

# **Rat Bladder Muscle Regeneration Induced by Local Delivery of an Engineered Insulin-Like Growth Factor 1 in Fibrin Gels**

THÈSE N° 4413 (2009)

PRÉSENTÉE LE 11 JANVIER 2010

À LA FACULTE SCIENCES DE LA VIE

CHAIRE MERCK-SERONO EN TECHNOLOGIES D'ADMINISTRATION DE MÉDICAMENTS (SV/SB/STI)  
PROGRAMME DOCTORAL EN BIOTECHNOLOGIE ET GÉNIE BIOLOGIQUE

ÉCOLE POLYTECHNIQUE FÉDÉRALE DE LAUSANNE

POUR L'OBTENTION DU GRADE DE DOCTEUR ÈS SCIENCES

PAR

**Lirong YANG**

acceptée sur proposition du jury:

Prof. V. Hatzimanikatis, président du jury

Prof. J. A. Hubbell, directeur de thèse

Prof. T. Barker, rapporteur

Prof. P. Frey, rapporteur

Prof. J. Southgate, rapporteur



ÉCOLE POLYTECHNIQUE  
FÉDÉRALE DE LAUSANNE

Suisse  
2010



## Table of Contents

<b>TABLE OF CONTENTS</b>	<b>3</b>
<b>ACKNOWLEDGEMENT</b>	<b>5</b>
<b>ABSTRACT</b>	<b>7</b>
<b>RESUME</b>	<b>11</b>
<b>ABBREVIATIONS</b>	<b>15</b>
<b>CHAPTER I INTRODUCTION AND BACKGROUND</b>	<b>19</b>
<b>CHAPTER II HIGH-LEVEL RECOMBINANT FIBRINOGEN PROTEIN PRODUCTION IN SUSPENSION CULTURED MAMMALIAN CELLS</b>	<b>49</b>
<b>CHAPTER III DEVELOPMENT OF A 3<sup>RD</sup> GENERATION FIBRIN DELIVERY SYSTEM: RECOMBINANT FIBRINOGEN IGF1 FUSION PROTEIN</b>	<b>71</b>
<b>CHAPTER IV LOCAL DELIVERY AND CONTROLLED RELEASE INSULIN-LIKE GROWTH FACTOR-1 FOR BLADDER MUSCLE REGENERATION</b>	<b>91</b>
<b>CHAPTER V RETROSPECTIVE AND OUTLOOK</b>	<b>141</b>
<b>ANNEX 1. HISTOLOGY STAINING OF RAT BLADDER SPECIMENS AT 4 WEEKS FOR FIRST SERIES EXPERIMENT</b>	<b>145</b>
<b>ANNEX 2. HISTOLOGY STAINING OF RAT BLADDER SPECIMENS AT 4 WEEKS FOR SECOND SERIES EXPERIMENT</b>	<b>158</b>
<b>CURRICULUM VITAE</b>	<b>179</b>



# Acknowledgement

I would like to express my deep appreciation and indebtedness to my thesis advisor Professor Jeffrey A. Hubbell for providing me with the opportunity to study in his laboratory. My gratitude should be extended for his invaluable guidance and continuous encouragement throughout my thesis work. His profound insight into the problems of tissue engineering and willingness to share his wealth of experience on numerous occasions gave me a great learning experience. Thank you, Jeff.

My sincere thanks go to Professor Peter Frey for his confidence, help and encouragement throughout this work. Thanks a lot, Peter.

My sincere thanks also go to Professor Thomas Barker for his scientific advice and encouragement for this thesis. Because of his help, my research career will be going in the direction that I wished.

I would like to thank my thesis committee members Professor Thomas Barker, Professor Jenny Southgate and Professor Peter Frey for accepting the invitation to examine my thesis. My special thanks go to Professor Jenny Southgate for her corrections to my thesis manuscript.

My thanks also go to Professor Vassily Hatzimanikatis for being the president of my thesis jury.

It is my great pleasure to acknowledge the kind assistance received from Dr. Lucia Baldi for suspension cell culture, Professor Susan Lord for supplying CHO<sub>fgn</sub> and CHO<sub>βγ</sub> cell lines, Dr. SeungTae Lee and Dr. Jung-Im Yun for real-time qPCR and RNA extraction, M.D. Lionel Micol for advice about animal experiments, Pierre Maillard for advice on cloning, Asad Qureshi for advice on protein purification, and Dr. Jacqueline Shields and V r ne Pignat for advice on protein phosphorylation.

I am grateful to Professor Jeffrey A. Hubbell, Dr. Conlin O'Neil, Dr. Jennifer Patterson, senior PhD student Catherine Sch tz, Dr. Yun Suk Jo and Dr. Catharina Adel w, for their corrections and useful suggestions to this manuscript.

I take this opportunity to thank many technicians and personnel in the institute, particularly Dr. Jessica Dessimoz, V ronique Garea, Dr. Graham Knott, Hautier Agn s, Dr. Otto Hagenbuehle, Diego Chiappe, Dr. Jacques Rougemont, Manuel Bueno, C dric George, Patrick Wenger, Carol Bonzon, Mich le Bonnard Giacobino and all others, for their responsibility and kindness.

A special note of thanks goes to my family, my husband and my child, for their support throughout my thesis work. I love you all.

Finally, I wish to thank all my friends and my colleagues for making my stay in the institute a memorable experience. Without them, this thesis would have been impossible to accomplish.

## Abstract

Currently, both congenital abnormalities and developmental problems of the bladder in children, and other dysfunctions in adults, require reconstructive surgery. Such correction involves transplant action of native tissues (such as gastrointestinal segments, or mucosa), homologous tissues from a donor, heterologous tissues or substances, or artificial materials to act as a replacement for normal bladder tissue. However, such surgery does not entirely restore the function, as the replacement tissue is either rejected due to immune system, fibrosis, contraction or causes metabolic complications due to a mismatch in different functional parameters, such as gastrointestinal segment for absorbance versus bladder for excretion. Tissue engineering is emerging as a significant alternative potential treatment for bladder dysfunction. To achieve this goal, we have explored fibrin gels as a natural material based scaffold to seed infiltrating smooth muscle cells to mimic the ontogeny of the bladder tissue.

Our interest in developing fibrin-based biomaterial technology is based on fibrin's central role in tissue binding and in the initiation of tissue repair and defence. It is well known that fibrinogen/fibrin binds to platelets as well as to different cells, growth factors, and extracellular matrix proteins, which is critical for the wound repair process.

Insulin-like growth factor I (IGF1) is well known as a key regulator in carbohydrate metabolism and growth. It can promote smooth muscle cell growth. In this thesis it was also chosen due to its simple active form, namely a single chain of low molecular weight, 10kDa. A novel engineered insulin-like growth factor I (IGF1) - factor XIIIa substrate fusion protein was chosen as the bioactive macromolecule to be released from the scaffold in order to control cellular growth and differentiation. Therefore, we can achieve close to the natural biomechanical environment in the regenerated tissue.

In this work, two generations of fibrin matrices for tissue engineering were developed. The first part of the work was devoted to preventing rapid diffusion of the growth factor from the matrix and to controlling its release. IGF1 was modified by inserting a factor XIIIa substrate sequence (denoted TG) based on the  $\alpha$ 2-plasmin inhibitor to cross-link into the fibrin gel during coagulation. This is so that the variant IGF1 will bind to the fibrin gel itself and will be released upon matrix degradation. In order to produce this recombinant protein TG-IGF1, IGF1 GST tag plasmid DNA was transformed into BL21 competent cells. After protein production, the recombinant TG-IGF1 protein was purified by GST affinity chromatography. The purified TG-

IGF1 was confirmed via SDS-PAGE and western blot with an anti-hIGF1 antibody. The sequence was confirmed using MALDI-TOF mass spectrometry.

The biological activity of TG-IGF1 was validated *in vitro* by receptor tyrosine phosphorylation and metabolic assay (MTT assay) with fibroblast 3T3 cells. The cell proliferation profile was similar for both TG-IGF1 and native recombinant IGF1. Although we were able to obtain relatively pure TG-IGF1 protein, the purification protocol may still require some development due to loss of protein via aggregation during protein production.

Using a three-dimension *in vitro* model, neonatal human bladder smooth muscle cells were seeded in the fibrin gel only, in the fibrin gel either with TG-IGF1 or native recombinant IGF1 as a control. The morphology of the seeded cells was analysed using ultra-structural transmission electron microscopy after three days. Secretory vesicles had not been found in the cells without IGF1. The cells with the TG-IGF1 displayed larger and more numerous secretory vesicles than those with native recombinant IGF1, presumably due to the rapid diffusional loss of the native recombinant IGF1 from the gel.

The bladder smooth muscle cell in the fibrin gel responses to either TG-IGF1 or native recombinant IGF1 at the genomic level were analyzed by qRT-PCR for extracellular matrix and adhesion molecules after 24 hours incubation. The cells in the fibrin gel only were used as control. We did not observe a difference in gene expression between the two groups.

The bioactivity of TG-IGF1 was also investigated *in vivo* utilizing a rat bladder model. A wound was induced via resection on the rat bladder. Either the TG-IGF1 or native recombinant IGF1 containing fibrin gel was then applied to the wound site, with a second control group receiving only the fibrin gel alone. Three classic histological stainings were done using Hematoxylin & Erythrosine (HE), Masson's Trichrome (TM) and Prussian Blue (PB). It was found that TG-IGF1 greatly enhanced rat bladder muscle layer regeneration compared to native recombinant IGF1 and the control group of fibrin gel according to the histology staining and quantitative analysis of the ratio of detrusor muscle regenerated / normal detrusor muscle ( $0.27 \pm 0.10$  for TG-IGF1 and  $0.23 \pm 0.10$  for native recombinant IGF1).

The second part of the work was devoted to making a new generation of fibrin matrices. Fibrinogen (Fgn), a soluble plasma protein found in all vertebrates, is a covalent dimer composed of pairs of three polypeptide chains called  $A\alpha$ -,  $B\beta$ - and  $\gamma$ -chains. Fibrinogen  $A\alpha$  chain can be truncated to  $B\beta$ - and  $\gamma$ -chains while maintaining the capacity to be assembled into a secreted, detectable fibrinogen. It is feasible to produce recombinant chimeric fibrinogen in cell



culture, which can then be used to incorporate growth factors into fibrin matrices as a fusion protein with fibrinogen at the genetic level. In this way, fibrin based natural material hydrogels can be formed which can bind and release signalling biomacromolecules for directed cellular growth and tissue regeneration.

In order to produce this new fibrinogen recombinant protein, a novel stable cell line of Chinese Hamster Ovary cells, CHO<sub>f<sub>gn</sub>-hIGF1</sub>, needed to be developed. This was accomplished via transfection of an FGA-hIGF1 plasmid DNA into CHO<sub>β<sub>γ</sub></sub> cells. After protein production, the recombinant chimeric fibrinogen variant hIGF1 fusion protein was purified by affinity chromatography. The successful production of these cell lines and the resultant variant IGF1 was confirmed via ELISA with fibrinogen and hIGF1 antibodies, and also by fluorescence activated cell sorting (FACS). Due to protein polymerisation in the column during purification, the protein purification step still requires additional development. Although the targeted fusion protein was successfully produced, overall protein yield was so low as to prevent further exploration.

By harnessing the powerful technique of protein engineering and using the fibrinogen/fibrin hydrogels developed in our lab, we were able to demonstrate a new type of multifunctional gel capable of regenerating smooth muscle type tissue with the aim to repair bladder function. Here we were able to demonstrate the production of the variant IGF1 factor XIIIa substrate fusion protein, its biological activity *in vitro*, and its application in an *in vivo* rat model.

Key words: Tissue engineering, biomaterials, fibrin gel, IGF1, SMC, smooth muscle cells, bladder, fibrinogen, muscle, fibrin matrices, CHO cells, regenerative medicine



## Résumé

Actuellement, les anomalies congénitales et les problèmes développementaux de la vessie chez les enfants, ainsi que d'autres dysfonctionnements chez les adultes exigent la chirurgie reconstructive comme traitement. Celle-ci implique l'implantation de tissus de l'hôte (tels que segments gastro-intestinaux, ou mucus), de tissus homologues d'un donateur, de tissus ou substances hétérologues, ou des matériaux artificiels pour reconstituer le tissu normal de la vessie. Cette chirurgie ne reconstitue toutefois pas entièrement la fonction, car le tissu de remplacement est rejeté par le système immunitaire, fibrose, contraction ou cause des complications métaboliques dues à une disparité dans différents paramètres fonctionnels, tels que des segments digestifs pour l'absorbance contre la vessie pour l'excrétion. L'ingénierie tissulaire est devenue un traitement potentiel alternatif significatif pour le dysfonctionnement de la vessie. Afin d'atteindre ce but, nous avons utilisé des gels de fibrine, une matrice naturelle,ensemencée de cellules musculaires lisses (SMCs) à imiter une ontogénèse du tissu urologique.

Notre intérêt pour développer une technologie des biomatériaux à base de fibrine est basé sur le rôle central de la fibrine dans l'adhésion, le déclenchement de la réparation et de la défense du tissu. La liaison entre fibrinogène/fibrine et des protéines, plaquettes d'hémostasies aussi bien qu'avec divers cellules, facteurs de croissance, et protéines de la matrice extracellulaire (ECM) est indispensable pendant le processus de réparation de blessure.

Le facteur de croissance insulino-mimétique (IGF1) est bien connu en tant que régulateur principal dans le métabolisme des hydrates de carbone et la croissance. Il peut favoriser la croissance de cellules musculaires lisses. Dans cette thèse, il a été choisi également pour sa forme active simple, une chaîne unique, et son faible poids moléculaire, 10kDa. Une nouvelle protéine recombinante de fusion IGF1 facteur XIIIa a été choisie en tant que macromolécule bioactive à être libérées de la matrice pour contrôler la croissance et la différenciation cellulaire. Ainsi, nous pouvons obtenir un environnement biomécanique presque naturel dans le tissu réparé.

Dans ce travail, deux générations de matrices fibrines pour ingénierie tissulaire sont planifiées. La première partie du travail est dédiée à empêcher la diffusion rapide du facteur de croissance de la matrice et contrôler sa libération retardée. L'IGF1 a été modifié en insérant une séquence TG du substrat de facteur XIIIa en base de l'inhibiteur  $\alpha$ 2-plasmine pour réticuler dans le gel de fibrine pendant la coagulation. C'est la raison pour laquelle le variant IGF1 est adhérent au gel de fibrine et libéré pendant la dégradation. Pour produire la protéine recombinante TG-IGF1, un

plasmide ADN d'IGF1 GST tagué a été transformé dans des cellules compétentes BL21. Après la production de la protéine, la protéine recombinante TG-IGF1 a été purifiée par chromatographie d'affinité GST. La pureté de TG-IGF1 a été vérifiée par SDS-PAGE et WB avec l'anticorps hIGF1. La séquence a été confirmée par spectrométrie de masse de MALDI-TOF.

Les activités biologiques de TG-IGF1 ont été validées *in vitro* par phosphorylation du récepteur et par essai MTT avec des cellules 3T3. Le profil de prolifération des cellules était semblable pour le TG-IGF1 et le naturel IGF1 recombinant. Bien que nous avons pu obtenir la protéine TG-IGF1 assez pure, le protocole de purification nécessiterait des développements supplémentaires dû à la protéine perdue via agrégation pendant la production de celle-ci.

Dans le modèle 3D, des SMCs humaines néonatales de vessie ont étéensemencées dans le gel de fibrine, dans le gel de fibrine incorporé respectivement avec TG-IGF1 et naturel IGF1 recombinant. La morphologie des cellulesensemencées a été analysée en utilisant la microscopie électronique à transmission (TEM) après 3 jours d'inoculation. Les vésicules sécrétrices n'ont pas été trouvées dans les cellules sans IGF1. Les cellules avec TG-IGF1 montraient de plus grandes et plus nombreuses vésicules sécrétrices que celles avec le naturel IGF1 recombinant. Ceci est dû à la diffusion de ce dernier du gel.

Les SMCs de vessie répondant respectivement au TG-IGF1 et au naturel IGF1 recombinant au niveau du gène ont été analysées par qRT-PCR dans le domaine des molécules d'adhérence et ECM après 24 heures d'inoculation. Les cellules dans le gel de fibrine étaient utilisées comme le contrôle. Aucune différence pour l'expression de gène pour ces cellules n'a été observée dans les deux cas.

La bio-activité de TG-IGF1 a également été étudiée *in vivo* dans le modèle de la vessie du rat. L'incision a été faite sous le microscope sur la vessie du rat. Soit TG-IGF1 soit le naturel IGF1 recombinant a été appliqué sur l'incision, avec le groupe de contrôle recevant que le gel de fibrine. Trois techniques classiques de coloration histologique ont été utilisées, Hématoxyline & éosine (HE), Masson's Trichrome (TM) et Blue Prusse (PB). Nous avons constaté que le TG-IGF1 a considérablement accéléré la régénération de la couche musculaire de vessie du rat, en comparant avec le naturel IGF1 recombinant et le groupe de contrôle d'après les colorations histologiques et l'analysis quantitative du rapport de muscle détrusor régénéré / muscle détrusor normal ( $0.27 \pm 0.10$  pour le TG-IGF1 et  $0.23 \pm 0.10$  pour le naturel IGF1).

La deuxième partie de ce travail a été dédiée à la fabrication d'une nouvelle génération de matrices de fibrine. Le fibrinogène (FGN), une protéine soluble de plasma présente dans tous

les vertébrés, est un dimère covalent composé de paires de trois chaînes de polypeptide, appelées  $A\alpha$ -,  $B\beta$ - and  $\gamma$ -chaînes. La chaîne du fibrinogène  $A\alpha$  peut être tronquée au  $B\beta$ - and  $\gamma$ -chaînes en gardant la capacité d'être réuni en fibrinogène sécrété et discernable. Il est faisable de produire le recombinant fibrinogène chimérique, qui dirige l'incorporation, au niveau génétique, du GF dans des matrices de fibrine. Dans ce cas, les hydrogels de matériel naturel basé sur la fibrine peuvent être faits en adhérant et libérant des bio-macromolécules signales pour diriger la croissance cellulaire et la régénération du tissu.

Pour produire cette nouvelle protéine fibrinogène recombinante, une nouvelle ligne cellulaire stable de cellules ovariées d'hamster chinois  $CHO_{\text{fgn-hIGF1}}$  a dû être développée. Elle a été faite par un plasmide ADN du FGA-hIGF1 transfecté dans les  $CHO\beta\gamma$  cellules. Après la production de la protéine, la protéine chimérique recombinante de fusion hIGF1 a été purifiée par la chromatographie d'affinité. La production avec succès de ces nouvelles lignes cellulaires stables et de IGF1 variante résultante a été confirmée par dosage d'immunosorption liée à une enzyme (ELISA) avec l'anticorps du fibrinogène et du hIGF1 et par le tri des cellules activées par la fluorescence (FACS). En raison de la polymérisation de protéine dans la colonne pendant la purification, l'étape de purification exige toujours un développement supplémentaire. Bien que la protéine ait été produite avec succès, le très bas rendement global était empêché le davantage de son exploration.

En utilisant la technique puissante de l'ingénierie de protéine et en employant les hydrogels de fibrinogène/fibrine développés dans notre laboratoire, j'ai pu démontrer un nouveau type de gel multifonctionnel capable de régénérer le tissu de type musculaire lisse avec le but de reconstruire la fonction de la vessie. Nous avons pu démontrer la production de la protéine de fusion variante IGF1facteur XIIIa, son activité biologique *in vitro* et son application *in vivo* dans un modèle de rat.

Mots clés: Ingénierie tissulaire, biomatériaux, gel de fibrine, IGF1, SMC, cellule musculaire lisse, vessie, fibrinogène, muscle, matrices de fibrine, CHO cellules, médecine régénérative



## Abbreviations

<b>ALS</b>	Acid-labile subunit
<b>bFGF</b>	Basic fibroblast growth factor
<b>BAM</b>	Bladder acellular matrix
<b>BSA</b>	Bovine serum albumin
<b>COL16A1</b>	Collagen, type XVI, alpha 1
<b>DNAse I</b>	Deoxyribonuclease I
<b>dNTPs.</b>	Nucleotides
<b>ELISA</b>	Enzyme-linked immunosorbent assay
<b>EPC</b>	Endothelial progenitor cells
<b>EtOH</b>	Ethanol
<b>FBS</b>	Fetal bovine serum
<b>FOXO</b>	Forkhead box O
<b>GH</b>	Growth hormone
<b>GnRH</b>	Gonadotropin-releasing hormone
<b>GSK-3<math>\beta</math></b>	Glycogen synthase kinase 3 beta
<b>GST</b>	Glutathione S-transferase
<b>HBSS</b>	Hanks Balanced Salt Solution
<b>H&amp;E</b>	Hematoxylin and eosin (erythrosine),
<b>His tag</b>	Polyhistidine-tag

<b>HH</b>	Hypogonadotropic hypogonadisms
<b>IGF1</b>	Insulin-like growth factor 1
<b>IGFBPs</b>	IGF binding proteins
<b>IGFD</b>	IGF1 deficiency
<b>IPTG</b>	Isopropyl $\beta$ -D-1-thiogalactopyranoside
<b>IRS1</b>	Insulin receptor substrate 1
<b>ITGA4</b>	Integrin, alpha 4 (antigen CD49D, alpha 4 subunit of VLA-4 receptor)
<b>ITGAV</b>	Integrin, alpha V (vitronectin receptor, alpha polypeptide, antigen CD51)
<b>KAL1</b>	Kallmann syndrome 1 sequence
<b>KS</b>	Kallmann's syndrome
<b>LAMA3</b>	Laminin, alpha 3
<b>LBA</b>	Luria-Bertani ampicillin
<b>MDCs</b>	Skeletal muscle-derived cells
<b>ml</b>	Milliliter
<b>MMP15</b>	Matrix metalloproteinase 15 (membrane-inserted)
<b>MMPs</b>	Matrix metalloproteinases
<b>MT</b>	Masson's Trichrome
<b>MTT</b>	3-(4,5-Dimethylthiazol-2-yl)-2,5-diphenyltetrazolium bromide (Thiazolyl Blue Tetrazolium Bromide)
<b>NaF</b>	Sodium fluoride
<b>OB</b>	Olfactory bulbs



<b>PB</b>	Prussian blue
<b>PBS</b>	Phosphate buffered saline
<b>PCR</b>	Polymerase chain reaction
<b>PDK1</b>	Phosphoinositide-dependent kinase-1
<b>PFA</b>	Paraformaldehyde
<b>PI3K</b>	Phosphoinositide 3 kinase
<b>PIP3</b>	Phosphatidylinositol (3,4,5)-trisphosphate
<b>PGA</b>	Polyglycolic acid
<b>PLA</b>	Polylactic acid
<b>PLGA</b>	Poly(lactic-co-glycolic acid)
<b>PMSF</b>	Phenylmethylsulphonyl fluoride
<b>PS</b>	Penicillin streptomycin
<b>qRT-PCR</b>	Quantitative real-time PCR
<b>RT</b>	Room temperature
<b>SDS-PAGE</b>	Sodium dodecyl sulphate polyacrylamide gel electrophoresis
<b>SFM</b>	Serum-free media
<b>SIS</b>	Small intestine submucosa
<b>SMCs</b>	Smooth muscle cells
<b>SPP1</b>	Secreted phosphoprotein 1 (osteopontin, bone sialoprotein I, early T-lymphocyte activation 1)
<b>THBS1</b>	Thrombospondin 1

<b>TBS</b>	Tris-Buffered Saline
<b>TBST</b>	Tris-Buffered Saline Tween-20 FBS
<b>TEM</b>	Transmission electron microscope
<b>TGF-<math>\alpha</math></b>	Transforming growth factor alpha
<b>TGF-<math>\beta</math></b>	Transforming growth factor beta
<b>THBS1</b>	Thrombospondin 1
<b>TIMP3</b>	TIMP metalloproteinase inhibitor 3 (Sorsby fundus dystrophy, pseudoinflammatory)
<b>TPO</b>	Thrombopoietin
<b>UC</b>	Urothelial cells
<b>VEGF</b>	Vascular endothelial growth factor

# Chapter I Introduction and Background

## ***Medical motivation for our research***

Insulin-like growth factor 1 (IGF1) is both a hormone and a tissue growth factor. It is normally produced throughout our life, and it plays some role in nearly every cell in the body. Since IGF1 was discovered in 1957, it has remained a top research topic in biology. Recently, IGF1 has been discovered to be an important factor or mediator for child growth, antineoplastic activity and treatment, cartilage and bone growth, skeletal muscle regeneration, and peripheral neurons apoptosis protection<sup>1-9</sup>. In August 2005, the FDA approved Tercica's IGF1 drug, Increlex, for severe primary IGF1 deficiency (IGFD), which is injected twice per day at a concentration of 10mg/ml. In December 2005, Insmed's Iplex, IGF1 with IGFBP3 complex, was also approved by the FDA for IGFD, which is injected only once per day<sup>4</sup>. There is still extensive work to be done before more IGF1 related drugs are approved by the FDA.

Biopharmaceutical companies have expressed more interest in IGF1 since 1987 when the IGF1 receptor was found to have relationship with human breast and colon cancer<sup>2</sup>. Several companies have developed therapeutic monoclonal antibodies against IGF1 to target IGF1 receptors for the treatment of different diseases (Table 1)<sup>2, 4</sup>, such as type 1 diabetes, type 2 diabetes, amyotrophic lateral sclerosis, and growth deficiency. One project for type 1 and 2 diabetes which was in a phase 3 clinical trial was withdrawn by Genentech due to severe side effects. Cephalon also withdrew a project for amyotrophic lateral sclerosis in 2001<sup>2, 10</sup>.

IGF1 concentration in the circulation is normally quite low, at 10-1000ng/ml<sup>90</sup>. Long-term IGF1 related drug use will disturb the IGF1 signalling pathway in the body and may result in severe irreversible side effects. The economic cost is also high, requiring large quantities of recombinant protein once or twice daily. So, development of an IGF1 protein formulation could be one solution to this problem. Controlled release of IGF1 could be another opportunity to avoid the effect of sudden spikes in IGF1 caused by large dose. The goal is to use IGF1 drugs safely and effectively by decreasing the quantity and frequency of IGF1 during the treatment.

Table 1. Several therapeutic monoclonal antibodies against IGF1 developed by divers' biopharmaceutical companies to target IGF1 receptors are undergoing clinical trial <sup>2, 4</sup>.

Company	Product	Development stage	Indication
Pfizer (New York)	CP-751,871 (fully human IgG2 mAb against IGF-1R extracellular domain)	Phase 3	Non-small-cell lung cancer
	CP-751,871 with Taxol (paclitaxel) and carboplatin	Phase 2	Non-small-cell lung cancer and Ewing's sarcoma
ImClone (New York)	IMC-A12 (fully human IgG1 mAb against IGF-1R extracellular domain)	Phase 2	Head-and-neck cancer
	IMC-A12 in combination with gemcitabine and Tarceva (erlotinib; targets EGFR tyrosine kinase domain)	Phase 1-2	Advanced pancreatic cancer
Genmab (Copenhagen)/Roche (Basel)	R1507 (fully human mAb targeting IGF-1R extracellular domain)	Phase 2	Recurrent or refractory sarcoma
Roche/Sarcoma Alliance for Research through Collaboration (Ann Arbor, Michigan)	R1507	Phase 2	Solid tumors, including sarcoma
Merck (Whitehouse Station, New Jersey)/Pierre Fabre (Paris)	MK-0646 (humanized IgG1 antibody targeting IGF-1R extracellular domain)	Phase 2	Metastatic colon cancer
Amgen (Thousand Oaks, California)/Takeda Bio (Tokyo)	AMG 479 (fully human mAb targeting IGF-1R extracellular domain) combined with anti-EGFR mAb panitumumab or gemcitabine	Phase 2	Advanced solid tumors
Sanofi-Aventis <sup>a</sup> (Paris)	AVE-1642 (humanized IgG1 <sub>κ</sub> mAb targeting IGF-1R extracellular domain) with Velcade (bortezomib)	Phase 1	Multiple myeloma
	AVE-1642 with Taxotere (docetaxel)	Phase 1	Solid tumors

mAb, monoclonal antibody; EGFR, epidermal growth factor receptor.

<sup>a</sup>Under license from ImmunoGen (Waltham, MA).

## ***Insulin-like growth factor 1 (IGF1)***

Growth factors are a class of proteins that can stimulate cellular growth, proliferation, differentiation and maturation<sup>11, 12</sup>. They act as signalling molecules between cells to regulate cellular effects. Several examples are thrombopoietin (TPO), insulin-like growth factor (IGF), transforming growth factor alpha (TGF- $\alpha$ ) and transforming growth factor beta (TGF- $\beta$ ), etc.

The insulin-like growth factors (IGFs) are single-chain polypeptides. They are well known as key regulators of energy metabolism and cellular growth for normal fetal and postnatal life. IGFs act as cell survivor factors because they simulate cell proliferation and inhibit apoptosis. The IGF system is composed of two ligands (IGF1 and IGF2), two receptors (IGF1R and IGF2R), six high-affinity IGF binding proteins (IGFBPs), a glycoprotein called the acid-labile subunit (ALS) and IGFBPs proteases. IGFBPs proteases allow IGFs to be released continuously from the inactive IGFs-IGFBPs conjugates<sup>13</sup>.

### **IGF1/GH axis**

Normally, the IGF/growth hormone axis (IGF/GH) refers specially to IGF1, because IGF2 expression is independent of GH activity. This axis (Fig. 1) plays a role in aging.

Growth hormone (GH) is a single polypeptide chain of 191 amino acids with 2 intramolecular disulfide bridges. It is produced and stored in secretory vesicles in the pituitary gland. GH is regulated by hypothalamic factors (GH releasing hormone (GHRH) and somatostatin (SMS)), ghrelin and the IGF1 negative feedback.

IGF1 is also called somatomedin C and is produced throughout life. Nearly every cell in the body is affected by IGF1. In the fetus, the supply of nutrition is the main regulator of IGF1 expression. In postnatal growth, GH is the essential regulator. Most circulating IGF1 is secreted by the liver as an endocrine hormone via stimulation by pituitary growth hormone (GH)<sup>14</sup>. It is also expressed by many target tissues as an autocrine or paracrine cytokine due to a number of regulatory influences, including stimulation by GH level and inhibition by malnutrition, GH insensitivity, GH receptors absent, or GH signalling pathway downstream failure<sup>14</sup>.

IGF1 is one of the most critical factors in the growth of children. It is the principal mediator for bone growth in the body. A deficiency in IGF1 (IGFD) causes abnormal growth. Severe primary IGFD refers to those children having normal or high GH levels, height lower than 3 standard deviation (<3SD) and IGF1 level in the blood <3SD. To catch up with the average height of their friends, these children can be treated with IGF1<sup>4</sup>.

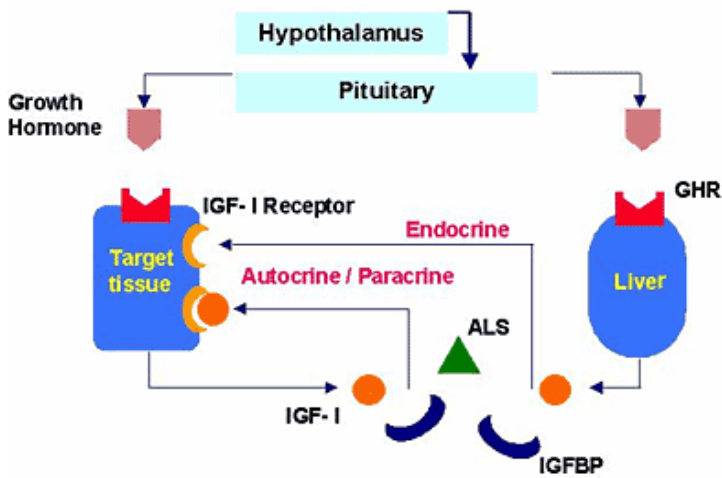


Fig 1. Relationships within the IGF1-GH system <sup>91</sup>.

Regulated by hypothalamic factors, growth hormone (GH) is synthesized in pituitary. Endocrine IGF1 is secreted primarily by the liver when GH binds to its GH receptor. Or autocrine/paracrine IGF1 is generated by target tissue when GH binds to its IGF1 receptor. Then IGF1 binds to both IGF-binding proteins (IGFBP) and acid-labile subunit (ALS) in the circulation to extend its half-life.

### The structure of IGF

Structurally, IGF1 is very similar to IGF2. IGF1 is a single chain basic polypeptide of 70 amino acids with three intramolecular disulfide bridges <sup>16</sup>. Its molecular weight is 7649 Dalton (Fig. 2). IGF2 is a single chain neutral polypeptide of 67 amino acids. The two proteins have different biological activities <sup>13</sup>.

IGF1 plays one important role in promotion of cell proliferation for maximal growth and inhibition of cell death (apoptosis). In contrast, IGF2 is one of the primary growth factors for early development. In this sense, it has a more specific function compared to IGF1.

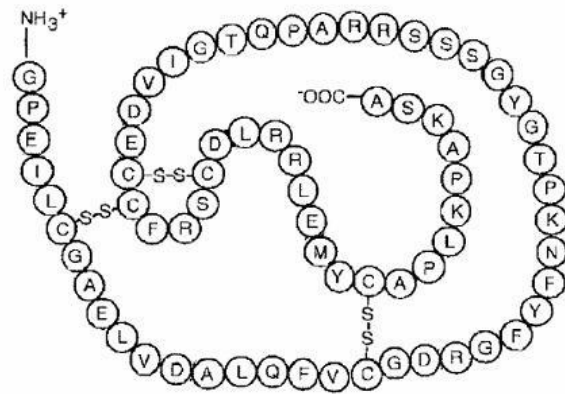


Fig 2. Primary amino acid sequence of human IGF1 structure <sup>15</sup>. It is a small polypeptide growth factor that consists of 70 amino acids in a single chain with three intramolecular disulfide bridges.

## IGF receptors

Because IGFs' molecular structure is similar to insulin, IGFs can also bind to the insulin receptor, but with much lower affinity than insulin. Both the insulin receptor and IGF1 receptor are tyrosine kinase receptors. The bioactivity of IGF1 is mediated by binding to IGF receptors present on many cell types<sup>14</sup>. The IGF1 receptor has a high degree of homology to the insulin receptor, while the IGF2 receptor is identical to the cation independent mannose 6-phosphate receptor<sup>17</sup>.

IGF2 can bind to both IGF1 and IGF2 receptors. The IGF2 receptor lacks a signal transduction capacity. So, the IGF2 receptor acts as a sink for IGF2 in order to decrease the chance of IGF2 binding to the IGF1 receptor. So, the IGF2 receptor was discovered to display tumour suppressor activity<sup>1,18</sup>.

The IGF1 receptor is a hetero-tetrameric transmembrane glycoprotein with two subunits<sup>1</sup>. Each subunit consists of one  $\alpha$ -chain containing an extracellular ligand binding domain and one  $\beta$ -chain containing an intracellular tyrosine kinase domain. The IGF1 receptor plays an important role in cancer<sup>2</sup>. Neoplastic cell lines and many human cancers express the IGF1 receptor. That is the reason why many cancer cell lines respond to physiological concentrations of IGFs.

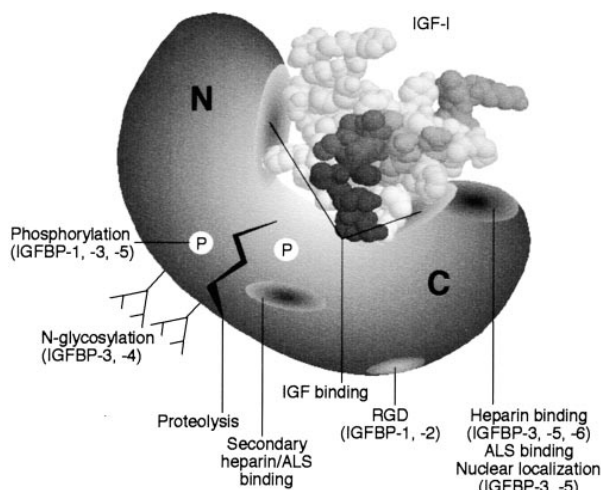
## IGF binding proteins (IGFBPs)

The interaction between IGF proteins and IGF receptors is regulated by IGFBPs<sup>19</sup>. Despite a similar molecular structure between IGFs and insulin, insulin can directly access its receptor, while IGFs are modulated by IGFBPs<sup>1</sup>. The main functions of IGFBPs are to transport the IGFs to the target tissues or cells, modulate the IGF bioactivity, limit the access of IGFs to IGF1 receptors and to extend IGFs half-life in the circulation.

There are six homologous multifunctional proteins in the IGFBPs gene family, named IGFBP1 to IGFBP6. Their precursor forms have secretory signal peptides from 20 to 39 amino acids. Their mature proteins have between 216 and 289 amino acids and are all extracellular<sup>18,20</sup>. Both the N-terminus and C-terminus of IGFBPs are rich in cysteine, containing an IGF binding domain (Fig. 3 and Table 2). The RGD integrin-binding and cell binding sites are also at the C-terminus. The central domain of IGFBPs contains the posttranslational modification, glycosylation, proteolytic cleavage sites and phosphorylation domains<sup>18,20,21</sup>.

IGFBPs also display various biological activities, which are both dependent and independent of their interactions with IGFs. It is known that they modulate cell functions and play a role in apoptosis for example.

The IGFBPs have the potential to stimulate or inhibit IGF1 action in IGF-dependent manner<sup>19, 20, 22</sup>. On the one hand, IGFBPs can enhance IGFs action by prolonging IGF half-life, increasing the IGFs concentration level around the IGFs receptor and cell exposure. On the other hand, IGFBPs can inhibit the IGF action via sequestration of the IGF from the receptor (Fig. 4).



Domain	Function	IGFBP
Amino terminal	IGF binding	IGFBP1, IGFBP2, IGFBP3, IGFBP5
	Insulin binding	IGFBP3
	Inhibition of insulin receptor autophosphorylation	IGFBP3
	Inhibition of mitogenesis	IGFBP3
Central	Heparin binding <sup>a</sup>	IGFBP2, IGFBP3, IGFBP5
	ALS binding <sup>a</sup>	IGFBP5
	Cell binding	IGFBP3
Carboxyl terminal	IGF binding	IGFBP1, IGFBP2, IGFBP3, IGFBP5
	Nuclear localization signal <sup>b</sup>	IGFBP3, IGFBP5
	Heparin-binding <sup>b</sup>	IGFBP3, IGFBP5
	ALS binding <sup>b</sup>	IGFBP3, IGFBP5
	Cell binding <sup>b</sup>	IGFBP3, IGFBP5
	Integrin binding	IGFBP1

Table 2. IGFBPs different functional domains. The N- and C-domains of IGFBPs both contain IGF binding site, which is important for the half-life of IGF<sup>20</sup>. At the C-terminus, there are also heparin binding, ALS binding, nuclear localization and RGD integrin-binding domains. The inhibitor domains are at the N-terminus. The central domains are highly variable containing sites for posttranslational modification.

Fig 3. IGFBPs structure. The family of six high affinity IGFBPs share common domain architecture: mid-region, highly conserved N- and C-domains. N- and C-domains are important for high affinity IGF1 binding to modulate the bioavailability and hence the action of IGF1<sup>20</sup>.

However each of the IGFBPs has unique sequences that underlie differentiating biochemical and functional properties, such as nuclear localization and RGD integrin binding. The central domains are sites of posttranslational modification, such as glycosylation, phosphorylation and IGFBP proteolysis.

When IGFBPs can not bind IGFs, they still have impact on the action of IGFs without activation or inhibition of type I IGF receptor in an IGF-independent manner<sup>19, 20, 22</sup>. IGFBP1 displays an effect on cell motility and adhesion through binding  $\alpha 5\beta 1$  integrin, such as healing stimulation in a dermal wound model. IGFBP3 can inhibit cancer cell growth and induce their apoptosis through a putative IGFBP3 receptor. IGFBP3 can also stimulate TGF $\beta$  signalling via the smad



pathway. IGFBP5 displays normal osteoblast mitogenesis stimulation through a putative IGFBP5 receptor (Fig. 5). Both IGFBP3 and IGFBP5 possess nuclear localisation sequence via importin  $\beta$ . But the mechanism of these activities is still unclear.

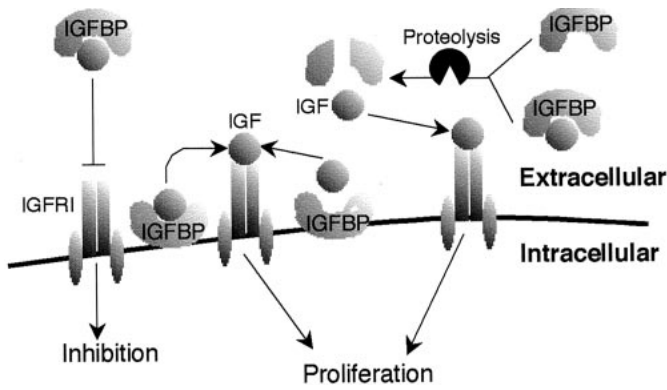


Fig 4. IGF-dependent IGFBPs action<sup>20</sup>. IGFBPs limite IGF bioavailability and decrease its activity by blocking its binding to IGF-receptor. The dissociation of the IGFBPs-IGF complex in the plasma of the target tissue enables IGF to interact with IGF-receptor on the cell membrane.

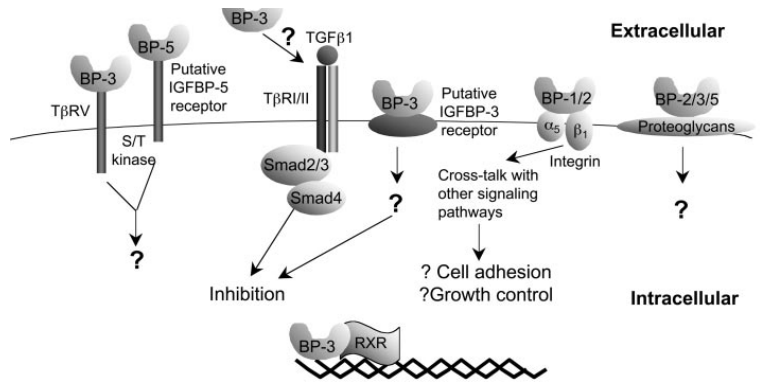


Fig 5. IGF-independent IGFBPs action<sup>20</sup>. IGFBPs can activate cell-surface receptors directly to stimulate cellular events in the absence of IGFs. For example, IGFBP1 can act on cell growth and adhesion through binding  $\alpha 5\beta 1$  integrin. IGFBP3 can inhibit cellular actions through interactions with putative IGFBP3 receptor or some other receptors.

## IGF1 actions in skeletal muscle

IGF1 can act either as a hormone or as a local growth factor<sup>6</sup>. It is essential for normal growth and development. It is a key regulator of skeletal muscle development. It enhances the ability for muscle to grow and undergoes repair throughout life<sup>23</sup>. It is one unique mitogenic growth factor that can stimulate both proliferation and differentiation of myoblasts in culture<sup>24</sup>. IGF1 is also known to function as survival factor to protect skeletal muscle cells from apoptosis<sup>17</sup>.

IGF1 can stimulate myoblast proliferation with the presence of mitogenic competence factor<sup>25</sup>. It is one important mediator of anabolic pathways in skeletal muscle cells. The effect of IGF1 on muscle protein metabolism is associated with the stimulation of muscle protein synthesis and the suppression of proteolysis<sup>26</sup>.

IGF1 controls the myogenesis in all skeletal muscle cells<sup>27</sup>. The family of myogenesis genes MyoD, myogenin, myf-5, and MRF4 is only expressed in skeletal muscle cells, not even in cardiac or smooth muscle cells<sup>28, 29</sup>. These genes functioned in similar ways are transcription

factors essential for the specification and determination of the muscle cell lineage. They can transform other cell types to the myogenic lineage. This muscle regulatory factor gene family is associated with terminal myogenic differentiation, which is crucial for normal skeletal muscle development. During myogenesis, myoblasts can be fused to form postmitotic myotubes, where the transcription factors MyoD and myf-5 plays a crucial role for the initial determination of the myogenic lineage<sup>27</sup>. Expression of MyoD is then downregulated shortly before myogenin<sup>30</sup>. The gene myf-5 is essential for the initial elevation of myogenin expression, which is then autocatalytic<sup>17</sup>. The expression of myogenin and MRF4 is activated during myoblast differentiation. Myogenin mRNA can be actively induced and elevated in treated cells. MRF4 is expressed only in the late phase of differentiation<sup>29</sup>.

Proliferation and differentiation are two opposing processes. It is found that IGF1 does not stimulate differentiation while it is stimulating proliferation<sup>31</sup>. There is one short separation time between two effects, which presented one perfect period for the repair of damaged tissue<sup>6</sup>. The cultured muscle cells exhibited a biphasic concentration dependent response to IGF1 treatment. At first cell proliferation was stimulated during which expression of myogenic factors is inhibited and then the myogenic differentiation was enhanced during which proliferative signals are down-regulated. During the stimulation of muscle cell differentiation by IGF1, the process was significant at relatively low IGF1 concentration. But at higher concentration (>100ng/ml IGF1), the process of differentiation was slowly, even stopped at very high IGF1 concentration<sup>17</sup>.

Disuse or denervation causes rapid atrophy. During atrophy, skeletal muscles exhibit a common set of biochemical and transcriptional changes, such as breakdown of myofibrillar proteins. Because 60-70% of the total cell protein is myofibrillar proteins in adult muscle, proteolysis will have important effect on muscle size and functional capacity<sup>32</sup>. Muscle atrophy results mainly from a general activation of the ubiquitin-proteasome pathway. FoxO family transcription factors play a critical role in this loss of cell protein<sup>33</sup>. When activated, FoxO3 causes expression of the atrophy-related ubiquitin ligases atrogen-1 and MuRF1 and profound loss of muscle mass. IGF1 is one important cytokine which maintains skeletal muscle mass. It can stimulate muscle protein synthesis and hypertrophy via the phosphatidylinositol 3-kinase (PI3K)-Akt pathway. Activation of this pathway can reduce muscle atrophy. Atrogen-1 is a regulated downstream target of PI3K. IGF1 can block protein degradation, which is associated with decreased expression of two muscle-specific ubiquitin ligases, atrogen-1 and MuRF1<sup>32</sup>. IGF1 can rapidly reduce atrogen-1 expression by blocking mRNA synthesis, while MuRF1 mRNA is just decreased slowly.

Contractile activity is necessary for postnatal muscle growth and for the maintenance of skeletal muscle mass in adults. Increased work can cause fiber hypertrophy. IGF1 mediates skeletal

muscle hypertrophy to activate of protein synthesis through PI3K-Akt pathway <sup>34</sup>. The key elements of this pathway are activation of PI3K, Akt and mTOR <sup>35</sup>.

### **IGF1 actions and signalling in skeletal muscle regeneration after injury**

Muscle deficiency or injury can result in a significant loss of function, which will have an impact on the quality of life. IGF1 is a central regulator of muscle regeneration <sup>6</sup>. IGF1 increases muscle mass and strength in two main ways. First, IGF1 acts directly on the muscle fibers to increase protein synthesis and muscle mass. Secondly, it can drive activated satellite cells to fuse to existing muscle fibers in order to repair damaged regions of the fibers and to promote muscle growth. It is the reason that IGF1 is a potential candidate for a therapeutic agent, both in aging and muscle disease <sup>23</sup>.

Muscle regeneration following injury is a coordinate process in which multiple factors are activated to maintain and preserve muscle structure and function on injured stimuli. There are four phases involved, degeneration, inflammation, regeneration, and fibrosis <sup>36</sup>. Injury results in the rapid necrosis of myofibers and the activation of inflammation, which is to remove necrotic materials and to secrete several cytokines and growth factors for activation of satellite cells <sup>5, 36</sup>. IGF1 can down-regulate proinflammatory cytokines, such as tumor necrosis factor- $\alpha$  and interleukin-1 $\beta$ , and modulate the expression of CC chemokines involved in the recruitment of monocytes and macrophages <sup>5</sup>. IGF1 can also act as a survival factor by prolonging the regenerative potential of skeletal muscle through increases in satellite cell activity <sup>6</sup>.

IGF1 initiates cellular action by directly binding to the IGF1 receptor  $\alpha$  subunit on the cell surface and subsequent phosphorylation of the IGF1 receptor  $\beta$  unit (Fig. 6) <sup>16</sup>. The phosphorylated receptor recruits and phosphorylates the insulin receptor substrate 1 (IRS1), which activates phosphoinositide 3 kinase (PI3K). PI3K transfers a phosphate group to the membrane bound phosphatidylinositol (3,4)-bisphosphate (PIP2) to generate phosphatidylinositol (3,4,5)-trisphosphate (PIP3). PIP3 serves as a nucleation site for Akt1 and phosphoinositide-dependent kinase-1 (PDK1) <sup>37, 38</sup>. PDK1 phosphorylates and activates Akt1, which in turn transfers phosphate groups to several substrates, mammalian target of rapamycin (mTOR), glycogen synthase kinase 3 beta (GSK-3 $\beta$ ) and forkhead box O (FoxO). The combined effects of PIP3, Akt1 and PDK1 are important for cell migration, growth and survival <sup>39-41</sup>.

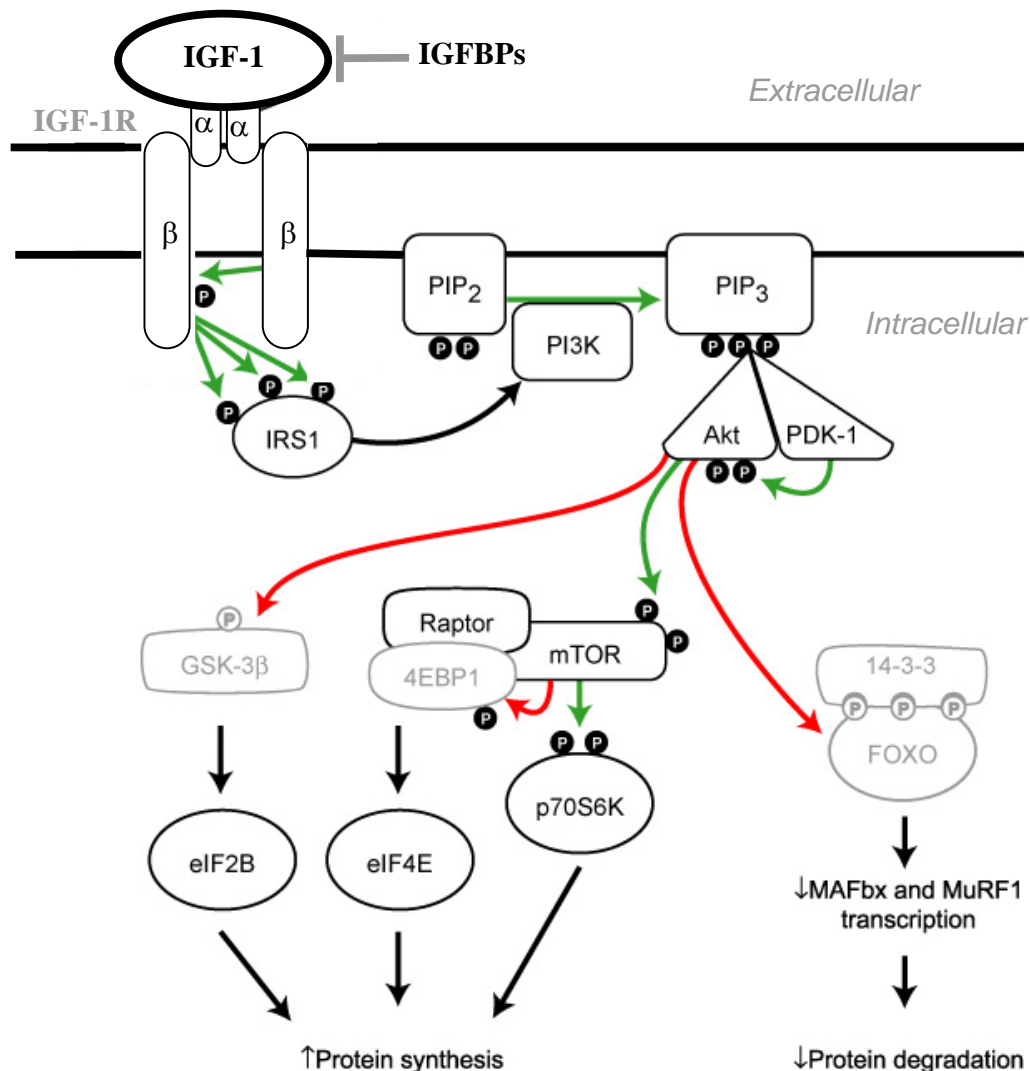


Fig 6. Mechanisms for IGF1-induced muscle growth promotion through PI3K/Akt pathway<sup>18, 38, 41, 42</sup>. IGF1 binds to IGF1 receptor resulting in receptor autophosphorylation, followed by tyrosine phosphorylation of several cellular substrates, such as insulin receptor substrate 1 (IRS1). Association of IRS-1 with phosphoinositide 3 kinase (PI3K) results in activation of Akt kinase. Akt can in turn activate mammalian target of rapamycin (mTOR) and inhibit both glycogen synthase kinase 3 beta (GSK-3β) and forkhead box O (FoxO). The combined effects result in increasing protein synthesis and reducing protein degradation. Activation of the pathway is indicated with green arrows. Inhibition of the pathway is indicated with red arrows.

Akt1-mediated phosphorylation and inhibition of GSK-3β activates the eukaryotic translation factor eIF-2B and increase protein synthesis. With the help of the protein Raptor, the phosphorylated

mTOR then phosphorylates and inhibits 4EBP1. mTOR also promotes protein synthesis also by activating ribosomal p70S6K<sup>42</sup>. At same time, down stream of the Akt mediated FoxO phosphorylation signalling pathway results in decreasing protein degradation.

So, the signalling cascades induced by IGF1 lead to increased muscle protein production and regenerate the muscle layer after injury and tissue damage.

### **IGF1 actions in smooth muscle**

IGF1 regulates the growth of smooth muscle cells (SMCs) of the vascular wall, bladder, myometrium, and gastrointestinal and respiratory tracts. This enables SMCs to have adaptive responses to injury, hormonal, or mechanical stimulation<sup>43</sup>. It is reported that smooth muscle hypertrophy secondary to partial urethral ligation is associated with increased IGF1 biosynthesis in the bladder wall<sup>44</sup>. The transgenic mice selectively overexpressing IGF1 in SMCs exhibited overexpression of IGF1 in all smooth muscle-rich tissues (*i.e.* bladder, stomach, intestine, uterus, and aorta), where the growth factor promotes a striking degree of hyperplasia without affecting plasma IGF1 levels or total body weight<sup>45</sup>.

The ligand occupancy of  $\alpha v \beta 3$  integrin is required for IGF1 stimulated SMCs proliferation and migration and DNA synthesis. The  $\alpha v \beta 3$  integrin occupancy is also important for the activation of IGF1 receptor dependent downstream signaling events, such as activation of PI3K and MAPK pathways. So, this integrin receptor has a significant role in regulating IGF1 receptor signalling<sup>46</sup>.

Vascular SMCs are the principal source of collagen and extracellular matrix, which maintain the tensile strength of atherosclerotic plaques. Apoptosis of vascular SMCs decreases the synthesis of collagen and extracellular matrix, and induces features of plaque instability<sup>47</sup>. Rupturing of plaques can result in thrombotic complications. Oxidative stress is increasingly implicated in the development of atherosclerosis<sup>48</sup>. It can induce vascular SMCs apoptosis in cell culture conditions. IGF1 receptor dependent signalling is a critical regulator for smooth muscle cell survival. Increased expression of the IGF1 receptor can rescue plaque vascular SMCs from oxidative stress-induced apoptosis<sup>49</sup>. A major downstream effector of IGF1 receptor signalling is the serine/threonine kinase Akt. Akt-dependent phosphorylation and subsequent inactivation of its downstream targets FoxO3a or GSK3 is important for vascular SMCs survival<sup>50</sup>.

**We will use IGF1 for bladder smooth muscle layer regeneration.**

## ***Biomaterials as delivery devices for growth factors***

The field of biomaterials research is a specialization within biomedical engineering that integrates engineering fundamentals in materials science with the principles of cell biology, chemistry and physiology to aid in the design and development of novel medical devices <sup>51</sup>. Using biomaterials is an increasingly utilized approach for wound healing and tissue regeneration. Biomaterials can serve as temporary scaffolds for tissue growth. They can direct cellular interactions, and also can provide bioactive signalling, such as in the delivery of growth factors <sup>52</sup>.

Biomaterials are already widely applied in biomedicine, such as in drug delivery systems, surgical implants, artificial organs, wound healing, and vaccines <sup>53, 54</sup>. Due to their wide application in clinical use, there are some design and production criteria, such as biocompatibility, sterility, favourable processing conditions, and stability in response to biological conditions. Biomaterials for tissue repair should display favourable biodegradation and bioresorption, with limited inflammation and toxicity to avoid long-term complications.

Generally, three classes of biomaterials have been used in tissue engineering: natural protein and polysaccharide based biomaterials (e.g., collagen and alginate), inorganic biomaterials (e.g., metals, ceramics and glasses for artificial hips in orthopaedic research) and synthetic polymers (e.g., polyglycolic acid (PGA), polylactic acid (PLA), and poly(lactic-co-glycolic acid) (PLGA)) <sup>55-58</sup>. These materials have been investigated using two- or three- dimensional models *in vitro* to mimic the multicellular ECM in order to guide morphogenesis in tissue repair <sup>59, 60</sup>.

In this thesis, one of these natural biomaterials, fibrin, was applied for bladder muscle layer regeneration. Natural biomaterials have the potential advantage of biological recognition, but also present some complexities associated with purification, immunogenicity and pathogen transmission. However, these limitations can be overcome using recombinant protein expression technologies <sup>60</sup>.

### **Fibrinogen structure**

Fibrinogen (also called coagulation factor I) is synthesised in the liver by hepatocytes and megakaryocytes. It is a rod-shaped dimeric glycoprotein (molecular weight, 340kDa) that circulates in the plasma (the pale yellow, protein-containing liquid part of blood in which the blood cells and platelets are suspended) at a concentration of 2 to 4 mg/ml with a normal half-life of 3 to 5 days. Each monomer is composed of three different polypeptides; the A $\alpha$  (610

amino acids, 67kDa), the B $\beta$  (461 amino acids, 55kDa) and the  $\gamma$  (411 amino acids, 47.5kDa) chains<sup>61</sup>. These three polypeptides are linked to one another through 13 pairs of disulfide bonds to form the fibrinogen monomer. The two monomers are then bridged together to form a symmetric dimer through three additional disulfide bonds located near the N-terminus, which enables the monomers to face each other, such that the N-terminus of the six chains colocalize near the center of the rod (Fig. 7). The amino-terminal region of the molecule (located in the middle of the rod) provides the thrombin-binding site and the polymerizing domains. The carboxy-terminal regions contain the principle cross-linking sites for factor XIIIa, the platelet-binding sites, and the fibronectin-binding domains. Two of the three chains, B $\beta$  and  $\gamma$ , have single N-linked carbohydrate clusters which are first added to the different chains during the translation/translocation event<sup>62</sup>.

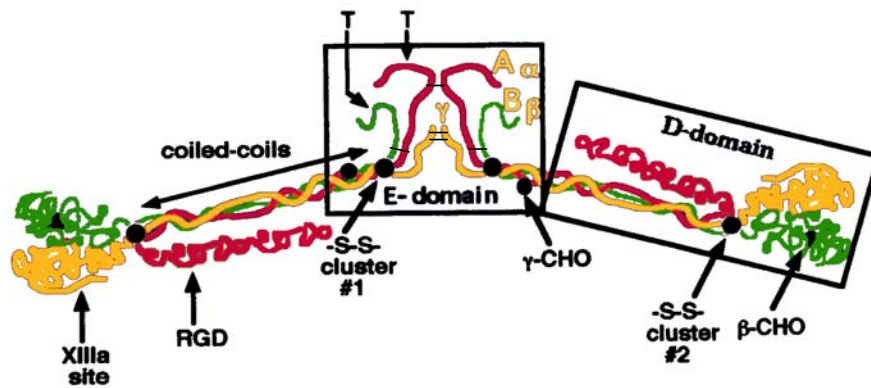


Fig 7. Schematic model of fibrinogen. T denotes the thrombin cleavage sites in central, or "E", domain located on the A $\alpha$  and B $\beta$  chains. The two disulfide clusters in the E domain and one each in the end, or "D", domains are referenced by "-S-S- cluster". The location of the carbohydrates on the  $\gamma$ - and B $\beta$ - subunits is noted by "CHO". The tightly wound supercoiled  $\alpha$ -helical regions are shown as coiled coils under the arrows. The C-terminal region of the B $\beta$  and  $\gamma$  chains form "random coils". In this region of the  $\gamma$  chain reside the Gln-Lys cross-linking sites catalyzed by activator factor XIIIa<sup>62</sup>.

## Fibrin tissue engineering

Fibrin is made from fibrinogen polymerisation. It is a specialized ECM protein network involved in blood clotting. Fibrinogen is transformed to fibrin by the coagulation enzyme thrombin (factor IIa). Thrombin catalyzes the hydrolysis of Arginyl-Glycine bonds. It binds to the N-terminal region of fibrinogen and initiates two steps of proteolysis to remove two acidic peptides. First is a rapid

removal of fibrinopeptide A ( $A\alpha$  chain, aa 1 to 16), followed by a slower hydrolysis of fibrinopeptide B ( $B\beta$  chain, amino acid from 1 to 14) <sup>62</sup>. The release of these peptides activates the fibrinogen molecule, which is thus designated the fibrin monomer. The molecular weights of fibrinogen and the fibrin monomer are identical. The only difference is that fibrinogen is more electronegative. The newly exposed amino termini ("knobs") are the principle contact sites during polymerization. In human fibrinogen, the  $A\alpha$  chain "knob" begins with the sequence Gly-Pro-Arg (G-P-R) while the  $B\beta$  chain starts with sequence Gly-His-Arg (G-H-R) <sup>62-64</sup>.

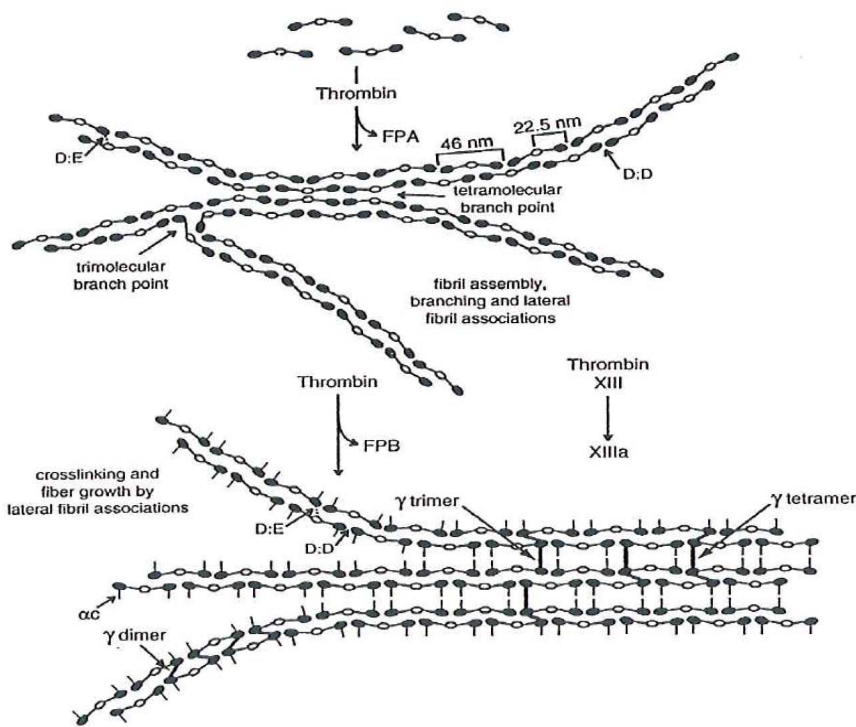


Fig 8. Schematic diagram of fibrin polymerisation and crosslinking <sup>65</sup>.

Thrombin cleavages fibrinopeptides A and B from the N-terminal ends of the fibrinogen  $A\alpha$  and  $B\beta$  chains, respectively. Then the assembly of fibrin begins with non-covalent interactions between E and D domains, followed by C-terminal ends of the  $A\alpha$  chains interact with other  $A\alpha$  domains to form a gel consisting of long polymers. Factor XIIIa catalyzes the covalent crosslinks between C-terminal sites in the  $\gamma$  chains and then  $A\alpha$  chains, which results in fibrin polymer web.

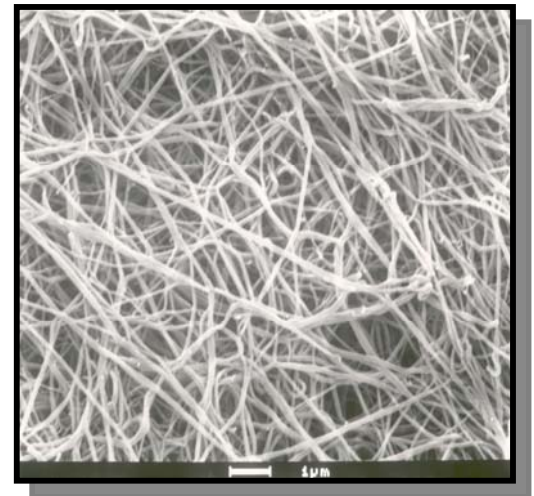


Fig 9. Scanning electron microscope (SEM) image of fibrous structure of fibrinogen scaffold with scale bar of 1 micrometer. Image was offered by Professor Thomas

Barker.



The first step of polymerization is the adherence of adjacent fibrinogen molecules in a half-overlapped fashion brought about following the removal of the charged clusters of the fibrinopeptides. Activation of the A $\alpha$  N-terminus leads to lateral aggregation of polymers by the association of the “knobs” with binding pockets, called “holes”, located at the C-terminal portions of both the B $\beta$  and  $\gamma$  chains. The mature fibrin product when A knobs are involved, are called fibrin I, and when A- as well as B-knobs are engaged, it is called fibrin II <sup>66</sup>. A second stage of fibrin polymer stabilization occurs, induced by the enzyme factor XIIIa, when the formation of isopeptide bonds between lysyl and glutamyl residues located at the C-terminus of the  $\gamma$ -chains that have aligned end to end (Fig. 8) <sup>62</sup>. Finally, the same coagulation enzyme factor XIIIa, forming  $\gamma$ - $\gamma$  crosslinking, introduces numerous covalent crosslinks between adjacent A $\alpha$ -chains.

The resulting fibrin web (Fig. 9) is capable of capturing platelets and red blood cells, effectively sealing a wound and stemming plasma (fluid) loss. Fibrin gels can be applied in tissue engineering by incorporating cells, adsorbing bioactive proteins or covalently bound peptides. These modifications can increase cell adhesion, or induce specific cell signalling pathways <sup>53, 59</sup>. Fibrin gels are sensitive to degradation by proteolytic enzymes activated by cells trapped inside. All cells that migrate activate plasminogen to plasmin and matrix metalloproteinase precursors to active matrix metalloproteinases. These active enzymes normally allow the cells to penetrate the extracellular matrix to degrade the fibrin gel in the nano- and micro-domain close to the cell surface. In this way, the cells can tunnel through the fibrin gel, which leads to a slow degradation and bioresorption of the biomaterials. At same time, these enzymes also liberate bound bioactive proteins or peptides from matrix <sup>52</sup>. This system has been used now for some time as a tissue adhesive/bioglue as well as a delivery system for growth factors and cells.

**We will use the fibrinogen/fibrin polymer system as a means to deliver a growth factor (IGF1) and cells infiltrating (bladder smooth muscle cells) for bladder muscle layer reconstruction.**

### ***Bladder tissue engineering***

#### **Tissue engineering**

Organ shortage and suboptimal prosthetic or biological materials for repair or replacement of diseased or destroyed human organs and tissues are the main motivation for increasing

research in the field of tissue engineering<sup>67</sup>. As one of the major disciplines in regenerative medicine, tissue engineering follows the principles of cell transplantation, materials science, and engineering toward the development of biologic substitutes that can restore and maintain normal function. Tissue engineering strategies generally fall into two categories: use of acellular matrices, where matrices are used alone and depend on the body's natural ability to regenerate for proper orientation and direction of new tissue growth, and use of matrices with cells<sup>68</sup>.

Acellular tissue matrices are usually prepared by removing cellular components from tissues via mechanical and chemical manipulation to produce collagen-rich matrices. These matrices tend to slowly degrade upon implantation and are generally replaced by the ECM proteins that are secreted by the ingrowing cells<sup>68-72</sup>.

When cells are used for tissue engineering, a small piece of donor tissue is dissociated *in vitro* into individual cells. These cells are either implanted directly into the host or are expanded in culture, attached to a support matrix, and then reimplanted into the host after expansion (Fig. 1). The source of donor tissue can be xenogeneic (different species, such as bovine), allogeneic (same species, different individual), or autologous (same individual). Ideally, both structural and functional tissue replacements will occur with minimal complications. The most preferred cells to use are autologous, where a biopsy of tissue is obtained from the host, the cells are dissociated and expanded in culture, and the expanded cells are implanted back into the host. The use of autologous cells avoids rejection, and thus the deleterious side effects of immunosuppressive medication use can be avoided<sup>67, 72</sup>.

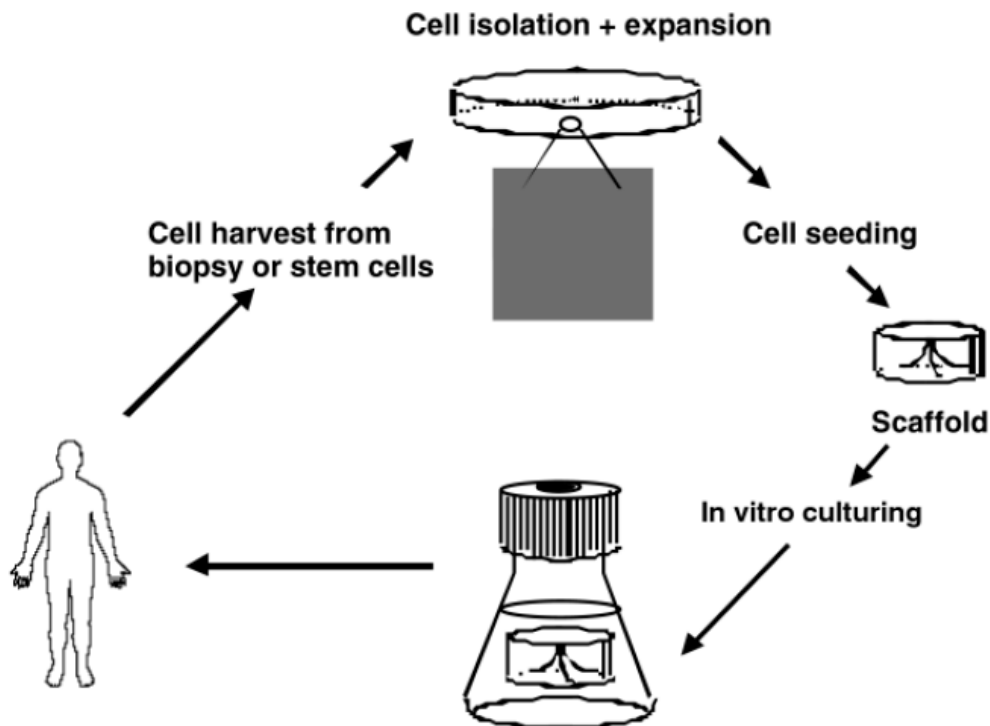


Fig 10. Concept of tissue engineering <sup>67</sup>. Cells can be taken from a biopsy of patient's body or differentiated from stem cells, and cultured until there is a sufficient quantity. Then the cells are seeded on a polymeric scaffold material where they grow *in vitro* in a bioreactor or incubator.

The regrown tissue can be implanted in the area of defect in patient's body.

For cell-based tissue engineering, expanded cells are seeded into a scaffold prepared with the appropriate biomaterial. In tissue engineering, biomaterials attempt to mimic the biologic and mechanical function of the native ECM found in tissues in the body by serving as an artificial scaffold. As a result, the ideal biomaterial should be biocompatible in that it is biodegradable and bioresorbable to support the replacement of normal tissue without inflammation. Furthermore, biomaterials provide a three-dimensional space for the cells to form into new tissues, and also can allow for the delivery of cells and appropriate biomolecules (*e.g.*, cell adhesion peptides, growth factors), to desired sites in the body <sup>68, 73, 74</sup>.

The formed hydrogel should provide a microenvironment in which the appropriate regulation of cell behavior (*e.g.*, adhesion, proliferation, migration, and differentiation) can occur so that the desired tissue can form. These interactions can include cell-adhesion ligands <sup>75</sup> and with soluble growth factors such as IGF1. Because the majority of mammalian cell types are anchorage dependent and will die if no cell-adhesion substrate is available, hydrogels also can act as cell-adhesion substrates. The formed hydrogels can also provide mechanical support against *in vivo*

forces such that the predefined three-dimensional structure is maintained during tissue development<sup>68</sup>.

In this way, hydrogels formed from biomaterials can provide for cellular growth and differentiation for a wide variety of cell types as well as a matrix whose elastic and viscous modulus can be well controlled. Tissue regeneration or replacement can be tailored for that specific medical application.

## Bladder wall

The urinary tract consists of the organs, tubes, and muscles that work together to make, move, store, and release urine, the liquid waste of the human body. The upper urinary tract includes the kidneys, which filter wastes and extra fluid from the blood, and the ureters, which carry urine from the kidneys to the bladder. There is a valve in the ureters that provides for a one-way flow, prohibiting reflux of urine from the bladder to the kidneys. The lower urinary tract includes the bladder, a balloon-shaped muscle that stores urine, and the urethra, a tube that carries urine from the bladder to the outside of the body during urination. The sphincter is a circular muscle that wraps around the bladder where it connects to urethra. Its purpose is to keep the connection closed so that urine does not leak out of the bladder (Fig. 11).

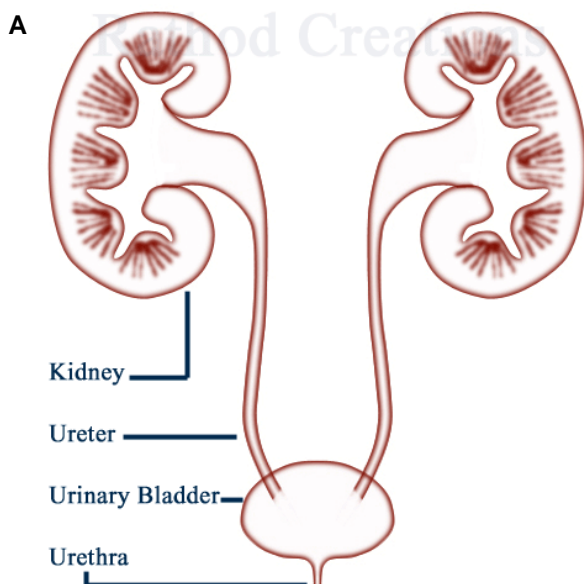


Fig 11. The urinary tract structure. The system includes two kidneys, two ureters, one bladder, two sphincter muscles, and one urethra.

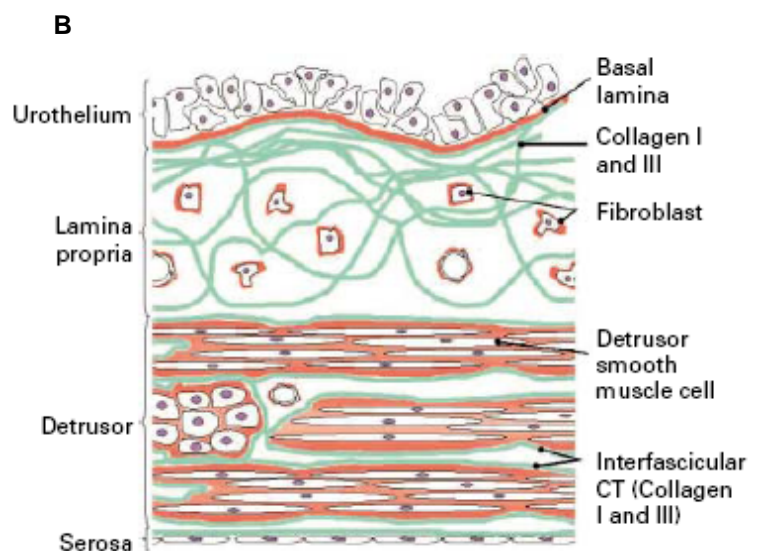


Fig 12. Bladder wall anatomy. It is composed of four principal layers, mucosa, submucosa, detrusor muscle and serosa<sup>76</sup>

The urinary bladder is unique and the most distensible organ in the body. It has a more or less spherical shape and is located at the end of both ureters, down in the abdomen, behind the pubic bone.

The bladder is capable, under normal circumstances, of storing 400-500 ml of urine at low pressure, and then to expel this completely, several times a day. When empty, it is no larger than a tennis ball. It is an autonomic organ under voluntary control. Contrary to what many people think, it is not the action of the abdominal wall muscles that empties the bladder, but the bladder contains its own smooth muscles.

Bladder compliance is determined by the structural properties of the extracellular matrix (ECM) and cells that make up the bladder wall. The bladder wall has a serous coat (serosa) over its upper surface. The serosa is a reflection of the peritoneum which covers only the superior surface and the upper part of the lateral surfaces. It is fibrous connective tissue. The other layers of the bladder wall are the fascial, muscular, submucosal, and mucosal coats.

The fascial coat (adventitia) is a layer of connective tissue between serosa and muscular coat.

The muscular coat (detrusor muscle) is composed of smooth muscle. The smooth muscle fibers are interwoven in all directions and collectively these are called the detrusor muscle. Contraction of this muscle expels urine from the bladder (Fig. 12)<sup>77</sup>. Detrusor smooth muscle cells are very elastic. During filling of the urinary bladder, the smooth muscle cells elongate and rearrange in the wall over a very large length interval. During expulsion, force generation and shortening are initiated comparatively fast, synchronized, and occur over a large length range<sup>77</sup>.

The submucosal coat (lamina propria) is composed of connective tissue with elastic fibers and supports the muscular coat. This layer contains blood vessels, nerves, and in some regions, glands.

The mucosal coat (mucosa or urothelium) is a transitional epithelium, composed of epithelial layer and basal lamina. It is the inner lining of the urinary bladder. When the bladder is empty, the mucosa has numerous folds called rugae. The rugae and transitional epithelium allow the bladder to expand as it fills. It contains no blood or lymphatic vessels and lines the bladder, ureters, and urethra. The basal lamina includes proteoglycans separating the epithelial layer from the lamina propria. It contains a sheet of extracellular material serving as a filtration barrier and supporting structure for the mucosal layer<sup>76</sup>.

## Bladder tissue engineering

Table 3 Recent studies on experimental bladder reconstruction <sup>79</sup>

Methodology	Authors	Year
<b>Animal derived matrix only</b>		
Small intestine submucosa (SIS)	Kropp <i>et al.</i>	1995
Bladder acellular matrix (BAM)	Sutherland <i>et al.</i>	1996
Collagen scaffold	Hattori <i>et al.</i>	2006
<b>Scaffold + autologous cell transplantation (tissue engineering)</b>		
Polymer scaffold + UC + SMC	Oberpenning <i>et al.</i>	1999
BAM/Collagen + UC	Moriya <i>et al.</i>	2003
Acellular bowel + UC + SMC + EPC	Schultheiss <i>et al.</i>	2005
Polymer scaffold + UC + SMC (clinical trial)	Atala <i>et al.</i>	2006
<b>Scaffold + growth factor loading</b>		
Bladder acellular matrix + bFGF	Kanematsu <i>et al.</i>	2003
Bladder acellular matrix + VEGF	Youssif <i>et al.</i>	2005
<b>Composite cystoplasty</b>		
Demucosalized gastric segment + UC sheet	Shiroyanagi <i>et al.</i>	2004
Demucosalized uterus/colon + UC	Fraser <i>et al.</i>	2004
Demucosalized colon + UC spray	Hafez <i>et al.</i>	2006

Reconstructive surgery is required for diseased and injured bladder. Currently, classical reconstruction is performed with native or homologous nonurologic tissues, such as small intestine (ileum), stomach, or mucosa. These techniques are called intestinal cystoplasty, gastrocystoplasty, ureterocystoplasty, vesicomomyectomy (autoaugmentation), seromuscular augmentation etc <sup>31,78</sup>. Due to complication after reconstruction and shortage of donors, bladder tissue engineering is emerging as a potential alternative to current treatment. Bladder tissue engineering is one part of regenerative medicine. It involves material science, engineering, cell

culture to develop biological substitutes for maintaining and reconstructing the normal function of bladder.

Bladder tissue engineering was begun in 1917 by Neuhof <sup>79</sup>. During the last decades, it is developing more and more fast. The main problem is to avoid covering a wound with a scar of fibrosis tissue. Three main classes of biomaterials are used as scaffold for bladder tissue engineering: naturally derived materials, acellular tissue matrices and synthetic polymer (Table 3). Acellular tissue matrices, such as bladder acellular matrix (BAM) and small intestine submucosa (SIS), are collagen-rich matrices and can be remodelled by ingrowing or transplanted cells. It contains cell adhesion sequences, such as RGD, which can attract many types of cells <sup>79</sup>.

Synthetic polymers, such as polyglycolic acid (PGA) and poly(lactic-co-glycolic acid) (PLGA) <sup>80</sup>, can be produced on a large scale. Their degradation rate and strength can be controlled. The growth factors can be loaded and cells can be seeded in the polymers. Urinary bladders in canines [55,<sup>80</sup> and humans <sup>81</sup> were made successfully using PGA/PLGA with autologous urothelial cells (UCs) and smooth muscle cells (SMCs).

The detrusor muscle in the bladder wall has a role predominant in bladder physiological function. It relaxes during bladder filling. It contracts during bladder voiding. A lot of causes can cause detrusor muscle failure, such as nerve damage, bladder stones, Parkinson's disease, prostate and stress. The malfunction of detrusor muscle results in bladder diseases, such as urinary incontinence and cystitis. So, the bladder muscle layer regeneration is an important topic in bladder tissue engineering. Researches were using acellular tissue matrices with mesenchymal cells, collagen and skeletal muscle-derived cells (MDCs). But actually no effective method is available to treat impaired detrusor dysfunction.

**We will use bladder tissue engineering methods for bladder muscle layer reconstruction.**

### ***Scope and survey of this thesis***

The bladder has two important functions, specifically filling and emptying of urine. These functions provide a significant mechanical challenge to the muscle component in the bladder wall where elasticity and compliance is required to accommodate the gross changes in volume <sup>77</sup>. From the time the fetus develops the bladder is exposed to a variety of possible deformities and injuries which may lead to bladder tissue damage or loss, requiring eventual bladder repair or replacement. Currently, gastrointestinal segments are commonly used for bladder

replacement or repair. However, gastrointestinal tissues are designed to absorb solutes, whereas bladder tissues are designed for the excretion of solutes<sup>82-86</sup>. Due to multiple complications encountered with the use of gastrointestinal segments and a severe shortage of donor tissues, alternative materials and tissues for bladder replacement or repair are being sought.

Over the last few decades the use of several bladder-wall substitutes has been attempted with both synthetic and natural biodegradable materials. They have usually failed due to either mechanical, structural, functional, or biocompatibility problems<sup>84, 85, 87-89</sup>. Tissue engineering using selective cell transplantation and matrices for tissue regeneration may provide for a means of creating functional new bladder segments.

IGF1 is used to supplement child growth and in short-term post-operational trauma in clinical trials. Due to severe side effects, an IGF1 formulation is being developed for long-term use. The IGF1 signalling pathway also plays an important role in maintaining skeletal muscle<sup>5</sup> and smooth muscle<sup>43</sup>. The goal of this thesis is to develop a fusion protein of IGF1 with a substrate for factor XIIIa, to allow binding to a fibrin matrix for bladder muscle layer regeneration. A second approach to the same end tried and reported first was to explore truncation mutants of fibrinogen, into which truncation site IGF1 would be grafted as a fusion protein. Thus two methods by which to incorporate IGF1 in bond form within fibrin matrices were evaluated.

Using the current fibrin gel platform technology developed in the lab, the IGF1 was modified by inserting one peptide TG, the first eight amino acids of  $\alpha_2$  plasmin inhibitor, at the N-terminal. The recombinant truncated TG-IGF1 was produced by E. Coli cells and purified by FPLC. The purified TG-IGF1 was characterized by SDS-PAGE and by western blot using anti-human IGF1 antibody. Then the bioactivity of TG-IGF1 was analyzed *in vitro* in 2-dimensional and in 3-dimensional models. In 2-dimensional model, 3T3 cells were used for cell metabolic assay (MTT assay) and IGF1 receptor phosphorylation assay. In 3-dimensional model, the fibrin gels were incorporated with neonatal bladder smooth muscle cells (SMCs). The quantitative real-time PCR (qRT-PCR) was used for genes expression about adhesion and extracellular matrix proteins by SMCs in fibrin gels. The morphology of SMCs in fibrin gels was characterized by the transmission electron microscopy (TEM). The bioactivity of TG-IGF1 was done also *in vivo*, where rat bladder model was used for muscle layer regeneration.

One new fibrin gel platform was tried to generate in this thesis by producing fusion fibrinogen IGF1 protein using mammalian CHO cells. The best growth and production media for CHO cells were screened among 23 commercial media by cell viability and cell number counting. For the



quantity and quality of recombinant protein produced, CHO cells were in the suspension and serum-free media culture. Then IGF1 protein was inserted at the C-terminal of truncated fibrinogen  $\alpha$ -chain in genetic level by cloning technology. The generated stable new CHO cell lines were characterized by ELISA using fibrinogen and human IGF1 antibodies. The fusion fibrinogen IGF1 protein was then produced by new CHO cell lines and purified by affinity chromatography. The purified fusion protein was analyzed by SDS-PAGE and western blot using fibrinogen antibody. The clot assay was done for the bioactivity of fusion protein.

**In this thesis, we will address the hypothesis that the delivery of an IGF1 fusion protein in a fibrin matrix will result in bladder muscle layer regeneration by promoting bladder smooth muscle cell infiltrating growth and differentiation.**

## ***References***

1. Pollak, M. Insulin and insulin-like growth factor signalling in neoplasia. *Nat Rev Cancer* **8**, 915-928 (2008).
2. Osborne, R. Commercial interest waxes for IGF-1 blockers. *Nat Biotechnol* **26**, 719-720 (2008).
3. Brower, V. Prostate-cancer link sours IGF-1. *Nat Biotechnol* **16**, 223 (1998).
4. Ratner, M. New IGF drug stirs competition in growth factor segment. *Nat Biotechnol* **23**, 1192 (2005).
5. Pelosi, L. et al. Local expression of IGF-1 accelerates muscle regeneration by rapidly modulating inflammatory cytokines and chemokines. *FASEB J* **21**, 1393-1402 (2007).
6. Musaro, A. et al. Localized IGF-1 transgene expression sustains hypertrophy and regeneration in senescent skeletal muscle. *Nat Genet* **27**, 195-200 (2001).
7. Musaro, A., McCullagh, K.J., Naya, F.J., Olson, E.N. & Rosenthal, N. IGF-1 induces skeletal myocyte hypertrophy through calcineurin in association with GATA-2 and NF-ATc1. *Nature* **400**, 581-585 (1999).
8. Delaughter, M.C., Taffet, G.E., Fiorotto, M.L., Entman, M.L. & Schwartz, R.J. Local insulin-like growth factor I expression induces physiologic, then pathologic, cardiac hypertrophy in transgenic mice. *FASEB J* **13**, 1923-1929 (1999).
9. Rabinovsky, E.D. et al. Targeted expression of IGF-1 transgene to skeletal muscle accelerates muscle and motor neuron regeneration. *FASEB J* **17**, 53-55 (2003).
10. Brower, V. IGF in the clinic. *Nat Biotechnol* **16**, 601-602 (1998).

11. Chen, Y., Capron, L., Magnusson, J.O., Wallby, L.A. & Arnqvist, H.J. Insulin-like growth factor-1 stimulates vascular smooth muscle cell proliferation in rat aorta in vivo. *Growth Horm IGF Res* **8**, 299-303 (1998).
12. Cheng, C.L., Gao, T.Q., Wang, Z. & Li, D.D. Role of insulin/insulin-like growth factor 1 signaling pathway in longevity. *World J Gastroenterol* **11**, 1891-1895 (2005).
13. Bayes-Genis, A., Conover, C.A. & Schwartz, R.S. The insulin-like growth factor axis: A review of atherosclerosis and restenosis. *Circ Res* **86**, 125-130 (2000).
14. Pollak, M. Targeting insulin and insulin-like growth factor signalling in oncology. *Curr Opin Pharmacol* **8**, 384-392 (2008).
15. Tokunou, T. et al. Engineering insulin-like growth factor-1 for local delivery. *FASEB J* **22**, 1886-1893 (2008).
16. Ren, J., Samson, W.K. & Sowers, J.R. Insulin-like growth factor I as a cardiac hormone: physiological and pathophysiological implications in heart disease. *J Mol Cell Cardiol* **31**, 2049-2061 (1999).
17. Florini, J.R., Ewton, D.Z. & Coolican, S.A. Growth hormone and the insulin-like growth factor system in myogenesis. *Endocr Rev* **17**, 481-517 (1996).
18. Hwa, V., Oh, Y. & Rosenfeld, R.G. The insulin-like growth factor-binding protein (IGFBP) superfamily. *Endocr Rev* **20**, 761-787 (1999).
19. Perks, C.M. & Holly, J.M. IGF binding proteins (IGFBPs) and regulation of breast cancer biology. *J Mammary Gland Biol Neoplasia* **13**, 455-469 (2008).
20. Firth, S.M. & Baxter, R.C. Cellular actions of the insulin-like growth factor binding proteins. *Endocr Rev* **23**, 824-854 (2002).
21. Flint, D.J., Tonner, E., Beattie, J. & Allan, G.J. Role of insulin-like growth factor binding proteins in mammary gland development. *J Mammary Gland Biol Neoplasia* **13**, 443-453 (2008).
22. Wheatcroft, S.B. & Kearney, M.T. IGF-dependent and IGF-independent actions of IGF-binding protein-1 and -2: implications for metabolic homeostasis. *Trends Endocrinol Metab* **20**, 153-162 (2009).
23. Barton, E.R. The ABCs of IGF-I isoforms: impact on muscle hypertrophy and implications for repair. *Appl Physiol Nutr Metab* **31**, 791-797 (2006).
24. Ewton, D.Z. & Florini, J.R. Effects of the somatomedins and insulin on myoblast differentiation in vitro. *Dev Biol* **86**, 31-39 (1981).

25. Napier, J.R., Thomas, M.F., Sharma, M., Hodgkinson, S.C. & Bass, J.J. Insulin-like growth factor-I protects myoblasts from apoptosis but requires other factors to stimulate proliferation. *J Endocrinol* **163**, 63-68 (1999).
26. Guha, N., Sonksen, P.H. & Holt, R.I. IGF-I abuse in sport: current knowledge and future prospects for detection. *Growth Horm IGF Res* **19**, 408-411 (2009).
27. Florini, J.R., Ewton, D.Z., Magri, K.A. & Mangiacapra, F.J. IGFs and muscle differentiation. *Adv Exp Med Biol* **343**, 319-326 (1993).
28. Florini, J.R., Ewton, D.Z. & Roof, S.L. Insulin-like growth factor-I stimulates terminal myogenic differentiation by induction of myogenin gene expression. *Mol Endocrinol* **5**, 718-724 (1991).
29. Rhodes, S.J. & Konieczny, S.F. Identification of MRF4: a new member of the muscle regulatory factor gene family. *Genes Dev* **3**, 2050-2061 (1989).
30. Cole, N.J. et al. Temperature and the expression of myogenic regulatory factors (MRFs) and myosin heavy chain isoforms during embryogenesis in the common carp *Cyprinus carpio* L. *J Exp Biol* **207**, 4239-4248 (2004).
31. Ewton, D.Z., Roof, S.L., Magri, K.A., McWade, F.J. & Florini, J.R. IGF-II is more active than IGF-I in stimulating L6A1 myogenesis: greater mitogenic actions of IGF-I delay differentiation. *J Cell Physiol* **161**, 277-284 (1994).
32. Satchek, J.M., Ohtsuka, A., McLary, S.C. & Goldberg, A.L. IGF-I stimulates muscle growth by suppressing protein breakdown and expression of atrophy-related ubiquitin ligases, atrogin-1 and MuRF1. *Am J Physiol Endocrinol Metab* **287**, E591-601 (2004).
33. Sandri, M. et al. PGC-1alpha protects skeletal muscle from atrophy by suppressing FoxO3 action and atrophy-specific gene transcription. *Proc Natl Acad Sci U S A* **103**, 16260-16265 (2006).
34. Barton-Davis, E.R., Shoturma, D.I., Musaro, A., Rosenthal, N. & Sweeney, H.L. Viral mediated expression of insulin-like growth factor I blocks the aging-related loss of skeletal muscle function. *Proc Natl Acad Sci U S A* **95**, 15603-15607 (1998).
35. Coolican, S.A., Samuel, D.S., Ewton, D.Z., McWade, F.J. & Florini, J.R. The mitogenic and myogenic actions of insulin-like growth factors utilize distinct signaling pathways. *J Biol Chem* **272**, 6653-6662 (1997).
36. Tidball, J.G. Inflammatory processes in muscle injury and repair. *Am J Physiol Regul Integr Comp Physiol* **288**, R345-353 (2005).

37. Leininger, G.M., Backus, C., Uhler, M.D., Lentz, S.I. & Feldman, E.L. Phosphatidylinositol 3-kinase and Akt effectors mediate insulin-like growth factor-I neuroprotection in dorsal root ganglia neurons. *FASEB J* **18**, 1544-1546 (2004).
38. Duan, C. The chemotactic and mitogenic responses of vascular smooth muscle cells to insulin-like growth factor-I require the activation of ERK1/2. *Mol Cell Endocrinol* **206**, 75-83 (2003).
39. Higuchi, M., Onishi, K., Kikuchi, C. & Gotoh, Y. Scaffolding function of PAK in the PDK1-Akt pathway. *Nat Cell Biol* **10**, 1356-1364 (2008).
40. Tisdale, M.J. The ubiquitin-proteasome pathway as a therapeutic target for muscle wasting. *J Support Oncol* **3**, 209-217 (2005).
41. Rommel, C. et al. Mediation of IGF-1-induced skeletal myotube hypertrophy by PI(3)K/Akt/mTOR and PI(3)K/Akt/GSK3 pathways. *Nat Cell Biol* **3**, 1009-1013 (2001).
42. Xu, T. et al. Phosphorylation of p70s6 kinase is implicated in androgen-induced levator ani muscle anabolism in castrated rats. *J Steroid Biochem Mol Biol* **92**, 447-454 (2004).
43. Zhu, B., Zhao, G., Witte, D.P., Hui, D.Y. & Fagin, J.A. Targeted overexpression of IGF-I in smooth muscle cells of transgenic mice enhances neointimal formation through increased proliferation and cell migration after intraarterial injury. *Endocrinology* **142**, 3598-3606 (2001).
44. Chen, Y. et al. Increase in insulin-like growth factor I in hypertrophying smooth muscle. *Am J Physiol* **266**, E224-229 (1994).
45. Wang, J. et al. Targeted overexpression of IGF-I evokes distinct patterns of organ remodeling in smooth muscle cell tissue beds of transgenic mice. *J Clin Invest* **100**, 1425-1439 (1997).
46. Ling, Y., Maile, L.A. & Clemmons, D.R. Tyrosine phosphorylation of the beta3-subunit of the alphaVbeta3 integrin is required for membrane association of the tyrosine phosphatase SHP-2 and its further recruitment to the insulin-like growth factor I receptor. *Mol Endocrinol* **17**, 1824-1833 (2003).
47. Clarke, M.C. et al. Apoptosis of vascular smooth muscle cells induces features of plaque vulnerability in atherosclerosis. *Nat Med* **12**, 1075-1080 (2006).
48. Stocker, R. & Keaney, J.F., Jr. New insights on oxidative stress in the artery wall. *J Thromb Haemost* **3**, 1825-1834 (2005).
49. Kavurma, M.M. et al. Oxidative stress regulates IGF1R expression in vascular smooth-muscle cells via p53 and HDAC recruitment. *Biochem J* **407**, 79-87 (2007).

50. Allard, D., Figg, N., Bennett, M.R. & Littlewood, T.D. Akt regulates the survival of vascular smooth muscle cells via inhibition of FoxO3a and GSK3. *J Biol Chem* **283**, 19739-19747 (2008).
51. Langer, R. Biomaterials in drug delivery and tissue engineering: one laboratory's experience. *Acc Chem Res* **33**, 94-101 (2000).
52. Hubbell, J.A. Cellular matrices: Physiology in microfluidics. *Nat Mater* **7**, 609-610 (2008).
53. Hubbell, J. Matrix-bound growth factors in tissue repair. *Swiss Med Wkly* **136**, 387-391 (2006).
54. Jones, K.S. Biomaterials as vaccine adjuvants. *Biotechnol Prog* **24**, 807-814 (2008).
55. Kim, B.S., Baez, C.E. & Atala, A. Biomaterials for tissue engineering. *World J Urol* **18**, 2-9 (2000).
56. Hubbell, J.A. Materials as morphogenetic guides in tissue engineering. *Curr Opin Biotechnol* **14**, 551-558 (2003).
57. Pariente, J.L., Kim, B.S. & Atala, A. In vitro biocompatibility assessment of naturally derived and synthetic biomaterials using normal human urothelial cells. *J Biomed Mater Res* **55**, 33-39 (2001).
58. Pariente, J.L., Kim, B.S. & Atala, A. In vitro biocompatibility evaluation of naturally derived and synthetic biomaterials using normal human bladder smooth muscle cells. *J Urol* **167**, 1867-1871 (2002).
59. Hubbell, J.A. Biomaterials in tissue engineering. *Biotechnology (N Y)* **13**, 565-576 (1995).
60. Lutolf, M.P. & Hubbell, J.A. Synthetic biomaterials as instructive extracellular microenvironments for morphogenesis in tissue engineering. *Nat Biotechnol* **23**, 47-55 (2005).
61. Binnie, C.G. & Lord, S.T. The fibrinogen sequences that interact with thrombin. *Blood* **81**, 3186-3192 (1993).
62. Doolittle, R.F. Fibrinogen and fibrin. *Annu Rev Biochem* **53**, 195-229 (1984).
63. Doolittle, R.F. & Wooding, G.L. The subunit structure of lamprey fibrinogen and fibrin. *Biochim Biophys Acta* **371**, 277-282 (1974).
64. Yang, Z., Mochalkin, I., Veerapandian, L., Riley, M. & Doolittle, R.F. Crystal structure of native chicken fibrinogen at 5.5-Å resolution. *Proc Natl Acad Sci U S A* **97**, 3907-3912 (2000).
65. Furlan, M. Sticky and promiscuous plasma proteins maintain the equilibrium between bleeding and thrombosis. *Swiss Med Wkly* **132**, 181-189 (2002).

66. Blomback, B. Fibrinogen and fibrin--proteins with complex roles in hemostasis and thrombosis. *Thromb Res* **83**, 1-75 (1996).
67. Stock, U.A. & Vacanti, J.P. Tissue engineering: current state and prospects. *Annu Rev Med* **52**, 443-451 (2001).
68. Koh, C.J. & Atala, A. Tissue engineering, stem cells, and cloning: opportunities for regenerative medicine. *J Am Soc Nephrol* **15**, 1113-1125 (2004).
69. Chen, F., Yoo, J.J. & Atala, A. Acellular collagen matrix as a possible "off the shelf" biomaterial for urethral repair. *Urology* **54**, 407-410 (1999).
70. Dahms, S.E., Piechota, H.J., Dahiya, R., Lue, T.F. & Tanagho, E.A. Composition and biomechanical properties of the bladder acellular matrix graft: comparative analysis in rat, pig and human. *Br J Urol* **82**, 411-419 (1998).
71. Piechota, H.J. et al. In vitro functional properties of the rat bladder regenerated by the bladder acellular matrix graft. *J Urol* **159**, 1717-1724 (1998).
72. Yoo, J.J., Meng, J., Oberpenning, F. & Atala, A. Bladder augmentation using allogenic bladder submucosa seeded with cells. *Urology* **51**, 221-225 (1998).
73. Kim, B.S. & Mooney, D.J. Development of biocompatible synthetic extracellular matrices for tissue engineering. *Trends Biotechnol* **16**, 224-230 (1998).
74. Hubbell, J.A. Tissue and cell engineering. *Curr Opin Biotechnol* **15**, 381-382 (2004).
75. Hynes, R.O. Integrins: versatility, modulation, and signaling in cell adhesion. *Cell* **69**, 11-25 (1992).
76. McCarthy, L.S., Smeulders, N. & Wilcox, D.T. Cell biology of bladder development and the role of the extracellular matrix. *Nephron Exp Nephrol* **95**, e129-133 (2003).
77. Andersson, K.E. & Arner, A. Urinary bladder contraction and relaxation: physiology and pathophysiology. *Physiol Rev* **84**, 935-986 (2004).
78. Gupta, N.P., Kumar, A. & Sharma, S. Reconstructive bladder surgery in genitourinary tuberculosis. *Indian J Urol* **24**, 382-387 (2008).
79. Kanematsu, A., Yamamoto, S. & Ogawa, O. Changing concepts of bladder regeneration. *Int J Urol* **14**, 673-678 (2007).
80. Jayo, M.J. et al. Long-term durability, tissue regeneration and neo-organ growth during skeletal maturation with a neo-bladder augmentation construct. *Regen Med* **3**, 671-682 (2008).
81. Atala, A., Bauer, S.B., Soker, S., Yoo, J.J. & Retik, A.B. Tissue-engineered autologous bladders for patients needing cystoplasty. *Lancet* **367**, 1241-1246 (2006).

82. Atala, A., Bauer, S.B., Hendren, W.H. & Retik, A.B. The effect of gastric augmentation on bladder function. *J Urol* **149**, 1099-1102 (1993).
83. Kaefer, M. et al. Continent urinary diversion: the Children's Hospital experience. *J Urol* **157**, 1394-1399 (1997).
84. Oberpenning, F., Meng, J., Yoo, J.J. & Atala, A. De novo reconstitution of a functional mammalian urinary bladder by tissue engineering. *Nat Biotechnol* **17**, 149-155 (1999).
85. Falke, G., Caffaratti, J. & Atala, A. Tissue engineering of the bladder. *World J Urol* **18**, 36-43 (2000).
86. Atala, A. Bladder regeneration by tissue engineering. *BJU Int* **88**, 765-770 (2001).
87. Pattison, M.A., Wurster, S., Webster, T.J. & Haberstroh, K.M. Three-dimensional, nano-structured PLGA scaffolds for bladder tissue replacement applications. *Biomaterials* **26**, 2491-2500 (2005).
88. Gleeson, M.J. & Griffith, D.P. The use of alloplastic biomaterials in bladder substitution. *J Urol* **148**, 1377-1382 (1992).
89. Atala, A. Tissue engineering for bladder substitution. *World J Urol* **18**, 364-370 (2000).
90. [http://en.wikipedia.org/wiki/Insulin-like\\_growth\\_factor\\_1](http://en.wikipedia.org/wiki/Insulin-like_growth_factor_1)
91. <http://www.endotext.org/neuroendo/neuroendo5a/ch01s02.html>





## **Chapter II High-level recombinant fibrinogen protein production in suspension cultured mammalian cells**

### ***Summary***

Mammalian cell culture is a widely used technique to produce many therapeutic recombinant proteins. To get relatively high quantities of protein, Chinese Hamster Ovary (CHO) cells are usually modified and grown in bioreactors. Due to the wide application of fibrin matrices in tissue engineering, recombinant fibrinogen was also tried to be obtained from CHO cells in serum free and suspension culture. However, expressed recombinant fibrinogen can be polymerized easily in cell culture due to proteases and trace of calcium ions present in the growth media. To resolve this problem, doxycycline-regulated pTet-on gene expression system was used. Because the fibrinogen expression is tightly controlled by the presence of doxycycline in the cell medium, this offers one new way to express a special gene from mammalian cells in culture. In this work, ProCHO5 cell medium was found to be the optimal growth and production medium among 23 media tested with CHO<sub>βγ</sub> cells (containing fibrinogen Bβ- and γ-chains) and CHO<sub>fgn</sub> cells (containing fibrinogen Aα-, Bβ- and γ-chains). CHO<sub>βγ</sub> cells were grown successfully in suspension and serum free culture. And some CHO<sub>βγ</sub> cells were transfected with fibrinogen Aα chain cDNA using pTet-on system to obtain CHO<sub>fgn</sub> cell line. Due to five vectors in CHO<sub>fgn</sub> cells (two vectors for pTet-on system and three vectors for fibrinogen Aα-, Bβ- and γ-chains respectively) and importance of conformational change in gene level in pTet-on system for fibrinogen on/off expression, up to date no stable CHO<sub>fgn</sub> cell line with pTet-on system was obtained.

### ***Introduction***

The primary role of fibrin is to provide for hemostasis and as a provisional structural scaffold for invading cells and an immuno-modulator of innate immune cells that will eventually repair the damaged tissue. Currently, the fibrin used in tissue engineering is derived from human plasma. It carries the risk (albeit small) of transmission of infectious agents and precipitating immunological reactions<sup>1</sup>. The development of recombinant sources of human fibrinogen could provide a reliable, predictable and chemically defined source of purified human fibrinogen that contains few additional components. Cultivated mammalian cells (such as CHO) have become the predominant system for the production of recombinant proteins for clinical applications because

of their capacity for proper protein folding, assembly and post-translational modification<sup>2</sup>. Due to the utility of fibrin, including use as a scaffold for tissue engineering constructs, and the risk of transmission of infectious agents, several systems for the production of the recombinant fibrinogen protein have been attempted, including anchorage-dependent CHO cell culture systems used in other laboratories<sup>3-5</sup>. However, the limitation in cell growth area in two-dimensional culture systems significantly limits large-scale cell culture. To overcome the limitation of cell growth area and to develop a system capable of producing industrially relevant quantities of recombinant soluble, bioactive fibrinogen, recombinant Chinese Hamster Ovary cells will be adapted to suspension culture in this aim. Even if it were to prove too difficult to recombinantly produce human fibrinogen at an acceptably low cost (the protein is used in matrices at concentrations > a few mg/ml), it may be possible to produce variant fibrinogen claims (such as IGF1 fusions) to be doped into fibrin produced from human plasma.

Fibrinogen is a dimeric glycoprotein. Each monomer is composed of three polypeptides, A $\alpha$ , B $\beta$  and  $\gamma$ <sup>6</sup>. CHO<sub>f $\gamma$ n</sub> cells refer to Chinese hamster ovary (CHO) cells expressing recombinant human fibrinogen, that is, these cells are capable of producing each of the three individual chains of fibrinogen and secrete the fully-assembled, bioactive protein. CHO<sub>B $\beta$  $\gamma$</sub>  cells refer to CHO cells containing human cDNAs encoding fibrinogen B $\beta$ - and  $\gamma$ -chains under the control of a constitutively-active promoter. These genetically-engineered CHO cells were obtained from Prof. ST Lord at University of North Carolina at Chapel Hill<sup>5, 7-9</sup>. They were anchorage-dependent and cultured in Dulbecco's modified Eagle media (DMEM)/F12 media (Invitrogen, UK) supplemented with 10% fetal bovine serum (FBS, Invitrogen, UK), 100U/ml penicillin (Invitrogen, UK), 100 $\mu$ g/ml streptomycin (Invitrogen, UK) and 0.4mg/ml G418 (Promega, USA). Both cell lines were grown at 37°C in 5% CO<sub>2</sub>.

Although calcium plays an important role in fibrinogen polymerisation<sup>10</sup>, trace amounts of calcium in the cell medium are required for the growth of CHO cells in culture. This is because calcium regulates cell proliferation, growth and apoptosis by Ras-MAPK pathway<sup>11, 12</sup>. So, it is a bad idea to neutralize calcium in cell medium as it is required to keep CHO cells in culture. To overcome this problem, fibrinogen expressed by CHO cells can be regulated by the doxycycline Tet-on gene expression system<sup>13</sup>. The "Tet-on" system contains two vectors, regulatory and response plasmids (Fig. 13).

The regulatory plasmid contains the regulatory protein, based on a reverse Tet repressor (rTetR)<sup>13, 14</sup>, which was created by four amino acid changes in TetR. The 37kDa protein is a fusion of amino acids 1-207 of rTetR and the C-terminal 127 amino acids of the Herpes simple virus VP16

activation domain. Addition of the VP16 domain converts the rTetR from a transcriptional repressor to a transcriptional activator, and the resulting hybrid protein is called the reverse tetracycline-controlled transactivator (rtTA). The pTet-on regulator plasmid contains a neomycin-resistance gene.

The response plasmid expresses the gene of interest under the control of the tetracycline-response element (TRE) <sup>14</sup>. The pTRE2 plasmid consists of seven direct repeats of a 42-bp sequence containing the tetO, located just upstream of the minimal CMV promoter ( $P_{minCMV}$ ).  $P_{minCMV}$  lacks the strong enhancer elements normally associated with the CMV immediate early promoter. Because these enhancer elements are missing, there is extremely low background expression of the gene of interest from the TRE in the absence of binding by the rTetR domain of rtTA. The pTRE2pur response plasmid contains puromycin-resistance gene. In the Tet-on system, rtTA binds to the TRE and activates transcription in the presence of doxycycline <sup>15</sup>.

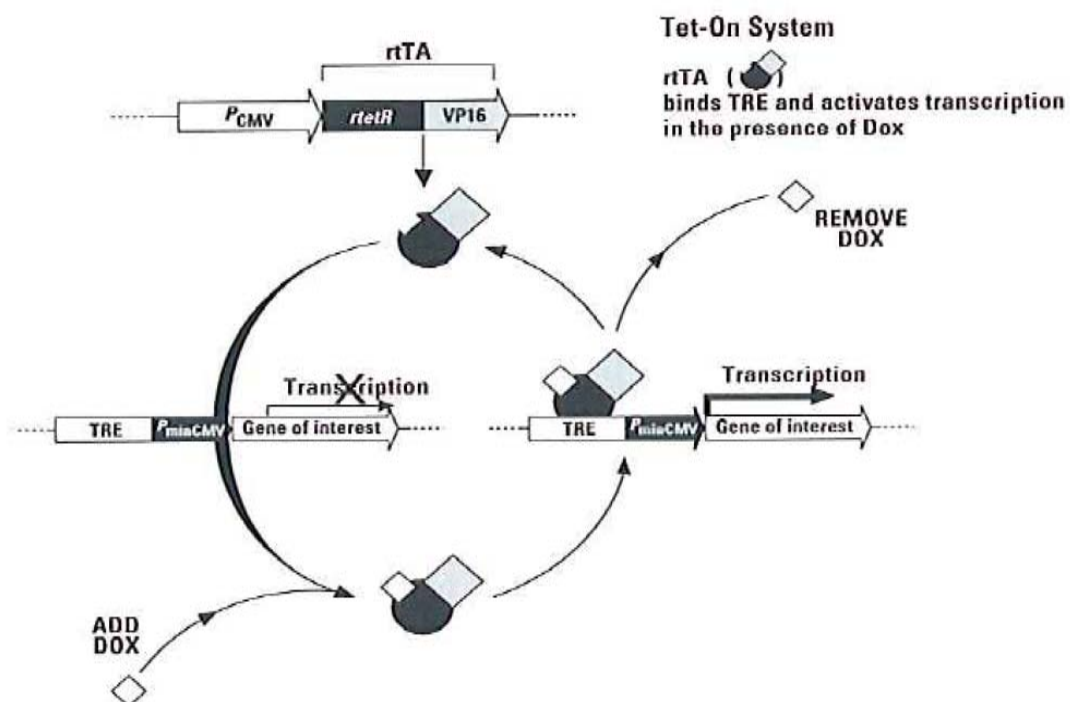


Fig 13. The Tet-on gene expression system. The system contains two vectors, regulatory and response plasmids. The regulatory plasmid contains the regulatory protein, based on a reverse Tet repressor (rTetR). The response plasmid expresses the gene of interest under the control of the tetracycline-response element (TRE). rtTA binds to the TRE and activates transcription in the presence of doxycycline.

In addition, the supplementation of cell culture media with serum components of animal origin is commonly used to provide cells necessary nutrition, shear protection, growth factors and cytokines for optimal growth<sup>16, 17</sup>. Because of its undefined composition, risk of contaminations, complication of desired protein purification and relatively expensive cost, rCHO will also be adapted to grow in serum free conditions.

Finally, the medium development is of utmost importance and has to be done on an individual basis, for each process and cell line. Commercial media for cell culture is now available with a variety of additives for cell growth. Optimal conditions for cell growth and fibrinogen production must be determined if recombinant wild-type fibrinogen and recombinant fibrinogen fusion proteins are to be produced in sufficient quantity and activity.

## ***Materials and methods***

### **Plasmid construction**

Plasmid DNA was amplified in the *E.coli* strain E10 and extracted using a plasmid Maxi Kit (QIAGEN GmbH, Germany). Purified plasmid was resuspended in sterile water and checked by gel electrophoresis and OD readings at 260 and 280 nm. Only the preparation of the highest purity ( $R_{260/280} > 1.8$ ) was used for transfection.

### **pTRE2pur-FgnA $\alpha$ full vector**

The Tet-on system used in this thesis is composed of pTRE2 response vector (Clontech, USA) and pTet-on regulator vector (Clontech, USA). The 1935 nucleotides fibrinogen A $\alpha$  full length gene was PCR-amplified from p584 A $\alpha$  plasmid (provided by Prof. Dr. Susan Lord) and purified by Genomed JETquick PCR product purification spin kit (Brunschiwig, Basel, Switzerland). The Forward primer was 5'- CGGGATCCCGATGTTTTCCATGAGGATCGT-3', in which a restriction enzyme BamHI sequence GGATCC (solid underline) was inserted before the FGN A $\alpha$  start codon ATG. The reverse primer was 5'- GAATTGCGGCCGCCCATTAACTTAGTCTA-3', in which another restriction enzyme NotI sequence GCGGCCGC (solid underline) was incorporated after the stop codon TAG. Then purified PCR product was digested with restriction enzymes BamHI and NotI. The band was purified from agarose gel by Genomed JetQuick gel extraction spin kit (Brunschiwig, Basel, Switzerland). The purified digested band was inserted into pTRE2pur plasmid to get pTRE2pur-FgnA $\alpha$  full vector. After ligation at 16°C, ligation

products were transformed into chemical competent E.coli subcloning Efficiency<sup>®</sup> DH5 $\alpha$ <sup>™</sup> cells. Colonies were grown on LB agar ampicillin plates and screened by restriction digest analyses.

### **pMYKpuro-FgnA $\alpha$ full vector**

Due to the availability of 23 commercial media which was required to be screened, a large quantity of fibrinogen A $\alpha$  plasmid DNA was needed for transfection. Polymerase chain reaction (PCR) is a commonly used method to amplify the quantity of cDNA. Native A $\alpha$  chain cDNA, in a shuttle vector, served as the template for the PCR reactions that used taq polymerase and reaction conditions recommended by the manufacturer. The Forward primer was 5'-ATATAGATATCTTAGAAAAGATGTTTTCCATGA-3', in which a restriction enzyme (EcoRV) sequence GATATC was inserted before the FGN A $\alpha$  start codon ATG. The reverse primer was 5'-GAATTGCGGCCGCCCATTTAACTTAGTCTA-3', in which another restriction enzyme (NotI) sequence CGCCGGCG was incorporated after the stop codon ATC.

The PCR products and PMYKpuro vector (Provided by F. Wurm) were digested with the appropriate restriction enzymes (EcoRV and NotI) and ligated at 16°C. Ligation products were transformed by electroporation into competent E.coli E10 cells. Colonies were grown on LB agar ampicillin plates and screened by restriction digest analyses.

## **Cell culture and transfection**

### **Cell culture**

For the cell culture, CHO $\beta\gamma$  cells were seeded in a bioreactor at a cell concentration of  $3 \times 10^5$  cells/ml in serum free ProCHO $_4$  medium (Cambrex, Belgium) supplemented with 100U/ml penicillin (Invitrogen, UK), 100 $\mu$ g/ml streptomycin (Invitrogen, UK), 0.2mM sodium hypoxanthine (Invitrogen, UK), 0.032mM thymidine (Invitrogen, UK) and 4mM L-Glutamine (Invitrogen, UK). The bioreactor was incubated in an incubator minitron (Infors HT, Switzerland) with a shaking speed 130rpm at 37°C in 5% CO $_2$ .

### **Transfection by lipofectamine 2000 reagent**

The transfection of Tet-on system into CHO $\beta\gamma$  cells was achieved in two steps. CHO $\beta\gamma$  cells were seeded in one 6-well plate at a density of  $2 \times 10^5$  cells/ml per well in 2ml medium without antibiotic G418. The transfection was carried out the following day in serum-free medium with lipofectamine 2000 (Invitrogen, UK) according to manufacturer's protocol. For each well, 4  $\mu$ g of pTet-on plasmid DNA in 125  $\mu$ l of OPTI-MEM<sup>®</sup>I Reduced Serum Medium without serum

(Invitrogen, UK) was transfected using 10  $\mu$ l of Lipofectamine 2000 Reagent. So the ratio of lipofectamine to plasmid is 5:2. 20 hours later, the cells were trypsinized, washed and seeded in one new 6-well plate, 2ml medium per well without antibiotics G418. The second transfection was carried out two days later using pTRE2pur-FgnAa full plasmid DNA. The process was exact same as the first transfection. Finally, 24 hours later after the second transfection, the CHO<sub>fgn</sub> pTet-on cells were selected in puromycin and neomycin containing medium, 20 $\mu$ g/ml puromycin (Brunschwig, Basel, Switzerland) and 0.4mg/ml G418, in 96-well plates.

### **Transfection by PEI reagent**

CHO <sub>$\beta$</sub>  cells were seeded in fresh serum free ProCHO<sub>4</sub> medium at  $5 \times 10^5$  cells/ml and transfected one day later. Transient transfection with polyethylenimine (PEI) was carried out in serum free conditions. Linear 25kDa PEI (Polysciences, Eppenheim, Germany) was prepared in water at a final concentration of 1mg/ml, pH 7.0, and sterilized by filtration.

The optimal PEI: DNA ratio used for this transient transfection was analysed from 1:1 to 1:14. The PEI (Polysciences, Germany)/DNA complexes were prepared in 150 mM NaCl, using a total of 2.5 $\mu$ g DNA /ml of cell culture. In all experiments, 2% EGFP (0.05 $\mu$ g) was mixed with 2.45 $\mu$ g plasmid DNA. Cells were resuspended in serum free RPMI medium at a density of  $2 \times 10^6$  cells/ml. After 4 hours post-transfection the culture was aliquot in 50 ml tubes (5ml per tube). These tubes were centrifuged at 800rpm for 10 minutes and the supernatant was removed. CHO cells were resuspended by adding 10 ml 23 different media.

### **Characterization**

Cell number, viability and aggregate number were determined using a Cedex HiRex cell analysis system (Innovatis AG, Germany).

The transfection efficiency was assessed using green fluorescent protein (pEGFP-N1 plasmid) by both green fluorescence microscope and FACS (CyAn<sup>TM</sup> ADP from Dakocytomation, Denmark).

Expressed recombinant fibrinogen by CHO<sub>fgn</sub> pTet-on cell line was analyzed by a sandwich ELISA using antibody against fibrinogen. The ELISA assay of the conditioned media was carried out in triplicate as described previously<sup>7, 18</sup>. This assay can just detect bioactivity of recombinant fibrinogen which has all three polypeptide chains fully-assembled. Briefly, 96-well assay plates (Milian) were bound with IgG fraction goat anti-human fibrinogen capture antibody (MP Biomedicals, USA) with dilution 1:1000 at room temperature for 1 hour. After washing three

times in PBST (0.05% Tween-20 in PBS, pH 7.4), the plates were blocked with 1% bovine serum albumin (BSA) (Sigma, Switzerland) in PBS for 30 minutes at room temperature. Then the conditioned medium of cultured CHO<sub>βγ</sub> cells and/or CHO<sub>fgn</sub> cells was collected after 24 hours and incubated in plates at room temperature for 2 hours. The fibrinogen standard was diluted serially to obtain several solutions of different concentration for standard curve. The solvent was served as zero standard (0ng/ml). The standard samples were also incubated in same plates as conditioned media. The plates were detected by goat anti-human fibrinogen peroxidase-conjugated detection antibody (MP Biomedicals, USA) using TMB peroxide substrate. Colour was developed and plates were measured at 450nm.

### Optimal growth and production medium for CHO cells

Table 4 Medium used for screening experiment

Medium	Supplier	URL
BD CHO medium	BD, USA	<a href="http://www.bd.com/">http://www.bd.com/</a>
ExCell 325 PF CHO CHO SFM	JRH Biosciences, USA	JRH Biosciences, Inc.
ExCell CD-CHO CHO SFM	JRH Biosciences, USA	JRH Biosciences, Inc.
CD CHO medium	Invitrogen, Switzerland	<a href="http://www.invitrogen.com/">http://www.invitrogen.com/</a>
HyQCDM4CHO	HyClone, USA	<a href="http://www.hyclone.com/">http://www.hyclone.com/</a>
ProCHO <sub>4</sub>	Cambrex, Belgium	<a href="http://www.cambrex.com/">http://www.cambrex.com/</a>
ProCHO <sub>5</sub>	Cambrex, Belgium	<a href="http://www.cambrex.com/">http://www.cambrex.com/</a>
ProMediaSelect K#1	Cambrex, Belgium	<a href="http://www.cambrex.com/">http://www.cambrex.com/</a>
↓	Cambrex, Belgium	<a href="http://www.cambrex.com/">http://www.cambrex.com/</a>
↓	Cambrex, Belgium	<a href="http://www.cambrex.com/">http://www.cambrex.com/</a>
ProMediaSelect K#16	Cambrex, Belgium	<a href="http://www.cambrex.com/">http://www.cambrex.com/</a>

Since i) the components of each commercial serum free medium vary, ii) the response to medium differs from one recombinant cell line to another, and iii) medium has a big impact on cell growth and protein production, screening the medium is a necessary procedure to find the optimal growth and production medium for the cell line.

Experiments were performed in triplicate in 50 ml bioreactor tubes (Fig. 14) containing 10ml of serum free media (SFM). Different commercial SFM for CHO cells were chosen (Table 4). Since CHO<sub>fgn</sub> cells were not able to be adapted to grow in suspension in serum free ProCHO<sub>4</sub> medium, transient transfection of CHO<sub>βγ</sub> cells with fibrinogen A $\alpha$  cDNA were used as a screening medium.



Fig 14. TubeSpin consisted of 50-ml ventilated centrifuge tubes for small-scale experiments in suspension culture. These 50ml sterile tubes have five openings and one gas-porous filter on the cap to regulate gas transfer. They are small bioreactors, used for large-scale parallel tests, optimization experiments and small-scale suspension culture.

## ***Results and discussion***

### **Growth of CHO cells in serum free culture**

CHO<sub>fgn</sub> and CHO<sub>βγ</sub> cells were grown at first in T flasks with 5% FBS and 0.4mg/ml G418 in DMEM/F12 media at 37°C under a humidified atmosphere of 5% CO<sub>2</sub>. G418 (Promega, USA) is a neomycin antibiotic analogue, called geneticine. The use of G418 in culture media provides selective pressure for cells stably expressing a neomycin resistance gene. CHO cells acquired from Dr Lord have been co-transfected with the cDNAs of fibrinogen and a neomycin resistance gene. Therefore, the genome of the cell population can be controlled.



After 3 successive passages, CHO<sub>fgn</sub> and CHO<sub>βγ</sub> cells were weaned from 5% to 2% FBS. The cells were left to grow in T flasks until the cells reach 80-90% of the flask confluence. Then cells were transferred into sterile square bottles or 50ml bioreactor tubes with 2% FBS and 0.4mg/ml G418 in ProCHO<sub>4</sub> media (Cambrex, Belgium), a media designed for suspension culture. The square bottles or 50ml bioreactor tubes were placed in an incubator under an atmosphere of 5% CO<sub>2</sub> with a relative humidity of 85% and shaken at 120-180rpm. The culture media was changed twice per week. During each passage, a new square bottle or a new bioreactor was used and the cell number was counted using a hemocytometer. The inoculum cell concentration was always adjusted to 3x10<sup>5</sup>cells/ml. If the cell concentration was higher, serum free ProCHO<sub>4</sub> media with G418 would be added to maintain 3x10<sup>5</sup>cells/ml. If cell concentration was lower, the cell culture would be centrifuged at 800 rpm for 5 minutes and about 90% supernatant would be removed, then the fresh media added to maintain 3x10<sup>5</sup>cells/ml. When the serum in the medium was infinitely diluted, it is assumed to be zero, or serum free. Once the cells were adapted to grow in suspension in serum free ProCHO<sub>4</sub> media, the cell culture was centrifuged at 800 rpm for 5 minutes at each passage and the supernatant was all removed and replaced by the fresh SFM media for cell expansion.

CHO<sub>βγ</sub> cells were able to be adapted to grow in suspension in serum free ProCHO<sub>4</sub> media. As shown in Fig. 15 and 16, CHO<sub>βγ</sub> cells displayed a regular proliferation curve with high viability (more than 85%) in ProCHO<sub>4</sub> medium supplemented with ProHT (hypoxanthine, thymidine) and 4mM L-glutamine for repeated-batch culture in square bottle. When CHO cells were cultivated in suspension, the unadapted cells either failed to grow or formed large aggregates with intercellular adhesion. The viability of cells in the large aggregates was often rather low.

CHO<sub>fgn</sub> cells were adapted to grow in serum free DMEM/F12 media supplemented with 15mM HEPES and 4mM L-glutamine (Fig. 17), but CHO<sub>fgn</sub> cells never adapted to growth in suspension. Under the microscope, large aggregates were observed. During one assay, it was found that if the culture medium was changed each day, CHO<sub>fgn</sub> cells could grow in suspension. It is known that fibrinogen is secreted from CHO<sub>fgn</sub> cells and fibrin network formation requires Ca<sup>++</sup> as a catalyser<sup>10</sup>. So, there are maybe some traces of Ca<sup>++</sup> in the medium which favour cell attachment to fibrin matrix. At same time, the calcium ion plays an important role in the cell cycle, and influences cell proliferation and growth<sup>11</sup>. So, using Ca<sup>2+</sup> binding reagent as anti-coagulant, such as EGTA, EDTA and dextran sulphate, would influence cell viability in the cell culture, which resulted in decreasing fibrinogen production by CHO cells. In this case, the doxycycline-regulatable Tet-on system was a good solution. CHO cells would not express the

fibrinogen protein when doxycycline was absent from the cell medium. So, the CHO<sub>fgn</sub>-pTet on cells would have no problem to grow in the serum free suspension cell culture. When the cell concentration was high enough for fibrinogen production, doxycycline would be added in the cell medium and the fibrinogen could be harvested in this way.

For the Tet-on system, the full pTRE2pur-fgnA $\alpha$  plasmid was obtained successfully by cloning. The PCR amplification product of the full length fibrinogen A $\alpha$  was analyzed on a 1% w/v agarose gel (Fig. 18) using GeneRuler™ 1kb DNA ladder (Fermentas, Germany) as standards. The result showed one visible band at about 2000bp, which corresponded to the size of full length fibrinogen A $\alpha$  DNA. Then full length fibrinogen A $\alpha$  DNA was inserted into response plasmid pTRE2pur using restriction enzymes. Several random clones of pTRE2pur-fgnA $\alpha$  full were selected from an ampicillin LB plate and analyzed by digestion using restriction enzymes, BamHI and NotI (Fig. 19). On a 1% w/v agarose gel, two bands around 2kb and 5kb were visible for clones #10 and 13, which corresponded to the size of full length fibrinogen A $\alpha$  DNA and response plasmid pTRE2pur. So, these two clones were sent to Microsynth Company for DNA sequence analysis. The analyse results confirmed that the clones #10 and 13 had the correct DNA sequences.

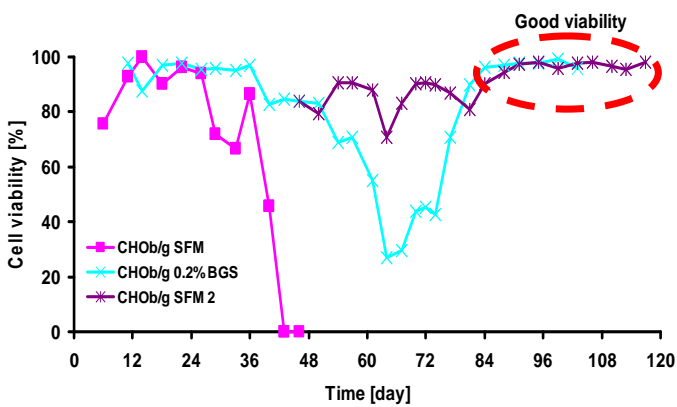


Fig 15. Viability curve of the repeated-batch culture of suspension CHO $\beta\gamma$  cells in ProCHO<sub>4</sub> medium. Suspension CHO $\beta\gamma$  cells showed the adaptation to the new serum concentration in ProCHO<sub>4</sub> medium by displaying a regular proliferation curve with high viability (more than 85%) for more than 30 days.

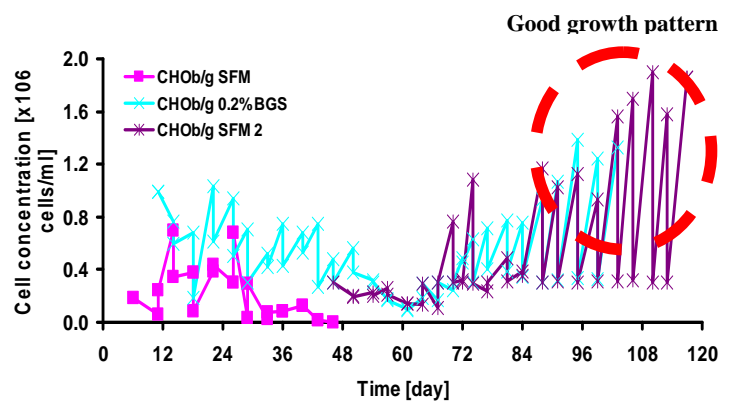


Fig 16. Growth curve of the repeated-batch culture of suspension CHO $\beta\gamma$  cells in ProCHO<sub>4</sub> medium. Suspension CHO $\beta\gamma$  cells showed the adaptation to the new serum concentration in ProCHO<sub>4</sub> medium by displaying a regular proliferation curve with cell concentration constantly up to more 1 million cells/ml from  $3 \times 10^5$  cells/ml after growth for 3 days.

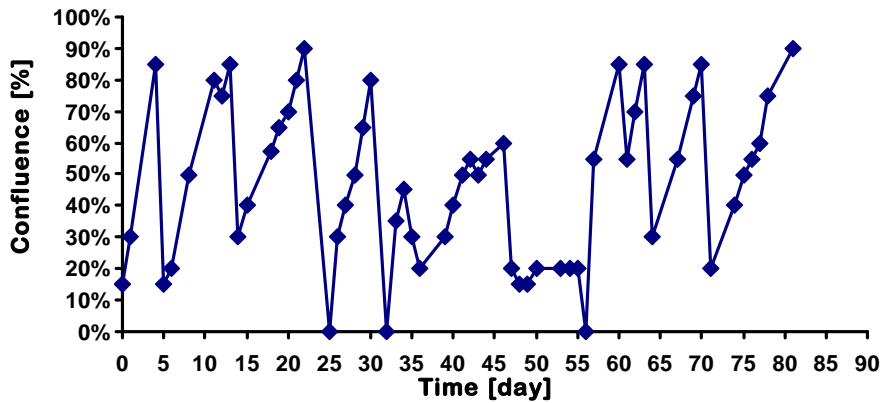


Fig 17. The repeated-batch culture of adherent CHO<sub>fgn</sub> cells in DMEM/F12 medium. Adherent CHO<sub>fgn</sub> cells showed the adaptation to the new serum concentration by displaying a regular growth confluence after several cell passages

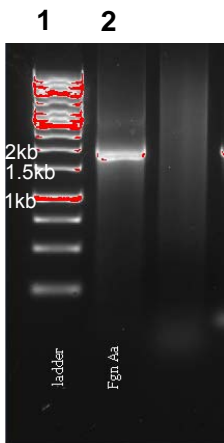


Fig 18. PCR fragment of fibrinogen A $\alpha$  full DNA about 2kbp showed on a 1% w/v agarose gel (lane 2). The DNA size marker is a commercial GeneRuler™ 1kb ladder (lane 1)

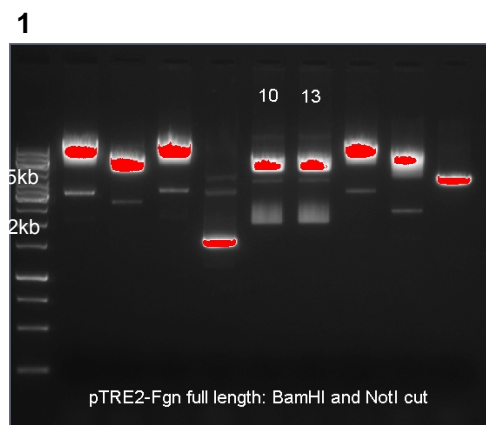


Fig 19. pTRE2pur-FgnA $\alpha$  full plasmid screening on a 1% w/v agarose gel. Restriction digest showing a similar fragment cut about 5kbp from plasmid vector and a fragment about 2kbp from fibrinogen A $\alpha$  full DNA insert (clones 10 and 13). Lane 1: commercial GeneRuler™ 1kb DNA ladder.

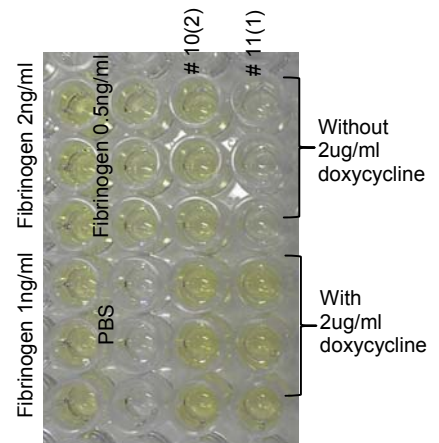


Fig 20. CHO<sub>fgn</sub>-pTet on cell line screening by fibrinogen ELISA. Samples in triplicate. The standard fibrinogen solutions were in first column, 2ng/ml (up) and 1ng/ml (down), and also in second column, 0.5ng/ml (up) and 0ng/ml (down). The same cell line was in 2 different cell medium, with 2ug/ml doxycycline (down, fibrinogen expression on) and without 2ug/ml doxycycline (up, fibrinogen expression off). 2 cell lines were analyzed, 10(2) and 11(1). The cell line 11(1) seems good.

The Tet-on system was transfected into CHO<sub>βγ</sub> cells in two steps using the lipofectamine 2000 reagents. After selection of cells in puromycin and neomycin containing media, two clones of CHO<sub>fgn</sub>-pTet on cell lines were selected. The cell medium was collected after 24 hours inoculation before and after 2μg/ml doxycycline (Sigma, Switzerland) was added. It should have no fibrinogen expression before adding doxycycline. According to a fibrinogen ELISA assay (Fig. 20), the color detection of the clone 11(1) was good. But three months later, the cells were dead due to the selection medium. This indicates that the plasmid failed to insert into the cell genome and was rejected by the cells. More clones were analyzed in the subsequent experiments.

There are two reasons that CHO<sub>fgn</sub> pTet-on cell line was difficult to produce. First, because pTet-on plasmid contains a neomycin resistance gene and CHO<sub>βγ</sub> cells are also neomycin resistant, the stable CHO<sub>βγ</sub> pTet-on cell line was not obtained, which is very important for Tet-on system application according to manufacturer's protocol. Instead, transient CHO<sub>βγ</sub> pTet-on cell line was transfected immediately by the pTRE2pur-FgnAα full plasmid, which was selected out by puromycin. That is the reason why it is difficult to obtain the CHO<sub>fgn</sub> pTet-on cell line. Secondly, during culture in selection medium, the CHO<sub>fgn</sub> pTet-on cell line may lose one or two plasmids of Tet-on system, which is expressed as cell death, fibrinogen expression leaking during doxycycline absence, and no fibrinogen expression during doxycycline presence. This is what was observed. One good clone was obtained according to color detection using the fibrinogen ELISA. But the cells were dead during culture in the selection medium. So, more cell clones would be chosen and analyzed in additional experiments.

### **Optimal growth and production medium for CHO cells**

CHO<sub>βγ</sub> cells were transfected with different PEI: DNA mass ratios (from 1 to 14) to determine the optimal charge ratio. During all transfection experiments, 2% mass of pEGFP-N1 (green fluorescent protein plasmid) was added into the other plasmid DNA. Two days post-transfection, transfected cells were analysed by FACS to check the transfection efficiency (Fig. 21) and cell viability was checked using a haemocytometer (Fig. 22). Results indicated that the transfection efficiency increased with higher charge ratios, but cell viability decreased dramatically. A charge ratio 5 (equivalent to mass ratio 2) was chosen for future CHO<sub>βγ</sub> cell transfection based on the combined transfection efficiency and cell viability.

Transient transfected CHO<sub>βγ</sub> cells were used to screen 23 commercially available medium for 10 days. Fluorescence microscopy on day 3 (Fig. 23) demonstrated the successful transfection and this was confirmed using FACS (Fig. 24) indicating that 41% of the cells were successfully

transfected. ELISA protein analysis indicates us that transfected CHO cells were capable of producing fibrinogen in several medium, such as CD CHO, ProCHO<sub>5</sub> and ProMedia Select k#10 (Fig. 25). Finally the cell growth curve (Fig. 26) indicated that cells passed the lag phase of 1 or 2 days during adaptation to the new medium. Following adaptation they grew more than 4 days in the same medium without exchange and maintained viability higher than 70% (Fig. 27). From the summary (Table 4), it was shown that several medium, such as Excell 325 PF, HyQCDM4CHO, ProMedia Select k#9 and ProMedia Select k#16, are good for cell growth. The cell concentration in these medium reached more than 3 million/ml on day 4 in the culture with a viability higher than 85%. However, ELISA data illustrated that these media were not good for fibrinogen production.

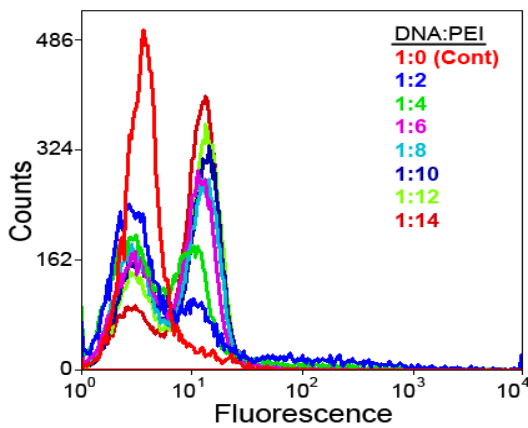


Fig 21. FACS Analysis of PEI transfection to CHO<sub>βγ</sub> cells using EGFP with eight different DNA:PEI ratios. The first peak represents the population of cells non-transfected. The second peak represents the population of cells transfected. Note that the population of cells transfected increased with DNA:PEI ratio.

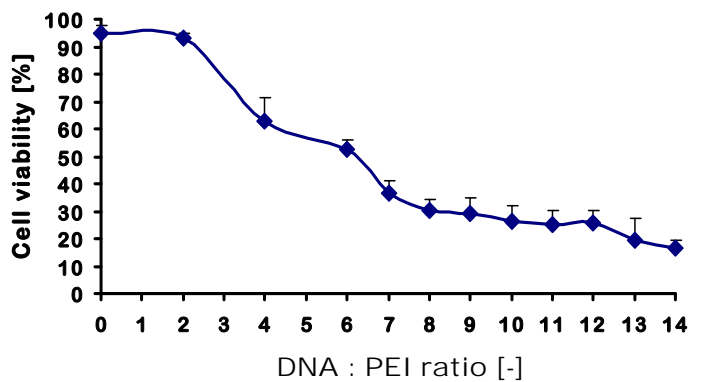


Fig 22. Cell viability of CHO<sub>βγ</sub> cells transfected using PEI reagent with eight different DNA:PEI ratios. Note that cell viability decreased with DNA:PEI ratio.

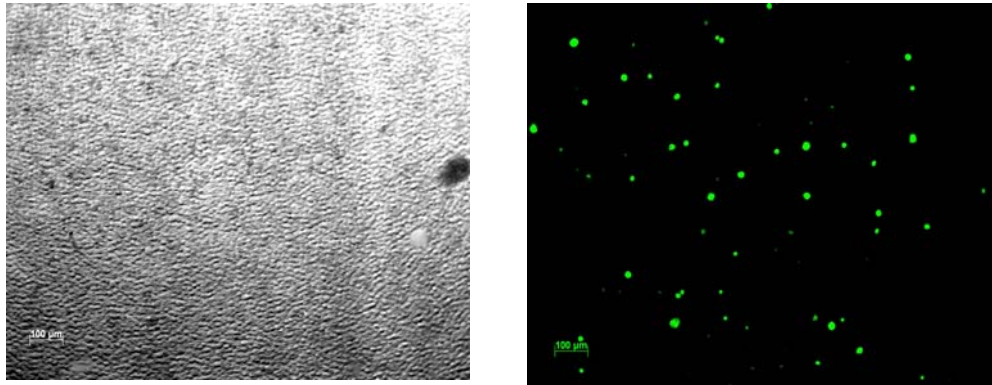


Fig 23. Imaging of CHO $\beta\gamma$  cells (3 days post-transfection) transfected using PEI reagent with DNA: PEI ratio 1:2. a) bright field (left) and b) Green fluorescence (right) under a fluorescence microscope, with scale bar 100 micrometers. It is evident that CHO $\beta\gamma$  cells showing green fluorescence were successfully transfected.

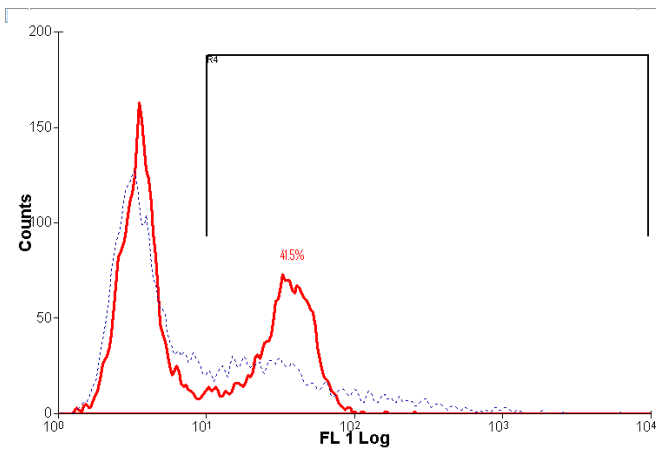


Fig 24. FACS analysis of CHO $\beta\gamma$  cells (3 days post-transfection) transfected using PEI reagent with DNA: PEI ratio 1:2. Note that about 41.5% cells were successfully transfected

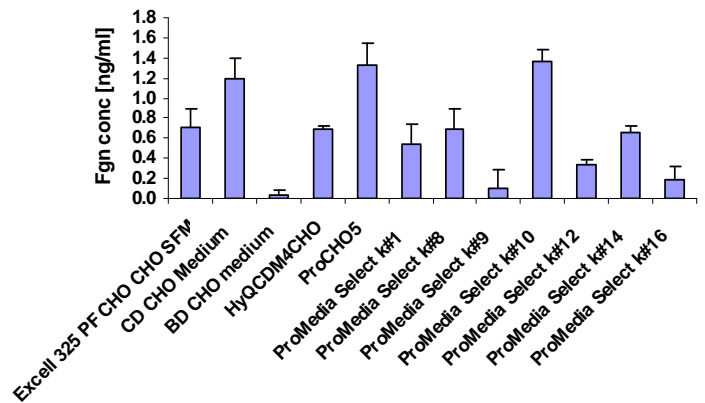


Fig 25. Fibrinogen ELISA analysis of CHO $\beta\gamma$  cells (2 days post-transfection) transfected using PEI reagent with DNA: PEI ratio 1:2. Note that fibrinogen expressed by transfected CHO $\beta\gamma$  cells was higher in three cell medium, CD CHO, ProCHO<sub>5</sub> and ProMedia Select k#10

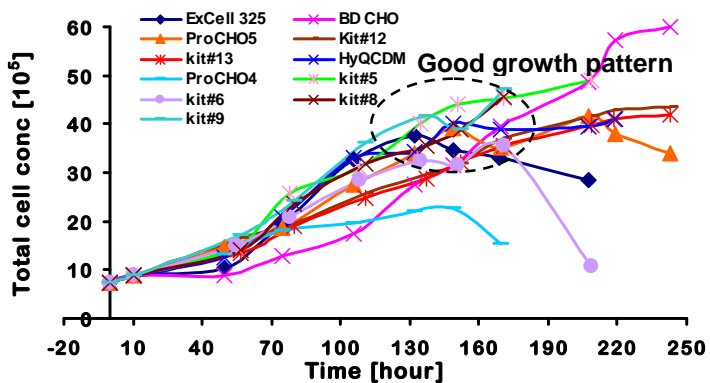


Fig 26: Growth curve of batch transfected CHO<sub>βγ</sub> cells culture in selected 11 commercial media for 10 days. Note that cells were adapted to the new medium very quickly, about 2 days, with nice cell growth pattern

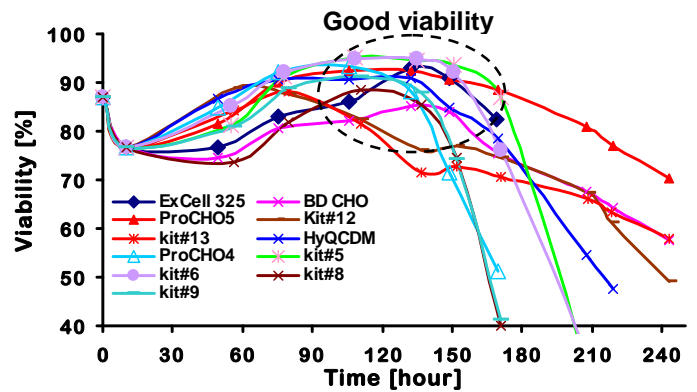


Fig 27. Cell viability curve of batch transfected CHO<sub>βγ</sub> cells culture in selected 11 commercial media for 10 days. Note that cells were adapted to the new medium very quickly, with high cell viability (>70%)

For batch culture, cells always proceed through four growth phases: lag phase, exponential growth phase, stationary phase and death phase (Fig. 28).

Lag phase: When first added to a medium, cells often have to adapt to the new medium which is different from that in which they have been growing. Adjusting to the new conditions takes time and during this period of gene expression and enzyme synthesis, no increase in cell number is observed causing a “lag” in the cell growth.

Exponential growth phase: Cells begin to divide and fairly quickly reach a maximal rate of division for the conditions present in the culture.

Stationary phase: Cell number in the culture reaches a maximum. Due to the depletion of a nutrients and/or accumulation of waste products, a small number of cells dying is equal to the number of slow growing cells

Death phase: Growing cell rate drops below death rate. The population slowly decreases over time at a rate that is normally much slower than the exponential growth phase <sup>19</sup>.

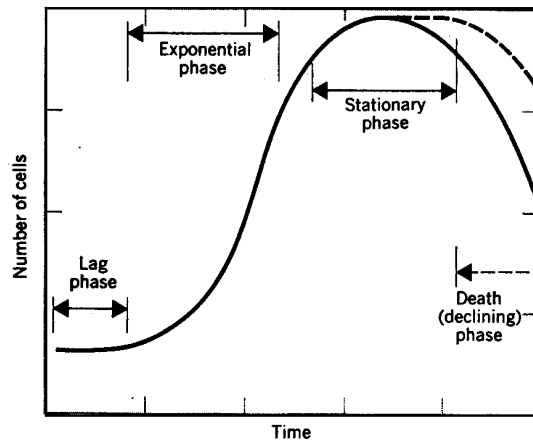


Fig 28. Typical batch cell culture growth curve <sup>19</sup>. It consists of 4 phases, lag phase, exponential phase, stationary phase and death (declining) phase.

The length of time spent in each phase and the growth rate during exponential phase is dependent upon the species and medium conditions. Cell growth rate  $\mu$  was calculated using  $N_t = N_0 \cdot \exp(\mu t)$  with  $N_t$  number of viable cells present at time  $t$  and  $N_0$  initial number of viable cells. As shown in Fig. 29 and Table 4, cell growth rates differed in different medium. Cells grew faster in Excell 325 PF CHO, HyQCDM4CHO, ProMedia Select k#5, k#8, k#9, k#10 and k#16 medium. And cell growth rate was slightly higher in ProMedia Select k#10 and Excell 325 PF.

As shown in Table 5 and Fig. 25, CD CHO, ProCHO<sub>5</sub> and ProMedia Select k#10 were the best production media. But they were not good growth media for the CHO cell line. The best growth medium among these three medium was ProCHO<sub>5</sub> where the cell concentration reached 3 million/ml. The worst was the CD CHO medium where cell growth rate was nearly 0 and cell concentration was less than 1 million/ml in 4 days.



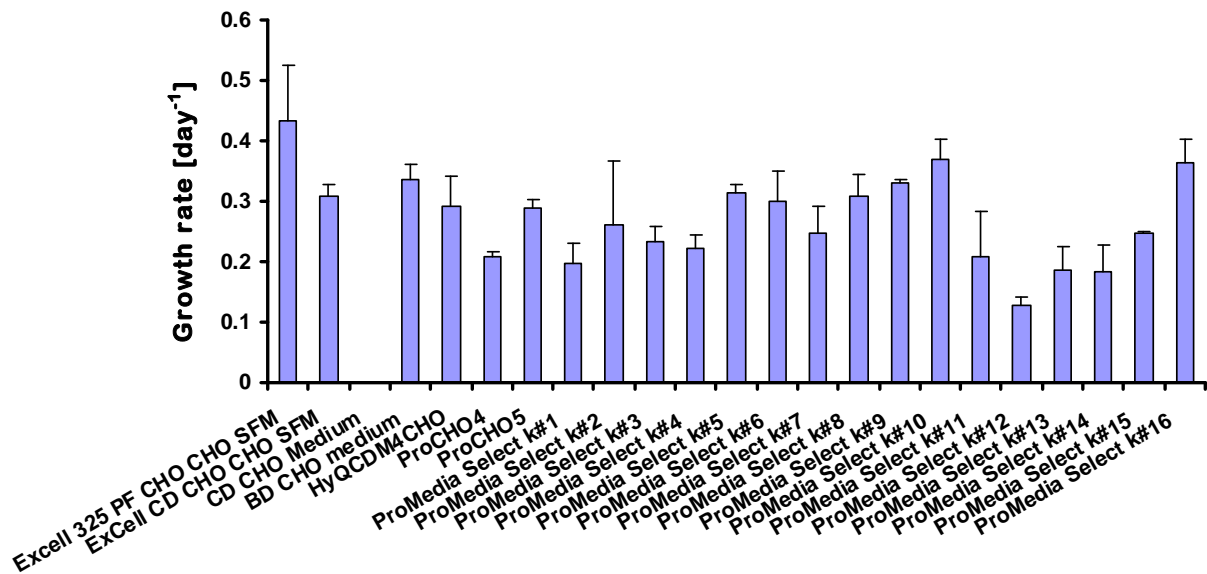


Fig 29. Growth rate curve of batch transfected CHO<sub>βγ</sub> cells culture in 23 commercial media for 10 days. Note that cell medium had definitively effects on cell growth rate and that cells grew faster in Excell 325 PF CHO, HyQCDM4CHO, ProMedia Select k#5, k#8, k#9, k#10 and k#16 medium. Low aggregate rate is another criterion for selection cell growth and production medium. Comparing cell aggregation rate in those medium at day 4 (Fig. 30) and at day 5 (Fig. 31), it was shown that cells were more easily aggregated in ProMedia Select k#6 and ProCHO<sub>4</sub> with an aggregate rate higher than 50% compared to k#16 and CD CHO medium with an aggregate rate of 20%.

It is shown that fibrinogen A $\alpha$  chain can be transfected to CHO<sub>βγ</sub> cells to produce secreted, detectable fibrinogen. Cell concentration can reach 6 million cells per ml 10 days after transient transfection and cell viability is still higher than 50%. For the optimal growth and production medium for CHO<sub>f<sub>gn</sub></sub> cells, Excell 325 PF CHO, HyQCDM4CHO, ProMedia Select k#9 and k#16 are shown to be the best growth medium for our CHO cells. ELISA results show us that CD CHO, ProCHO<sub>5</sub> and ProMedia Select k#10 are the best production medium. The growth rate tells us that Excell 325 PF CHO and ProMedia Select k#10 are the best. Finally cell aggregate rate shows us that ProCHO<sub>4</sub> and ProMedia Select k#6 are not ideal. Based on the available data, ProCHO<sub>5</sub> was determined to be the optimal production and growth medium for CHO<sub>βγ</sub> and CHO<sub>f<sub>gn</sub></sub> cells (Table 5). Alternatively we may grow our CHO cells in Excell 325 PF CHO medium to the desired cell number then transfer to ProCHO<sub>5</sub> or ProMedia Select k#10 medium for fibrinogen production. This screening result provides us an optimal means for the future production of recombinant chimeric fibrinogen.

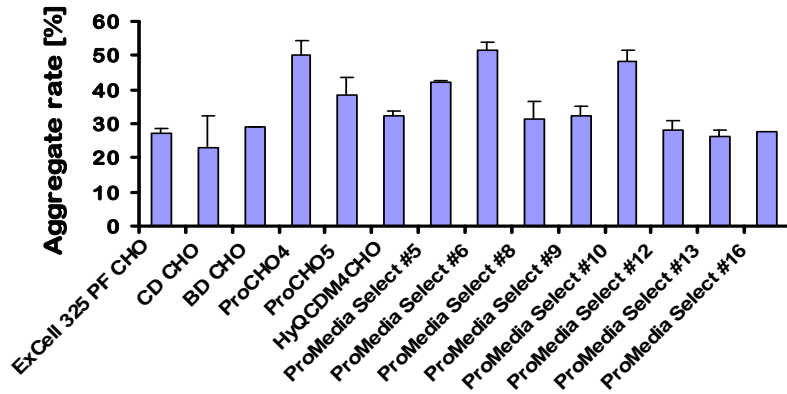


Fig 30. Aggregate rate curve of batch transfected CHO<sub>βγ</sub> cells culture in selected 14 commercial media at day 4. Note that cell medium had definitively effects on cell aggregate rate and that cells aggregated easily in ProMedia Select k#6, k#10 and ProCHO<sub>4</sub>

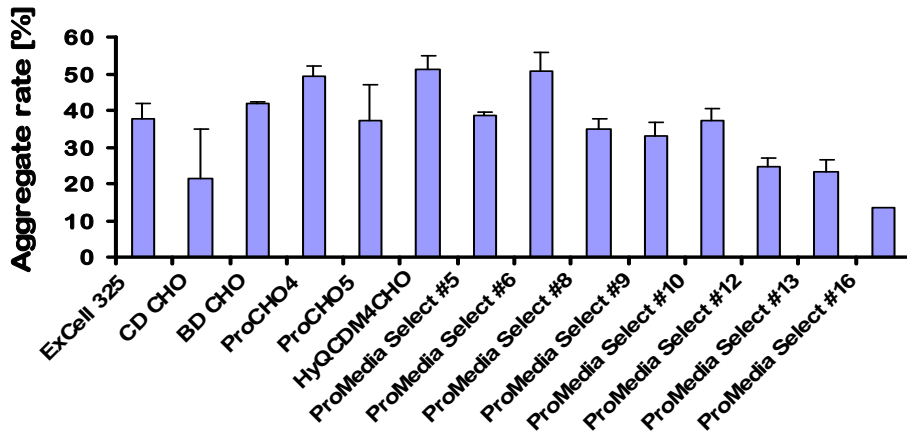


Fig 31. Aggregate rate curve of batch transfected CHO<sub>βγ</sub> cells culture in selected 14 commercial media at day 5. Note that cell medium had definitively effects on cell aggregate rate and that cells aggregated easily in HyQCDM4CHO, ProMedia Select k#6 and ProCHO<sub>4</sub>

Table 5 Summary of optimal growth and production medium for CHO<sub>fgn</sub> and CHO<sub>βγ</sub> cells

Medium	Fgn conc [ng/ml]	Total cell number d4 [10 <sup>6</sup> ]	Viability d4 [%]	Growth rate [day <sup>-1</sup> ]	Aggregate rate d4 [%]
<b>Excell 325 PF</b>	<b>0.70±0.02</b>	<b>3.29±0.36</b>	<b>86.16±2.07</b>	<b>0.434</b>	<b>27.10±1.48</b>
CD CHO	1.19±0.10	0.88±0.16	19.90±6.47	0.000	22.83±9.41
HyQCDM4CHO	0.69±0.03	3.32±0.10	90.65±0.88	0.293	32.33±1.46
ProCHO <sub>4</sub>	0	1.95±0.12	93.46±0.17	0.209	50.07±4.50
<b>ProCHO<sub>5</sub></b>	<b>1.33±0.09</b>	<b>2.75±0.23</b>	<b>92.45±3.46</b>	<b>0.288</b>	<b>38.33±5.16</b>
ProMedia k#5	0	3.08±0.05	95.15±0.35	0.314	42.13±0.59
ProMedia k#6	0	2.86±0.09	94.85±0.17	0.300	51.47±2.51
ProMedia k#8	0.70±0.06	3.18±0.01	88.51±2.41	0.307	31.37±4.98
ProMedia k#9	0.11±0.02	3.62±0.32	91.15±0.50	0.331	32.17±2.89
ProMedia k#10	1.36±0.01	1.62±0.10	88.55±0.72	0.370	48.07±3.51
ProMedia k#12	0.33±0.05	2.57±0.09	82.33±1.22	0.127	28.33±2.78
ProMedia k#16	0.19±0.03	3.72±0.39	86.35±0.86	0.365	27.43±4.22

d4: at day 4

## **Conclusion**

Due to the wide application of fibrin matrices in tissue engineering, recombinant fibrinogen produced by CHO cells is a new way to obtain this bioactive protein. Furthermore since natural fibrin purified from blood could cause problems, such as purification and contamination, recombinant fibrinogen could overcome these shortcomings and is developing well in the laboratory. To produce relatively high quantities, CHO cells are grown in suspension using serum free culture conditions. In this chapter, CHO<sub>βγ</sub> cells are shown to adapt to grow in serum free medium in suspension which is difficult for CHO<sub>fgn</sub> cells. Due to trace calcium in the cell medium, fibrinogen expressed by CHO<sub>fgn</sub> cells were polymerized to form cell aggregates. In this way, all CHO cells were trapped in the matrix and precipitated to the bottom of the spin bottle. For CHO<sub>fgn</sub> cells in suspension culture, the problem of calcium should be resolved. Since calcium plays an important role in cell growth, the Tet-on system was used to resolve the expressed fibrinogen polymerisation problem by regulating the fibrinogen expression. The Tet-on system was composed of one response plasmid, pTRE2pur, and one regulator plasmid. One good clone of CHO<sub>fgn</sub> pTet-on cell line was obtained according to a fibrinogen ELISA assay. However the cells were dead during culture in the selection medium due to plasmid rejections by CHO cells. So, additional development is required to get CHO<sub>fgn</sub> cells in suspension culture, such as screening more cell clones by ELISA.

During screening for optimal growth and production medium for CHO cells, ProCHO5 was chosen for several reasons, such as cell viability, cell growth rate, cell number and the low cell aggregation rate. For CHO cells in serum free suspension culture, optimal medium ProCHO5 plays one key role for cell viability. In future studies, ProCHO5 was used as standard cell medium for CHO cells in suspension culture.

## **Acknowledgement**

The p584 A $\alpha$  plasmid and CHO<sub>βγ</sub> cell line are kindly provided by prof. Dr. Susan Lord, Department of Chemistry, University of North Carolina at Chapel Hill, Chapel Hill, NC 27599, USA.

I am grateful to Dr. Lucia Baldi for helpful discussions about suspension cell culture and Dr. Thomas Barker for teaching me cell line isolation.

## Reference

1. Lutolf, M.P. & Hubbell, J.A. Synthetic biomaterials as instructive extracellular microenvironments for morphogenesis in tissue engineering. *Nat Biotechnol* **23**, 47-55 (2005).
2. Wurm, F.M. Production of recombinant protein therapeutics in cultivated mammalian cells. *Nat Biotechnol* **22**, 1393-1398 (2004).
3. Mullin, J.L., Gorkun, O.V., Binnie, C.G. & Lord, S.T. Recombinant fibrinogen studies reveal that thrombin specificity dictates order of fibrinopeptide release. *J Biol Chem* **275**, 25239-25246 (2000).
4. Gorkun, O.V., Veklich, Y.I., Weisel, J.W. & Lord, S.T. The conversion of fibrinogen to fibrin: recombinant fibrinogen typifies plasma fibrinogen. *Blood* **89**, 4407-4414 (1997).
5. Lord, S.T., Strickland, E. & Jayjock, E. Strategy for recombinant multichain protein synthesis: fibrinogen B beta-chain variants as thrombin substrates. *Biochemistry* **35**, 2342-2348 (1996).
6. Doolittle, R.F. Fibrinogen and fibrin. *Annu Rev Biochem* **53**, 195-229 (1984).
7. Binnie, C.G., Hettasch, J.M., Strickland, E. & Lord, S.T. Characterization of purified recombinant fibrinogen: partial phosphorylation of fibrinopeptide A. *Biochemistry* **32**, 107-113 (1993).
8. Binnie, C.G. & Lord, S.T. The fibrinogen sequences that interact with thrombin. *Blood* **81**, 3186-3192 (1993).
9. Lord, S.T., Byrd, P.A., Hede, K.L., Wei, C. & Colby, T.J. Analysis of fibrinogen A alpha-fusion proteins. Mutants which inhibit thrombin equivalently are not equally good substrates. *J Biol Chem* **265**, 838-843 (1990).
10. Furlan, M., Steinmann, C., Jungo, M. & Lammle, B. Binding of calcium ions and their effect on clotting of fibrinogen Milano III, a variant with truncated A alpha-chains. *Blood Coagul Fibrinolysis* **7**, 331-335 (1996).
11. Cook, S.J. & Lockyer, P.J. Recent advances in Ca<sup>2+</sup>-dependent Ras regulation and cell proliferation. *Cell Calcium* **39**, 101-112 (2006).
12. Machaca, K. Ca<sup>2+</sup> signaling differentiation during oocyte maturation. *J Cell Physiol* **213**, 331-340 (2007).
13. Gossen, M. et al. Transcriptional activation by tetracyclines in mammalian cells. *Science* **268**, 1766-1769 (1995).

14. Scimmenti, C.R., Baba, E.J. & Calos, M.P. An extrachromosomal tetracycline-regulatable system for mammalian cells. *Nucleic Acids Res* **28**, E80 (2000).
15. Vieyra, D.S. & Goodell, M.A. Pluripotentiality and conditional transgene regulation in human embryonic stem cells expressing insulated tetracycline-ON transactivator. *Stem Cells* **25**, 2559-2566 (2007).
16. Ryu, J.H., Kim, M.S., Lee, G.M., Choi, C.Y. & Kim, B.S. The enhancement of recombinant protein production by polymer nanospheres in cell suspension culture. *Biomaterials* **26**, 2173-2181 (2005).
17. Korke, R. et al. Genomic and proteomic perspectives in cell culture engineering. *J Biotechnol* **94**, 73-92 (2002).
18. Snouwaert, J.N., Kariya, K. & Fowlkes, D.M. Effects of site-specific mutations on biologic activities of recombinant human IL-6. *J Immunol* **146**, 585-591 (1991).
19. <http://www.dentistry.leeds.ac.uk/OROFACE/PAGES/micro/expgrow.gif>

## Chapter III Development of a 3<sup>rd</sup> generation fibrin delivery system: recombinant fibrinogen IGF1 fusion protein

### *Summary*

The development of fibrin-based biomaterials is based on fibrin's central role in tissue binding and in the initiation of tissue repair and defence. The binding of Fgn/fibrin to hemostasis proteins and platelets as well as to different cells, growth factors, and extracellular matrix proteins is indispensable during the wound repair process. Technologies have been developed with some success for the incorporation of growth factors into fibrin, ranging from simple admixing to covalent incorporation using the coagulation transglutaminase factor XIIIa. Here we explore a novel platform technology where the growth factor is incorporated into Fgn's A $\alpha$ -chain at the genetic level. We have chosen this region since evidence suggests that the C-terminus of Fgn's A $\alpha$ -chain is not required for bioassembly or polymerization.

Here we produced truncation and fusion variants of the fibrinogen A $\alpha$  chain, denoted FGA5aa, in which the C-terminus of the fibrinogen A $\alpha$  chain was truncated to 5 amino acid residues of the second disulfide cluster; FGA5aa-IGF1, in which the truncation was fused with IGF1, and FGA5aa-MMP-IGF1, in which an MMP substrate was inserted between the two fusion domains.

In this work, the cell lines CHO<sub>FGA5aa-IGF1</sub> and CHO<sub>FGA5aa-MMP-IGF1</sub> were made and protein variants of fibrinogen expressed. Fibrinogen was detectable by fibrinogen antibody using an ELISA assay. From the ELISA results, it was discovered that CHO<sub>FGA5aa-MMP-IGF1</sub> cell line was more immune-reactive than the CHO<sub>FGA5aa-IGF1</sub> cell line due to the stoichiometric concentration ratio of fibrinogen to IGF1. The ratio expected was 0.5 because fibrinogen structure contains 2 A $\alpha$ -polypeptide chains. According to experimental result, this ratio was 15.8:1 for the CHO<sub>FGA5aa-MMP-IGF1</sub> cell line and 152.8 for the CHO<sub>FGA5aa-IGF1</sub> cell line. So, it was guessed that the structure of FGA5aa-MMP-IGF1 was more flexible than FGA5aa-IGF1 due to linker matrix metalloproteinase MMP substrate site. The fusion fibrinogen protein produced by the cell lines was collected and purified by saturated ammonium sulphate and by fibrinogen binding peptide AAGPRP or fibrinogen antibody IF-1 affinity chromatography consecutively. The release profile and functional significance of this novel fibrin-delivery system will be addressed in the future.

## ***Introduction***

The use of fibrin instead of other materials is based on its central role in the initiation of tissue repair. The three-dimensional fibrin network can induce cell proliferation and migration <sup>1</sup>. As invading cells migrate into the fibrin matrix they produce and activate another enzyme, plasmin, at the leading edge of the cell. This enzyme degrades the fibrin polymer in a highly regulated manner and leaves the polymer intact where cells have not yet invaded, and where structural support is still required <sup>2</sup>. These activities of this system make fibrin an attractive material for medical applications. The interest in fibrin was sparked in 1998 when the FDA approved the fibrin polymer to be commercially used for tissue hemostasis, called Tisseel VH kit (Baxter AG). To enhance wound healing and regeneration, several bioactive proteins have been successfully incorporated into the fibrin matrices as developmental signals, such as adhesion factors and growth factors <sup>3-5</sup>.

In our laboratory, we have developed a fibrin platform to deliver bioactive proteins in a controlled manner, which resulted in a more effective wound healing process. Up to date, this platform has two generations (Fig. 32). The first generation was used to incorporate the heparin-affinity bioactive proteins, heparin and a heparin-binding peptide into fibrin matrices during polymerization. This peptide was composed of a factor XIIIa substrate from the  $\alpha_2$ -plasmin inhibitor at N-terminus and one heparin-binding site based on the antithrombin III (ATIII) at the C-terminus. This peptide, which was covalently cross-linked into the fibrin matrix, was used to immobilize heparin electrostatically in fibrin. Then the immobilized heparin was used to bind electrostatically the heparin-affinity bioactive proteins <sup>3</sup>. This system provided for an indirect but strong affinity between heparin-affinity bioactive proteins and the fibrin. The second generation was to covalently bind a mutant form of a bioactive protein into the fibrin matrices <sup>5</sup>. This mutant protein contained a factor XIIIa substrate sequence NQEQVSPL from the  $\alpha_2$ -plasmin inhibitor ( $\alpha_2$ PI<sub>1-8</sub>) at the N-terminus, which would attach to fibrin during coagulation through the action of factor XIIIa. In this chapter, the third generation of the fibrin platform was explored, a genetic modification of fibrinogen A $\alpha$  polypeptide chain itself.



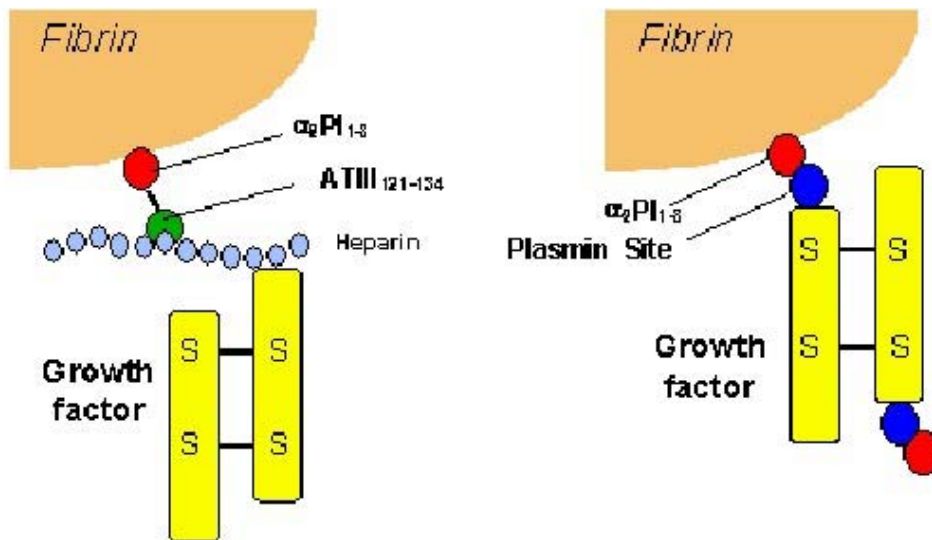


Fig 32. Two generations of the fibrin platform in our lab. The first generation (left) incorporated peptides, heparin and heparin-affinity growth factor in fibrin matrices. The second generation (right) was to create a mutant form of growth factor X, named  $\alpha_2\text{PI}_{1-8}\text{-X}^5$

It has been found that  $\gamma$ -chains and B $\beta$ -chains were relatively constant in size among most species of 30 mammalian fibrins surveyed, but the carboxyl domains of the A $\alpha$ -chains varied considerably. These domains ( $\alpha\text{C}$ ) contained a series of repeated sequences, which resulted in the flexible nature of the region. This region was easily trimmed away by proteolysis and was often referred to as “free-swimming appendages”<sup>6</sup>. As described by R. Doolittle, chicken fibrinogen A $\alpha$ -chain lacked these  $\alpha\text{C}$  repeats and the A $\alpha$  C-terminus was neither required for fibrinogen bioassembly nor did it participate in the formation of fibrin polymer<sup>7, 8</sup>. Engineered truncations of the fibrinogen A $\alpha$  chain could create about 40 kDa of space available for the fusion of other bioactive proteins respecting the fact that the disulfide bridges at the C-terminus of the coiled-coils were absolutely essential for fibrinogen stability (Fig. 33).

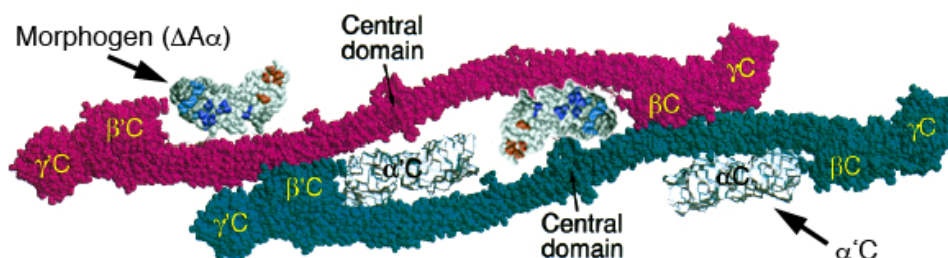


Fig 33. Diagram of the third generation of fibrin platform. The carboxyl terminal region of the fibrinogen A $\alpha$  chain ( $\Delta\text{A}\alpha$ ) can be replaced by bioactive protein chosen<sup>8</sup>.

One preliminary screening experiment by fibrinogen ELISA was manipulated to determine how many amino acids of A $\alpha$  C-terminus from the second S-S ring were sufficient for proper fibrinogen assembly while its native bioactivity remained. This ELISA assay can just detect bioactivity of truncated fibrinogen which has all three polypeptide chains fully-assembled.

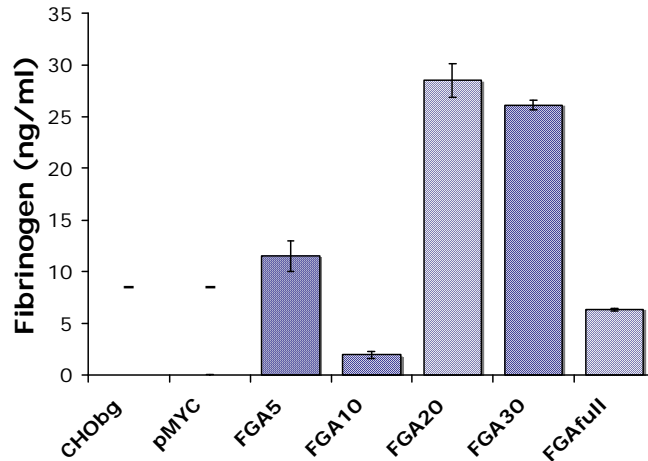


Fig 34. Fibrinogen ELISA assay for detection of truncated fibrinogen expressed by CHO cells. Here pMYC vector was a negative control, no fibrinogen expression detectable. It was clear that fibrinogen antibody could not detect mutant fibrinogen expressed by CHO $\beta\gamma$  cells because of just B $\beta$ -and  $\gamma$ -chains, lack of fibrinogen A $\alpha$  chain. Note that fibrinogen expressed by all truncated fibrinogen species CHO cells could be detectable by fibrinogen antibody. FGA5 represented 5 amino acids of A $\alpha$  C-terminus from the second disulfide cluster.

FGA10 represented 10 amino acids of A $\alpha$  C-terminus from the second disulfide cluster.

FGA20 represented 20 amino acids of A $\alpha$  C-terminus from the second disulfide cluster.

FGA30 represented 30 amino acids of A $\alpha$  C-terminus from the second disulfide cluster.

FGAfull represented full length of fibrinogen A $\alpha$  chain.

According to fibrinogen ELISA results (Fig. 34), fibrinogen expression of all truncated fibrinogen species (A $\alpha$ 189, 194, and 199) could be detectable by the fibrinogen antibody. This confirmed that the C-terminus of fibrinogen A $\alpha$ -chain could be cut as short as only 5 amino-acids from the second disulfide cluster (FGA5aa). It provided at least 40kDa of free space in FGA5aa for therapeutic DNA insertion. This discovery showed us a means for the direct incorporation, at the genetic level, of protein therapeutics such as growth factors into fibrin matrices without additional enzymes. This technology should extend the residence time of growth factors in the matrix for enhanced tissue regeneration. Among growth factors, IGF1 was suggested as one example of a bioactive protein that could be incorporated into fibrinogen A $\alpha$  chain due to its single chain and

small mass weight of 10kD. So, a new protein engineering system was proposed in this chapter: genetic fusion of IGF1 to the fibrinogen A $\alpha$  polypeptide chain C-terminus. The advantage of this new generation was a high level of control of the release profile of the desired bioactive protein and that the incorporation of the bioactive protein into the fibrin matrices was independent of coagulation.

## Materials and methods

### Materials

The mammalian expression vector pMYKpuro was provided by Dr. Lucia Baldi, EPFL. Plasmid p584 A $\alpha$ , containing cDNA for the A $\alpha$  chain of human fibrinogen, was provided by Prof. Dr. Susan Lord, the University of North Carolina at Chapel Hill. Plasmid pCR2.1-hIGF1, containing cDNA of hIGF1, was provided by Prof. Aebischer, EPFL. CHO $\beta\gamma$  cells, expressing both B $\beta$  and  $\gamma$  chains of human fibrinogen, were provided by Prof. Dr. Susan Lord, the University of North Carolina at Chapel Hill. All enzymes used were purchased from New England Biolabs. Unless otherwise specified, all cell culture reagents were supplied by Invitrogen, UK.

### Construction of expression vector

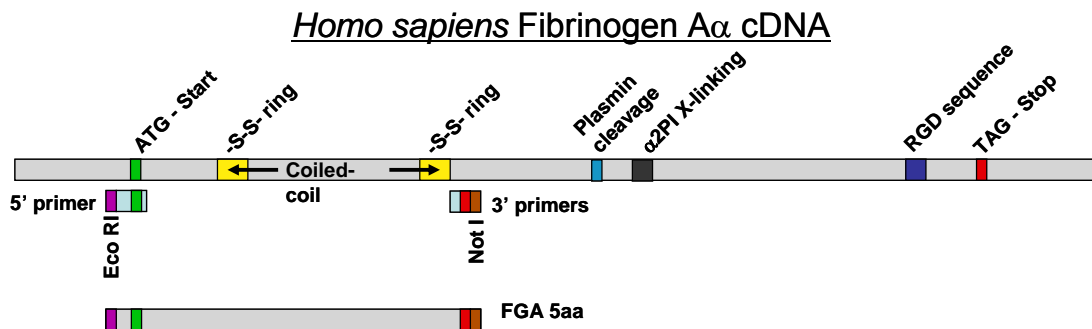


Fig 35. Truncated FGA5aa DNA generation. Fibrinogen A $\alpha$  full length cDNA is showed above. One fragment of DNA is taken from the start codon ATG to 5 amino acids after the second S-S ring. Then EcoRI restriction enzyme is added before ATP start codon and NotI restriction enzyme is added after the 5<sup>th</sup> amino acid DNA sequence by PCR using two primers coding EcoRI and NotI restriction enzyme sequence separately.

The cDNA encoding fibrinogen A $\alpha$  chain 1-567 nucleotides was cloned into an expression vector pMYKpuro using a 5' primer containing the EcoRI restriction site and a 3' primer containing the

NotI restriction site (Fig. 35). Then a restriction enzyme XbaI sequence TCTAGA was added closely after the 3'-terminus of fibrinogen A $\alpha$  chain by PCR as a unique fusion cloning site. This vector was called pMYKpuro FGA5aafus.

Human IGF1 cDNA was obtained from the plasmid pCR2.1-hIGF1 by PCR with both termini containing the XbaI restriction sites. The Forward primer was 5'-GCTCTAGAGGAAAAATCAGCAGTCTTCC-3'. The reverse primer was 5'-GCTCTAGACTACATCCTGTAGTTCTTGT-3'. The restriction enzyme XbaI sequence was solid underlined in both primers. The IGF1 PCR product was inserted downstream and immediately adjacent to and in frame with truncated fibrinogen A $\alpha$  chain at the XbaI site of the vector pMYKpuro FGA5aafus. The resulted vector was called pMYKpuro FGA5aaIGF1.

Construction of the vector for the mutant human IGF1 was obtained by adding one MMPs sensitive sequence, which corresponded to the 8 amino acids GPQG $\uparrow$ IWGQ<sup>9</sup> with cleavage site indicated  $\uparrow$  and double underlined in the forward primer. This primer was 5'-GCTCTAGAGGACCTCAGGGTATTGGGGACAAGGAAAAATCAGCAGTCTTCC-3'. The added MMP sensitive sequence was to allow for the cleavage of human IGF1 from fibrinogen A $\alpha$  chain by several MMP enzymes. The resulted vector was called pMYKpuro FGA5aaMMPIGF1.

## DNA transfection and cell culture

CHO $\beta\gamma$  cells were growing in Dulbecco's modified Eagle media (DMEM)/F12 media supplemented with 10% Fetal Bovine Serum (FBS), 100U/ml penicillin, 100 $\mu$ g/ml streptomycin and 0.4mg/ml G418 (Promega, USA) at 37°C in 5% CO<sub>2</sub>. These cells were used as the host for all transfections.

The Plasmids DNA sequences were analyzed by Microsynth. The plasmid DNA was amplified in the *E.coli* strain E10 and extracted using a plasmid Maxi Kit (QIAGEN GmbH, Germany). The purified plasmid was resuspended in sterile water and checked by gel electrophoresis and by OD readings at 260 and 280 nm. Only the preparation of the highest purity ( $R_{260/280} > 1.8$ ) was used for transfection.

CHO $\beta\gamma$  cells for stable transfection were seeded in one 6-well plate at a density of 2x10<sup>5</sup> cells/ml per well in 2ml medium without antibiotic G418. The transfection was carried out the following day in serum-free medium with lipofectamine 2000 reagent according to manufacturer's protocol. For each well, 4  $\mu$ g of plasmid DNA in 125  $\mu$ l of OPTI-MEM<sup>®</sup>I Reduced Serum Medium without

serum was transfected using 10  $\mu$ l of Lipofectamine 2000 Reagent. Thus the ratio of lipofectamine to plasmid is 5:2 (Fig. 36). Cells were incubated with precipitated DNA for 24 hours. The medium was removed. After washing in PBS, the cells were trypsinized. After cell counting using the Trypan blue exclusion method, the cells were distributed to 96-well plates, 1cell per well. Three days later, the cells were selected in puromycin and neomycin containing medium, 20 $\mu$ g/ml puromycin (Brunschwig, Basel, Switzerland) and 0.4mg/ml G418. The cell medium was changed twice per week.

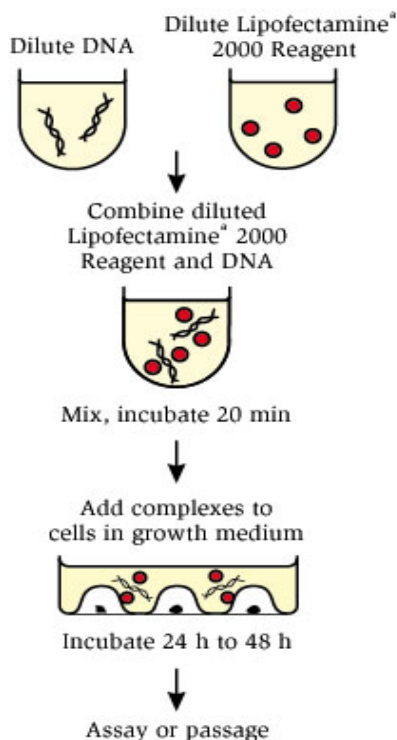


Fig 36. DNA transfection process by Lipofectamine 2000 reagent. It is one fast and efficient transfection method. In brief, diluted DNA and Lipofectamine 2000 reagent were mixed and incubated at room temperature for 20 minutes. And then the complexe was added to cells in growth medium for 24h up to 48h.

Individual colonies were picked from 96-well plates and tested for fibrinogen antibody detection. Positive cell lines were kept. The cell lines which expressed the highest quantity of truncated fibrinogen were grown to confluence and stored in a liquid nitrogen container. Large-scale cell growth was performed in a 10-layer cell factory Nunclon™ $\Delta$  (Milian, USA) in serum free

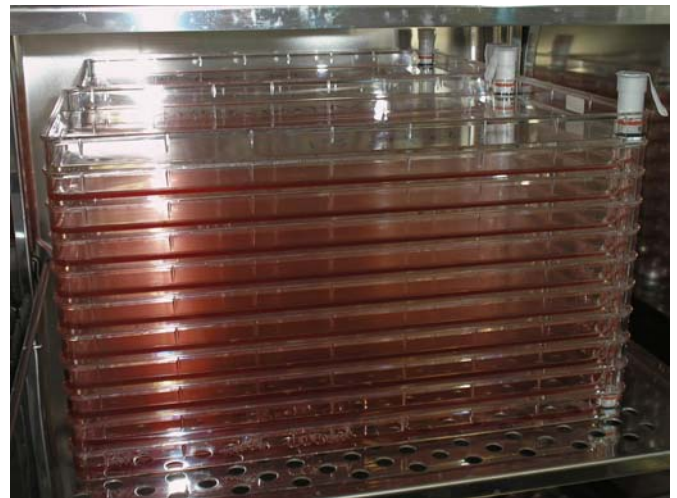


Fig 37. Large-scale cell growth in 10-layer cell factory Nunclon™ $\Delta$ . The surface equals to 36xT-175 flasks. Thus it is one space saving cell culture device, easy change of medium, single-use and sterile. It is excellent for large-scale recombinant protein production from mammalian cells.

DMEM/F12 supplemented with 1% PS, 10U/ml Aprotinin (Roche, Basel, Switzerland) and 1mg/100ml ITS for truncated fibrinogen production (Fig. 37).

### **Immunostaining detection and FACS**

For immunostaining, 0.1 million cells were seeded overnight in one 12-well plate. Immunostaining was carried out using a goat anti-human fibrinogen (MP Biomedicals, USA) as the primary antibody and Alexa Fluor 488 donkey anti-goat IgG (H+L) as the secondary antibody. BD Cytfix/Cytoperm fixation/permeabilization kit (BD, Basel, Switzerland) was used for the staining process. Each sample was added to four wells on the plate. To the first well, 0.5 $\mu$ l of primary antibody was added while 1.5 $\mu$ l primary antibody was added into the second well. In the third well, no primary antibody was added. In the fourth well, no secondary antibody was added. The last two wells were there to act as negative controls. Finally PFA 1% solution was added for fixation. FACS was used to characterize the cell population of each group using CyAn™ ADP flow cytometer (Dakocytomation, Glostrup, Denmark). Data was acquired using Summit® software and analysed with FlowJo® software.

### **ELISA (enzyme-linked immunosorbent assay)**

Expressed truncated fibrinogen from CHO<sub>FGA5aa-IGF1</sub> and CHO<sub>FGA5aa-MMP-IGF1</sub> cell lines were analyzed by a sandwich ELISA for assembly capacity. An ELISA assay of the conditioned media was carried out in triplicate as described previously<sup>10, 11</sup>. Briefly, 96-well assay plates (Milian, USA) were bound with IgG fraction goat anti-human fibrinogen capture antibody (MP Biomedicals, USA) with a dilution of 1:1000 at room temperature for 1 hour. After washing three times in PBST (0.05% Tween-20 in PBS, pH 7.4), the plates were blocked with 1% BSA (Sigma, Switzerland) in PBS for 30 minutes at room temperature. The conditional medium which was collected after 24 hours was incubated in plates at room temperature for 2 hours. The plates were detected using the goat anti-human fibrinogen peroxidase-conjugated detection antibody (MP Biomedicals, USA) and TMB peroxidase substrate. Color was developed and plates were read at 450nm.

For human IGF1 ELISA, the Quantikine Human IGF-1 immunoassay kit (R&D, USA) was used according to the manufacturer's protocol.

## Fibrinogen-IGF1 protein production and purification

Recombinant chimeric fibrinogen-IGF1 fusion protein expressed by CHO cells was secreted in the cell medium. During large-scale protein production, one liter of ITS cell medium was collected every seven days from the 10-layer cell factory. The same batch of CHO cells could produce the fusion protein for one month. EDTA-free protease inhibitor (Roche) was added to avoid fusion protein degradation. Recombinant fibrinogen was precipitated slowly at 4°C from the medium with saturated ammonium sulphate which reached a final concentration of 40%. After centrifugation at high speed (12000xg for 50 minutes at 4°C), the supernatant was discarded carefully to avoid disturbing the pellets. The pellets were then redissolved in 50ml HBSS containing Ca<sup>2+</sup> and Mg<sup>2+</sup> and applied to a thiopropyl Sepharose 4B column 5ml coupled with peptide AAGPRP<sup>12</sup>, specific for fibrinogen.

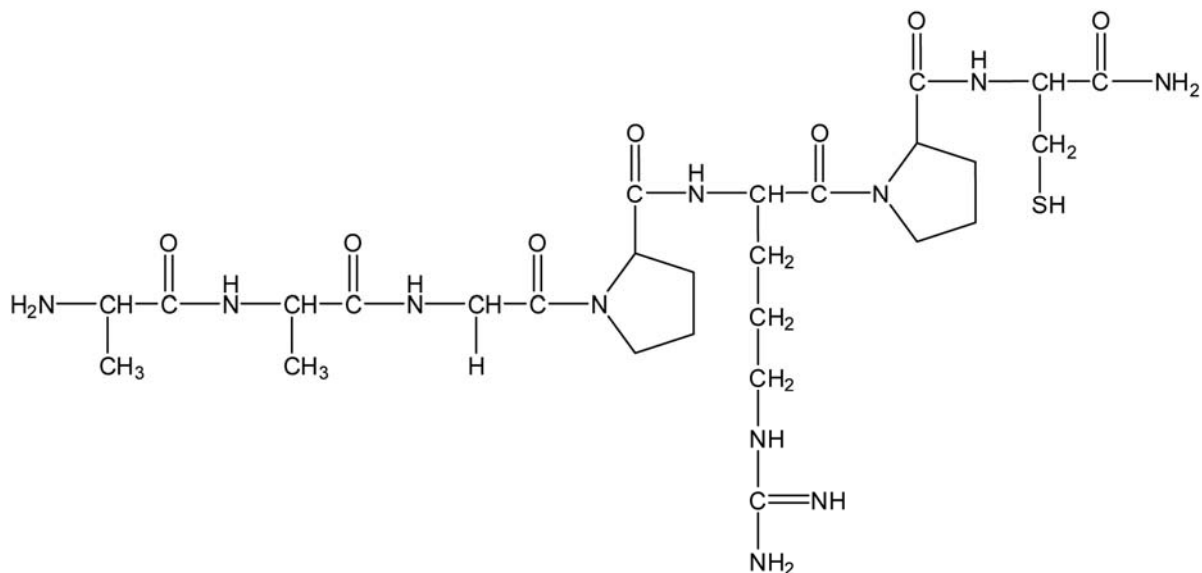


Fig 38. The peptide AAGPRPC structure. A cysteine was added at the carboxy (C) terminus of peptide GPRP (that is, GPRPC) for conjugation to the functional groups presented in the thiopropyl Sepharose 4B polymers via the free thiol through Michael-type addition<sup>13</sup>. Two alanines acted as protection group and added at the N-terminus of the peptide GPRP.

The AAGPRP peptide (Fig. 38) was synthesized in the lab using standard Fmoc chemistry. A cysteine was added at the C-terminal end of the peptide for conjugation to the functional groups that are present in the thiopropyl Sepharose 4B polymers. In brief, 334mg of thiopropyl Sepharose 4B (GE Healthcare Bio-Sciences) was prepared according to the manufacturer's

instructions to give a 1ml gel. 30mg of peptide, AAGPRP, was immobilized in the gel. After washing, the column was stored at 4°C cold room and ready for mutant fibrinogen purification.

For purification, the binding buffer was 0.1M HEPES with 20mM CaCl<sub>2</sub>, pH7.4. The washing buffer was HBSS containing Ca<sup>2+</sup> and Mg<sup>2+</sup>. The elution buffer was 1M NaBr and 50mM NaAc, pH5.3. During elution, pH value of the buffer was 5.3, which was too acidic for fibrinogen. So, several drop of 1M HEPES was added in each elution tube to adjust the pH to 7.4, which required 10μl of 1M HEPES for each 1ml of elution buffer.

The recombinant fibrinogen concentration was determined at A<sub>280</sub> using the extinction coefficient ε<sub>280</sub>=1.506 for a 1mg/ml fibrinogen solution. The purity of the proteins was analyzed by 9% reducing SDS-polyacrylamide gel electrophoresis.

## Results and discussion

### Gene cloning and vector construction

All PCR amplification requires the use of cDNA templates, two primers, Ampli Taq Gold DNA polymerase (Applied Biosystems), deoxynucleoside triphosphates (dNTP) and Mg<sup>2+</sup>. The amplified PCR products with predicted size of about 500bp were observed in lane 2 (Fig. 39) by 1% agarose gel. If there were no cDNA templates or no primers in the PCR amplification solution, then no PCR product band was visible (lane 3 and 4).

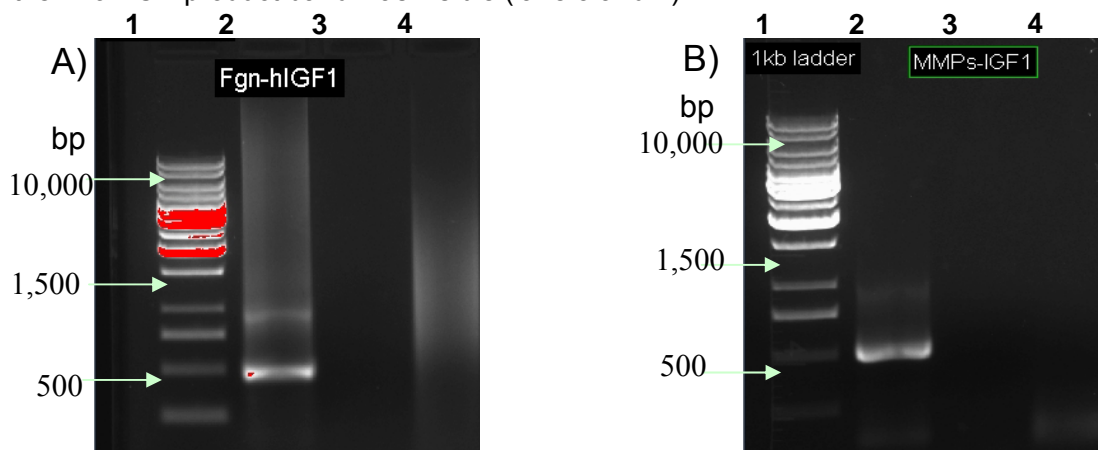


Fig 39. PCR amplification fragment of human IGF1 insert about 500bp showed on a 1% w/v agarose gel. A) plasmid pMYKpuro<sub>FGA5aaIGF1</sub> (left); B) plasmid pMYKpuro<sub>FGA5aaMMPsIGF1</sub> (right); lane 1: Commercial 1kb DNA ladder; lane 2: PCR with both cDNA and primers; lane 3: PCR with cDNA and without primers; lane 4: PCR with primers and without cDNA. Lanes 3 and 4 were the negative controls. It was showed that only one band at lane 2 was visible.



After cloning, the plasmids of pMYKpuro<sub>FGA5aaIGF1</sub> and pMYKpuro<sub>FGA5aaMMPIGF1</sub> were transformed into subcloning Efficiency<sup>®</sup> DH5 $\alpha$ <sup>™</sup> Competent cells (chemical competent cells) for clone selection. Using designed primers (Table 6) and PCR amplification, partial insert fragments were analyzed on 1% Agarose gel using GeneRuler<sup>™</sup> 1kb DNA ladder (Fermentas). Selected clones were due to one visible band at about 250bp, such as clones 3 and 6 of pMYKpuro<sub>FGA5aaIGF1</sub> and clones 2 and 3 of pMYKpuro<sub>FGA5aaMMPIGF1</sub> (Fig. 40). According to DNA sequence results from Microsynth, clones 3 and 6 of pMYKpuro<sub>FGA5aaIGF1</sub> and clone 2 of pMYKpuro<sub>FGA5aaMMPIGF1</sub> had the right DNA sequences expected, which would be used for mammalian cells transfection.

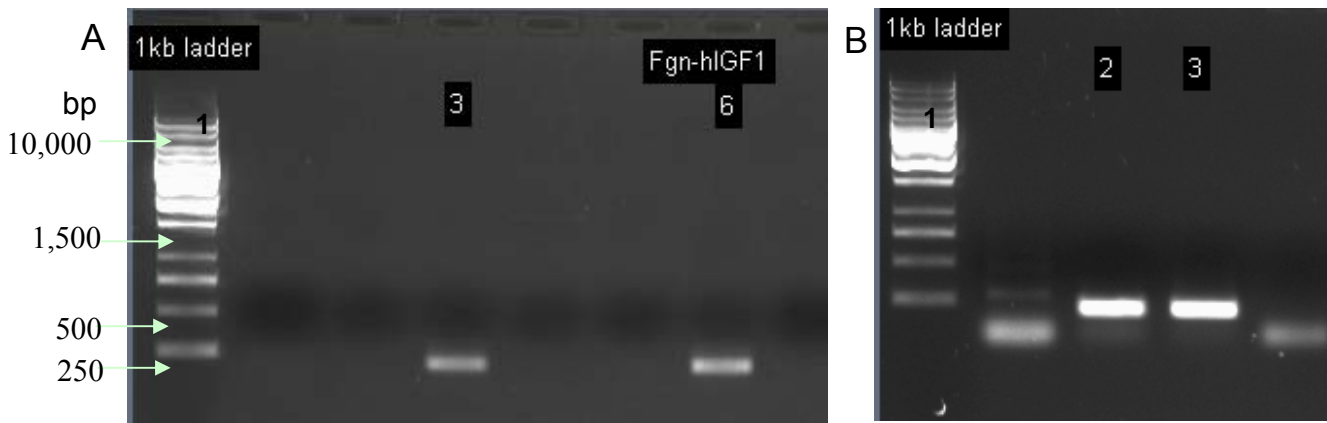


Fig 40. Clones screening by PCR amplification using designed primers on a 1% w/v agarose gel. A) plasmid pMYKpuro<sub>FGA5aaIGF1</sub> (left); B) plasmid pMYKpuro<sub>FGA5aaMMPIGF1</sub> (right). The DNA size marker is a commercial GeneRuler<sup>™</sup> 1kb ladder (lane 1). A band about 250bp was visible at clones 3 and 6 of plasmid pMYKpuro<sub>FGA5aaIGF1</sub> and at clones 2 and 3 of plasmid pMYKpuro<sub>FGA5aaMMPIGF1</sub>.

Table 6 Primers used for plasmids clones selection.

Plasmid construction/primer name	Oligonucleotide sequences (5' → 3')
pMYKpuro <sub>FGA5aaIGF1</sub> :	
fgnhIGFliftprimer	GAAACGACTGGAGGTGGACATTG
fgnIGFrevprimer	GGTAGAAGAGATGCGAGGAGGAC
pMYKpuro <sub>FGA5aaMMPIGF1</sub> :	
fgnhIGFliftprimer	GAAACGACTGGAGGTGGACATTG
MMPIGFrevprimer	GGTAGAAGAGATGCGAGGAGGAC

## Cell lines analysis

Transfected CHO cells were cultured in the selection medium containing puromycin and G418 to eliminate cells non-transfected for two months. Fibrinogen ELISA was effectuated once per week to check fibrinogen expression by different truncated fibrinogen CHO cell lines. After selection based on several consecutive fibrinogen ELISA results, the cells that expressed most truncated chimeric fibrinogen were transferred and grown in 10cm plates. Using these cells, highest quantity of fibrinogen could be obtained at the same volume of medium. Because transfected CHO cell lines intend to reject the transfected plasmid, it is important to keep several cell clones of same cell line.

Because during manipulation it was difficult to distribute exactly one cell per well in 96-well plates, it was important to analyze the cell population of each cell line to be sure that these cell lines originated from the same cell. The goal was to guarantee the optimal fibrinogen production by these cells. The monoclonal cell line was characterized by FACS. Because the truncated fibrinogen was expressed and secreted by the cells, the immunostaining process was more straightforward compared to the analysis of the whole cell lysate method.

According to FACS results (Fig. 41), three cell lines CHO<sub>FGA5aa</sub>, CHO<sub>FGA5aaIGF1</sub> and CHO<sub>FGA5aaMMPIGF1</sub> were all monoclonal due to only one cell population peak, in the blue colour. It meant that the cells had the same profile of fibrinogen expression. So, these cell lines were stored in liquid nitrogen for further truncated fibrinogen production.

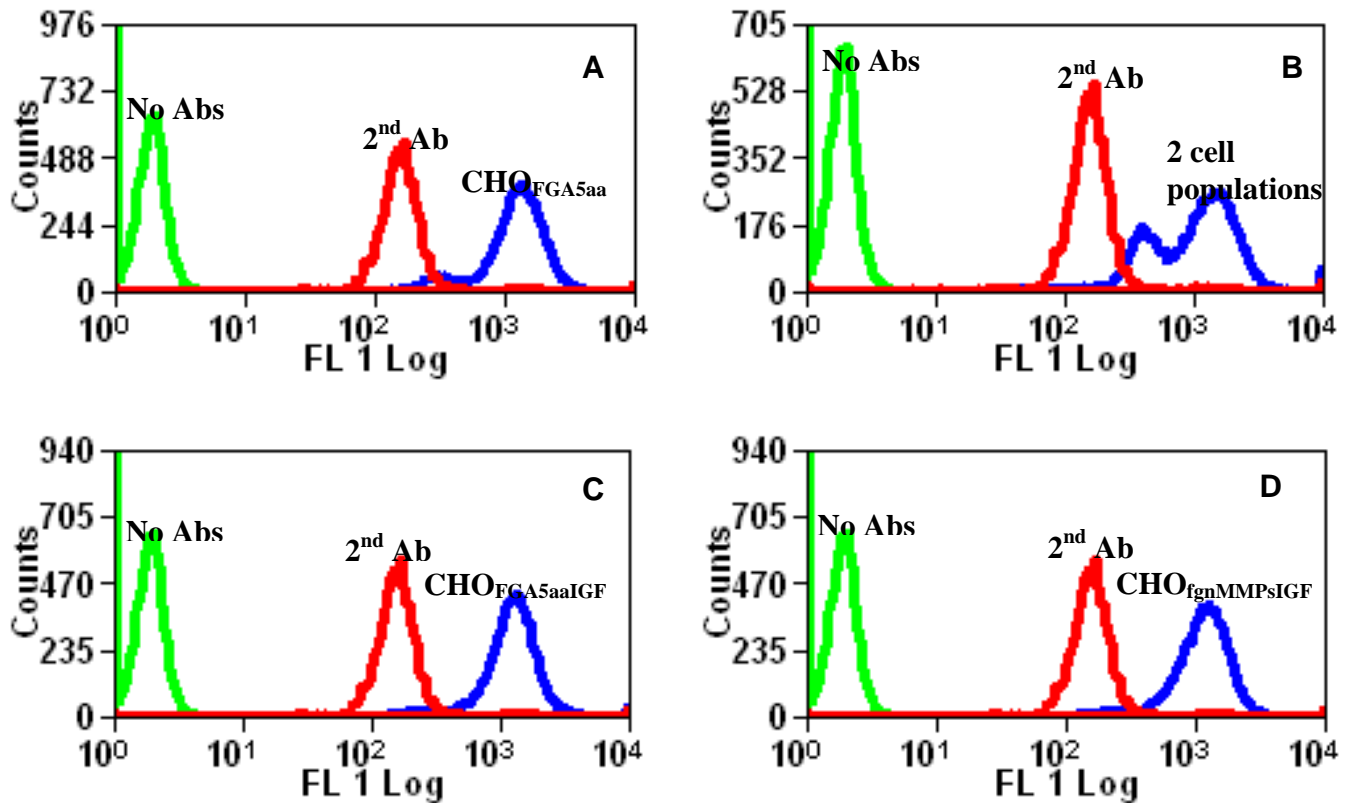


Fig 41. FACS characterisation of monoclonal cell line. A)  $\text{CHO}_{\text{FGA5aa}}$  cell line; B) mixing 2 cell lines together; C)  $\text{CHO}_{\text{FGA5aaIGF1}}$  cell line; D)  $\text{CHO}_{\text{FGA5aaMMPIGF1}}$  cell line. The first peak (green) represents the population of cells non-stained, neither first nor second antibodies added. The second peak (red) represents the population of cells stained with second antibody only. The third peak (blue) represents the population of cells stained with both first and second antibodies. The cell population in the first and second peaks is used as negative control. Note that there are 2 peaks for 2 cell populations for cell line B. Three cell lines, A, C, and D, representing  $\text{CHO}_{\text{FGA5aa}}$ ,  $\text{CHO}_{\text{FGA5aaIGF1}}$  and  $\text{CHO}_{\text{FGA5aaMMPIGF1}}$  were all monoclonal due to one cell population peak (blue). Ab: antibody

### Characterization of recombinant fusion protein secretion

In 10cm plates, 1 million  $\text{CHO}_{\text{FGA5aaIGF1}}$  and  $\text{CHO}_{\text{FGA5aaMMPIGF1}}$  cells were seeded separately and inoculated for 36 hours in ITS medium for fusion protein production. Then ELISA was performed to quantify the production of the fusion proteins fibrinogen-IGF1 by CHO cells. Each sample was made in triplicate.

According to the ELISA results (Table 7 and Fig. 42), the quantity of truncated fibrinogen expressed by the two cell lines was about the same, around 0.025 $\mu$ g/ml. But the quantity of truncated IGF1 detected by antibody was very different, 0.157 ng/ml for CHO<sub>FGA5aaIGF1</sub> cells and 1.65 ng/ml for CHO<sub>FGA5aaMMPIGF1</sub> cells. For the stoichiometric concentration ratio of fibrinogen to IGF1, we observed 15.8 for CHO<sub>FGA5aaIGF1</sub> cell line and 152.8 for CHO<sub>FGA5aaMMPIGF1</sub> cell line. So, CHO<sub>FGA5aaMMPIGF1</sub> cells expressed the more immune-reactive IGF1 than CHO<sub>FGA5aaIGF1</sub> cells. It seemed that the protein structure of Fgn-MMP-IGF1 was more flexible than that of Fgn-IGF1 due to the MMP linker between fibrinogen and IGF1. We believe that adding the MMP linker in the fusion protein increased the enzymes invasion and improved antibody detection.

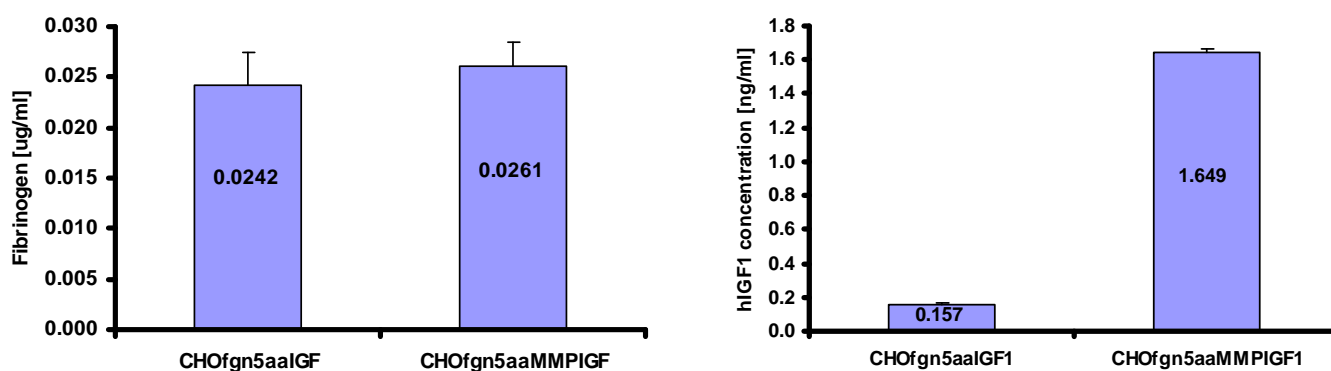


Fig 42. The concentration of protein expressed by CHO<sub>FGA5aaIGF1</sub> and CHO<sub>FGA5aaMMPIGF1</sub> cell lines was detected by antibody using a fibrinogen ELISA (left) and a hIGF1 ELISA (right). It showed that according to ELISA results, for both cell lines fibrinogen expression was similar and that hIGF1 expression was significantly different. The quantity of hIGF1 expressed by CHO<sub>FGA5aaMMPIGF1</sub> cell line was much higher than that by CHO<sub>FGA5aaIGF1</sub> cell line, 1.649ng/ml and 0.157ng/ml respectively.

Table 7. Protein concentration detected by antibody

Cell line	Fibrinogen		IGF1	
	Concentration [µg/ml]	SD	Concentration [ng/ml]	SD
CHO <sub>FGA5aaIGF1</sub>	0.0242	0.0033	0.157	0.0065

## Truncated chimeric fibrinogen purification

The purification of recombinant fibrinogen from conditioned serum-free media (SFM) was achieved by two steps in a 4°C cold room. The first step was to precipitate the recombinant fibrinogen from SFM via saturated ammonium sulphate. The second step was using fast protein liquid chromatography (FPLC) (GE Healthcare, USA). An AAGPRP affinity column was made using a Sepharose 4B column coupled with the peptide AAGPRP synthesized in the lab. The idea of using the peptide AAGPRP was from the fibrinogen coagulation cascade. When thrombin cleaved amino termini of fibrinogen A $\alpha$ - and B $\beta$ -chains, the exposed N-terminal of A $\alpha$ -chain was Gly-Pro-Arg-Val (GPRV) and that of B $\beta$ -chain was Gly-His-Arg-Pro (GHRP). This step activated fibrinogen coagulation cascade to fibrin polymerization. So, the modified Gly-Pro-Arg-Pro (GPRP) was used to binding fibrinogen<sup>12, 14-16</sup>. But due to GPRP similar to GPRV, which played an important role in the fibrinogen coagulation process, fibrinogen polymerized in the AAGPRP affinity column during purification. In Fig. 43, one visible elution peak was observed. But when the eluted samples were analyzed by SDS-PAGE on 10% gels and stained with SimplyBlue™ SafeStain, there was no band visible on the gel.

To avoid fibrinogen polymerization during purification, monoclonal fibrinogen antibody IF-1 affinity chromatography was proposed<sup>17-19</sup>. IF-1 was purchased from Kamiya Biomedical Company (Thousand Oaks, California). The purification was in development in Prof. Thomas Barker's lab at Georgia Tech. Recombinant fibrinogen was precipitated with saturated ammonium sulphate. The pellets were then redissolved in buffer containing 10mM CaCl<sub>2</sub> and applied to a Sepharose 4B column coupled with monoclonal antibody IF-1, specific for fibrinogen. Fibrinogen was eluted with a buffer containing 5 mM EDTA; dialyzed against 20mM HEPES (pH 7.4), 150mM NaCl, and 1mM CaCl<sub>2</sub> for one change and then extensively against 20mM HEPES (pH 7.4) and 150mM NaCl; and stored at -70°C. The fibrinogen concentration would be determined at A<sub>280</sub> using the extinction coefficient  $\epsilon_{280}=1.506$  for a 1mg/ml fibrinogen solution. Purity of the proteins would be analyzed by 9% reducing SDS-polyacrylamide gel electrophoresis.

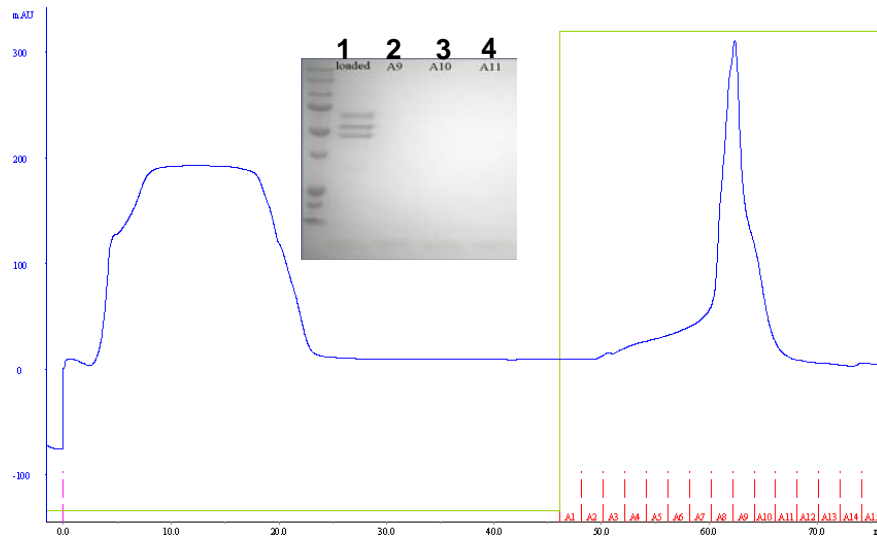


Fig 43. Purification of recombinant fibrinogen by AAGPRP affinity chromatography. The first peak represents flow through. The second peak represents eluate. The eluted fractions were collected separately and shown on stained 10% reducing polyacrylamide SDS-PAGE (lanes 2, 3 and 4). Lane 1: starting material. Molecular weight marker is a commercial prestained protein ladder. It showed no band on the gel, which means no purified recombinant fibrinogen obtained.

## Conclusion

Fibrinogen (Fgn), a soluble plasma protein found in all vertebrates, is a covalent dimer composed of pairs of three polypeptide chains called  $A\alpha$ -,  $B\beta$ - and  $\gamma$ -chains. Fibrinogen  $A\alpha$  chain can be truncated to amino acid 189 while maintaining the capacity to be assembled into a secreted, detectable fibrinogen. It is feasible to produce recombinant chimeric fibrinogen, which directly incorporates, at the genetic level, growth factors of interest into fibrin matrices. We believe this new generation of the fibrin delivery system represents a significant advance over current delivery systems. This novel approach could allow for near-complete incorporation of protein species into fibrin polymers resulting in high levels of control over the delivered protein factor.

Human IGF1 was chosen for its simple active form (single chain) and low molecular weight (10kDa). The modified plasmids DNA containing FGA5aa-hIGF1 and FGA5aa-MMP-hIGF1 were transfected into CHO $_{\beta\gamma}$  cells separately using Lipofectamine 2000 reagent, followed by puromycin selection. Fibrinogen ELISA was used to select the optimal truncated fusion protein expression clone of cell lines. The optimal stable cell lines CHO $_{\text{FGA5aaIGF1}}$  and CHO $_{\text{FGA5aaMMPIGF1}}$  were characterized by ELISA with fibrinogen and human IGF1 antibody and by FACS. During

the characterization of the cell lines, it was found that the fusion protein structure of fgn-MMP-IGF1 was more immune-reactive than that of fgn-IGF1 because the stoichiometric concentration ratio of fibrinogen to hIGF1 for the CHO<sub>FGA5aaMMPIGF1</sub> cell line was closer to the expected value. The optimal cell lines were monoclonal as observed by FACS, growing from the same single cell. These cell lines were chosen for the production of recombinant chimeric fibrinogen hIGF1 fusion protein.

Recombinant fibrinogen was secreted in the production medium by CHO cells due to the secretion genes in the expression vector. Fibrinogen was precipitated preliminarily from the cell medium, and collected with 40% saturated ammonium sulphate. We then tried to purify the recombinant truncated fibrinogen by AAGPRP affinity chromatography according to the literature. Due to fibrinogen polymerization in the column during purification, we switched to an IF-1 affinity column. The monoclonal antibody IF-1, specific for fibrinogen, was coupled in a Sepharose 4B column. Purified recombinant fibrinogen was analyzed by SDS-PAGE under reducing conditions at 10% gel. When the gels were stained with Coomassie blue, there should be three bands representing mutant A $\alpha$ -(41kDa), B $\beta$ -(55kDa) and  $\gamma$ -(47.5kDa) chains. Finally, the purified recombinant fibrinogen should be analyzed by western blot and the amino acid sequence would be confirmed by mass spectrometry.

The purification process for the recombinant fibrinogen variants is still under development. When the recombinant fibrinogen is purified, the bioactivity analysis will be performed, such as the clotting assay (fibrinogen polymerization) and cell proliferation assay (for the hIGF1 component). This still requires additional development.

### ***Acknowledgement***

The p584 A $\alpha$  plasmid and CHO <sub>$\beta\gamma$</sub>  cell line are kindly provided by prof. Dr. Susan Lord, Department of Chemistry, University of North Carolina at Chapel Hill, Chapel Hill, NC 27599, USA.

I would like to thank Prof. Aebischer for the cDNA of human IGF1.

I am grateful to Prof. Thomas Barker for teaching me cell line isolation, FACS and AAGPRP affinity chromatography for fibrinogen purification.

## Reference

1. Kodama, M. et al. Role of D and E domains in the migration of vascular smooth muscle cells into fibrin gels. *Life Sci* **71**, 1139-1148 (2002).
2. Walker, J.B. & Nesheim, M.E. The molecular weights, mass distribution, chain composition, and structure of soluble fibrin degradation products released from a fibrin clot perfused with plasmin. *J Biol Chem* **274**, 5201-5212 (1999).
3. Sakiyama-Elbert, S.E. & Hubbell, J.A. Controlled release of nerve growth factor from a heparin-containing fibrin-based cell ingrowth matrix. *J Control Release* **69**, 149-158 (2000).
4. Schense, J.C., Bloch, J., Aebischer, P. & Hubbell, J.A. Enzymatic incorporation of bioactive peptides into fibrin matrices enhances neurite extension. *Nat Biotechnol* **18**, 415-419 (2000).
5. Zisch, A.H., Schenk, U., Schense, J.C., Sakiyama-Elbert, S.E. & Hubbell, J.A. Covalently conjugated VEGF--fibrin matrices for endothelialization. *J Control Release* **72**, 101-113 (2001).
6. Doolittle, R.F. & Wooding, G.L. The subunit structure of lamprey fibrinogen and fibrin. *Biochim Biophys Acta* **371**, 277-282 (1974).
7. Yang, Z., Mochalkin, I., Veerapandian, L., Riley, M. & Doolittle, R.F. Crystal structure of native chicken fibrinogen at 5.5-A resolution. *Proc Natl Acad Sci U S A* **97**, 3907-3912 (2000).
8. Yang, Z., Kollman, J.M., Pandi, L. & Doolittle, R.F. Crystal structure of native chicken fibrinogen at 2.7 A resolution. *Biochemistry* **40**, 12515-12523 (2001).
9. Rizzi, S.C. & Hubbell, J.A. Recombinant protein-co-PEG networks as cell-adhesive and proteolytically degradable hydrogel matrixes. Part I: Development and physicochemical characteristics. *Biomacromolecules* **6**, 1226-1238 (2005).
10. Binnie, C.G., Hettasch, J.M., Strickland, E. & Lord, S.T. Characterization of purified recombinant fibrinogen: partial phosphorylation of fibrinopeptide A. *Biochemistry* **32**, 107-113 (1993).
11. Snouwaert, J.N., Kariya, K. & Fowlkes, D.M. Effects of site-specific mutations on biologic activities of recombinant human IL-6. *J Immunol* **146**, 585-591 (1991).
12. Kostelansky, M.S., Betts, L., Gorkun, O.V. & Lord, S.T. 2.8 A crystal structures of recombinant fibrinogen fragment D with and without two peptide ligands: GHRP binding



- to the "b" site disrupts its nearby calcium-binding site. *Biochemistry* **41**, 12124-12132 (2002).
13. Lutolf, M.P. & Hubbell, J.A. Synthesis and physicochemical characterization of end-linked poly(ethylene glycol)-co-peptide hydrogels formed by Michael-type addition. *Biomacromolecules* **4**, 713-722 (2003).
  14. Laudano, A.P. & Doolittle, R.F. Synthetic peptide derivatives that bind to fibrinogen and prevent the polymerization of fibrin monomers. *Proc Natl Acad Sci U S A* **75**, 3085-3089 (1978).
  15. Laudano, A.P. & Doolittle, R.F. Studies on synthetic peptides that bind to fibrinogen and prevent fibrin polymerization. Structural requirements, number of binding sites, and species differences. *Biochemistry* **19**, 1013-1019 (1980).
  16. Yamazumi, K. & Doolittle, R.F. The synthetic peptide Gly-Pro-Arg-Pro-amide limits the plasmin digestion of fibrinogen in the same fashion as calcium ion. *Protein Sci* **1**, 1719-1720 (1992).
  17. Lord, S.T., Strickland, E. & Jayjock, E. Strategy for recombinant multichain protein synthesis: fibrinogen B beta-chain variants as thrombin substrates. *Biochemistry* **35**, 2342-2348 (1996).
  18. Gorkun, O.V., Veklich, Y.I., Weisel, J.W. & Lord, S.T. The conversion of fibrinogen to fibrin: recombinant fibrinogen typifies plasma fibrinogen. *Blood* **89**, 4407-4414 (1997).
  19. Mullin, J.L., Gorkun, O.V., Binnie, C.G. & Lord, S.T. Recombinant fibrinogen studies reveal that thrombin specificity dictates order of fibrinopeptide release. *J Biol Chem* **275**, 25239-25246 (2000).



## **Chapter IV Local delivery and controlled release insulin-like growth factor-1 for bladder muscle regeneration**

### ***Summary***

Human insulin-like growth factor-1 (IGF1) has been under investigation by biotech companies for decades because of its potential therapeutic functions. But the wide application of IGF1 in clinical trials has been discouraged by its deleterious side effects due to the required high frequency of dosing and concentration used for treatment. The controlled release of IGF1 to mimic physiological patterns is considered a promising approach. In this study, local delivery and controlled release of IGF1 in fibrin-based biomaterials are investigated. A novel fusion protein (TG-IGF1) was designed with one transglutaminase enzyme factor XIIIa substrate for covalent crosslinking into fibrin gels at the N-terminus and the bioactive part of native IGF1 at the C-terminus. Determined by one commercial IGF1 ELISA kit, the quantity of purified TG-IGF1 obtained per liter bacteria culture was about 5ug. The sequence of the purified fusion protein was confirmed by MALDI-TOF mass spectrometry. The bioactivity of the fusion protein was analyzed *in vitro* compared with recombinant native IGF1. The cell proliferation profile was similar for both wild-type and engineered IGF1 proteins using the metabolic MTT assay. An assay for IGF receptor tyrosine phosphorylation showed that both wild-type and engineered IGF1 proteins were bioactive and activated the IGF receptor. In a three-dimensional model, neonatal human bladder smooth muscle cells (SMCs) were seeded in the fibrin gel incorporated with TG-IGF1 and recombinant native IGF1 respectively. The morphology of the seeded cells was analysed ultra-structurally using transmission electron microscopy (TEM) 3 days after inoculation. According to the morphology of cells seeded in the fibrin gel only, the cells with TG-IGF1 displayed larger and more secretory vesicles than those with recombinant native IGF1 due to the rapid diffusion of the recombinant native IGF1 from the fibrin gel. Confocal imaging revealed that both wild-type and engineered IGF1 proteins did not stimulate neonatal SMCs to form elastin in the fibrin gel after 5 days. The response of the bladder SMCs in the fibrin gel to the IGF1 fusion and native protein was analyzed by qRT-PCR for extracellular matrix and adhesion molecules 24 hours after inoculation. The bladder SMCs in the fibrin gel without any IGF1 was used as control. No statistical difference for gene expression between those cells was noticed. These data demonstrate that TG-IGF1 is fully bioactive, and additionally by design has the beneficial ability to be entrapped within and released from fibrin gels.

The experiment *in vivo* assessed in smooth muscle repair in rat bladder model, in which a resection of the muscle was made. Fibrin gels incorporating TG-IGF1 or (free) recombinant native IGF1 were applied directly on the top of the tissue defected. The fibrin gel without any IGF1 was utilized as negative control. After 28 days, the rats were sacrificed, and the bladders were formaldehyde-fixed and permeabilized. After bladders were paraffin-bedded and sectioned, three histological stainings were made, Hematoxylin & Erythrosine (HE), Masson's Trichrome (TM) and Prussian Blue (PB). All histological images taken were approved by pathologist Dr. Taminelli. The histological staining revealed that the rats treated by fibrin gels containing TG-IGF1 displayed bladder muscle layer regeneration without fibrosis formation which was a superior result compared to the control groups. Due to complete fibrin gel degradation, no bioactive IGF1 was remained after tissue repair. Thus, its systemic side effects were limited. The area of muscle regenerated was quantified blindly with Dr. Hasegawa using program Fiji according to images taken previously. The value was normalised by the area of muscle intact in the same bladder section. It showed that detrusor muscle layer was regenerated about 27% (second experiment) up to 31% (first experiment) for TG-IGF1 compared to 23% (second experiment) for recombinant native IGF1. The percentage of detrusor muscle regenerated for two control groups was around 10%.

## ***Introduction***

In 1957, IGF1 was discovered by Samon and Daughaday<sup>1, 2</sup> as a sulphation factor. In 1972, IGF1 received its second name as somatomedin<sup>3</sup> because of the relationship between IGF1 and growth factor (GH). In 1976, IGF1 received its current name due to its bioactive presence in serum and its similar structure to insulin<sup>4</sup>. From then on, more and more functions of IGF1 have become known. IGF1 is secreted by many tissues and affects nearly every cell in the human body. IGF1 plays an important role in growth<sup>5</sup>. IGF1 deficiency during childhood results in growth retardation and impaired skeletal development<sup>6, 7</sup>. IGF1 has an amino acid sequence similar to insulin and can bind to the insulin receptor. So, it has insulin-like activity, such as increasing glucose uptake by peripheral tissues<sup>8, 9</sup>. Use of IGF1 treatment in clinical trials has been shown to improve glucose metabolism, reduce the need of insulin for insulin-dependant diabetic patients, increase insulin sensitivity and limit related obesity<sup>10, 11</sup>. In addition, IGF1 can regulate cell growth and proliferation. Cells need IGF1 to complete the cell cycle through G1 to S phase<sup>12-14</sup>. IGF1 can also increase the probability of cancer cell survival through the IGF1 receptor<sup>15-17</sup>. Use of the IGF1 receptor inhibitors is being investigated in cancer patients<sup>18</sup>. Furthermore, IGF1 can protect neurons of the peripheral nervous system (PNS) from apoptosis

<sup>19, 20</sup>. IGF1 could also be used in life-threatening situations, such as with burns and postsurgical trauma <sup>20</sup>. Finally, IGF1 can accelerate skeletal muscle regeneration and maintain skeletal muscle structure and function <sup>21-23</sup>. These are the reasons that IGF1 is one of most studied growth factors in the body. Its wide applications in the clinic have been investigated since 1987 <sup>24</sup>, but due to severe side effects observed during treatment, the quantity of IGF1 used and the exposure duration of IGF1 to injured tissues have to be resolved.

Currently, biomaterials are commonly used for the controlled release of IGF1, such as silk fibroin embedding PLGA <sup>25</sup> and hyaluronan (HA) <sup>26</sup>. In this work fibrin matrices, which is FDA approved as a biomaterial for tissue hemostasis (Tisseel VH kit, Baxter AG), were used as scaffold. An advantage of fibrin as a system as we propose it for implementation used is that IGF1 can incorporate covalently into the fibrin matrices instead of simple entrapment, because of the addition of a small peptide group called TG. TG is the first eight amino acids of the  $\alpha_2$ -plasmin inhibitor ( $\alpha_2$ PI<sub>1-8</sub>), sequence NQEQVSPL <sup>27, 28</sup>. It is also the substrate for the Factor XIIIa, which is the transglutaminase enzyme for fibrinogen coagulation <sup>29</sup>. Thrombin, calcium and Factor XIIIa catalyze fibrinogen polymerization to form a three dimensional matrix. Factor XIIIa can cross-link proteins bearing the TG sequence to fibrin during matrix polymerization. This system provides a direct and strong binding between IGF1 and the fibrin matrix and therefore eliminates the possibility of IGF1 diffusing out of the formed gel. When cells invade the fibrin matrix, plasmin and matrix metalloproteinases (MMPs) are produced and activated by the leading edge of the cells. These enzymes degrade the fibrin matrix around the invaded cells, and liberating the bound IGF1. The rest of the matrix including the IGF1 bound inside is left intact due to no cells having invaded yet, until the cells invade the entire matrix and replace it as new tissue growth <sup>29, 30</sup>. In this way, the fibrin matrix can “release” IGF1 during a short-term period until the injured tissue regenerates or is repaired. For this system, a mutant IGF1 protein containing one Factor XIIIa substrate  $\alpha_2$ -PI<sub>1-8</sub> at N-terminus should be made.

The injured tissue chosen for this work was the bladder wall. The bladder is a very elastic organ. Urine is filled and expelled several times per day, in volumes up to 500ml each time. The elasticity of the bladder wall comes from the detrusor muscle layer <sup>31</sup>. The peripheral neurons are also important to its physiological function <sup>32</sup>. Surgical or traumatic injury and disease, which induce bladder wall dysfunction, require muscle layer regeneration with the participation of smooth muscle cells (SMCs) <sup>33, 34</sup>. IGF1 can stimulate SMC growth and proliferation through the integrin  $\alpha_v\beta_3$  <sup>35-37</sup>, prevent neuronal apoptosis and improve the injured neuron repair <sup>23</sup>. IGF1 is also known to improve heart function, regenerate injured heart muscle (Fig. 44) <sup>38</sup> and

accelerate injured skeletal muscle and neuron repair<sup>21, 23</sup>. However chronic IGF1 administration can induce pathologic cardiac hypertrophy and fibrosis<sup>39, 40</sup>. The purpose of this study was to examine injured bladder muscle regeneration using IGF1 cross-linked fibrin gels delivered locally at the site of injury.

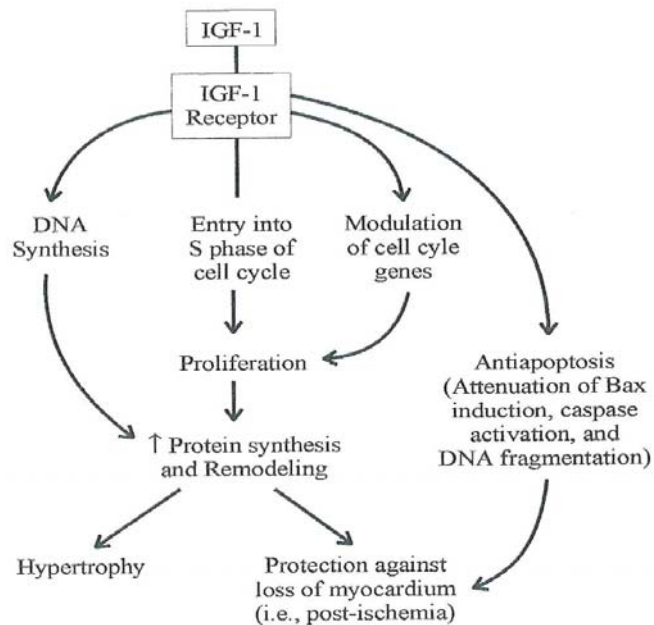


Fig 44. Schematic drawing showing IGF1 mediated signal transduction pathways to regulate cell survival in myocardial tissue<sup>11</sup>. When IGF1 engages and activates IGF1 receptor on the cell surface, several signalling pathways are activated and mediate cardiomyocytes DNA synthesis, growth, remodelling, and anti-apoptosis. Thereby protein synthesis is stimulated and myocardial apoptosis is decreased, which result in increasing cardiac muscle mass (Hypertrophy), protection against losing myocardium, and maintaining myocardial function.

## **Materials and methods**

### **Construction of $\alpha_2\text{PI}_{1-8}$ -IGF1**

Human IGF1 cDNA was obtained by PCR from the plasmid pCR2. 1-hIGF1, was kindly provided by Prof. Aebischer, EPFL. To obtain the  $\alpha_2\text{PI}_{1-8}$ -IGF1 cDNA, a factor XIIIa substrate sequence NQEQVSPL must be added at the N-terminus of the mature human IGF1 protein. For the truncated mutant IGF1 protein purification, the pGEX6P1 expression vector was chosen. The expression vector pGEX6P1 was purchased from GE Healthcare (USA), and prescission protease at 4°C was used to cleave the glutathione S-transferase (GST) tag. Due to inefficient

cleavage, the thrombin cleavage sequence LVPRGS was added at N-terminus of  $\alpha_2\text{PI}_{1-8}$ -IGF1. To avoid purification problems, a polyhistidine-tag (His tag) sequence HHHHHH was added at the C-terminus of  $\alpha_2\text{PI}_{1-8}$ -IGF1. All added sequences were in frame with IGF1 cDNA (Fig. 45).



Fig 45. A schematic view of gene construction. A factor XIIIa DNA substrate sequence was added at 5' of mature human IGF1 cDNA (that is  $\alpha_2\text{PI}_{1-8}$ -IGF1) for binding to fibrin matrices. Six histidines DNA sequence was added at 3' of mature human IGF1 cDNA for protein purification by His-affinity chromatography. Thrombin cleavage DNA sequence was added at 5' of  $\alpha_2\text{PI}_{1-8}$ -IGF1 DNA for final cleavage of  $\alpha_2\text{PI}_{1-8}$ -IGF1 from fusion protein. For insertion  $\alpha_2\text{PI}_{1-8}$ -IGF1 DNA into plasmid vector, two restriction enzymes, BamHI and XhoI, were added at 5' and 3' terminal separately.

Due to a primer length limitation, PCR amplification was separated into two steps. For the first step of PCR amplification, the Forward primer was 5'-AAGAACAAGTCAGTCCCCTTATGGGACCGGAGACGCTCTG-3'. The reverse primer was 5'- TGGTGATGACGACCTTCGATAGCTGACTTGGCAGGCTTGA-3'. For the second step of PCR amplification, the Forward primer containing BamHI restriction site (single dark underlined) was 5'-CGCGGATCCCCTGGTTCGCGTGGATCTAATCAAGAACAAGTCAGTCCCCTT-3'. The reverse primer containing XhoI restriction site (single dark underlined) was 5'-CCGCTCGAGTCAATGGTGATGGTGGTGATGACGACCTTCGAT -3'. The thrombin cleavage sequence was discontinuous underlined. The  $\alpha_2\text{PI}_{1-8}$  sequence was double underlined. The 6xHis tag sequence was single underlined.

### Cloning of pGEX6p1- $\alpha_2\text{PI}_{1-8}$ -IGF1

Using AmpliTaq DNA polymerase kit (Applied Biosystems, USA), the PCR component was prepared according to the formulation in Table 8. The final reaction volume was 100ul.

Polymerase chain reaction (PCR) is a technique widely used in molecular biology. There are three steps in PCR (Fig. 46).

1. Denaturation: This step is to denature the DNA template by heating, which would disrupt the hydrogen bonds between complementary bases of the DNA strands to yield single strands of DNA.

2. Annealing: This step is to anneal the primers to the single-stranded DNA template. The polymerase binds to the primer-template hybrid then begins the DNA synthesis. The melting temperature is determined by the primers used.
3. Elongation: This step is to synthesize a new DNA strand complementary to the DNA template strand by adding nucleotides (dNTPs). The temperature depends on the DNA polymerase used.

Table 8. PCR required reagents for AmpliTaq DNA polymerase kit

Sequences added	Component	Volume per rx	Final concentration
2	10x QIAGEN PCR buffer	10 $\mu$ l	1X
3	dNTP mix (10mM each)	2 $\mu$ l	200 $\mu$ M of each dNTP
3	MgCl <sub>2</sub> 25mM	6 $\mu$ l	
4	Primer A (4 $\mu$ M stock)	5 $\mu$ l	0.1-0.5 $\mu$ M
4	Primer B (4 $\mu$ M stock)	5 $\mu$ l	0.1-0.5 $\mu$ M
Last	Taq DNA polymerase	.1 $\mu$ l	2.5 units/rx
1	Distilled water	Variable, 70 $\mu$ l	-
5	Template DNA, A $\alpha$ chain	.1 $\mu$ l (1.7 $\gamma$ / $\lambda$ )	$\leq$ 1 $\mu$ g/rx

The PCR program used for AmpliTaq DNA polymerase kit was made according to the kit manufacturer's protocol. Using a PCR machine (Fig. 47, Applied Biosystems, USA), the reaction was running with the following program:

94°C	12 minutes	X1	
95°C	45 seconds	X30	
64°C	59 seconds	X30	
72°C	120 seconds	X35	<1k bp
72°C	8 minutes	X1	
4°C	Indefinite		



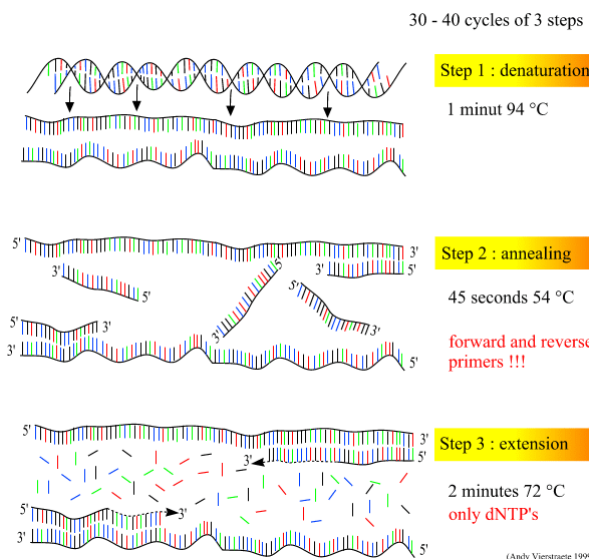


Fig 46. Schematic drawing of the PCR cycle. There are three steps in the reaction, denaturation at 94°C, annealing at about 54°C and extension at 72°C. One cycle is shown here.



Fig 47. One thermal cycler (Applied Biosystems, USA) used for PCR amplification in this manuscript.

5% PCR product was identified by agarose gel electrophoresis on 1% gel with GelRed nucleic acid stain staining (Brunschwig, Switzerland).

After identification, 95% PCR product was purified using a JetQuick PCR purification spin kit (Brunschwig, Switzerland) to delete small base pair molecules, such as primers. Then the purified PCR product and expression vector pGEX6P1 were digested by BamHI and XhoI restrictions enzyme in BamHI buffer at 37°C for 5 hours. Digested pGEX6p1 expression vector was purified on agarose gel using Jetquick gel extraction spin kit (Brunschwig, Switzerland), while the digested PCR product was purified by JetQuick PCR purification spin kit (Brunschwig, Switzerland). Then ligation was carried out between PCR fragment and digested vector at 16°C for 14 hours with T4 DNA ligase. The proportion used of components for the ligation was according to the equation below:

$$\frac{ng.of .vector * kb.size.of .insert}{kb.size.of .vector} * molar.ratio.of . \frac{insert}{vector} = ng.of .insert$$

Then the ligation solution was transformed into subcloning Efficiency<sup>®</sup> DH5 $\alpha$ <sup>™</sup> chemical competent cells (Invitrogen, USA). Furthermore, the transformation solution was spread on pre-

warmed LB-Agar plates containing 100 µg/ml of Ampicillin. The plates were incubated overnight with parafilm around the edge at 37°C.

Finally, the colonies were picked up randomly from LBA plates and screened by PCR. The Forward primer was 5'- GGGCTGGCAAGCCACGTTTGGTG-3'. The reverse primer was 5'- CCGGGAGCTGCATGTGTGTCAGAGG-3'. The PCR product was identified using agarose gel electrophoresis.

### **TG-IGF1 protein expression, extraction and purification**

The pGEX6p1-IGF1 plasmid was transformed into BL21 competent cells (Amersham) for protein expression. A colony was picked randomly from the overnight Luria-Bertani ampicillin (LBA) plates and grown in 5ml LBA medium at 37°C with speed 220rpm for 12 hours. Then 2ml bacteria culture was diluted in 1000ml 2xYT ampicillin medium supplemented with 1% glycerol (1g per 100ml) in 1x2.0-liter Erlenmeyer flask. The bacteria culture was incubated with shaking 230rpm at 37°C for about 5.5 hours until OD<sub>600</sub> about 1.2. 10ml 100mM Isopropyl β-D-1-thiogalactopyranoside (IPTG) (Axon lab, Switzerland) was added inside to induce protein expression at 30°C with speed 230rpm for 5 hours.

After the TG-IGF1 protein was expressed in BL21 bacteria culture, the culture was centrifuged at 4000g for 20 min at 4°C to sediment the pellets. The pellets were placed on ice and resuspended in 40ml ice-cold 1x Phosphate buffered saline (PBS) pH 7.4 supplemented with Complete Protease Inhibitor Cocktail (Roche, Switzerland). The cells were lysed by adding 0.1 volume of a 10mg/ml lysozyme solution in 1xPBS and followed by sonication on ice three times 15 seconds at max speed without foaming. Then 10U/µl deoxyribonuclease I (DNase I) (Fluka, USA) was added to a final concentration 10U/ml. The lysate was gently mixed for 30 minutes to dissolve the fusion protein at 4°C. Finally, the mixture was centrifuged at 10,000xg for 30 minutes at 4°C to remove insoluble components. The supernatant containing extracted TG-IGF1 protein was filtered through a 0.22µm pore filter into a fresh container. The solution was stored at 4°C before preceding the purification procedure (flow chart in Fig. 48).

The purification procedure was separated in two steps and performed using ÄKTA FPLC (Amersham Pharmacia Biotech, USA). The first step was with a GSTPrep™ FF 16/10 20ml column (Amersham Pharmacia Biotech) for GST-TG-IGF1 fusion protein purification. The loading rate was 1ml/min and PBS was used as binding buffer. The elution buffer was 50mM Tris-HCl and reduced with 10mM glutathione at pH 8.0.

The purified GST-TG-IGF1 fusion protein was digested by 20U/mg thrombin protease (stock concentration 1U/ $\mu$ l, Amersham) at RT for 16 hours.

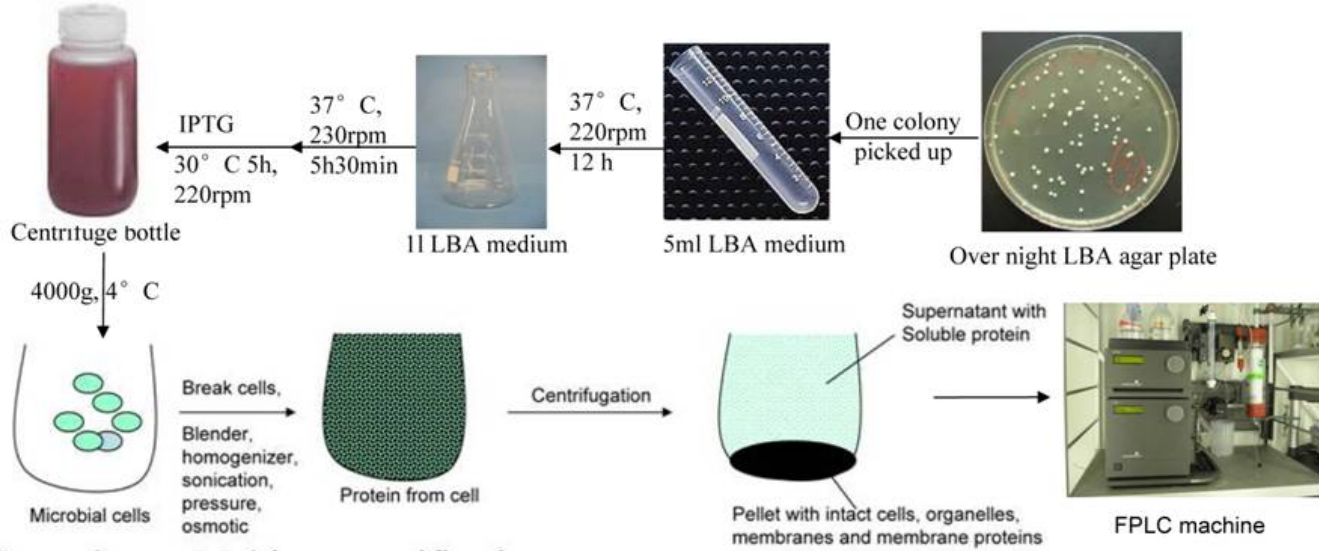


Fig 48. Flow chart of TG-IGF1 protein production and purification. From a LBA agar plate, one colony was picked up and grew in 5ml LBA medium for 12 hours. 2ml fresh bacteria culture was then growing in 1L LBA medium for about 5.5 hours. After adding IPTG, the bacteria culture was growing for additional 5 hours. Finally the pellets were collected from centrifugation. The extracted cytosol solution was purified using FPLC machine.

The second step of purification was to remove GST tag from the GST-TG-IGF1 fusion protein. The system was washed with 1xPBS solution; the sample was loaded into the charging column with a syringe. The HiTrap Benzamide FF column (for binding thrombin) was connected to the GStap FF column (for binding GST). Then the system was switched to the “inject” position. PBS was used as the binding buffer. The purified TG-IGF1 protein was collected in the flow through. The elution buffer, 50mM Tris-HCl and 10mM reduced glutathione at pH 8.0, was used to recondition the column and to remove the GST tag from the column. The other elution buffer, 0.05M Glycine-HCl pH 3.0, was to remove thrombin from the Benzamide FF column. The columns were finally conditioned in PBS for storage.

The TG-IGF1 protein concentration was determined at  $A_{280}$  using the extinction coefficient  $\epsilon_{280}=0.48$ . The size of protein expected was 10.4kD (PI 6.3). The purity of the proteins was analyzed by 10% reducing sodium dodecyl sulphate polyacrylamide gel electrophoresis (SDS-PAGE). Then using one commercial IGF1 ELISA kit, the quantity of obtained purified TG-IGF1 was measured.

## MTT cell proliferation assay <sup>41</sup>

The MTT assay is a quantitative colorimetric method to determine cell proliferation. It is an alternative to the thymidine incorporation test which measures cell proliferation by determining the amounts of incorporated tritiated thymidine into freshly synthesized DNA. The MTT assay measures the changes in colour following the metabolism of the reagent in the mitochondria. 3-(4,5-Dimethylthiazol-2-yl)-2,5-diphenyltetrazolium bromide (MTT, Thiazolyl Blue Tetrazolium Bromide) was purchased from Fluka, USA. This assay measures the activity of the mitochondria in cells to reduce a yellow tetrazolium component (MTT) into an insoluble purple formazan product (reaction in Fig. 49). So, this assay was also a measurement for cell viability as dead cells would not produce the color change.

3T3 cells were seeded in 96-well plates before assay, each sample triplicate. During the assay, the cell medium was removed. 100µl PBS and 20µl MTT (5mg/ml) were added into each well. The cells were incubated at 37°C for 2 hours. Then the MTT medium was removed again and 100µl isopropanol was added into each well to lyse the cells and to solubilize the colored formazan crystals. The plates were wrapped in aluminium foil to avoid the light and incubated at 37°C for another 30 minutes. Finally, the samples were read using an Enzyme-linked immunosorbent assay (ELISA) plate reader (Tecan, Männedorf, Switzerland, Fig. 50) at a wavelength of 570 nm. The amount of color produced was directly proportional to the number of viable cells.

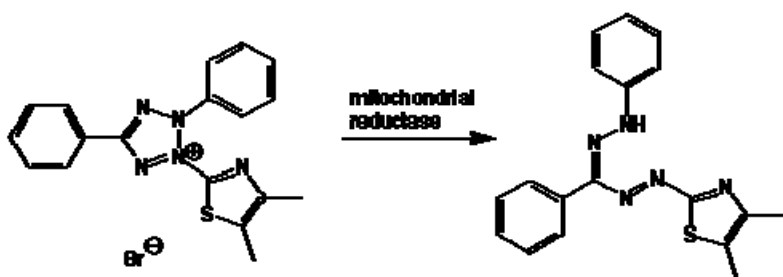


Fig 49. Reaction schema showing MTT assay mechanism. Yellow MTT was reduced to purple formazan by mitochondrial reductase in living cells. A solubilisation solution was added to dissolve the insoluble purple formazan product into a colored solution. The absorbance of this colored solution could be quantified by a spectrometer.



Fig 50. Plate reader Tecan Safire2 (Männedorf, Switzerland) used for absorbance measurement in this manuscript. It is a fully modular monochromator-based microplate detection system.

## Receptor phosphorylation assay

There exist three kinds of phosphorylation receptors, phosphoserine, phosphothreonine and phosphotyrosine. IGF1 receptor belongs to the tyrosine kinase family. IGF1 function on cell proliferation and development is carried out through its binding to the IGF1 receptor at the cell surface, which leads to autophosphorylation and phosphorylation of several receptor substrates. So, IGF1 receptor phosphorylation is very important in the regulation of the signalling pathways for various biological responses<sup>42-44</sup> (Fig. 51). It also offers a good method to test the bioactivity of the engineered recombinant protein TG-IGF1.

For the IGF1 receptor phosphorylation assay, 3T3 cells were seeded on 6-well plates until the confluence about  $\geq 80\%$ . Then the cell medium was removed. The cells were washed three times by 1xPBS buffer. Finally 2ml fresh 1% penicillin streptomycin (PS) DMEM/F12 medium was added into each well. The same quantity 60ng/ml of TG-IGF1 and recombinant native IGF1 were added into each well to activate IGF1 receptor for 20 minutes at 37°C

The cells were washed 1x with cold PBS on the ice. To each well was added 100 $\mu$ l RIPA lysis buffer (Sigma Aldrich) cocktail supplemented with protease inhibitor (Roche), 200x sodium orthovanadate, 100x Okadaic acid (Brunschwig, Switzerland), 100x phenylmethylsulphonyl fluoride (PMSF) (Sigma Aldrich, USA) and 20x Sodium fluoride (NaF). The cells were immediately scraped with a cell scraper. The total cell lysates were transferred into low-binding 1.5ml eppendorf tubes and rotated at 4°C for 30 minutes. The solutions were boiled for 5 minutes at 95°C after reduced 6x Lamelli buffer was added.

The total cell lysates were loaded on 13% polyacrylamide gels and run at 100mV for 1 hour. Then the proteins in gels were transferred to nitrocellulose membranes at 80mV for 1 hour. After blocking in 5% bovine serum albumin (BSA) / Tris-Buffered Saline Tween-20 (TBST) pH 7.4 for 1 hour at room temperature (RT), the membranes were incubated overnight at 4°C in 5% BSA/TBST containing 1:1000 rabbit polyclonal to IGF1 receptor antibody (phospho Y1165+Y1166) (Abcam, UK). The membranes were rinsed 4x5 minutes in TBST and incubated at room temperature for 1 hour in 5%BSA/TBST containing 1:10,000 goat anti-rabbit IgG (H+L)-HRP conjugate (Bio-rad, USA). After the second antibody solution was removed, the membranes were washed 6x5 minutes in TBST. Finally, the membranes were incubated 5 minutes with SuperSignal west pico chemiluminescence detection solutions (Pierce, USA). The phosphorylation bands around 100kD were visualized by timed exposures to CL-XPosure Film (Pierce, USA).

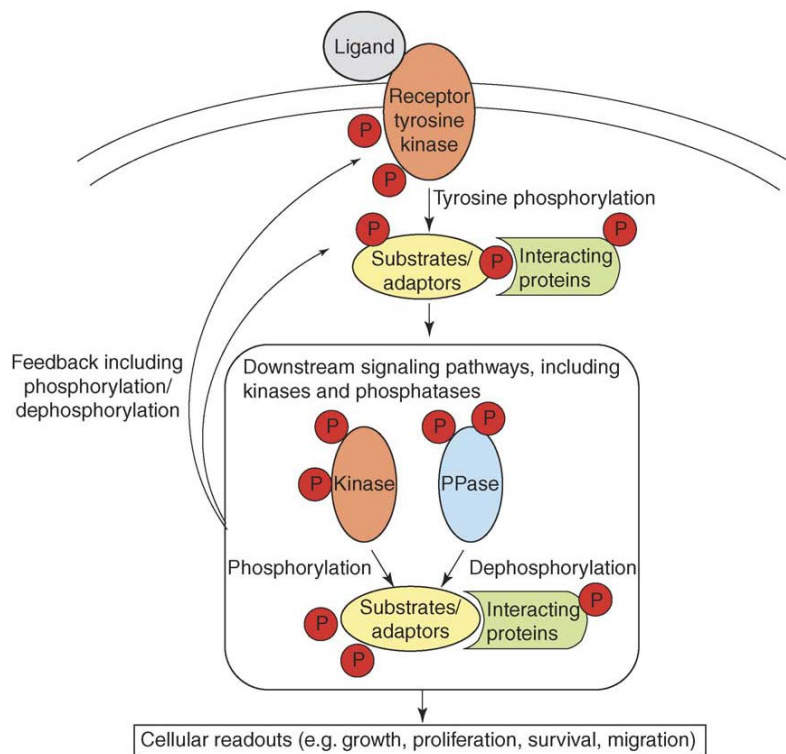


Fig 51 Simplified scheme showing tyrosine receptor phosphorylation pathway<sup>42</sup>. Upon binding of a ligand, autophosphorylation of the receptor is followed by tyrosine phosphorylation of several receptor substrates. These substrates interact with other proteins to activate several downstream pathways. Each pathway can themselves phosphorylate and dephosphorylate the receptor tyrosine kinase and its substrates leading to a complex picture of phosphorylation and dephosphorylation events. The activation of a signaling pathway will result in various phenotypic effects, including changes in migration, apoptosis and proliferation. P, phosphate; PPase, phosphatase.

After the membranes were stripped in western blot stripping buffer (Pierce, USA), the membranes were re-blocked in 5% BSA/TBST for 1 hour at room temperature. Then the membranes were incubated overnight at 4°C in 5% BSA/TBST containing 1:1000 rabbit polyclonal to IGF1 receptor antibody (Abcam, UK). The remaining steps were the same as the previous ones. The second antibody solution used was 5% BSA/TBST containing 1:10,000 goat anti-rabbit IgG (H+L)-HRP conjugate (Bio-rad, USA). This time, the bands of total IGF1 receptors around 100kD were visualized by timed exposures to CL-XPosure Film (Pierce, USA).

## **Fibrin gel formation**

Human fibrinogen (Pg, vWF & Fn depleted) was purchased from Enzyme Research Laboratories (USA). It was dissolved in sterile Tris-Buffered Saline (TBS) pH 7.4 solution 1 hour at 37°C at 25mg/ml. The resulting solution was sterilized by filtration through a 0.22  $\mu$ m syringe filter. Then the fibrinogen solution in 10 kD cut-off dialysis cassette (Pierce, USA) was dialysed against 1000 volumes of TBS for 24 hours at room temperature to remove salts presented in the initially protein buffer. The resulting fibrinogen concentration was determined by measuring the absorbance at 280 nm using the extinction coefficient 1.51. The solution was stored at -80 °C.

Fibrin gels (70 $\mu$ l) were made by mixing the various components in an ultra low binding 96-well plate (Corning, USA). SMCs were trypsinized and washed 3 times with PBS and resuspended in serum-free media (SFM) to obtain high cell concentrations. Final concentrations of 6 mg/ml fibrinogen, 76  $\mu$ g/ml fibronectin, 5 mM Ca<sup>2+</sup>, 2 NIH units/ml of Factor XIIIa, 2 NIH units/ml of human thrombin, 20 % (v/v) cell solution, 100ng/ml TG-IGF1 or recombinant native IGF1 (R&D systems, USA) and 17  $\mu$ g/ml aprotinin were obtained in the solution. During this experiment, the control sample was with fibrin gel alone without IGF1. Finally the gels were transferred to a 48-well plate containing 300  $\mu$ l of cell medium supplemented with 10 % fetal bovine serum (FBS) to mimic physiological condition.

## **Isolation of human bladder smooth muscle cells**

Human bladder tissue was obtained kindly from Professor Peter Frey. The smooth muscle cells were isolated from bladder tissue by antibody conjugated magnetic beads. 12.5 $\mu$ l anti-human epithelial antigen, clone Ber-EP4 (Dako Cytomation, Denmark) and 4 $\mu$ l anti-human fibroblast antigen, Thy-1/CD90 (Dianova, Germany) were conjugated separately to 100 $\mu$ l dynabeads pan mouse IgG (Invitrogen, USA) at a final concentration 1 $\mu$ gAb/1x10<sup>7</sup>beads.

Fresh bladder tissue, transported in sterile Hanks Balanced Salt Solution (HBSS) supplemented with 5% PS, was washed twice by HBSS. Then the tissue was cut into narrow strips (~3x10mm) to facilitate epidermal removal. After HBSS was removed, the tissue was incubated in 0.5mg/ml liberase blendzyme I (Roche, Switzerland) at 37°C for 2 hours. Using 70 $\mu$ m cell strainer, the pellets were separated from the remaining tissues. After centrifugation at 800rpm for 5 minutes at 4°C, the tissue cells were resuspended in 2ml cell medium.

20 $\mu$ l epithelial beads were added per ml cell culture. The cell medium was rotated gently at 4°C for 15 minutes. The magnetic separator was used to collect the supernatant. In this way, the

epithelial cells were removed from the tissue cells. Then 20ul fibroblast beads were added per millilitre (ml) cell culture. Again the cell medium was rotated gently at 4°C for 15 minutes. The magnetic separator was used to collect the supernatant. This time, the fibroblast cells were also removed from the isolated tissue cells. Finally 20ul dynabeads CD31 (Invitrogen, USA) were added per ml cell culture. The same steps were repeated to remove endothelial cells from the isolated tissue cells. Thus, there were only smooth muscle cells (SMCs) in the supernatant. After centrifugation at 800rpm for 5 minutes at 4°C, the tissue cells were resuspended in 10 ml alpha-MEM/F10 media supplemented with 10% fetal bovine serum, 1% penicillin streptomycin (PS) and 1% fungizone, spread in one T-25 flask and incubated at 37°C under humidified 5% CO<sub>2</sub>. The medium was renewed every 3 or 4 days. The cells were cultured until 90% confluence and then sub-cultivated.

### **Transmission electron microscopy (TEM)**

TEM is a powerful tool to reveal the crystallographic structure and the surface states of nanoparticles on an atomic scale. It can also be used to analyze the morphology and even composition of a specimen. It is also used to deduce the correlation between microstructures and their properties<sup>45</sup>.

In this work, TEM (Fig. 52) was used to analyze the SMCs cellular morphology in fibrin gels. The cultured cells in the fibrin matrix were fixed for 4 hours with a cold (4°C) solution of 2% paraformaldehyde (PFA) and 2.5% glutaraldehyde in 0.1M phosphate buffer, pH 7.4. To ensure good fixation, the gels were cut into small (1 mm<sup>3</sup>) blocks shortly after the fixation was begun. After fixation the blocks were washed thoroughly three times for 5 minutes each with 0.1M cacodylate buffer, pH 7.4. The blocks were subsequently fixed for 1 hour in 1% osmium tetroxide and 1.5% potassium ferrocyanide in 0.1M cacodylate buffer, pH 7.4 and then 40 minutes in 0.1M 1% osmium tetroxide alone in cacodylate buffer, pH 7.4. The subsequent washing was performed in distilled water two times for 3 min each. Then the blocks were stained in 1% uranyl acetate for 40 minutes. The next step involved washing in distilled water for 5 minutes, and the subsequent dehydration was performed through increasing concentrations of ethanol in 50%, 70%, 2x96% and 2x100% ethanol, three times for 3 min each. In the next step, we used 30 min incubation in a mixture of equal volume of 100% ethanol and Durcupan. The blocks were washed in durcupan ACM (Fluka, Switzerland) three times for buffer exchange. Then the blocks were embedded in fresh Durcupan ACM resin at least for 4 h. The resin with hardened for 24 hours in a 65°C oven and then the blocks trimmed with glass knives. The ultra-thin sections were obtained at 50 nm thickness using a diamond knife (Diatome, Switzerland) and



ultramicrotome (Leica UCT). The sections were placed on grids (SPI, West Chester, PA, USA) and contrasted with lead citrate. Images were captured digitally on a CCD camera (SIS Morada, Munich) inside a Philips CM10 transmission electron microscope (Aachen, Germany) at a filament voltage of 80kV.

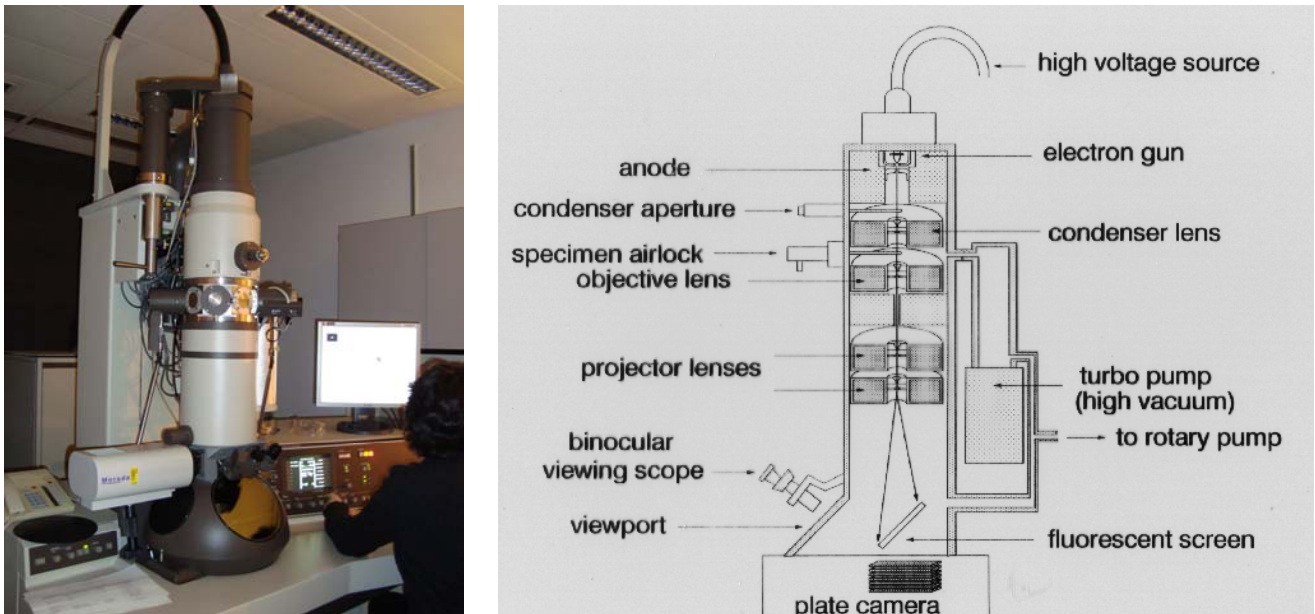


Fig 52. The Philips CM10 TEM used in this manuscript. It is a stable instrument, used primarily for biological samples, also used for materials research on nanoparticles.

### Total RNA extraction

Total RNA from SMCs was extracted with Trizol (Invitrogen, USA) and RNeasy Mini Kit (Qiagen, USA) according to the manufacturer's protocol. This method was used to extract total RNA from small amount of cells ( $10^6$ - $10^7$ ). In brief, human SMCs were incubated in fibrin gels at 37°C with 5% CO<sub>2</sub> for 24 hours and then isolated from gels using high purity trypsin 5mg/ml (Calbiochem, Germany) in one RNase-pyrogen free tube. After centrifugation at 1500rpm for 5 minutes, SMCs were resuspended in 800ul Trizol and incubated at room temperature for 10 minutes. Then 160ul phenol-chloroform-isoamyl alcohol mixture (Fluka, USA) was added. The tubes were shaken vigorously by hand for 15 seconds and incubated at room temperature for 3 minutes. Then the tubes were spun for 15 minutes at 4°C at 12,000xg, and the aqueous phase was removed. The organic phase was re-extracted two times more with 500ul phenol-chloroform-isoamyl alcohol mixture. After centrifugation for 2 minutes at room temperature at 12,000xg, the aqueous phase was removed. Three fractions of aqueous phase were collected and mixed with

equal volume of 70% ethanol (EtOH). The solutions were loaded onto RNeasy mini columns, up to 700ul per time. The columns were spun for 15 second at 10,000rpm. The columns were washed with 350ul RW1 and spun for 15 second at 10,000rpm. Then the columns were incubated for 15 minutes at room temperature in 10ul DNase I stock solution and 70ul RDD buffer. The columns were again washed with 350ul RW1 and spun for 15 second at 10,000rpm. Then the new collection tubes were used. The columns were washed with 500ul RPE and spun for 15 second at 10,000rpm. The columns were washed again with 500ul RPE and spun for 15 second at 10,000rpm. The flow through was discarded. Finally, total RNA was eluted with 30ul RNase free H<sub>2</sub>O in one new 1.5ml RNase-pyrogen free tube by spinning for 1 minute at 10,000rpm. The eluted RNA was stored at -70°C.

The concentration and purity of the RNA were estimated spectrophotometrically using a ND-1000 spectrophotometer (Nanodrop; Wilmington, DE). The integrity of the extracted total RNA was assessed using the Agilent 2100 Bioanalyzer and RNA6000 Nano LabChip Kit (Agilent Technologies, Palo Alto, CA) prior to qRT-PCR assay.

## **Gel immuno-staining**

Fibrin gels (70ul each) were taken out of the cell medium for elastin immuno-staining. After washing twice in PBS, the gels were fixed in 4% paraformaldehyde (PFA) at 4°C for 30 minutes. Washing twice again in PBS, the cell membranes were weakened with 0.1% Triton X-100 for 10 minutes at room temperature. After washing twice in PBS, the gels were blocked in 2% FBS in PBS for 30 minutes at room temperature (RT). Rabbit polyclonal elastin antibody (Abcam, UK) was used as primary antibody at 1:50 dilution in PBS with 2% BSA. The gels were then incubated in primary antibody solution overnight at 4°C.

After washing three times with fresh PBS, 30 minutes-1 hour each at RT, the gels were in Alexa Fluor 488 goat anti-rabbit IgG from Molecular Probes (Invitrogen, USA) at 1:100 dilution in PBS with 2% BSA with few drops of 0.5% Triton over night at 4°C.

After washing three times with fresh PBS, 1 hour each at RT, the gels were incubated in the second antibody solution of Rhodamin Phalloidin (20ul in 0.8ml PBS with 2% BSA) from Molecular Probes (Invitrogen, USA) over night at 4°C for F-actin staining.

After washing three times with fresh PBS, 30 minutes-1 hour each at RT, the gels were counterstaining of nuclei stain in diluted Hoechst 33342 5uM (Invitrogen, USA) (2.5ul in 2ml 1%

BSA/PBS) 1 hour at RT. Finally, after washing three times with fresh PBS, 30minutes-1 hour each at RT, the gels were stored at 4°C and ready for confocal imaging.

### **Confocal fluorescence microscopy**

Fluorescence microscopy was performed using a LSM 510 META - ConfoCor 2 system (Carl Zeiss Jena GmbH, Jena, Germany). The Zeiss laser scanning confocal system was equipped with 5 lenses, including a 63 magnification oil immersion objective of numerical aperture (NA) 1.4 and a 40 magnification oil immersion objective of numerical aperture (NA) 1.3. There were seven laser lines to be selected for fluorescence images. All parameters used in the image acquisition step had to be standardized (output laser power, pinhole diameter, detector gain, amplifier offset) to maintain high reproducibility. Because of overlapping of the excitation/emission spectrum between different fluorochromes, the fluorescence ratio images might be multitrack analyzed. Image analysis was performed using the LSM510 software. Each image was represented by 512x512 pixels.

### **Quantitative real-time PCR (qRT-PCR) assay**

To get the first strand of cDNA from RNA, the reverse transcription kit used was SuperScript III first-strand synthesis system for RT-PCR (Invitrogen, USA). The volume of samples was normalized using the same quantity of total RNA.

Real-time RT-PCR was performed using a Bio-Rad iCycle IQ multicolour detection system (Bio-Rad, USA). PCR primers were purchased from SaBiosciences (USA) to amplify and detect 84 genes in the field of extracellular matrix and adhesion molecules. These primers were loaded in 96-well plate, containing 5 housekeeping genes and one genomic DNA. Real-time PCR amplifications were carried out in a 25ul volume containing 12.5ul iQ SYBR Green Supermix (Bio-Rad), 1ul first strand cDNA and 11.5ul H<sub>2</sub>O. The running program was set according to manufacturer's recommendation. In Brief, the reactions were run at an initial denaturation step at 95° C for 10 min followed by 40 cycles consisting of 95°C for 15 sec and 60°C for 1 minute. Finally the dissociation curve was run at 95°C for 1 minute, 65°C for 2 minutes and from 65°C to 95°C at 2°C per minute. Reactions were performed in triplicate and threshold cycle values were averaged. The data was normalized using the  $\Delta\Delta C_t$  method.

## **Animal experiments**

Sprague-Dawley female rats 250g (12 weeks of age) were used in this study. Two series of animal experiments were carried out. During the first series, twelve rats were randomly divided into three groups of four rats each, fibrin gel without IGF1, fibrin gel with 100ng TG-IGF1 and no fibrin gel. During the second series experiment, twenty rats were randomly divided into four groups of five rats each, fibrin gel without IGF1, fibrin gel with 100ng TG-IGF1, fibrin gel with 100ng recombinant native IGF1 and no fibrin gel. All surgical procedures and experimental manipulations were in accordance with a protocol approved by the Veterinary Authorities of the Canton Vaud according to Swiss law (protocol number 2146).

Induced by an inhalation reagent isoflurane (4% of inspired concentration) and oxygen, rats underwent one general anesthesia procedure. Receiving 50ul Morphasol-4 subcutaneous for analgesia due to the surgery and drops of Viscotears on eyes to prevent eyes from drying during the operation, rats were put on a heating carpet to maintain their body temperature during operation. Anaesthesia was maintained with isoflurane (1% inspired concentration) and oxygen. The abdomen of rats was shaved by razor and sterilized by betadine and 70% ethanol. Working under sterile conditions, the urinary bladder was isolated. Using a scalpel, a straight Vannas spring scissors (FST, USA) and a stainless steel mini Dumont #M5S (WPI, USA) under a microscope, three resections about 1 to 2mm diameter were made on the posterior wall of the bladder, where the muscle layer was removed and the mucosal lining was intact (Fig. 53). Then a 100ul fibrin gel was directly applied on the top to cover three resections using a low binding 0.5ml tube (Milian). After surgery, the muscular layer of the abdomen was sutured with resorbable #5.0 Dafilon (B.Braun, Switzerland) and the skin was sutured with stapler proximate plus MD 35 R (Johnson & Johnson, Switzerland). Betadine gel was used to sterilize the sutured abdomen. Then the rats were kept on a heating carpet (35°C) until awake. The total duration of the experiment was 28 days.

The staples were removed 10 days after surgery. The state of rats was observed every day after surgery until dissection.

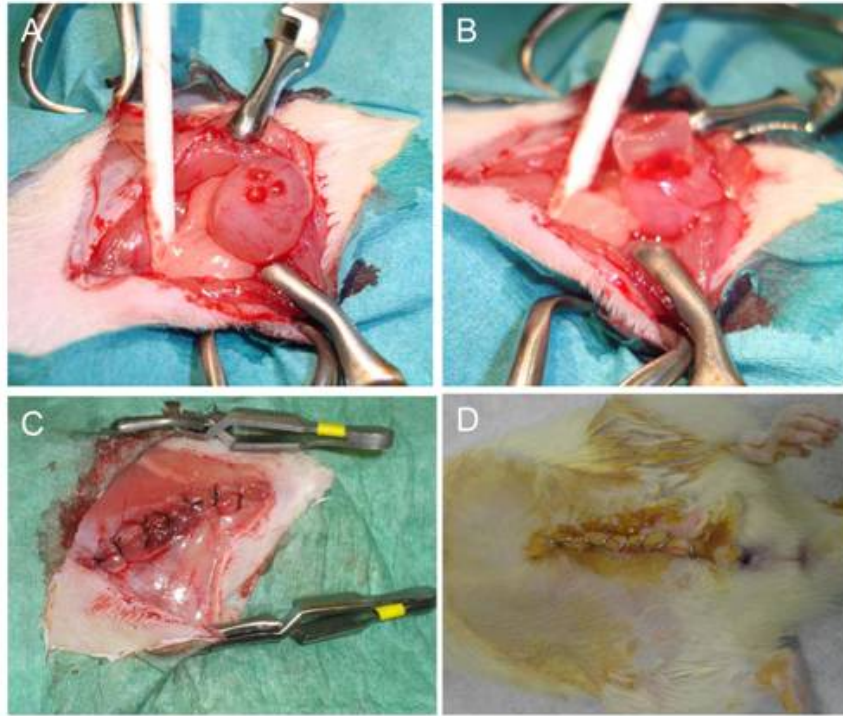


Fig 53. Flow chart showing animal experimental manipulation: A) three resections made on the bladder wall; B) 100ul fibrin gel was made on the top of three resections; C) The abdomen muscle layer was sutured by absorbable #5.0 Dafilon; D) The abdomen skin was sutured by staples

### **Animal dissection**

28 days after surgery, rats were sacrificed by carbon dioxide asphyxiation. The bladder was found and the urethra was tied by one suture. Then around 100ul fresh 4% paraformaldehyde (PFA) solution was injected via the urethra into the urinary bladder by needle for fixation (Fig. 54). The bladder was then cut vertically at the bottom of the ventral knot and removed in a suitable container filled with fresh 4% PFA solution, where the fixation of the bladder was continued at 4°C.

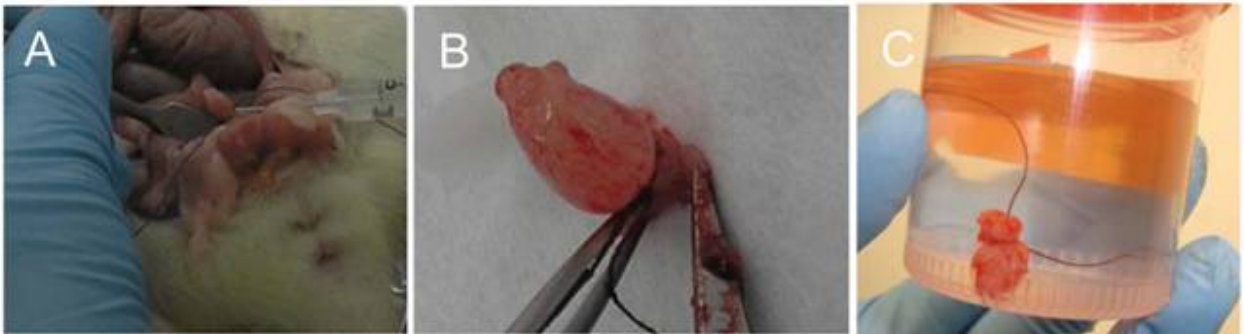


Fig 54. Rat dissection and bladder fixation: A) The bladder was injected about 100ul 4% PFA; B) The bladder was cut off; C) The bladder was fixed in one container with 4% PFA

### **Histological analysis**

Bladders were washed by PBS and then dehydrated in 75%, 96%, 100% ethanol and xylene consecutively. Finally, the bladders were immersed in paraffin overnight. Paraffin-embedded bladder tissues were cut at 5um thickness by microtome. The sections were stained with hematoxylin and eosin (erythrosine) (H&E). This stain was a simple method for general morphology of the tissue. The sections were stained also with Masson's Trichrome (MT). Trichrome staining was a collection of techniques designed to selectively demonstrate muscle, collagen fibers, fibrin and erythrocytes. Finally the sections were stained with Prussian Blue (PB). This stain was identifying hemosiderines in the site of injection. All histological images taken were approved by pathologist Dr. Taminelli.

### **Quantification blindly of detrusor muscle regenerated**

The area of muscle regenerated was quantified blindly with Dr. Hasegawa by the program Fiji according to approved images taken previously. The value was normalised by the area of muscle intact in the same bladder section. The means and standard error were calculated for each experimental group.

### ***Results and discussion***

#### **Construction vector of pGEX6p1- $\alpha_2$ PI<sub>1-8</sub>-IGF1**

The first and second PCR fragments of  $\alpha_2$ PI<sub>1-8</sub>-IGF1 were obtained because we could observe a visible band around 250bp using a 1% agarose gel. Each time, 5% PCR product was run on 1%

agarose gel. It was obvious that second PCR fragment band was higher and clearer than the first one because the size of second PCR fragment was larger and concentration was higher (Fig. 55).

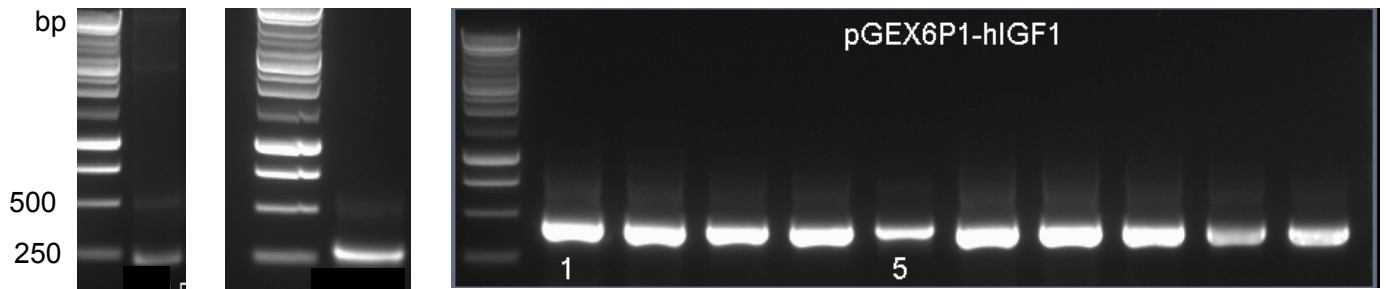


Fig 55. PCR amplification fragment on a 1% w/v agarose gel: the first step of PCR for  $\alpha_2\text{PI}_{1-8}$ -IGF1 DNA (left); the second step of PCR for DNA insert “BamHI-thrombin- $\alpha_2\text{PI}_{1-8}$ -IGF1-6xHis-XhoI” (middle); Screening of 10 colonies of pGEX6p1- $\alpha_2\text{PI}_{1-8}$ -IGF1 using standard primers (right). The DNA size marker is a commercial 1kb ladder. A band about 250bp was visible for  $\alpha_2\text{PI}_{1-8}$ -IGF1 DNA insert (left and middle). A band about 450bp was visible for every colony.

After screening 10 random colonies of pGEX6P1-IGF1 on a LB ampicillin plate using pGEX5' and pGEX3' primers, one visible band between 250 and 500bp was observed on a 1% agarose gel. The expected size of the inserted  $\alpha_2\text{PI}_{1-8}$ -IGF1 was 459bp. So, it seemed that these 10 colonies were all good. Randomly, two colonies, colony 1 and 5, were chosen for DNA sequencing by Fasteris (Geneva, Switzerland). The DNA sequencing results showed that both colonies contained the correct DNA sequence. Therefore, they could be used for TG-IGF1 protein production.

### **TG-IGF1 protein expression and purification**

It was discovered that recombinant IGF1 produced by *E.coli*<sup>46</sup> could maintain its bioactivity. It means that IGF1 protein did not require post translational modification for bioactivity. This finding facilitated the production of recombinant IGF1.

*E.coli* BL21 is a cell strain which lacks OmpT and Lon protease production. According to the GST gene fusion system handbook (Amersham Biosciences), this cell strain could give high levels of expression of GST fusion proteins. So, in this work, this cell strain was chosen for TG-IGF1 protein expression.

During the TG-IGF1 protein production by BL21, it was found that the most of TG-IGF1 was in inclusion bodies. To facilitate the purification TG-IGF1 from the inclusion bodies, another cloning was performed using pET-22b(+) (Novagen, Germany) as an expression vector in order to obtain TG-IGF1 by a one step purification (His tag affinity column) instead of two step purification (GST tag affinity column). Consistent with the small size of the His tag at the C-terminus, it was demonstrated that the His tag did not influence the bioactivity of TG-IGF1. So, it was not necessary to enzymatically remove the His tag from TG-IGF1. During the preliminary experiment, it was difficult to obtain very pure TG-IGF1 by His affinity purification due to relatively weak affinity of His-tag compared to GST-tag. It was also found that TG-IGF1 purified from the inclusion bodies was easily precipitated but did not display significant bioactivity, as expected. Finally, TG-IGF1 was purified by GST affinity column.

Due to a small elution peak, a small quantity of GST-IGF1 was purified from the cytoplasm of one liter of bacteria culture (Fig. 56). The final product TG-IGF1 was in the flow through fractions. Using an Amicon Ultra-15 Centrifugal filter unit with membrane 5 kDa (Milian, Switzerland), the flow through fractions of the second purification step were concentrated to 1ml solution.

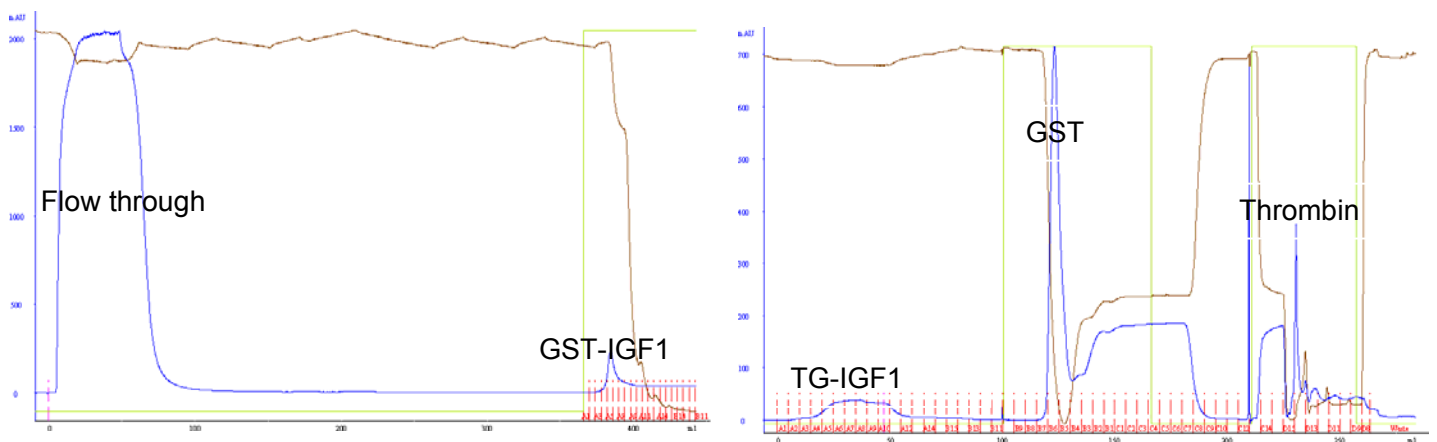


Fig 56. Purification of TG-IGF1 by GST affinity chromatography. The first step of GST-IGF1 purification (left); the second step of TG-IGF1 purification (right). The first peak represents flow through. The second and third peak represents eluate. For the first step of GST-IGF1 purification (left), the eluted fractions were collected, which contained GST-IGF1. For the second step of TG-IGF1 purification (right), the flow through fractions were collected, which contained TG-IGF1.

The purity of TG-IGF1 was analyzed by SDS-PAGE using a 12% gel. 5ul of sample was mixed with 5ul reduced 1xloading buffer. After heating at 95°C for 5 minutes, 10μl sample was loaded



on the gel. After, the gel was stained with SimplyBlue™ SafeStain solution (Invitrogen), only one band at about 10kD was visible on the gel (Fig. 57, left). Therefore, the collected protein was very pure. To further identify this protein, the band was transferred onto a membrane to perform a western blot analysis. The mouse monoclonal [1F6-3H10] to IGF1 (Abcam, UK) was used as the first antibody at a dilution 1:5000. 10% milk in PBST was used as the blocking buffer. Only one band at about 10kD on the film developed (Fig. 57, right). So, this protein was TG-IGF1. The quantity of purified TG-IGF1 was determined by Quantikine® human IGF-I immunoassay (R&D systems, USA), which was about 10ug from 2 liters bacteria culture.

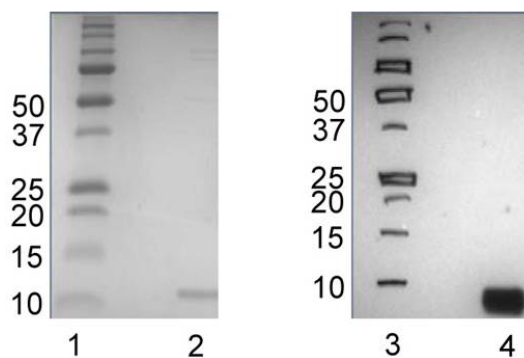


Fig 57. Purified recombinant TG-IGF1 shown on stained 12% reducing polyacrylamide SDS-PAGE (lane 2) and on membrane reacted with anti-IGF1 antibody, visualized by chemiluminescence (lane 4). Lanes 1 and 3: molecular weight marker broad range in kDa (prestained; Bio-rad).

The TG-IGF1 protein purification process was repeated several times. Each time, the same result was obtained on SDS-PAGE and by western blot. 100ul protein, loaded on the reduced SDS-PAGE gel and stained by SimplyBlue™ SafeStain solution, was cut and sent to proteomics facility in EPFL for amino acid sequencing by MALDI-TOF mass spectrometry. After analysis, the resolved amino acid sequence from fragmentation and parent ion mass was first compared to the expected sequence to check the coverage rate and then was secondly compared to the sequences of all proteins in the database of the host expression cell, such as E. coli in this case. The sequencing results showed that there were two close bands on the gel about 10kD and that both of them were TG-IGF1. There was very weak sequence coverage between the protein sent and the E. coli proteins sequences in the database. But there was strong sequence coverage, up to 80%, between the protein sent and the expected sequence. Two close bands on the gel were due to slight difference between two 3D conformations of TG-IGF1. This is a common

phenomenon in protein engineering. Thus, we proved unambiguously that the TG-IGF1 was produced and thoroughly purified.

### MTT cell proliferation assay

For the MTT cell proliferation assay, a standard curve was determined to find the optimal cell number for the MTT assay.

Four cell densities of HeLa cells were seeded on one 96-well plate,  $6 \times 10^3$ ,  $1.2 \times 10^4$ ,  $2.5 \times 10^4$  and  $5 \times 10^4$  cells. The samples were made in triplicate for each cell number. 12 hours after seeding, the cell medium was removed and MTT assay was running as usual.

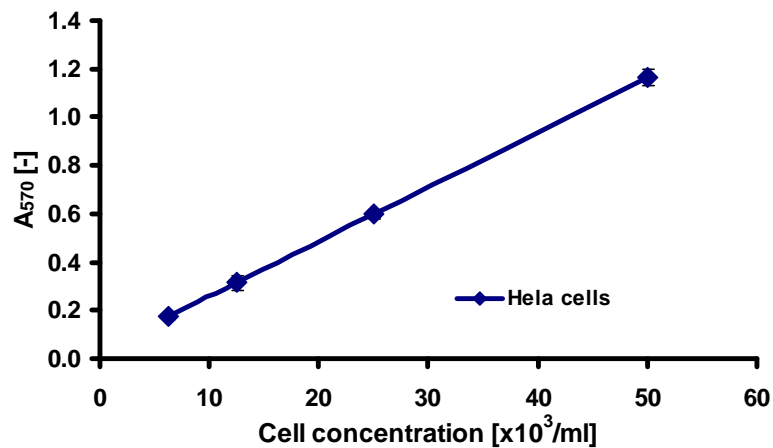


Fig 58. Standard curve to determine optimal cell number for MTT cell proliferation assay. Axis x was cell concentration in 1000 cells per ml. Axis y was optical density at 570nm. It showed optical density increased with cell concentration. Due to test of cell proliferation with time, the cell number chosen was  $1 \times 10^4$  for this assay.

Because IGF1 stimulated cell proliferation, the cell number chosen should be the lowest value in the linear part of the standard curve (Fig. 58) to avoid the cell overgrowth during the MTT assay. So, the cell number chosen was  $1 \times 10^4$  for the MTT assay.

3T3 cells were trypsinized and washed three times by PBS buffer. After cell counting,  $1 \times 10^4$  cells were seeded in serum free medium in 96-well plates, which were pre-coated by 1% BSA/PBS. Ten different IGF1 concentrations were added in each well to stimulate 3T3 cells proliferation, 0, 1, 3, 6, 9, 12, 15, 18, 21 and 24ng/ml. The different effect of recombinant native IGF1 and TG-IGF1 on 3T3 proliferation was also compared in this assay. Two time points were taken, each sample in quadruplet. After 46 hours and 77 hours of cell proliferation, the cell medium was

removed and an MTT assay was performed. From the Fig. 59, it showed that TG-IGF1 and recombinant native IGF1 stimulated 3T3 cell proliferation in the same profile. For the 46 hours stimulation, the cell number was in the stationary state for IGF1 concentration higher than 12ng/ml. When cell proliferation was stimulated by IGF1 for 77 hours, the cell number was nearly independent on IGF1 concentration.

From this assay, it showed that recombinant TG-IGF1 was the same in terms of bioactivity as the recombinant native IGF1 for cell proliferation.

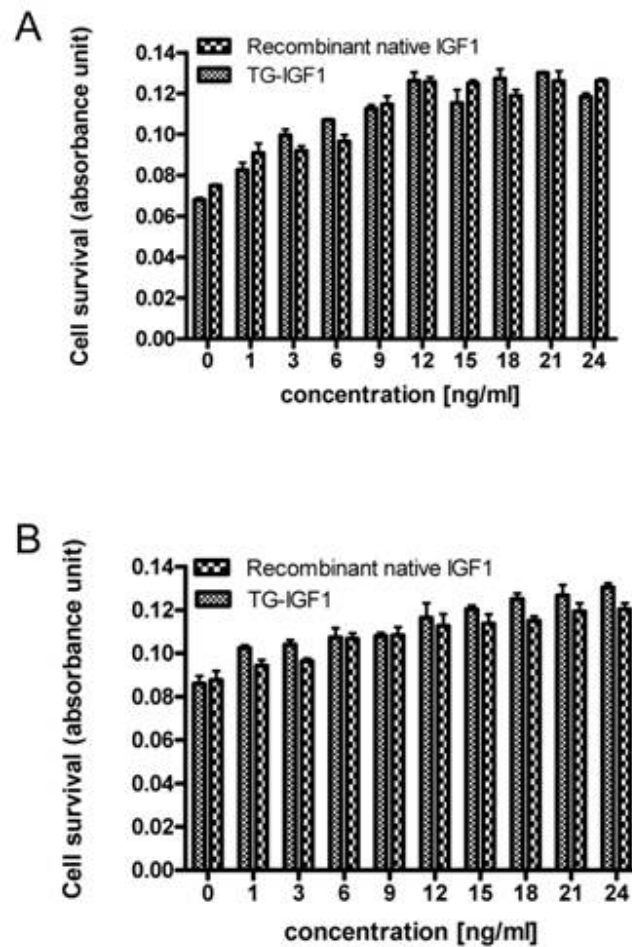


Fig 59. Effect of recombinant native IGF1 and TG-IGF1 on fibroblast 3T3 cell proliferation. The cells (10,000 per well) were seeded in 96-well plates overnight and then treated separately with various concentrations (0-24ng/ml) of IGF1 for 46 hours (A) and for 77 hours (B). Cell proliferation was estimated on the basis of optical density. The data represent the mean ( $\pm$ SEM) of 4 wells.

## Receptor phosphorylation assay

For the phosphorylation assay, it was difficult to retain phosphorylation, which dissappeared very quickly. Many factors could influence the result of this assay, such as the time used to stimulate 3T3 cells by IGF1, time to lyse the cells and the presence of protein phosphatases in the cells. All the components in the cell lysis buffer were to inhibit protein phosphatase activity, including Okadaic acid <sup>47</sup>. So, this assay was needed to be performed quickly and on ice. 3T3 cells were stimulated by IGF1 less than 20 minutes. Each sample was made in duplicate.

From the Fig. 60, it reveals that TG-IGF1 and commercial recombinant IGF1 could bind to the IGF1 receptor of 3T3 cells to stimulate the formation of phosphorylated IGF1 receptor, which was visualized by receptor phosphorylation antibody (Fig. 60A). For the negative control without IGF1 stimulation, no phosphorylated receptor was visible on the film.

For the proteins on the same membrane, there were IGF1 receptors in all samples, which were visualized on the film due to the IGF1 receptor antibody. Due to the 2 subunits in the IGF1 receptor, there were 2 bands visible on the film (Fig. 60B).

From this assay, it was revealed that recombinant TG-IGF1 displayed the same bioactivity as the native recombinant IGF1 for IGF1 receptor phosphorylation stimulation.

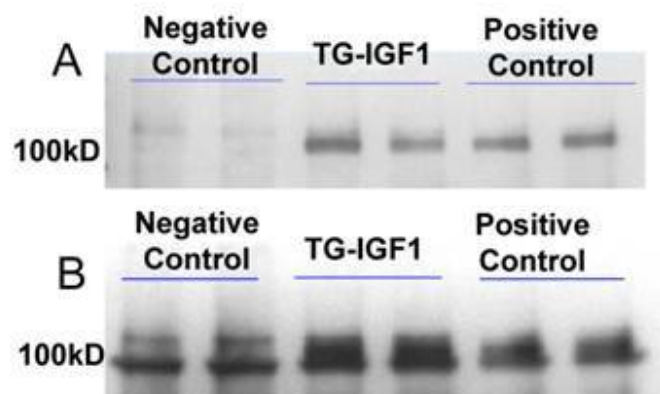


Fig 60. Western blot analysis of receptor phosphorylation assay showing one band at 100kD corresponding to IGF1 receptor. 3T3 cell lysates were probed with a phosphospecific IGF1 receptor antibody (A) and with a correspondent IGF1 receptor (B). Negative control was with no IGF1 added. TG-IGF1 was TG-IGF1 stimulated cell lysate. The positive control was recombinant native IGF1 stimulated cell lysate.

## Isolation of human bladder smooth muscle cells

To confirm the identity of the isolated neonatal human smooth muscle cells (SMCs), SMCs markers were used, such as the alpha smooth muscle actin antibody, smooth muscle myosin heavy chain 1 antibody, calponin antibody and caldesmon antibody. Alpha smooth muscle actin is a differentiation cell marker for SMCs <sup>48</sup>. Smooth muscle myosin heavy chain 1 <sup>49</sup>, calponin and caldesmon <sup>50</sup> were three proteins related to SMCs contraction. The antibodies were purchased from Abcam (UK).

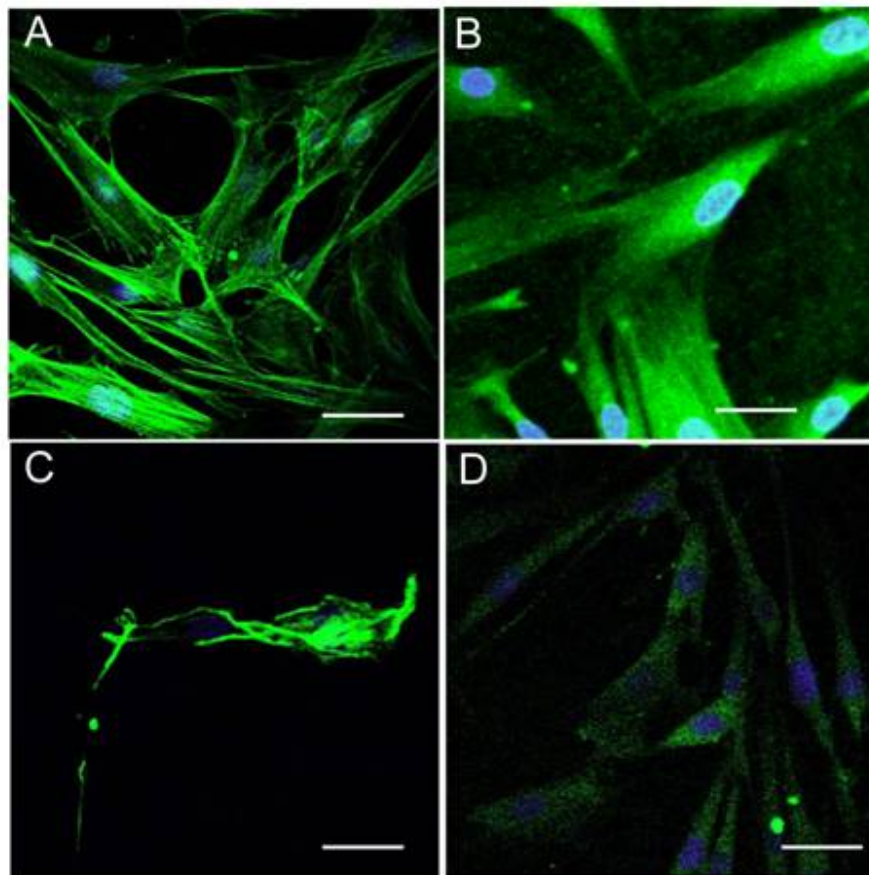


Fig 61. Isolation of neonatal human bladder SMCs. After isolation process, the cells in 2D cultures on polystyrene tissue culture plastic ware were immunofluorescence stained with cell markers (green): A) alpha smooth muscle actin antibody, B) smooth muscle myosin heavy chain 1 antibody, C) calponin and D) caldesmon. The nuclei were counter staining with DAPI (blue). Scale bars represent 200 $\mu$ m.

The cells were washed twice with PBS and then mixed with 4% PFA for 1 hour. After washing three times with PBS, the cells were permeabilized with 0.1% Triton-X for 5 minutes at RT, and

then washed again three times with PBS. After blocking in 2% BSA with 10% goat serum in PBS for 1 hour at RT, the cells were immersed overnight in the first antibody solution in blocking buffer. After washing four times with PBS, the cells were suspended in the second antibody solution for 1 hour at RT. The cells were washed again six times with PBS. Finally, the cells were counted after staining by Hoechst 33258 in blocking solution for 30 minutes at RT to label the cell nuclei.

From the immunofluorescence staining (Fig. 61), the conclusion could be made that the isolated bladder cells were indeed SMCs.

### **Transmission electron microscopy (TEM)**

Three types of fibrin gels (70ul each), without IGF1 (as negative control), with 50ng/ml native recombinant IGF1 (as positive control) and with 50ng/ml TG-IGF1, were prepared containing  $2.1 \times 10^5$  isolated neonatal human bladder SMCs per gel, each sample in triplicate.

These nine gels were placed into a 48-well plate, to which 500ul alpha-MEM medium supplemented with 10% FBS, 1% PS, 17  $\mu\text{g/ml}$  aprotinin and 1mg/ml  $\epsilon$ -aminocaproic acid were added per well. 50ng/ml native recombinant IGF1 was also added in the cell medium for the positive control fibrin gel. Three days later, these gels were treated for TEM imaging.

From the TEM imaging (Fig. 62), secretory vesicles were more numerous and bigger in the SMCs in the fibrin gels with TG-IGF1 than in the SMCs with the control samples. So, some proteins were produced by SMCs after stimulation by TG-IGF1 and were accumulated in the secretory vesicles until release into the extracellular environment. TG-IGF1 was released from the fibrin gel during gel degradation by cleavage. Thus, SMCs were stimulated by TG-IGF1 in the gel during three days' incubation.

The morphology of SMCs was similar in the positive and negative fibrin gels. The reason was maybe native recombinant IGF1 not cross-linked with fibrin gels, which resulted in its diffusion from the gel to the cell medium with the time. Even 50ng/ml native recombinant IGF1 was added in the cell medium, the SMCs in the positive fibrin gels were nearly in the same situation as cells in the negative control fibrin gels without IGF1, or maybe only slightly better.

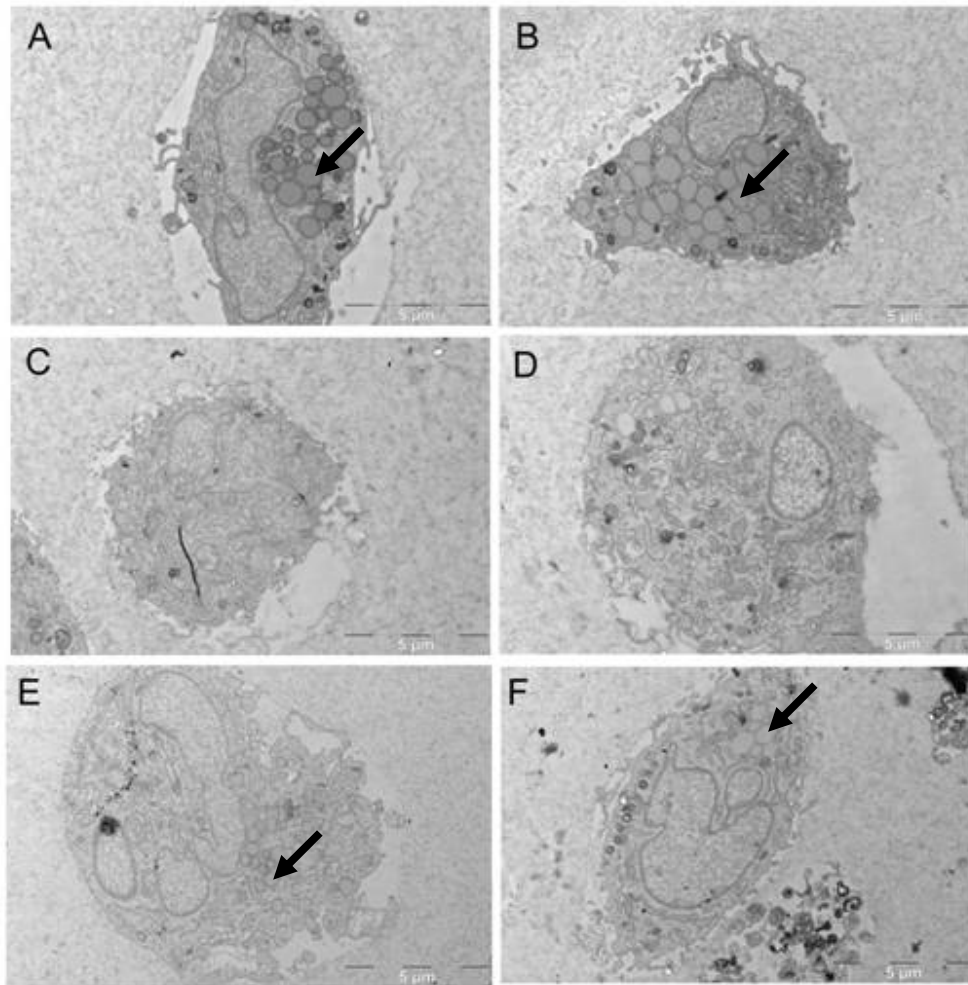


Fig 62. Bright field TEM images. A) and B) represent SMCs in fibrin gel with TG-IGF1. The obvious secretory vesicles in SMCs were indicated by the arrows. C) and D) showed SMCs in fibrin gel only (negative control); no secretory vesicles were found in the cells. E) and F), SMCs in fibrin gel with commercial IGF1 (positive control) had some small secretory vesicles (indicated by the arrows). Scale bars represent 5 $\mu$ m.

Because of these observations, we believe that the TG-IGF1 was in fact bioactive. It had some functions on SMCs due to obvious secretory vesicles in the cells. In contrast, gels without IGF1, or gels with IGF1 added to the gels by simple mixing did not reveal substantial changes in the cell morphology.

## Total RNA extraction for qRT-PCR assay

Table 9. The total RNA data summary

Sample	Concentration [ng/ul]	A260/280	A260/230	RIN (over 10)
Neonatal negative control 1	53.6	1.87	0.26	8.30
Neonatal negative control 2	38.56	1.87	0.83	7.50
Neonatal negative control 3	123.02	2.03	2.03	9.60
Neonatal negative control 4	133.97	2.04	1.78	9.80
Neonatal negative control 5	104.91	2.07	1.54	9.90
Neonatal TG-IGF1 1	187.27	2.01	1.85	9.70
Neonatal TG-IGF1 2	175.1	2.04	2.04	9.70
Neonatal TG-IGF1 3	167.72	2.02	1.57	9.70
Neonatal TG-IGF1 4	86.15	2.03	1.72	10
Neonatal TG-IGF1 5	114.34	2.05	1.21	9.80
Neonatal recombinant native IGF1 1	184.05	2.02	0.66	9.80
Neonatal recombinant native IGF1 2	176.53	2.04	2.07	9.80
Neonatal recombinant native IGF1 3	180.58	2.01	1.07	9.50
Neonatal recombinant native IGF1 4	116.96	2.04	1.90	10
Neonatal recombinant native IGF1 5	124.52	2.04	1.61	10

For characterization of gene expression, three types of fibrin gels were prepared (210ul each), without IGF1 (as negative control), with 100ng/ml recombinant native IGF1 (as positive control) and with 100ng/ml TG-IGF1, containing isolated neonatal human bladder SMCs, each sample in quintuplicate. The gels were added to a 24-well plate, 1ml alpha-MEM medium supplemented with 10% FBS 1% PS and 17 µg/ml aprotinin was added per well. 100ng/ml commercial hIGF1 was also added in the cell medium for the positive control fibrin gels. The gels were incubated for 24 hours at 37°C.



After 24 hours induction by IGF1, the total RNA were extracted from the neonatal human bladder SMCs cells in the fibrin gels according to the protocol. The concentration of total RNA extracted was measure by Nanodrop spectrophotometry (Thermo Scientific, Wilmington USA).

For the qRT-PCR analysis, three values of total RNA extracted were important, A260/280 for DNA contamination, A260/230 for chemical purity and the RIN for RNA integrity number (Table 9). It is better to obtain similar values in the same triplicate group.

According to the obtained results, the quality of two samples, neonatal negative control 1 and 2, were not as high quality as the other samples. So, they were not used for qRT-PCR assay.

### Quantitative real-time PCR (qRT-PCR) assay

The total RNA was extracted from SMCs and analyzed as mentioned above. An RT<sup>2</sup> Profiler™ PCR array plate, containing various primers for 84 genes in the field of ECM and cell adhesion, was purchased from SABiosciences (USA). The efficiency of the primers was estimated to be 2. The experiment was conducted in triplicate. The qRT-PCR array data analysis was performed using the  $\Delta\Delta C_t$  method.

The relationship between the original gene expression level (L) for each gene of interest and the threshold cycle (Ct) is expressed as:

$$L = 2^{-Ct}$$

To normalize the gene expression level for each gene of interest (GOI) to a housekeeping gene (HKG), the expression levels of the two genes are divided as:

$$\frac{2^{-Ct(GOI)}}{2^{-Ct(HKG)}} = 2^{-(Ct(GOI)-Ct(HKG))} = 2^{-\Delta C_t}$$

To determine the fold change in gene expression, the normalized gene expression of the GOI in the experimental sample is divided by that in the control sample:

$$\frac{2^{-\Delta C_t(\text{expt})}}{2^{-\Delta C_t(\text{control})}} = 2^{-\Delta\Delta C_t} \quad \text{Where } \Delta\Delta C_t \text{ is equal to } \Delta C_t(\text{expt}) - \Delta C_t(\text{control})$$

The complete calculation for  $\Delta\Delta C_t$  method is as following:

$$\frac{\frac{2^{-Ct(GOI)} \text{ expt}}{2^{-Ct(HKG)} \text{ expt}}}{\frac{2^{-Ct(GOI)} \text{ control}}{2^{-Ct(HKG)} \text{ control}}} = \frac{2^{-(Ct(GOI)-Ct(HKG))} \text{ expt}}{2^{-(Ct(GOI)-Ct(HKG))} \text{ control}} = \frac{2^{-\Delta C_t} \text{ expt}}{2^{-\Delta C_t} \text{ control}} = 2^{-\Delta\Delta C_t}$$

There were three experimental groups, TG-IGF1, recombinant native IGF1 and no IGF1, each group in triplicate. Each data set was characterized by its mean and standard deviation. The population was assumed to be normally distributed. So, a Student's T-test, one of the most frequently used tests, was applied to determine whether the means were different. This statistic relies on an uncertain estimate of standard deviation rather on a precisely known value. A null hypothesis of this test is that the variances of two distributed populations are supposed to be normally equal. The P value of the Student's T-test indicates the confidence level, statistical significance. It represents the false discovery rate. It is more important than a fold change, which reveals the magnitude of differential expression but not significance.

Table 10. All genes down-regulated with  $p \leq 0.05$

Sample ratio	well	symbol	Gene description	Fold change	T-test P value
TG-IGF1/no IGF1	D09	KAL1	Kallmann syndrome 1 sequence	0.53	0.0371
	G01	SPP1	Secreted phosphoprotein 1 (osteopontin, bone sialoprotein I, early T-lymphocyte activation 1)	0.37	0.0468
	G03	THBS1	Thrombospondin 1	0.76	0.0250
TG-IGF1 /recombinant native IGF1	G03	THBS1	Thrombospondin 1	0.82	0.0446
Recombinant native IGF1/no IGF1	A11	COL16A1	Collagen, type XVI, alpha 1	0.56	0.0124
	C08	ITGA4	Integrin, alpha 4 (antigen CD49D, alpha 4 subunit of VLA-4 receptor)	0.66	0.0169
	D03	ITGAV	Integrin, alpha V (vitronectin receptor, alpha polypeptide, antigen CD51)	0.90	0.0493
	D09	KAL1	Kallmann syndrome 1 sequence	0.38	0.0737
	D12	LAMA3	Laminin, alpha 3	0.38	0.0151
	E10	MMP15	Matrix metalloproteinase 15 (membrane-inserted)	0.16	0.0104
	G01	SPP1	Secreted phosphoprotein 1 (osteopontin, bone sialoprotein I, early T-lymphocyte activation 1)	0.36	0.0620
	G08	TIMP3	TIMP metalloproteinase inhibitor 3 (Sorsby fundus dystrophy, pseudoinflammatory)	0.41	0.0411

Normally it often chooses fold-change with P value lower than 5%. It means that 95% chance to have this observed fold change value represent a statistical difference. If the calculated P value is below the threshold chosen for statistical significance (usually 0.05 level), the null hypothesis which usually states that the two groups do not differ is rejected. These two groups do differ.

According to Student's T-test statistic, if the fold change is greater than 2 and the P value less than 0.05, the gene may be reported as up-regulated. If the fold change is less than 0.5 and P value less than 0.05, then the gene may be reported as down-regulated.

To compare the expression level of each gene in TG-IGF1 with that in native recombinant IGF1, there was just one gene with a probability lower than 0.05. This gene was called THBS1 (Table 10). But the fold change was 0.82, close to 1.0. Thus, there was no difference between the gene expressions by SMCs stimulated by TG-IGF1 and by native recombinant IGF1.

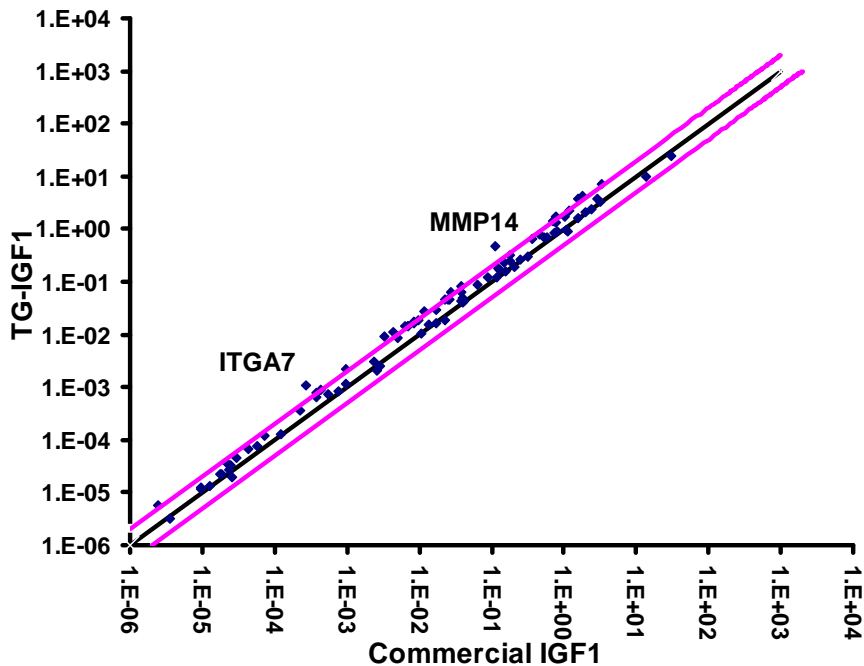


Fig 63. Comparison of relative expression by neonatal human bladder SMCs in 210ul fibrin gels for 84 genes related to adhesion and extracellular matrix molecules between 100ng/ml TG-IGFI and 100ng/ml commercial IGFI. The scatter plot depicts the relative expression level of each gene between TG-IGFI (y-axis) and commercial IGFI (x-axis). The red lines indicate a two-fold change in gene expression threshold. Two genes, ITGA7 and MMP14, have the value of fold change higher than 2.

The gene expression results were also represented in scatter plot (Fig. 63). A scatter plot can suggest various kinds of correlations between variables with a certain confidence level. Correlations may be positive (rising), negative (falling), or null (uncorrelated). It is one of the basic tools of quality control.

The scatter plot indicated that up-regulation was observed in 2 genes, Matrix metalloproteinase 14 (MMP14) and Integrin, alpha 7 (ITGA7), which demonstrated at least a 3-fold difference in gene expression by neonatal human bladder SMCs in fibrin gels between TG-IGFI and commercial IGFI. But no gene was statistically significant due to  $p > 0.05$  (Table 11). So, we did not observe a difference between the TG-IGF1 and the recombinant native IGF1 on the neonatal bladder SMCs.

Table 11. Fold changes in expression for genes related to adhesion and extracellular matrix molecules between TG-IGFI and commercial IGFI. Only genes, ITGA7 and MMP14, in Figure 7 exhibiting a three-fold or greater change in expression are listed. But their p-value of Student's t-test was too high, around 0.2. So, the statistic difference was insignificant.

Gene	Fold change TG-IGFI / Commercial IGFI	t-Test p value	Average raw Ct	
			Commercial IGFI	TG-IGFI
Matrix metalloproteinase 14 (MMP14)	4.10	0.2639	23.23	21.77
Integrin, alpha 7 (ITGA7)	3.94	0.2184	32.47	30.77

The gene expression results (Table 10) identified two down-regulated genes (with  $p < 0.05$  and  $> 2$ -fold change) between TG-IGF1 stimulated bladder SMCs and no IGF1 stimulated SMCs upon 24 hours of stimulations. According to microarray studies, both Kallmann syndrome 1 (KAL1) and Secreted phosphoprotein 1 (SPP1) were dramatically down-regulated in response to TG-IGF1 in neonatal bladder SMCs.

SPP1, also named osteopontin, is an extracellular structural protein. It is expressed in many types of cells, such as smooth muscle cells. It has chemotactic properties, which promote cell recruitment to inflammatory sites. It also functions as an adhesion protein, involved in cell attachment and wound healing. These integrins,  $\alpha v \beta 3$ ,  $\alpha v \beta 5$  and  $\alpha 5 \beta 1$  [51, 52], bind to the RGD site in SPP1 and mediate cell adhesion, migration, and survival. This molecule was down-regulated 2.7-fold in neonatal bladder SMCs cultured with TG-IGF1 ( $p < 0.05$ ) in reference to no IGF1.

The KAL1, also named anosmin-1, is an adhesion fibronectin-containing heparin-binding protein and is responsible for Kallmann's syndrome (KS). KS is defined as a hypogonadotropic hypogonadisms (HH) and an olfactory deficit (anosmia) [53]. The KAL1 is involved in the embryonic development of the olfactory bulbs (OB). The key role of KAL1 is to facilitate gonadotropin neuron migration from the olfactory placode to the Gonadotropin-releasing hormone (GnRH) neurons of the hypothalamus. This neuronal migration defect will also result in GnRH deficiency and hypogonadism [54]. This molecule was down-regulated 1.9-fold in neonatal bladder SMCs cultured with TG-IGF1 ( $p < 0.05$ ) in reference to no IGF1.

Thrombospondin 1 (THBS1) is an adhesive extracellular glycoprotein mediating cell-to-cell and cell-to-matrix interaction. It plays a role in angiogenesis and wound healing. It can interact with fibronectin, fibrinogen and integrins  $\alpha v \beta 3$ ,  $\alpha v \beta 1$  and  $\alpha v \beta 6$  [55, 56]. This molecule was down-regulated 1.3-fold in neonatal bladder SMCs cultured with TG-IGF1 ( $p < 0.05$ ) in reference to no IGF1.

The gene expression results (Table 9) also identified five down-regulated genes (with  $p < 0.08$  and  $> 2$ -fold change) between recombinant native IGF1 stimulated bladder SMCs and no IGF1 stimulated SMCs upon 24 hours of stimulation. It means that native recombinant IGF1 down-regulated KAL1, SPP1, LAMA3, MMP15 and TIMP3 genes expression in neonatal bladder SMCs. So, two genes, SPP1 and KAL1, were both down-regulated in SMCs cultured in fibrin gels with either TG-IGF1 or native recombinant IGF1 compared to the fibrin gels only.

KAL1 was down-regulated 2.63-fold in neonatal bladder SMCs cultured with native recombinant IGF1 ( $p = 0.07$ ) in reference to no IGF1, while SPP1 was down-regulated 2.78-fold ( $p = 0.06$ ). So, for SMCs in fibrin gels *in vitro*, TG-IGF1 or native recombinant IGF1 down-regulated significantly SPP1 and KAL1 ( $n = 3$ ).

Laminin is a base membrane protein in extracellular matrix. Each laminin is a heterotrimer, composed of alpha-, beta- and gamma-chains. Laminin alpha 3 (LAMA3) is the alpha 3 chain of laminin 5, a glycoprotein. It is involved in cell adhesion and signal transduction. This molecule was down-regulated 2.63-fold in neonatal bladder SMCs cultured with native recombinant IGF1 ( $p < 0.05$ ) in reference to no IGF1.

Matrix metalloproteinases (MMPs) consist of 24 zinc-dependent endopeptidases. They are involved in the cleavage all kinds of extracellular matrix proteins in normal physiological processes. They are synthesized and secreted in latent forms. MMPs need extracellular activation. Matrix metalloproteinase 15 (MMP15) is a membrane-type metalloproteinase (MT-

MMP). This molecule was down-regulated 6.25-fold in neonatal bladder SMCs cultured with native recombinant IGF1 ( $p < 0.05$ ) in reference to no IGF1.

The tissue inhibitors of metalloproteinases (TIMPs) are specific endogenous inhibitors for the matrix metalloproteinases (MMPs). There are 4 members in this family, TIMP1, TIMP2, TIMP3 and TIMP4. TIMP3 was down-regulated 2.44-fold in neonatal bladder SMCs cultured with native recombinant IGF1 ( $p < 0.05$ ) in reference to no IGF1.

Collagen is the main connective tissue protein in animals. Up to date there are more than 28 types of collagen discovered. Collagen, type XVI, alpha 1 (COL16A1) is a member of the fibril-associated collagens with interrupted helices (FACIT) collagen family. This molecule was down-regulated 1.79-fold in neonatal bladder SMCs cultured with native recombinant IGF1 ( $p < 0.05$ ) in reference to no IGF1.

Integrins are receptors mediating cell-to-cell and cell-to-matrix communication and interaction. They are involved in the attachment of the cells to the extracellular matrix (ECM), the signal transduction from the ECM to the cells and vice versa. There are 19 alpha and 8 beta subunits. Integrin alpha 4 (ITGA4) was down-regulated 1.52-fold in neonatal bladder SMCs cultured with native recombinant IGF1 ( $p < 0.05$ ) in reference to no IGF1, while integrin alpha V (ITGAV) was down-regulated 1.11-fold ( $p < 0.05$ ).

Table 12. Real-time qPCR primer sequence

Gene	Forward	Reverse
hTropoelastin	GGT GGC TTA GGA GTG TCT GC	CCA GCA AAA GCT CCA CCT AC
hLysyl oxidase	CAG AGG AGA GTG GCT GAA GG	CCA GGT AGC TGG GGT TTA CA
hElastin	CAT TTC CCC CGA AGC TCA G	GCT TTG GCG GCT GCT TTA G
hRPI13A	AGG TAT GCT GCC CCA CAA AA	TGC CGT CAA ACA CCT TGA GA
hRPL27	TGT CCT GGC TGG ACG CTA CT	CTG AGG TGC CAT CAT CAA TGT T

At same time, gene expression of tropoelastin, lysyl oxidase and elastin were analysed using extracted neonatal bladder SMCs RNA. Tropoelastin is a soluble monomer of elastin. Lysyl oxidase is a cross-linker to polymerize tropoelastin to elastin. hRPI13A and hRPL27 are used as house keeping genes (Primer sequence in Table 12). All primers used were checked by standard curve using universal human reference RNA (Stratagene, USA). According to standard

curve (Fig. 64), the PCR efficiency for these primers was around 100%. So, these primers could be used for RT-qPCR experiment.

The fold-change ratio results (Fig. 65) identified that TG-IGF1 and native recombinant IGF1 down-regulated three genes expression, tropoelastin, lysyl oxidase and elastin. It showed that TG-IGF1 and native recombinant hIGF1 had nearly same function on neonatal bladder smooth muscle cells in the fibrin gels.

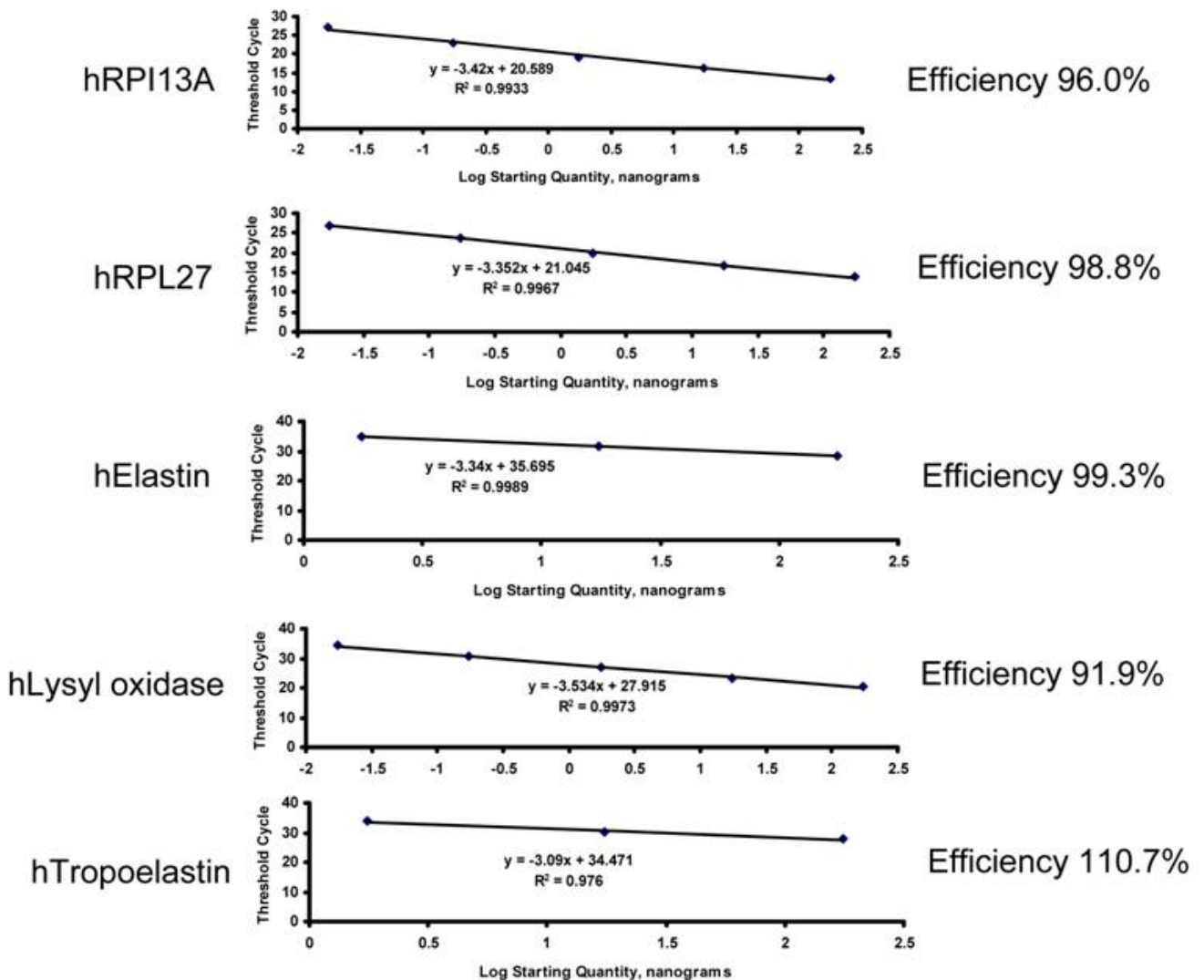


Fig 64. Standard curves for five primers, hRPI13A, hRPL27, hElastin, hLysyl oxidase, and hTropoelastin, using universal human reference RNA (Stratagene, USA). Note that efficiency of standard curve for these 5 primers is around 100%. So, the primers are validated for further experiments of RT-qPCR.

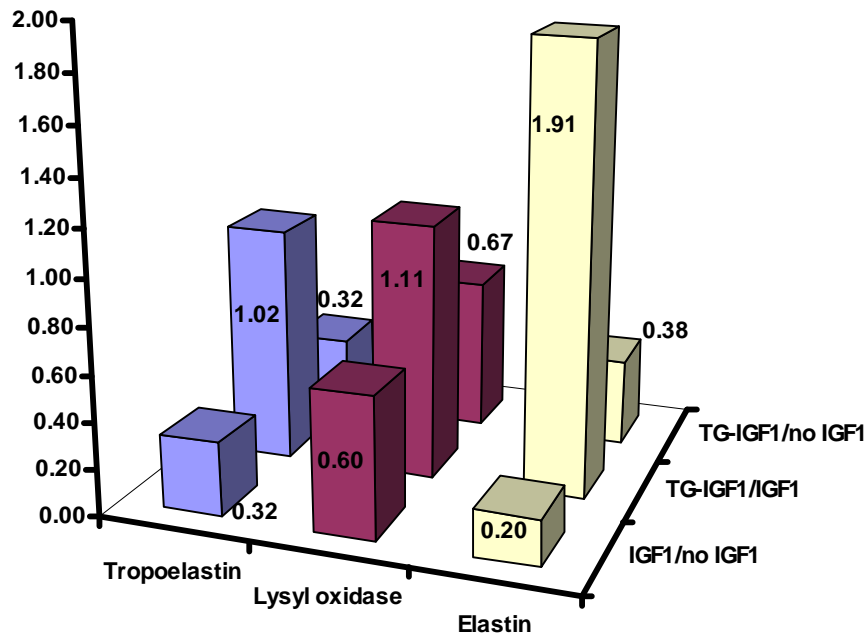


Fig 65. Fold-change ratio result for gene expression of tropoelastin, lysyl oxidase and elastin responding to TG-IGF1, recombinant native IGF1 or no IGF1. Note that two genes, tropoelastin and lysyl oxidase, were down-regulated in same fold-change ratio by TG-IGF1 and native recombinant IGF1.

### Confocal imaging for elastin detection

Nine fibrin gels (70ul each) were made for confocal imaging, three gels per group. 100ng/ml TG-IGF1 or recombinant native IGF1 was incorporated in fibrin gels. The fibrin gels only were acted as the negative control. The gels were inoculated in a 48-well plate for 5 days, 300ul 10% FBS 1% PS alpha-MEM medium with aprotinin was added per well. For the gel with 100ng/ml native recombinant hIGF1, 100ng/ml native recombinant hIGF1 was also added in the cell medium. After 5 days inoculation, the gels were immuno-stained for elastin. The samples were sectioned and analyzed by confocal laser scanning microscopy.

All imaging was carried out using a Zeiss x63 Apochromat objective in three different locations per gel with a z stack of 20 images each. Background fluorescence was determined by imaging the negative control gel, fibrin gel without IGF1. Elastin was green-labelled. The cell skeletal F-



actin was red-labelled. The cell nuclei were blue-labelled (Fig. 66). From the confocal imaging, no elastin was formed by neonatal bladder SMCs in the fibrin gel due to no detectable green colour.

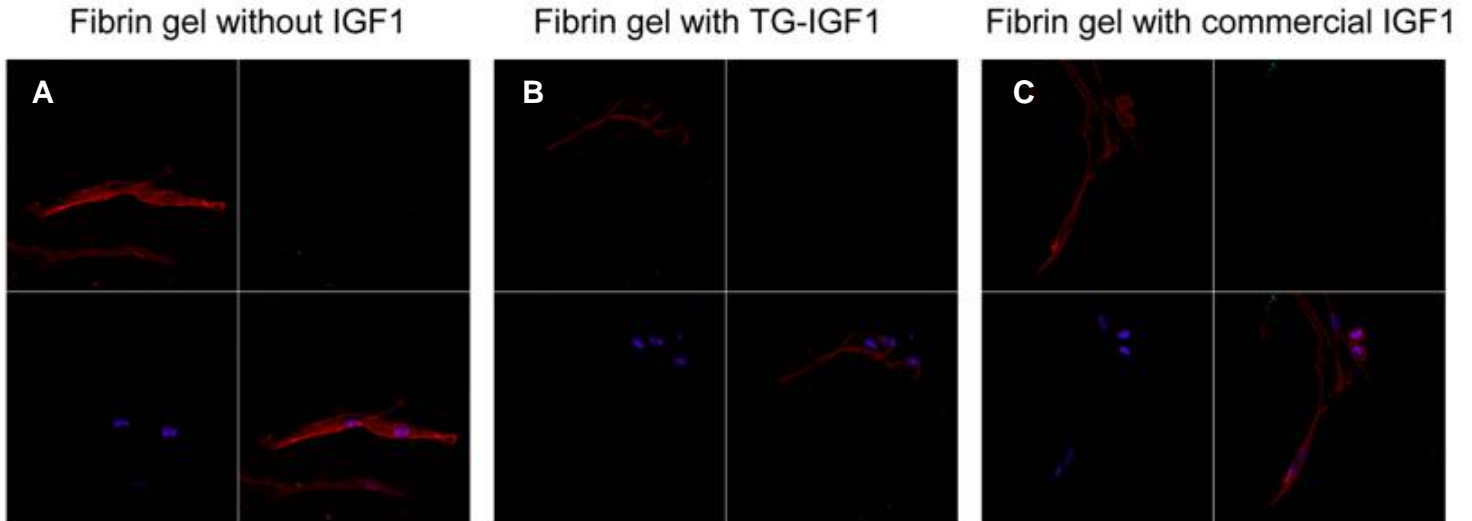


Fig 66. Confocal imaging of elastin (green) formation by neonatal bladder SMCs seeded in the fibrin gels after 5 days stimulation. A) fibrin gel without IGF1; B) fibrin gel with TG-IGF1; C) fibrin gel with native recombinant IGF1. The cell filamentous actin (F-actin) was staining with rhodamine–phalloidin (red). The nuclei were counter staining with DAPI (blue). Sale bars represent 200 $\mu$ m. Note that no elastin was formed by neonatal bladder SMCs.

### TG-IGF1 retention in fibrin gel matrices

Because TG is supposed to crosslink IGF1 in the fibrin matrices, it is important to compare TG-IGF1 and recombinant native IGF1 retention in the fibrin gel matrices under the same condition.

In this experiment, two kinds of 100 $\mu$ l fibrin gel matrices containing 50ng/ml TG-IGF1 or recombinant native IGF1 were prepared in a UltraLow binding plates 96 well plate (Corning, Lowell, USA), each kind of gel in triplicate. The gels were transferred into a 1.5ml low binding Eppendorf tube (Vaudaux Eppendorf, Hambourg, Germany) containing 1.2ml Tris-buffered saline pH 7.4 (TBS). During inoculation in TBS buffer, TG-IGF1 or recombinant native IGF1 was released from fibrin gels at the indicated time points was determined by a Quantikine human IGF-1 kit (R&D systems, USA). An IGF1 standard curve was also determined according to manufacture's instruction. So, TG-IGF1 or recombinant native IGF1 retained in the fibrin gel could be determined. The fixed time points were 0h, 30 minutes, 1h, 2h, 6h, 12h, 18h, 24h, 35h,

52h and 55h for TG-IGF1 and 0h, 30 minutes, 1h, 2h, 6h, 12h, 24h, 30h, 41h, 52h and 55h for recombinant native IGF1.

As indicated in Fig. 67, it was observed that at the beginning of 30 minutes, about 4% TG-IGF1 was burst from the fibrin gel matrices. Then after 6 hours incubation, about 8% TG-IGF1 was released from the fibrin gel matrices. Within the 60h incubation period, about 88% of added TG-IGF1 remained within fibrin gel (n=3, values were means  $\pm$  SEM).

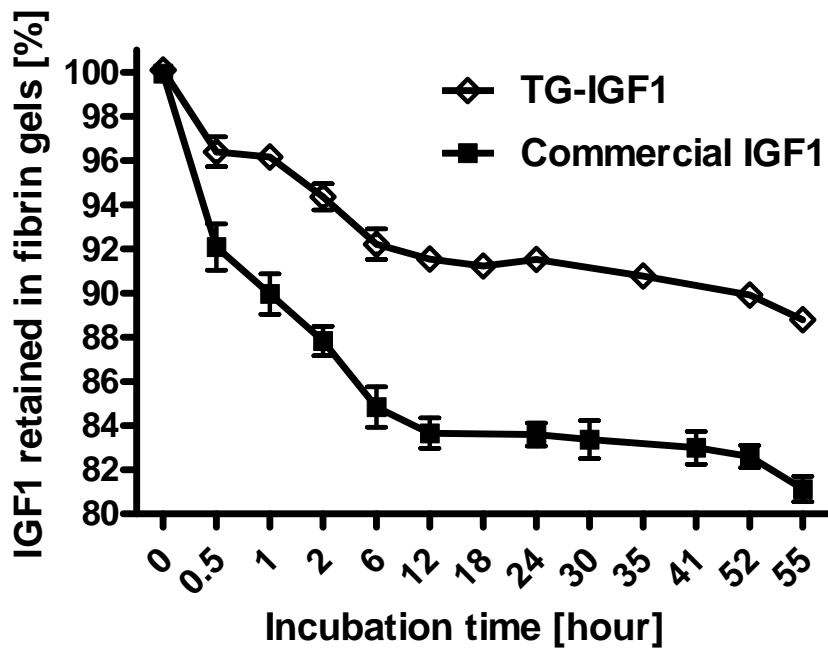


Fig 67. Determination of TG-IGF1 and commercial IGF1 controlled releasing from fibrin gels in percentage vs incubation time in hour. 100ul fibrin gels with 50ng/ml TG-IGF1 or commercial IGF1 respectively were incubated in 1.5ml TBS at 37°C. At the indicated time points, released IGF1 concentration in TBS was determined by ELISA with human IGF1 antibody (n=3, value were mean  $\pm$  SEM).

It was also showed that at the beginning of 30 minutes, about 8% recombinant native IGF1 was burst from the fibrin gel matrices, double quantity more than TG-IGF1. Then after 6 hours inoculation, about 16% recombinant native IGF1 was released from the fibrin gel matrices, which was also nearly double quantity more than TG-IGF1. Within the 60h incubation period, about 81% of added recombinant native IGF1 remained within fibrin gel (n=3, values were means  $\pm$  SEM). So, for 100ul fibrin gel, TG-IGF1 was 7% more controlled released from gels than recombinant native IGF1 under the same physiologic condition.

## Rat bladder muscle layer regeneration

HEK-Blue LPS detection kit (Invitrogen, USA) was used to determine the endotoxin value for TG-IGF1. This kit is based on the ability of Toll like receptor 4 (TLR4), to recognize structurally different LPS from gram-negative bacteria and in particular lipid A, their toxic moiety.

HEK-blue-4 cells, which are very sensitive to lipopolysaccharide (LPS), were seeded 30'000 cells per well in one 48-well plate. Three days later, the cell medium was removed. 360ul HEK-blue detection medium was added into each well. Then 40ul dilution medium containing different quantities of TG-IGF1 were added into each well. The samples were tested in duplicate. Then the plate was incubated for 18 hours at 37°C. Finally, the plate was read at 640nm. According to the standard curve, the endotoxin value for TG-IGF1 was  $\leq 1$  EU/ug. The endotoxin value for recombinant native IGF1 was also  $< 1$  EU/ug. Thus, the endotoxin value for TG-IGF1 was slightly higher than that of the native recombinant IGF1. Both were judged to be acceptable for implantation.

During two series of animal experiments, no mortality was observed. During the first series, there were four rats in the negative control group, resection only. There were four rats in the fibrin gel only group. There were also four rats in the fibrin gel with 100ng TG-IGF1. The rats were distributed randomly to each group. The experiment was conducted for 28 days. In the 4-week specimens, there were a few unusual formations in three bladders, one in the negative control group (#1), and two in fibrin gel only group (#2 and 3). The images of H&E staining of all specimens are in Annex 1.

From the standard histological staining results (Fig. 68), it was noticed that the rat bladder regenerated its muscle layer in the fibrin gel with TG-IGF1 group, but also involved lymphocytes and mast cells. Lymphocytes were involved due to inflammation, which may be caused by endotoxin present in the TG-IGF1 and by wound. Among the 4 rats in this group, three bladders displayed different degrees of bladder muscle layer regeneration. During animal surgery, fibrin gels were made *in-situ* with a sterile low binding eppendorf tube on the top of three resections. About one minute later, the gel was cut off the wall of tube. Due to an inflated surface, one fibrin gel with TG-IGF1 leaked during gel polymerization in one eppendorf tube and formed glue. The speed of both infiltrating SMCs and gel degradation was related to the contacted gel surface. Thus gel degradation was slower than glue. This could be one reason that this rat bladder muscle layer was not regenerated due to glue formation.

There was no bladder muscle layer regeneration in the negative control group. The bladder muscle layer was slightly regenerated in the fibrin gel only group, but much less than the bladder regenerated in the fibrin gel with TG-IGF1 group. Due to no TG-IGF1 incorporation, there were few lymphocytes and mast cells involved in the muscle layer regeneration in two control groups.

For the quantification of detrusor muscle regenerated over normal detrusor muscle, it was  $0.12 \pm 0.08$  (mean $\pm$ SEM, Fig. 70) for resection only group and  $0.00 \pm 0.00$  for fibrin gel only group. It was  $0.31 \pm 0.18$  for TG-IGF1 group. So, defected detrusor muscle layer tissue was indeed regenerated by fibrin gel incorporated with TG-IGF1.

During the second series, there were five rats in the negative control group, resection only. There were five rats in the fibrin gel only group, five rats in the fibrin gel with 100ng TG-IGF1 group, and five rats in the fibrin gel with 100ng native recombinant IGF1 group. The rats were distributed randomly to each group. The experiment was conducted also for 28 days. The only difference of manipulation between two series experiment was the resection method. For the first series, the resection was made by directly cutting off the muscle layer under the microscope. For the second series, the resection was made by opening the muscle layer using a scalpel and tweezers. In the 4-week specimens, there was just one bladder in the negative control group displaying some abnormal tissue after H&E staining. The images of H&E staining of all specimens are located in Annex 2.

From the standard histological staining results (Fig. 69), it was noticed that the rat bladder wall did not regenerate its muscle layer after 28 days in the resection only group. In the fibrin gel only group, the rat bladder muscle layer did regenerate, but very little. In the fibrin gel with native recombinant IGF1 group, the rat bladder muscle layer was regenerated, more than fibrin gel only group. In the fibrin gel with TG-IGF1 group, the rat bladder muscle layer was the most regenerated. This observation was confirmed by the quantitative analysis of detrusor muscle regenerated over normal detrusor muscle. The value was  $0.08 \pm 0.07$  (mean $\pm$ SEM, Fig. 70) for resection only group and  $0.11 \pm 0.09$  for fibrin gel only group. Due to detrusor muscle regeneration, the value was much higher for IGF1 groups. It was  $0.23 \pm 0.10$  for native recombinant IGF1 group and  $0.27 \pm 0.10$  for TG-IGF1 group. So, defected detrusor muscle layer tissue was indeed regenerated by fibrin gel incorporated with IGF1, especially with TG-IGF1. This suggests that TG-IGF1 is released in a controlled manner from the fibrin gel matrices and have longer effect on muscle layer regeneration than the native recombinant IGF1.

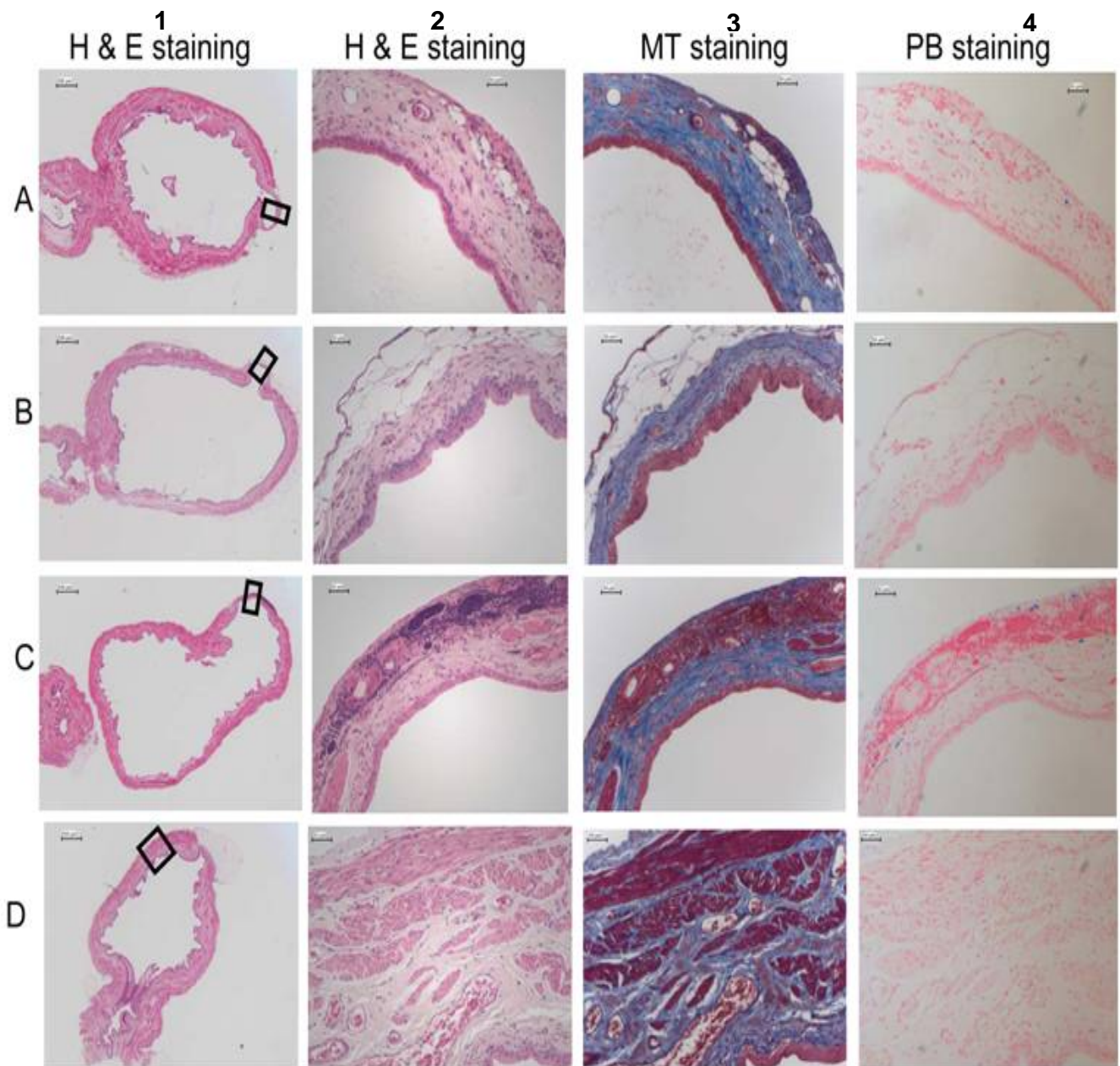


Fig 68. Rat bladder wall histology staining (H&E, MT and PB) for the first series experiment (n=4). All images were approved by pathologist Dr. Taminelli. For H&E, the muscle was stained deep pink red. For MT, the muscle was stained pink red. For PB, the hemosiderine were stained blue, representing the site of injection. Group A was resection only, nearly no detrusor muscle regenerated. Group B was 100ul fibrin gel only, hardly detrusor muscle regenerated. Group C was 100ul fibrin gel with 100ng TG-IGFI, with obviously some detrusor muscle regenerated. Group D was normal bladder tissue. Scale bars=500um for lane 1 and scale bars=50um from lane 2 to 4.

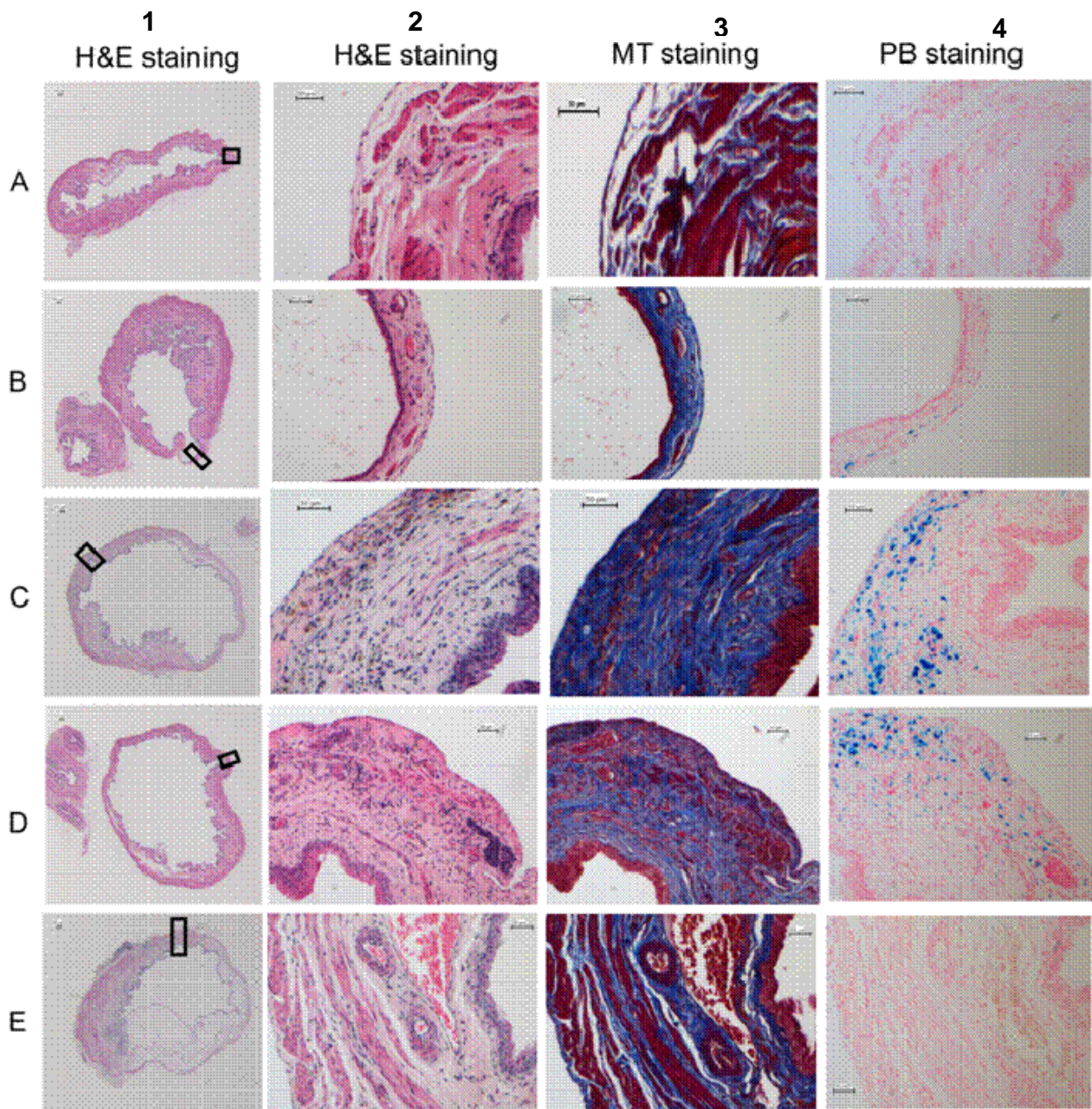
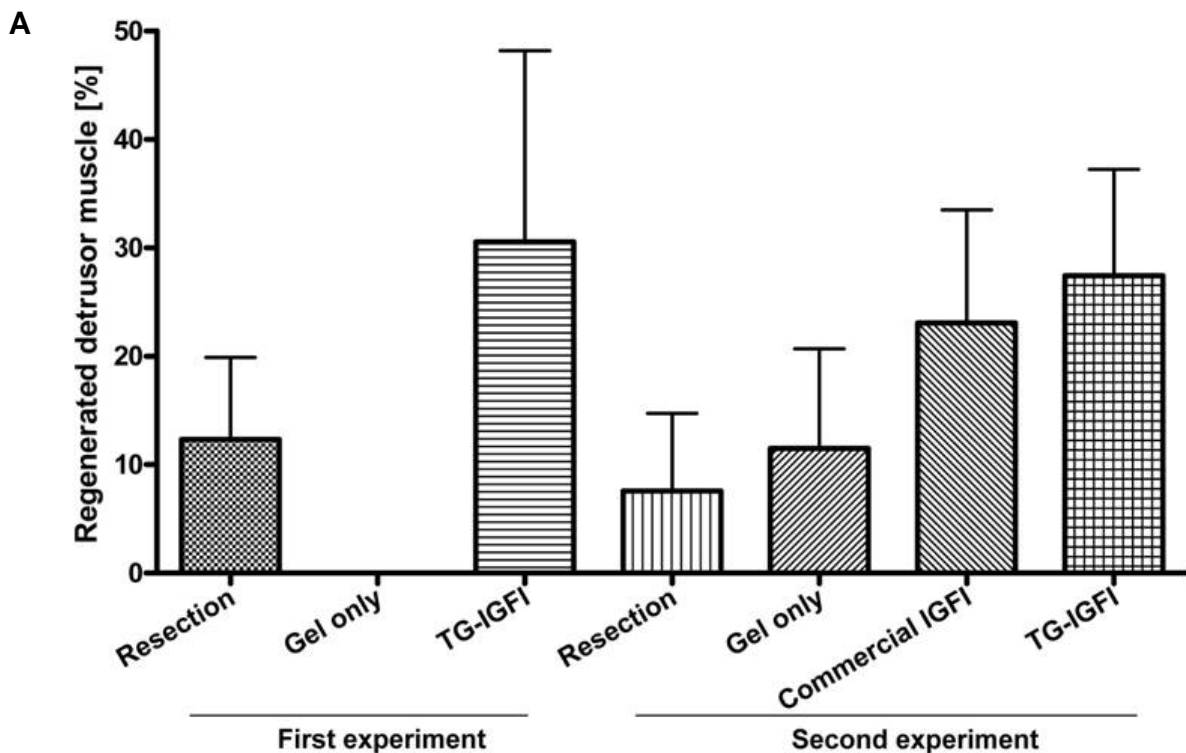


Fig 69. Rat bladder wall histology staining (H&E, MT and PB) for the second series experiment (n=5). All images were approved by pathologist Dr. Taminelli. For H&E, the muscle was stained deep pink red. For MT, the muscle was stained pink red. For PB, the hemosiderine were stained blue, representing the site of injection. Group A was resection only. Group B was 100ul fibrin gel only. For Groups A and B, there was nearly no detrusor muscle regenerated. Group C was 100ul fibrin gel with 100ng commercial IGFI. Group D was 100ul fibrin gel with 100ng TG-IGFI. For Groups C and D, there was some detrusor muscle regenerated. Group E was normal bladder tissue. Scale bars=500um for lane 1 and scale bars=50um from lane 2 to 4.



**B**

Groups	Resection only	Fibrin gel only	Commercial IGFI	TG-IGFI
First experiment	0.12±0.08	0.0±0.0	NA	0.31±0.18
Second experiment	0.08±0.07	0.11±0.09	0.23±0.10	0.27±0.10

Fig 70. Quantitative analyze data of two series of rat bladder wall regeneration for 28 days using

A) graphic representation of regenerated detrusor muscle in percentage and B) table representation of regenerated detrusor muscle in ratio. The data, blindly analyzed with Dr. Hasegawa using program Fiji, showed that for both experiments, fibrin gel with TG-IGFI regenerated more detrusor muscle defected than two control groups, resection only and fibrin gel only. In the second experiment, fibrin gel with TG-IGFI (27%) could regenerate slightly more detrusor muscle defected than the gel with commercial IGFI (23%). The measurement is presented as mean ± SEM. P value is not significant.

For two series experiments, according to results from the section staining and from quantitative analysis of detrusor muscle area regenerated over normal detrusor muscle area, defected detrusor muscle was regenerated much more by fibrin gel with TG-IGFI (27%-31%) or fibrin gel

with native recombinant IGF1 (23%) than by fibrin gel only (0%-11%) or resection only (8%-12%). So, TG-IGF1 can stimulate bladder smooth muscle regeneration.

## **Conclusion**

Recombinant TG-IGF1 protein produced by E.coli was successfully purified by GST affinity chromatography and maintained its bioactivity. 5ug purified TG-IGF1 can be obtained per liter bacteria culture. Its purity was analyzed by SDS-PAGE and western blot. The amino acid sequence was confirmed by MALDI-TOF mass spectrometry. More than 88% of TG-IGF1 could be retained in the fibrin gel after 55 hours incubation. Its bioactivity was analyzed both in vitro and in vivo. TG-IGF1 could bind to IGF1 receptors to stimulate receptor phosphorylation and result in 3T3 cell proliferation using the MTT assay. In fibrin gels, TG-IGF1 could stimulate SMCs to synthesize proteins. This was the reason why SMCs displayed more abundant and larger secretory vesicles as showed in the TEM imaging compared to control samples. TG-IGF1 could also down-regulate two genes in SMCs in the field of ECM and adhesion molecules, the same as native recombinant IGF1. TG-IGF1 in fibrin gels could also accelerate rat bladder muscle layer regeneration (27%-31%), more than native recombinant IGF (23%) after 28 days treatment. It is due to TG-IGF1 cross-linked and controlled releasing in fibrin gels. So, recombinant TG-IGF1 is more bioactive than native recombinant IGF1 in fibrin gel, which can better stimulate bladder smooth muscle proliferation and regeneration.

## **Acknowledgement**

I would like to thank Dr. Jessica Dessimoz, Véronique Garea, Stéphanie Rosset, Dr. Graham Knott and Dr. Otto Hagenbuchle for their technical assistance. I acknowledge Professor Dr. Thomas Barker, Dr. SeungTae Lee, Dr. Jung-Im Yun, M.D Lionel Micol, Pierre Maillard, Asad Qureshi, Dr. Jacques Rougemont, Dr. Lucia Baldi, Véréne Pignat, Dr. Jacqueline Shields, Véronique Borel, Manuel Bueno, Dr. Yunsuk Jo, Dr. André Van der Vlies, Dr. Catharina Adelöw, Stephane Kontos, Dr. Alessandra Calabrese and Julia Braunecker for their advice concerning divers techniques. Moreover, this work was funded by a grant from 3G-scaff and CTI.

## **Reference**

1. Salmon, W.D., Jr. & Daughaday, W.H. A hormonally controlled serum factor which stimulates sulfate incorporation by cartilage in vitro. *J Lab Clin Med* **49**, 825-836 (1957).



2. Laron, Z. Insulin-like growth factor 1 (IGF-1): a growth hormone. *Mol Pathol* **54**, 311-316 (2001).
3. Daughaday, W.H. et al. Somatomedin: proposed designation for sulphation factor. *Nature* **235**, 107 (1972).
4. Rinderknecht, E. & Humbel, R.E. Polypeptides with nonsuppressible insulin-like and cell-growth promoting activities in human serum: isolation, chemical characterization, and some biological properties of forms I and II. *Proc Natl Acad Sci U S A* **73**, 2365-2369 (1976).
5. Abuzzahab, M.J. et al. IGF-I receptor mutations resulting in intrauterine and postnatal growth retardation. *N Engl J Med* **349**, 2211-2222 (2003).
6. Ratner, M. New IGF drug stirs competition in growth factor segment. *Nat Biotechnol* **23**, 1192 (2005).
7. Bautista, C.M., Mohan, S. & Baylink, D.J. Insulin-like growth factors I and II are present in the skeletal tissues of ten vertebrates. *Metabolism* **39**, 96-100 (1990).
8. Russell-Jones, D.L. et al. A comparison of the effects of IGF-I and insulin on glucose metabolism, fat metabolism and the cardiovascular system in normal human volunteers. *Eur J Clin Invest* **25**, 403-411 (1995).
9. Rajpathak, S.N. et al. Insulin-like growth factor-(IGF)-axis, inflammation, and glucose intolerance among older adults. *Growth Horm IGF Res* **18**, 166-173 (2008).
10. Fontana, L. The scientific basis of caloric restriction leading to longer life. *Curr Opin Gastroenterol* **25**, 144-150 (2009).
11. Ren, J., Samson, W.K. & Sowers, J.R. Insulin-like growth factor I as a cardiac hormone: physiological and pathophysiological implications in heart disease. *J Mol Cell Cardiol* **31**, 2049-2061 (1999).
12. Rubin, R. & Baserga, R. Insulin-like growth factor-I receptor. Its role in cell proliferation, apoptosis, and tumorigenicity. *Lab Invest* **73**, 311-331 (1995).
13. Stiles, C.D. et al. Dual control of cell growth by somatomedins and platelet-derived growth factor. *Proc Natl Acad Sci U S A* **76**, 1279-1283 (1979).
14. Banskota, N.K., Taub, R., Zellner, K., Olsen, P. & King, G.L. Characterization of induction of protooncogene c-myc and cellular growth in human vascular smooth muscle cells by insulin and IGF-I. *Diabetes* **38**, 123-129 (1989).
15. Heuson, J.C. & Legros, N. Influence of insulin deprivation on growth of the 7,12-dimethylbenz(a)anthracene-induced mammary carcinoma in rats subjected to alloxan diabetes and food restriction. *Cancer Res* **32**, 226-232 (1972).

16. Pollak, M.N., Perdue, J.F., Margolese, R.G., Baer, K. & Richard, M. Presence of somatomedin receptors on primary human breast and colon carcinomas. *Cancer Lett* **38**, 223-230 (1987).
17. Pollak, M. Targeting insulin and insulin-like growth factor signalling in oncology. *Curr Opin Pharmacol* **8**, 384-392 (2008).
18. Pollak, M. Insulin and insulin-like growth factor signalling in neoplasia. *Nat Rev Cancer* **8**, 915-928 (2008).
19. Lewis, M.E. et al. Insulin-like growth factor-I: potential for treatment of motor neuronal disorders. *Exp Neurol* **124**, 73-88 (1993).
20. Brower, V. Prostate-cancer link sours IGF-1. *Nat Biotechnol* **16**, 223 (1998).
21. Pelosi, L. et al. Local expression of IGF-1 accelerates muscle regeneration by rapidly modulating inflammatory cytokines and chemokines. *FASEB J* **21**, 1393-1402 (2007).
22. Musaro, A. et al. Localized IGF-1 transgene expression sustains hypertrophy and regeneration in senescent skeletal muscle. *Nat Genet* **27**, 195-200 (2001).
23. Rabinovsky, E.D. et al. Targeted expression of IGF-1 transgene to skeletal muscle accelerates muscle and motor neuron regeneration. *FASEB J* **17**, 53-55 (2003).
24. Osborne, R. Commercial interest waxes for IGF-1 blockers. *Nat Biotechnol* **26**, 719-720 (2008).
25. Wenk, E., Meinel, A.J., Wildy, S., Merkle, H.P. & Meinel, L. Microporous silk fibroin scaffolds embedding PLGA microparticles for controlled growth factor delivery in tissue engineering. *Biomaterials* **30**, 2571-2581 (2009).
26. Kothapalli, C.R. & Ramamurthi, A. Benefits of concurrent delivery of hyaluronan and IGF-1 cues to regeneration of crosslinked elastin matrices by adult rat vascular cells. *J Tissue Eng Regen Med* **2**, 106-116 (2008).
27. Zisch, A.H., Schenk, U., Schense, J.C., Sakiyama-Elbert, S.E. & Hubbell, J.A. Covalently conjugated VEGF--fibrin matrices for endothelialization. *J Control Release* **72**, 101-113 (2001).
28. Schense, J.C., Bloch, J., Aebischer, P. & Hubbell, J.A. Enzymatic incorporation of bioactive peptides into fibrin matrices enhances neurite extension. *Nat Biotechnol* **18**, 415-419 (2000).
29. Hubbell, J. Matrix-bound growth factors in tissue repair. *Swiss Med Wkly* **136**, 387-391 (2006).

30. Walker, J.B. & Nesheim, M.E. The molecular weights, mass distribution, chain composition, and structure of soluble fibrin degradation products released from a fibrin clot perfused with plasmin. *J Biol Chem* **274**, 5201-5212 (1999).
31. Korossis, S., Bolland, F., Southgate, J., Ingham, E. & Fisher, J. Regional biomechanical and histological characterisation of the passive porcine urinary bladder: Implications for augmentation and tissue engineering strategies. *Biomaterials* **30**, 266-275 (2009).
32. Drake, M.J. The integrative physiology of the bladder. *Ann R Coll Surg Engl* **89**, 580-585 (2007).
33. Baskin, L.S. et al. Growth factors in bladder wound healing. *J Urol* **157**, 2388-2395 (1997).
34. Kanematsu, A. et al. Induction of smooth muscle cell-like phenotype in marrow-derived cells among regenerating urinary bladder smooth muscle cells. *Am J Pathol* **166**, 565-573 (2005).
35. Ling, Y., Maile, L.A. & Clemmons, D.R. Tyrosine phosphorylation of the beta3-subunit of the alphaVbeta3 integrin is required for membrane association of the tyrosine phosphatase SHP-2 and its further recruitment to the insulin-like growth factor I receptor. *Mol Endocrinol* **17**, 1824-1833 (2003).
36. Maile, L.A., Capps, B.E., Ling, Y., Xi, G. & Clemmons, D.R. Hyperglycemia alters the responsiveness of smooth muscle cells to insulin-like growth factor-I. *Endocrinology* **148**, 2435-2443 (2007).
37. Upadhyay, J., Aitken, K.J., Damdar, C., Bolduc, S. & Bagli, D.J. Integrins expressed with bladder extracellular matrix after stretch injury in vivo mediate bladder smooth muscle cell growth in vitro. *J Urol* **169**, 750-755 (2003).
38. Barton, P.J. et al. Myocardial insulin-like growth factor-I gene expression during recovery from heart failure after combined left ventricular assist device and clenbuterol therapy. *Circulation* **112**, 146-50 (2005).
39. Delaughter, M.C., Taffet, G.E., Fiorotto, M.L., Entman, M.L. & Schwartz, R.J. Local insulin-like growth factor I expression induces physiologic, then pathologic, cardiac hypertrophy in transgenic mice. *FASEB J* **13**, 1923-1929 (1999).
40. Musaro, A., McCullagh, K.J., Naya, F.J., Olson, E.N. & Rosenthal, N. IGF-1 induces skeletal myocyte hypertrophy through calcineurin in association with GATA-2 and NF-ATc1. *Nature* **400**, 581-585 (1999).

41. Weichert, H., Blechschmidt, I., Schroder, S. & Ambrosius, H. The MTT-assay as a rapid test for cell proliferation and cell killing: application to human peripheral blood lymphocytes (PBL). *Allerg Immunol (Leipz)* **37**, 139-144 (1991).
42. Schmelzle, K. & White, F.M. Phosphoproteomic approaches to elucidate cellular signaling networks. *Curr Opin Biotechnol* **17**, 406-414 (2006).
43. Schmelzle, K., Kane, S., Gridley, S., Lienhard, G.E. & White, F.M. Temporal dynamics of tyrosine phosphorylation in insulin signaling. *Diabetes* **55**, 2171-2179 (2006).
44. Kim, J.J. & Accili, D. Signalling through IGF-I and insulin receptors: where is the specificity? *Growth Horm IGF Res* **12**, 84-90 (2002).
45. Zhang, Z. & Su, D. Behaviour of TEM metal grids during in-situ heating experiments. *Ultramicroscopy* (2009).
46. Upton, Z. et al. Evolution of insulin-like growth factor (IGF) function: production and characterization of recombinant hagfish IGF. *Gen Comp Endocrinol* **105**, 79-90 (1997).
47. Mahadevan, L.C., Willis, A.C. & Barratt, M.J. Rapid histone H3 phosphorylation in response to growth factors, phorbol esters, okadaic acid, and protein synthesis inhibitors. *Cell* **65**, 775-783 (1991).
48. Skalli, O. et al. Alpha-smooth muscle actin, a differentiation marker of smooth muscle cells, is present in microfilamentous bundles of pericytes. *J Histochem Cytochem* **37**, 315-321 (1989).
49. Chi, M., Zhou, Y., Vedamoorthyrao, S., Babu, G.J. & Periasamy, M. Ablation of smooth muscle myosin heavy chain SM2 increases smooth muscle contraction and results in postnatal death in mice. *Proc Natl Acad Sci U S A* **105**, 18614-18618 (2008).
50. Durand-Arczynska, W., Marmy, N. & Durand, J. Caldesmon, calponin and alpha-smooth muscle actin expression in subcultured smooth muscle cells from human airways. *Histochemistry* **100**, 465-471 (1993).

## Chapter V Retrospective and Outlook

### *Retrospective*

During this thesis I was able to learn a great deal regarding protein engineering, and how to bring together various research methods and techniques to create new functional fusion proteins towards bladder tissue repair. Towards this goal, I was able to generate both a peptide-protein biomacromolecule comprised of a factor XIIIa substrate and IGF1 (TG-IGF1), as well as a new IGF1-fibrinogen fusion protein. The goal of my research was to deliver IGF1 to an induced wound site using a rat bladder *in vivo* model. Towards this goal, I was able to produce the fusion protein variants and test the TG-IGF1 fusion protein both *in vitro* and *in vivo* with very favourable results. During this thesis, I was required to also learn about advanced cell culture techniques, and various other skills to characterize the *in vitro* and *in vivo* systems I used to produce this thesis. These include cloning, western blot, RT-qPCR, TEM, MTT cell proliferation assay, phosphorylation assay, recombinant protein production both by E.Coli and by mammalian CHO cells, mammalian cells in serum free and suspension culture, cell line isolation, recombinant protein purification, fibrin gel formation, cell and gel staining, animal experiment, histological stainings, etc. Learning these techniques will provide for a sound foundation to continue my scientific career, whether in industry or academia.

The peptide TG was the first eight amino acids NQEQVSPL of  $\alpha_2$ -plasmin inhibitor ( $\alpha_2$ PI<sub>1-8</sub>). It was the factor XIIIa substrate to mediate IGF1 cross-linking into fibrin gels during polymerization. The goal of adding TG sequences was to control release IGF1 from fibrin gels and then to strengthen IGF1 function by increasing its life span. TG-IGF1 produced by E. coli was successfully purified by GST affinity chromatography. Its purity was visible on SDS-PAGE using 1% agarose gel and western blot using IGF1 antibody. Its amino acid sequence was confirmed by MALDI-TOF mass spectrometry.

Then TG-IGF1 bioactivity was analyzed *in vitro*. TG-IGF1 showed its bioactivity same as native recombinant IGF1 in MTT cell proliferation assay and in IGF1 receptor phosphorylation assay using IGF1 receptor and phosphor-IGF1 receptor antibodies. TG-IGF1 also showed its advantage to the morphology of SMCs seeded on the fibrin gels. TEM images were taken when SMCs was inoculated for 3 days in three types of fibrin gels, fibrin gel only, fibrin gel with native recombinant IGF1 and fibrin gel with TG-IGF1. There were more and bigger secretory vesicles in SMCs when fibrin gel was incorporated with TG-IGF1. It was maybe TG-IGF1 controlled

released from fibrin gels so that IGF1 could act longer in SMCs than native recombinant IGF1. Gene expression level was also performed by RT-qPCR from SMCs inoculated in three types of fibrin gels for 24 hours. Gene expression level by SMCs to TG-IGF1 and to native recombinant IGF1 was similar among 84 genes of extracellular matrix and adhesion molecules. Two genes, SPP1 and KAL1, were down-regulated in SMCs cultured in fibrin gels with either TG-IGF1 or native recombinant IGF1 compared to the fibrin gels only. As we know that IGF1 plays one role in SMCs migration and angiogenesis. SPP1 mediates angiogenesis during pregnancy while KAL1 is involved in angiogenesis during cancer. So, for SMCs in fibrin gels *in vitro*, TG-IGF1 or native recombinant IGF1 down-regulated significantly SPP1 and KAL1 (n=3, p<0.07).

The bioactivity of TG-IGF1 was also performed *in vivo* using rat bladder model. Three resections were made in the detrusor muscle layer. Three different kinds of fibrin gels were made *in-situ* on the top of the injury with ingrowing autologous SMCs. The bladder muscle layer was able to be regenerated by local delivery of TG-IGF1 in fibrin gels. From histological stainings HE, MT and PB, the structure of repaired tissue was similar to the native tissue and there was no fibrous tissue formed on the place of resection (group=3, n=4; group=4, n=5). The quantitative analyze data showed detrusor muscle regeneration rate of TG-IGFI, about 31% or 27%. For second series of experiment, due to native recombinant IGFI diffusing from gels to environment, it lost slightly its quantity compared to cross-linked and controlled releasing TG-IGFI in fibrin gels. So, fibrin gels with native recombinant IGFI regenerated defect bladder muscle layer less than TG-IGFI, 23% instead of 27%. During dissection, injured bladders with TG-IGF1 in fibrin gels had one size bigger than others due to containing urine, which was a good signal for normal bladder physiological function. This is another indication that defected detrusor muscle layer was much better regenerated by TG-IGF1 than control groups. This work offered one opportunity in treatment for bladder dysfunction. And it would be interesting to analyze gene expression *in vivo* of angiogenesis molecules, such as SPP1 and KAL1.

During dissection of rats, no more fibrin gels were found. All fibrin gels were degraded and no bioactive IGFI remained after tissue repair. On one hand, the detrusor muscle regeneration was not complete yet, 31% at most. So, to strengthen TG-IGFI effect on the detrusor muscle regeneration, more quantity of TG-IGFI could be added in the fibrin gel. On the other hand, systemic side effects were limited. The histological staining also revealed that the rats treated by fibrin gels with TG-IGFI displayed bladder muscle layer regeneration without fibrosis formation up to 4 weeks. It demonstrated that the design of TG-IGFI incorporated fibrin gels was useful in tissue engineering for wound healing and tissue regeneration.

Two new cell lines were made in this work, CHO<sub>FGA5aaIGF1</sub> and CHO<sub>FGA5aaMMPIGF1</sub>. These cell lines were characterized by FACS using fibrinogen antibody and ELISA using both IGF1 and fibrinogen antibodies. Purified recombinant fusion protein fibrinogen-IGF1 would be used to make fibrin gels with IGF1 covalently linked. Recombinant fibrinogen protein produced by these CHO cells met purification problem due to low quantity of fibrinogen expressed (about 20ng/ml), which should be resolved in the near future. Although I was unable to purify the fibrinogen fusion proteins, a great deal was learned in the process, especially regarding the protein production and purification.

## **Outlook**

Due to donor shortage, metabolic and immune problems of traditional treatment, bladder tissue engineering offers one alternative treatment to bladder dysfunction. It is one important part of tissue engineering. During the repair and regeneration process in the body, the body's response to the injury is the summary of all factors and can trigger a lot of mechanisms, which can result in fibrosis tissue and scar formation. So, fibrosis is one challenge for tissue engineering.

In order to restore bladder function and structure without side effect, several technologies are developing. First, nanoscale materials can be used as scaffold to facilitate the communication between cells. Secondly, tissue bioreactors can be employed to imitate bladder mechanical environment to enhance artificial bladder tissue formation *in vitro*. Thirdly, stem cells, such as mesenchymal stem cells, can be used and differentiated into smooth muscle cells for bladder wall regeneration. Fourthly, beside collagen-based matrix, more biomaterials can be provided as scaffold with and without cells and proteins, such as growth factors. Atala's research group had successfully made one neo-bladder *in vitro* using synthetic scaffold PLGA/PGA with UCs and SMCs seeded on two sides. Finally the bladder tissue engineering is also related to the angiogenesis/vasculature and nerve system regeneration of injured tissue.

In this work, although the mechanisms of detrusor muscle regeneration are not well understood, we attempted to restore and maintain bladder function by regenerating or repairing bladder using IGF1. Because TG-IGF1 showed its bioactivity and its controlled releasing profile in fibrin gels in the diver assays and in animal experiment, more animal models can be used to testify its bioactivity, such as pig bladder muscle layer regeneration and rat heart muscle regeneration. Due to fibrin gels too soft and lack of mechanical strength, TG-aprotinin to controlled release TG-IGF1 from fibrin gel or synthetic polymers, such as PLGA and PEG, can be incorporated with fibrin gels and be used as co-polymer biomaterials.

Although a great deal of research has been produced regarding both natural materials and synthetic tissue engineering, few products have produced approved therapeutics. In this sense, we are still in the early stage of tissue engineering. During this thesis I was able to display rat bladder smooth muscle cell regeneration using a relatively simple fibrin gel / TG-IGF1 fusion protein matrix. However, this is only the beginning. Further research must be directed at not only repair of an induced wound, but total bladder regeneration. Towards this goal delivery of novel fusion proteins, peptide, and small molecules will need to be deployed to achieve the complex signal cascade necessary to achieve this result. This could be accomplished by the fusion of synthetic nanocarriers such as hydrolytically sensitive hydrogel microspheres or polymersomes, and or functionalized polymeric micelles to release hydrophobic small molecules.

To solve the problem about low fibrinogen expression by CHO cell lines, there are several options. First, more new cell lines showing higher fibrinogen expression should be made. Secondly, the expression system for CHO cell line can be changed. But CHO<sub>f<sub>gn</sub></sub> cells grew difficult in suspension cell culture due to sticky fibrinogen polymerisation. The problem is resolving slowly. If this problem can be resolved one day, more CHO cells, expressing therapeutic bioactive substance, can be culture in suspension using pTet-on system. It offers one new way to produce recombinant protein in industry for clinical application. Thirdly, cell culture medium can be changed or improved, such as feeding some special ingredients (glucose, certain amino acids, vitamins, etc.) which is very important for this cell line. Finally, the culture conditions should be modified, such as temperature, pH. Sometime lower temperature, such as 30-33°C, can increase CHO cell productivity.

For the purification of fusion protein fibrinogen-IGF1, new more affinity peptides to fibrinogen can be found using phage library technology. Then affinity chromatography column can be made specially to purify fusion fibrinogen proteins. After the bioactivity of fusion protein is analyzed in vitro, two generations of fibrin gels can be compared in animal models, such as rat bladder detrusor muscle layer regeneration.

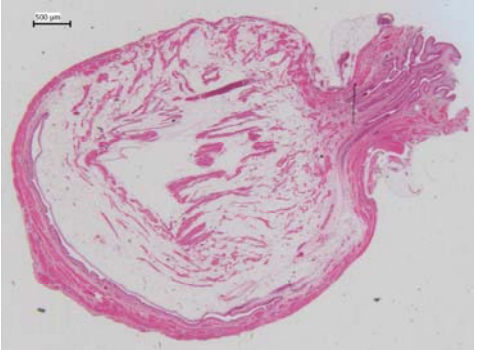
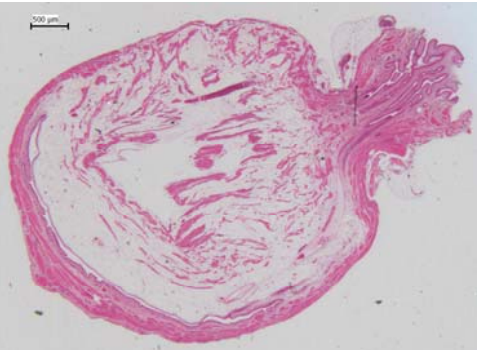


**Annex 1. Histology staining of rat bladder specimens at 4 weeks for first series experiment**



Resection only

**Resection only**

<p><b>Hematoxylin &amp; Erythrosine staining</b> Nuclei are stained blue-black. Muscle is stained deep pink red</p>	<p><b>Masson's Trichrome staining</b> Nuclei are stained braun. Muscle is stained pink red. Collagen is stained blue</p>	<p><b>Prussian Blue</b> Iron (hemosiderine) is stained blue. Asbestos bodies are stained blue-black. Nuclei are stained red</p>	
			
			

Resection only

Hematoxylin & Erythrosine staining

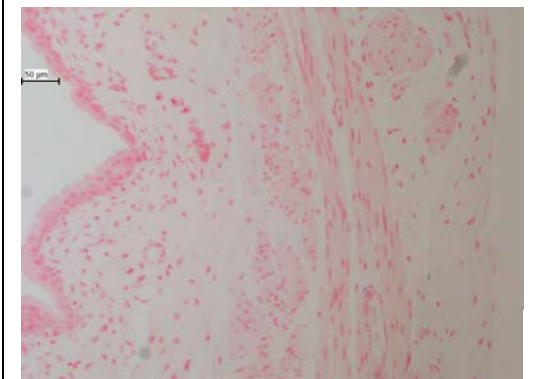
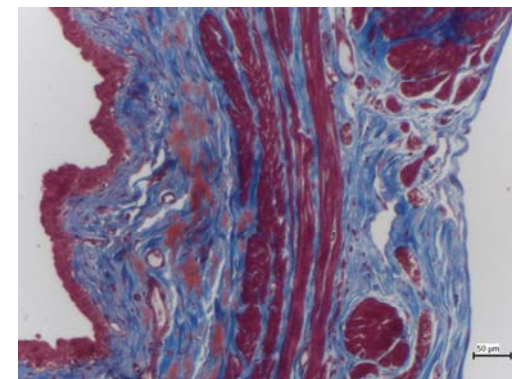
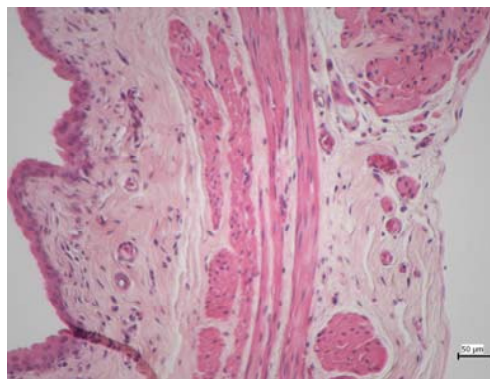
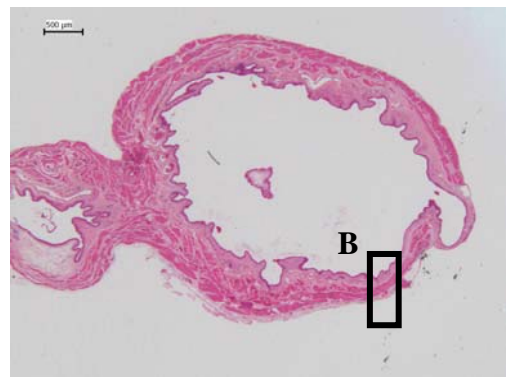
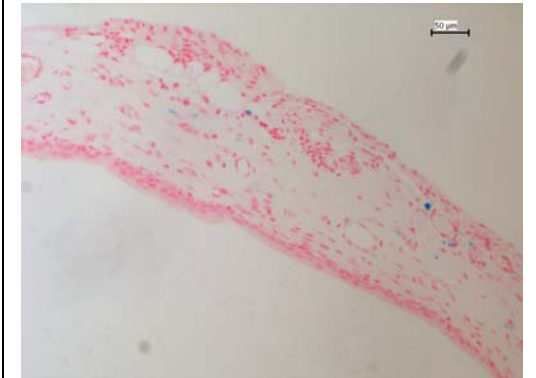
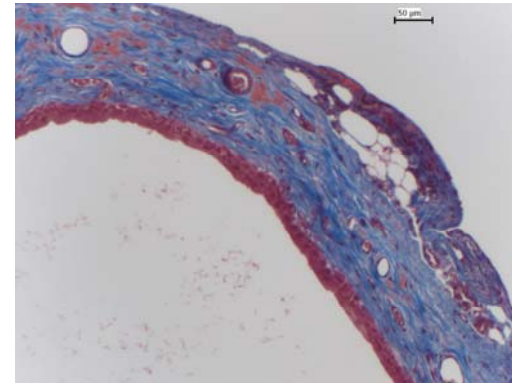
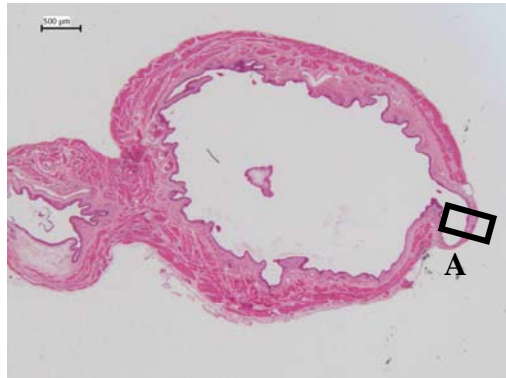
Nuclei are stained blue-black.  
Muscle is stained deep pink red

Masson's Trichrome staining

Nuclei are stained brown.  
Muscle is stained pink red.  
Collagen is stained blue

Prussian Blue

Iron (hemosiderine) is stained blue.  
Asbestos bodies are stained blue-black.  
Nuclei are stained red



Resection only

Hematoxylin & Erythrosine staining

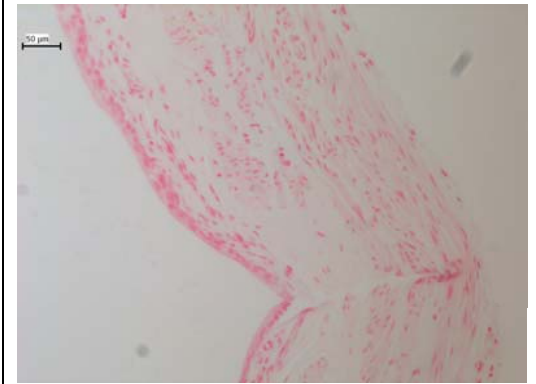
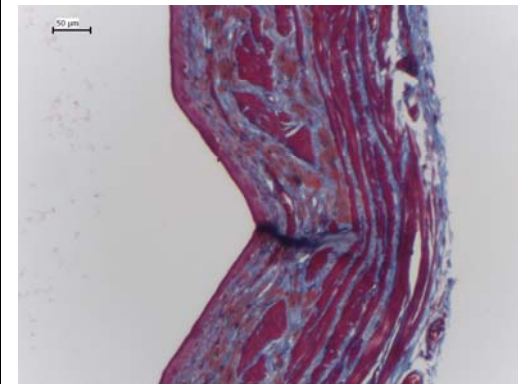
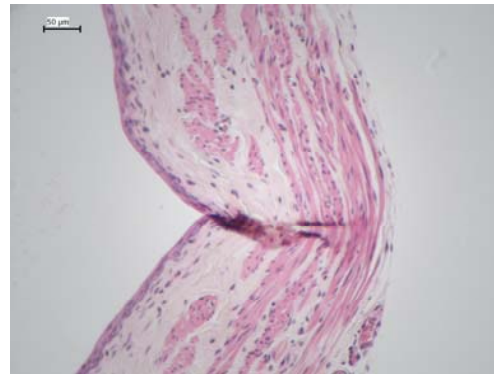
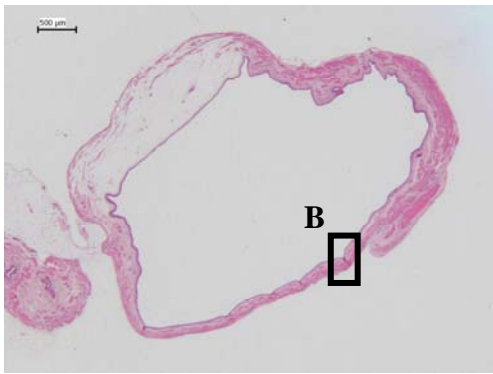
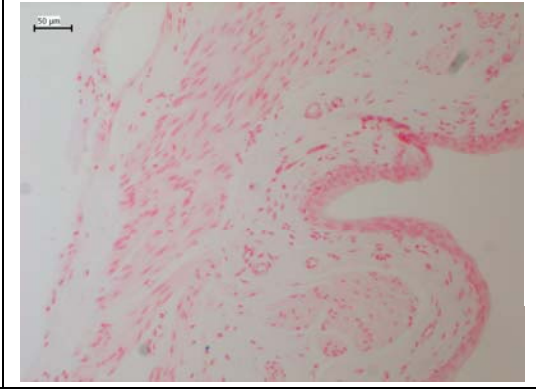
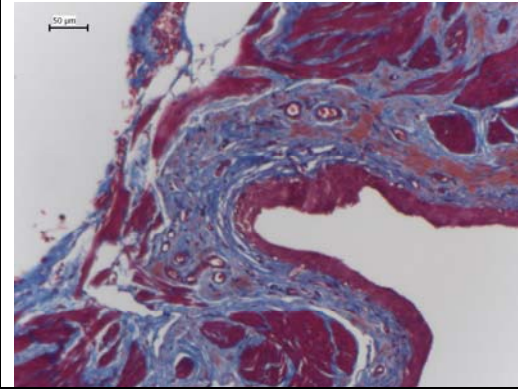
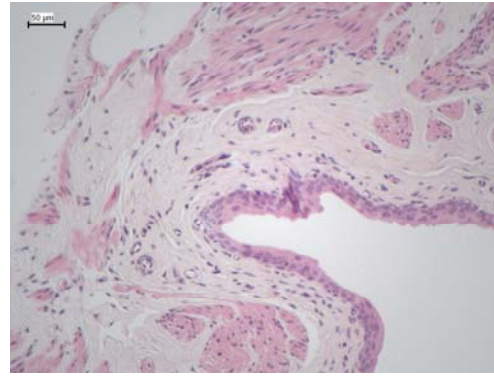
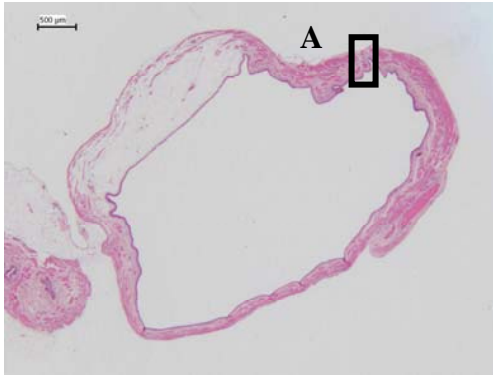
Nuclei are stained blue-black.  
Muscle is stained deep pink red

Masson's Trichrome staining

Nuclei are stained braun.  
Muscle is stained pink red.  
Collagen is stained blue

Prussian Blue

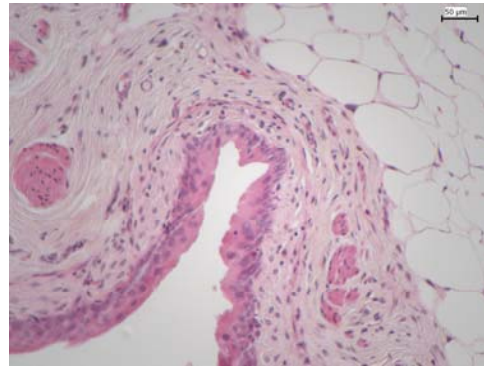
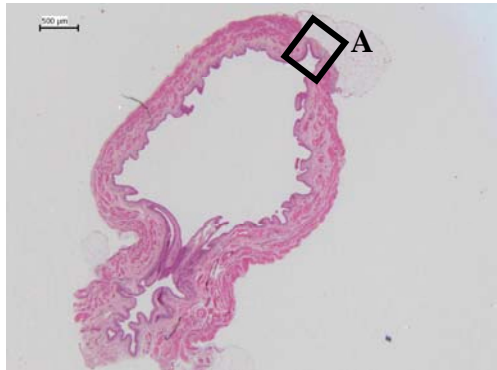
Iron (hemosiderine) is stained blue.  
Asbestos bodies are stained blue-black.  
Nuclei are stained red



Resection only

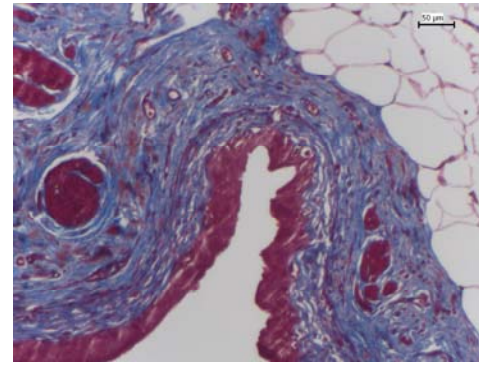
Hematoxylin & Erythrosine staining

Nuclei are stained blue-black.  
Muscle is stained deep pink red



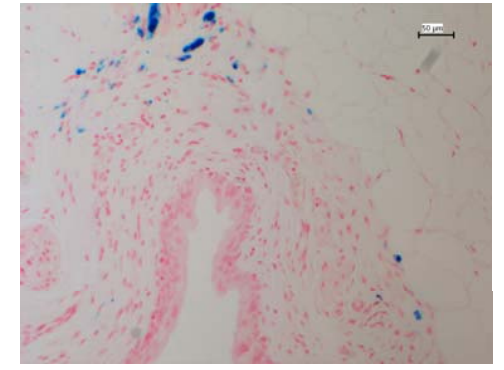
Masson's Trichrome staining

Nuclei are stained braun.  
Muscle is stained pink red.  
Collagen is stained blue

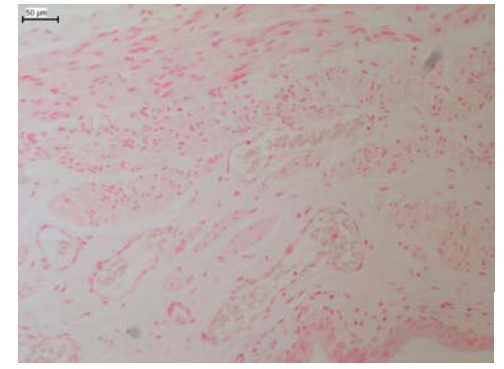
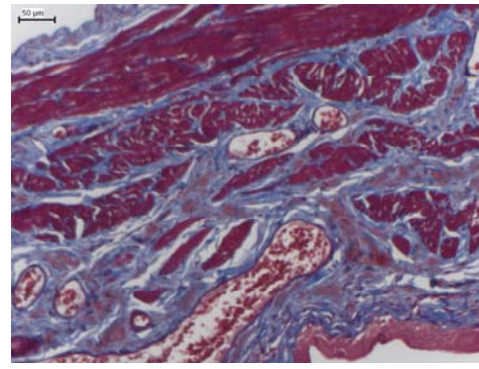
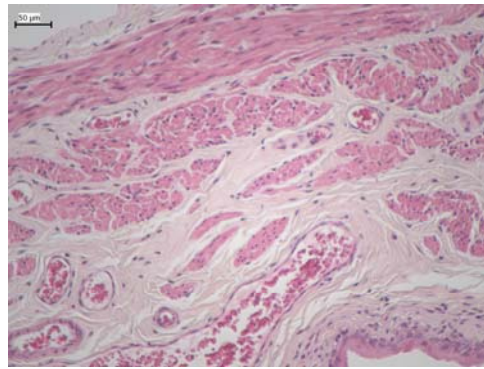
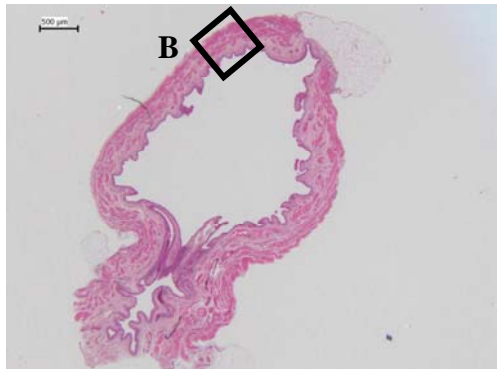


Prussian Blue

Iron (hemosiderine) is stained blue.  
Asbestos bodies are stained blue-black.  
Nuclei are stained red

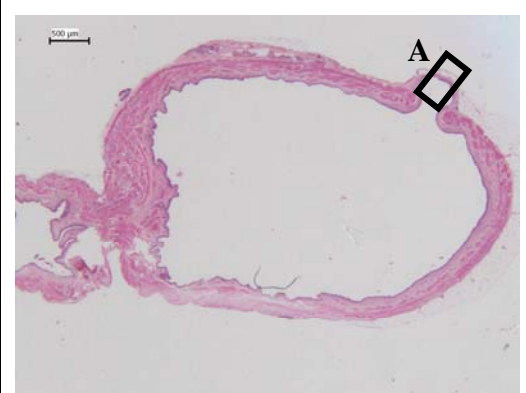
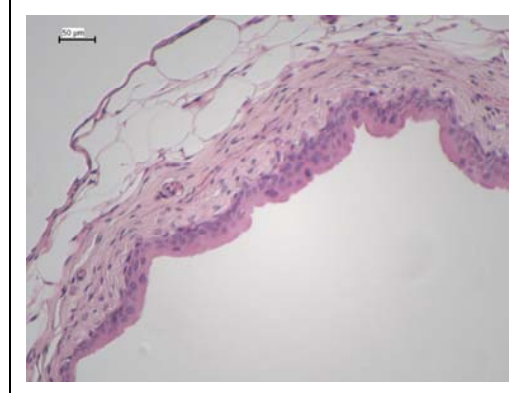
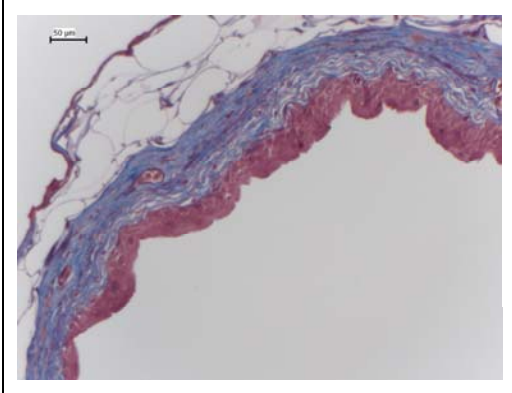
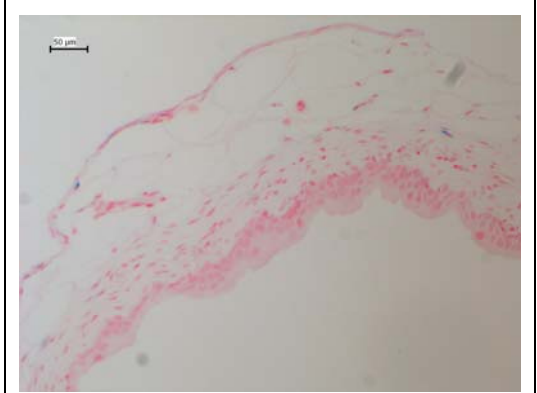
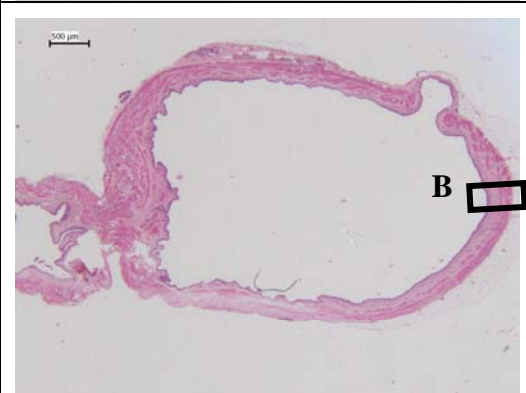
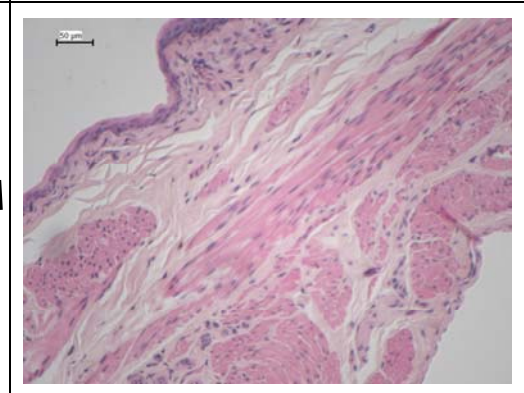
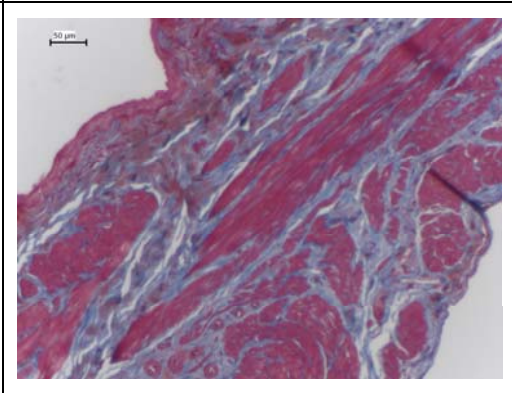
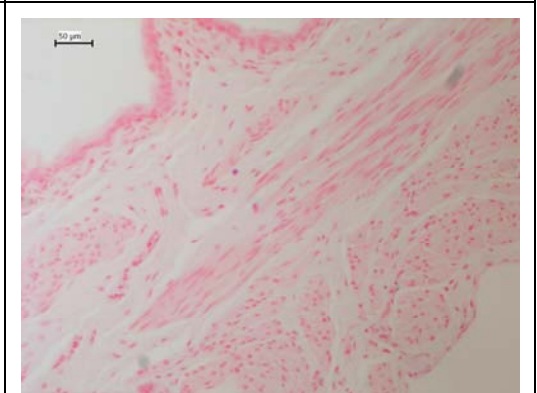


B

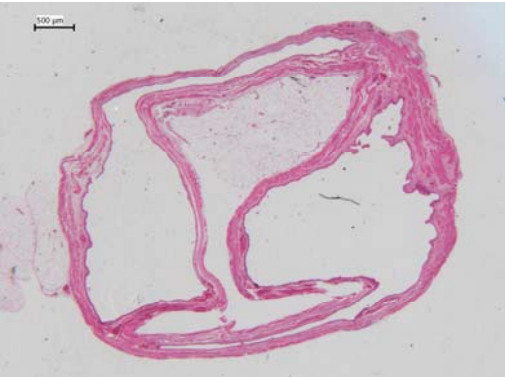
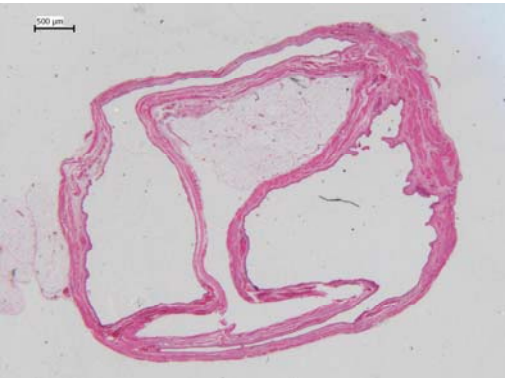


Fibrin gel only

### Fibrin gel only

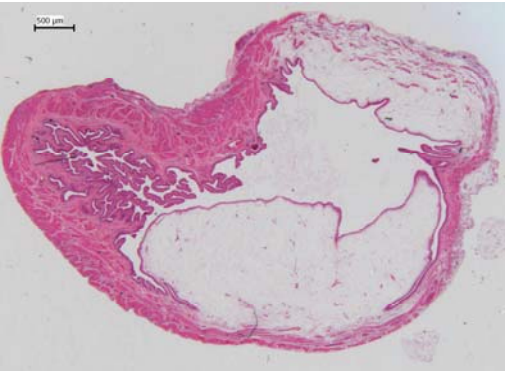
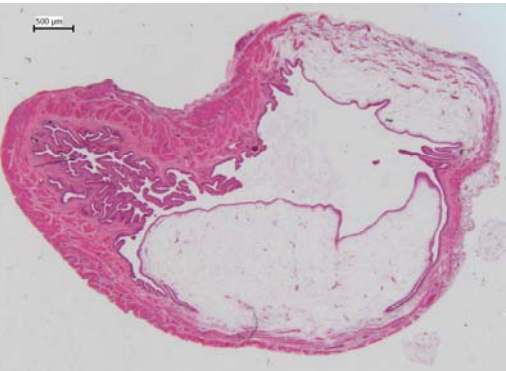
<p>Hematoxylin &amp; Erythrosine staining Nuclei are stained blue-black. Muscle is stained deep pink red</p>	<p>Masson's Trichrome staining Nuclei are stained braun. Muscle is stained pink red. Collagen is stained blue</p>	<p>Prussian Blue Iron (hemosiderine) is stained blue. Asbestos bodies are stained blue-black. Nuclei are stained red</p>	
			
			

Fibrin gel only

<p><b>Hematoxylin &amp; Erythrosine staining</b> Nuclei are stained blue-black. Muscle is stained deep pink red</p>	<p><b>Masson's Trichrome staining</b> Nuclei are stained braun. Muscle is stained pink red. Collagen is stained blue</p>	<p><b>Prussian Blue</b> Iron (hemosiderine) is stained blue. Asbestos bodies are stained blue-black. Nuclei are stained red</p>	
			
			



Fibrin gel only

<p><b>Hematoxylin &amp; Erythrosine staining</b> Nuclei are stained blue-black. Muscle is stained deep pink red</p>	<p><b>Masson's Trichrome staining</b> Nuclei are stained braun. Muscle is stained pink red. Collagen is stained blue</p>	<p><b>Prussian Blue</b> Iron (hemosiderine) is stained blue. Asbestos bodies are stained blue-black. Nuclei are stained red</p>	
			
			

Fibrin gel only

Hematoxylin & Erythrosine staining

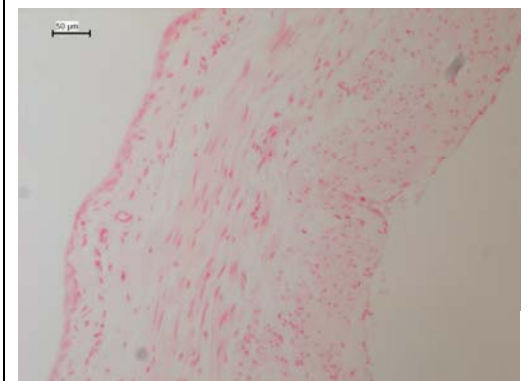
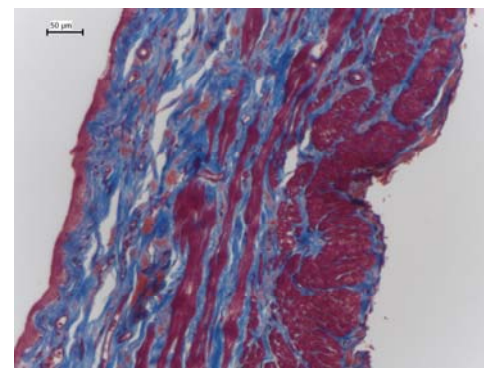
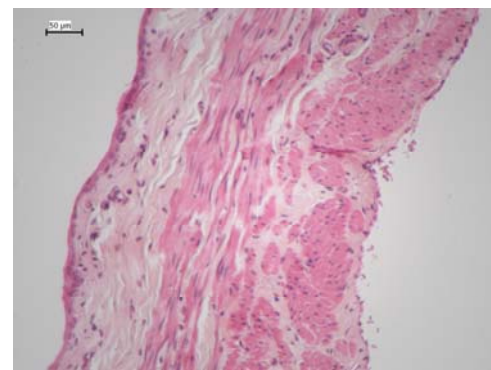
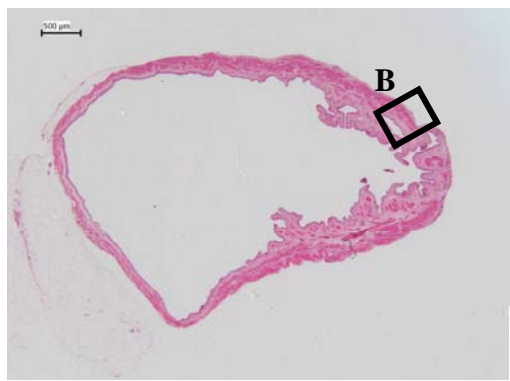
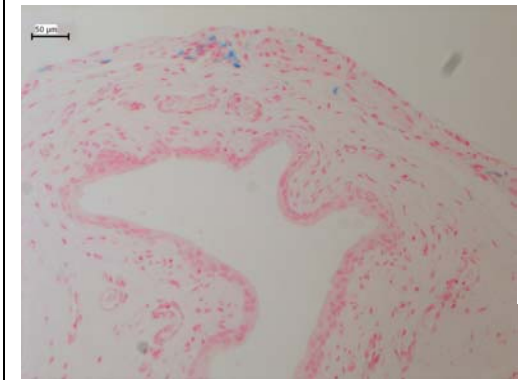
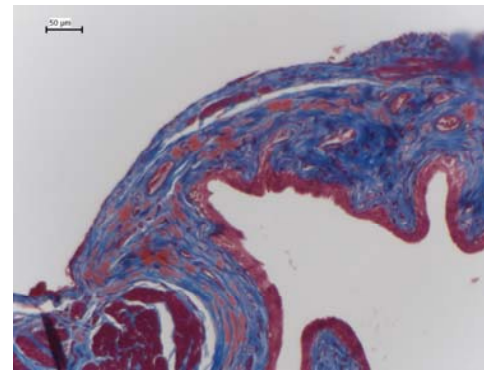
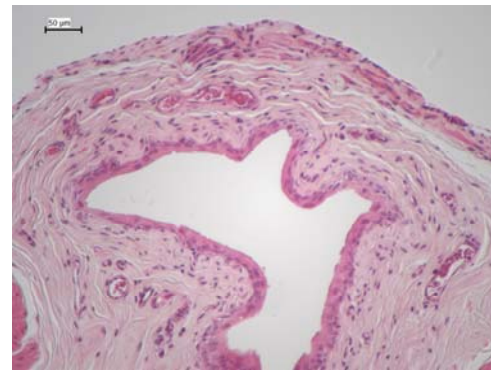
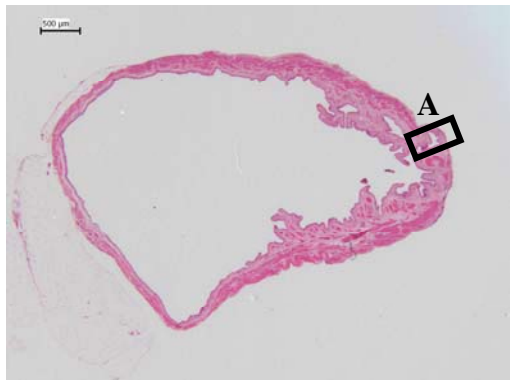
Nuclei are stained blue-black.  
Muscle is stained deep pink red

Masson's Trichrome staining

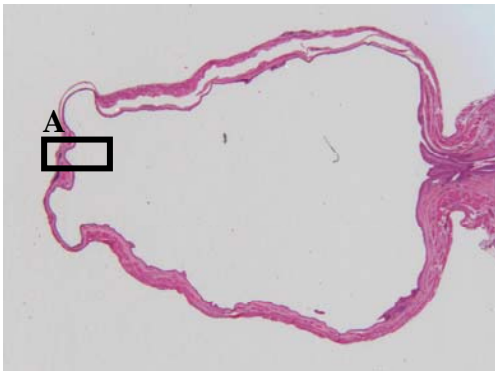
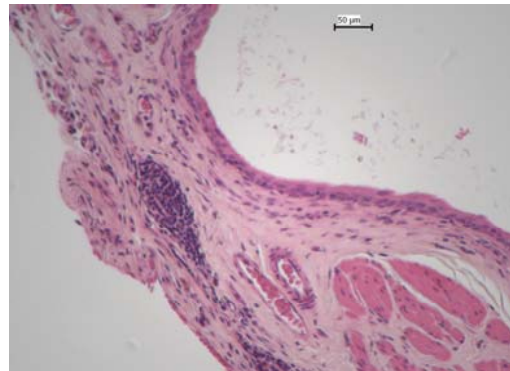
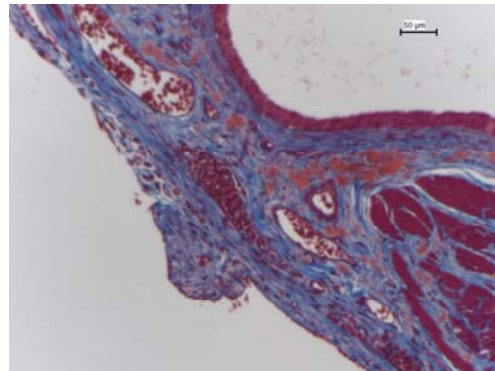
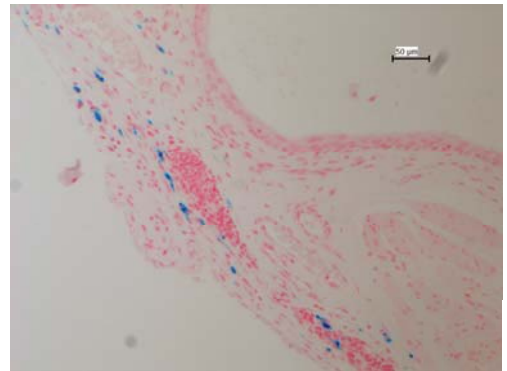
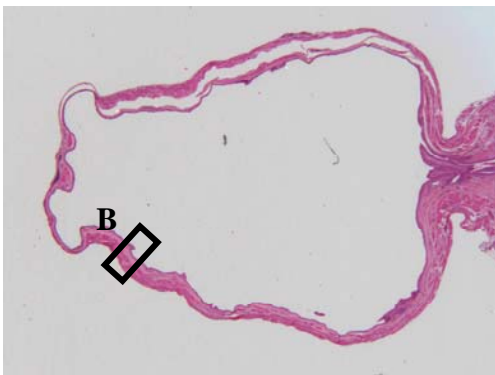
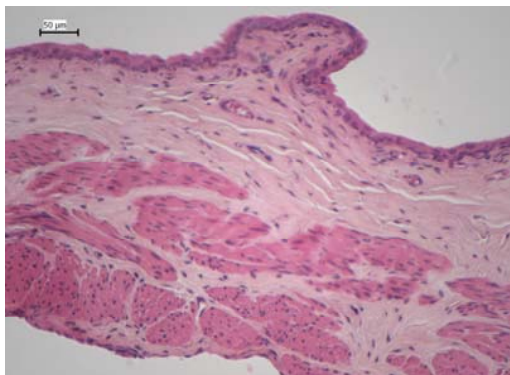
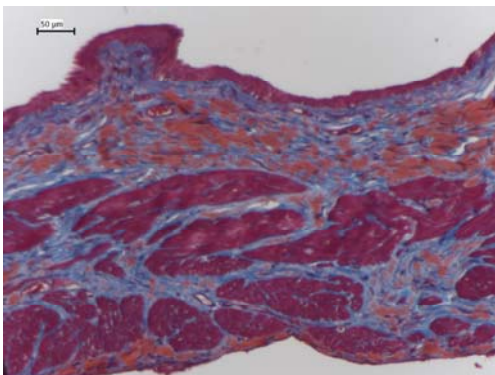
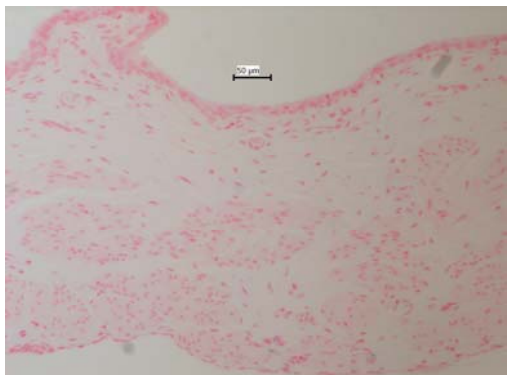
Nuclei are stained braun.  
Muscle is stained pink red.  
Collagen is stained blue

Prussian Blue

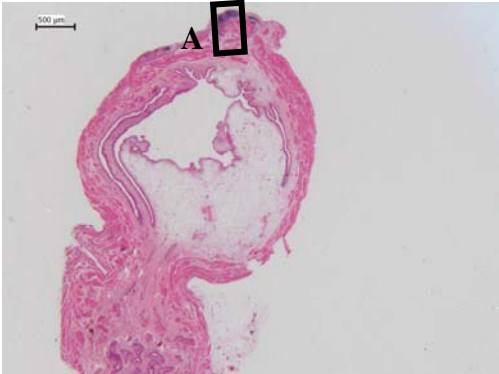
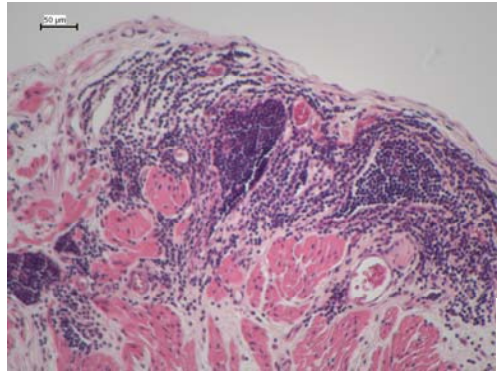
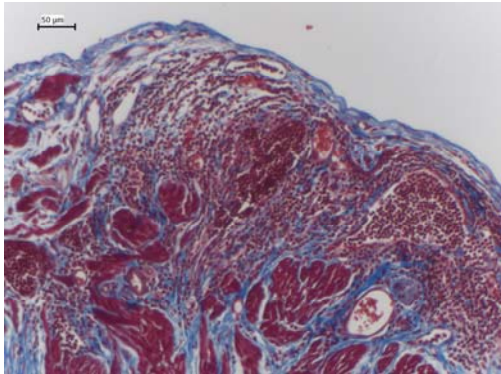
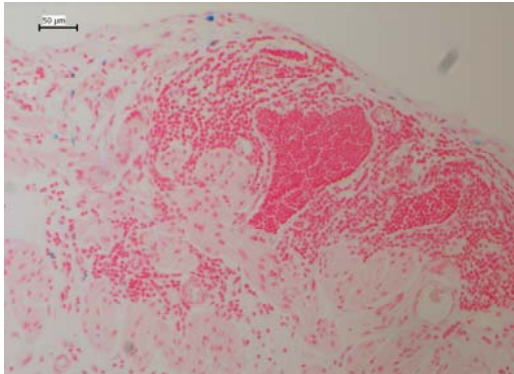
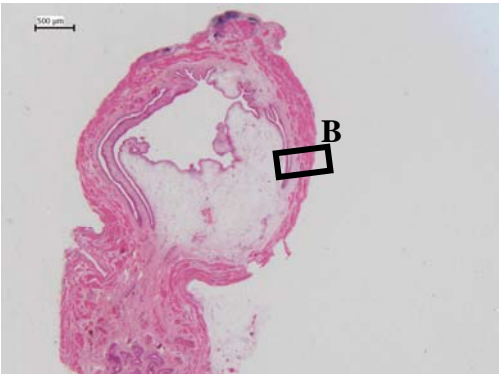
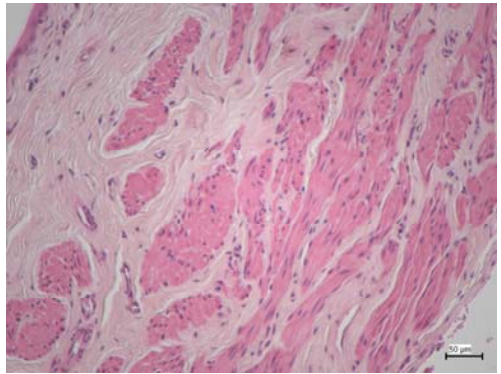
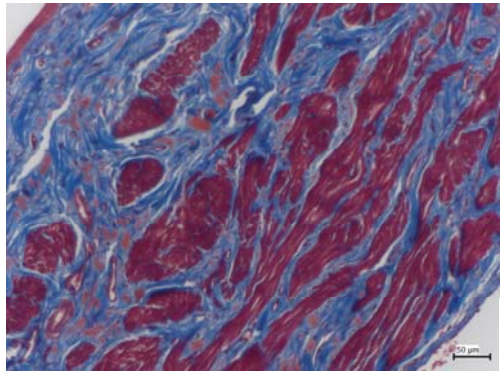
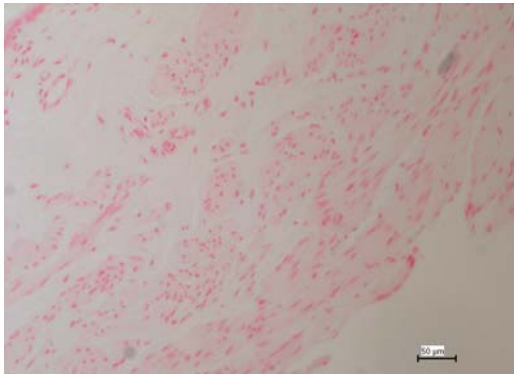
Iron (hemosiderine) is stained blue.  
Asbestos bodies are stained blue-black.  
Nuclei are stained red



### Fibrin gel with TG-IGF1

<p>Hematoxylin &amp; Erythrosine staining Nuclei are stained blue-black. Muscle is stained deep pink red</p>	<p>Masson's Trichrome staining Nuclei are stained braun. Muscle is stained pink red. Collagen is stained blue</p>	<p>Prussian Blue Iron (hemosiderine) is stained blue. Asbestos bodies are stained blue-black. Nuclei are stained red</p>	
			
			

Fibrin gel with TG-IGF1

<p>Hematoxylin &amp; Erythrosine staining Nuclei are stained blue-black. Muscle is stained deep pink red</p>	<p>Masson's Trichrome staining Nuclei are stained braun. Muscle is stained pink red. Collagen is stained blue</p>	<p>Prussian Blue Iron (hemosiderine) is stained blue. Asbestos bodies are stained blue-black. Nuclei are stained red</p>	
			
			

Fibrin gel with TG-IGF1

Hematoxylin & Erythrosine staining

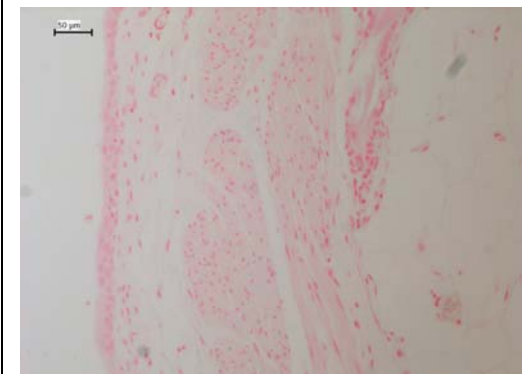
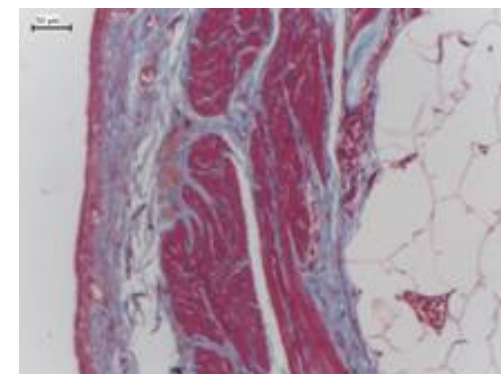
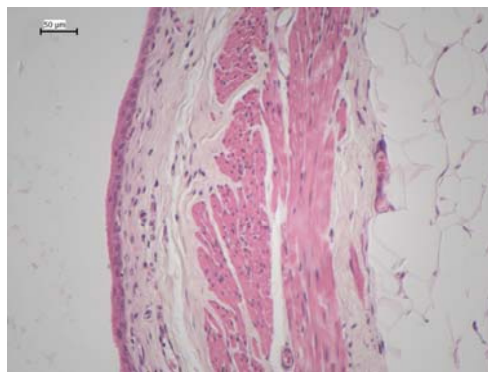
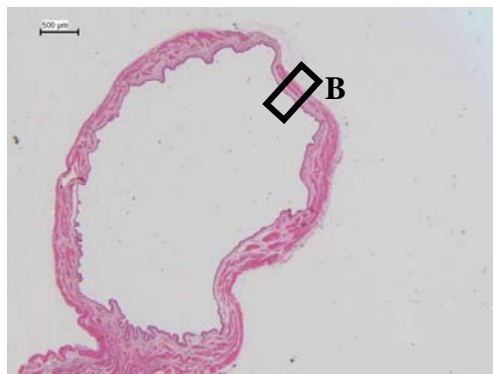
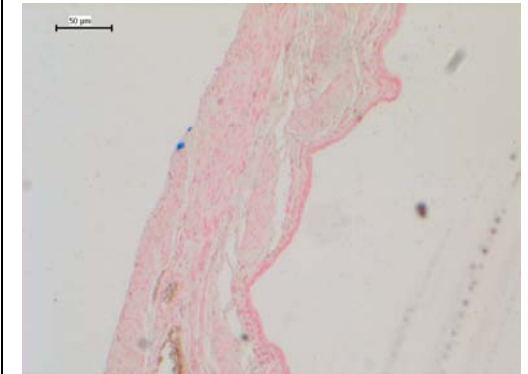
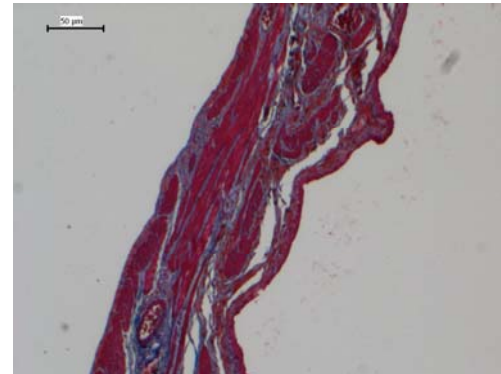
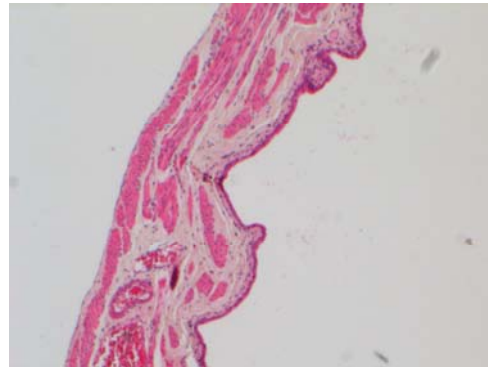
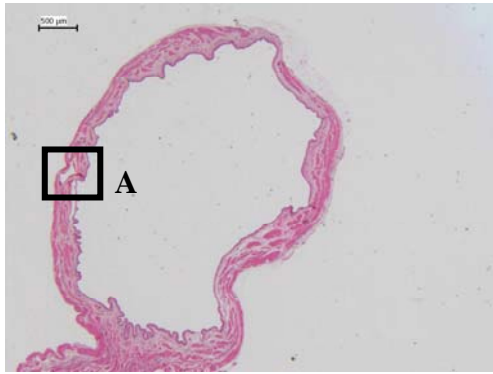
Nuclei are stained blue-black.  
Muscle is stained deep pink red

Masson's Trichrome staining

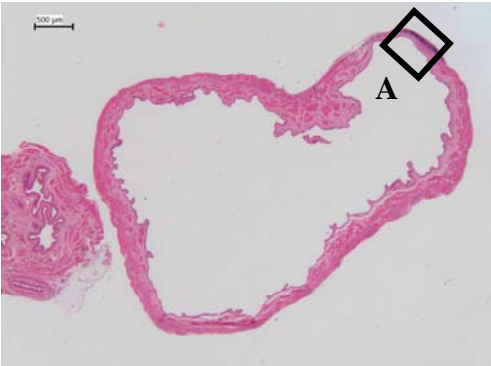
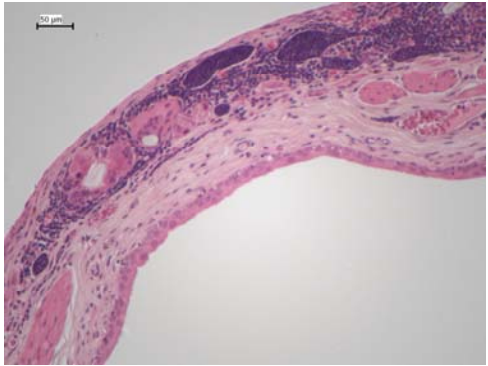
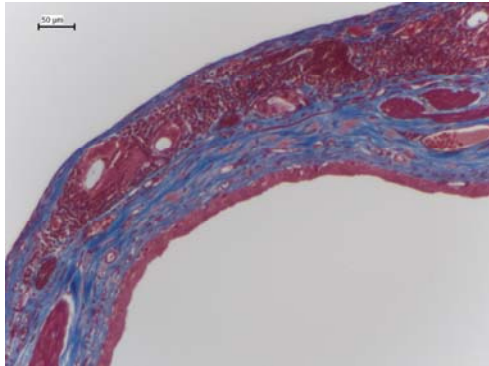
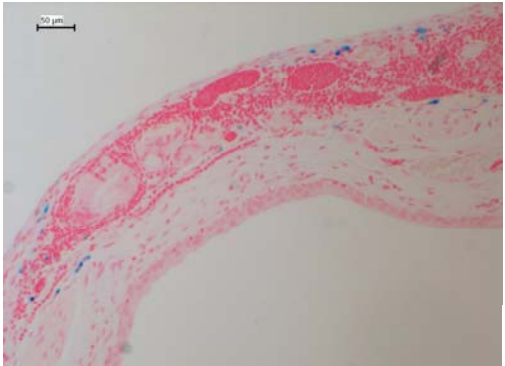
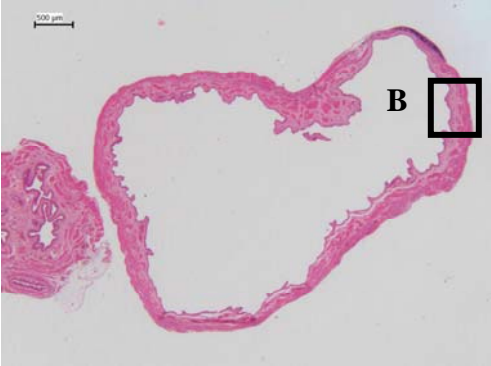
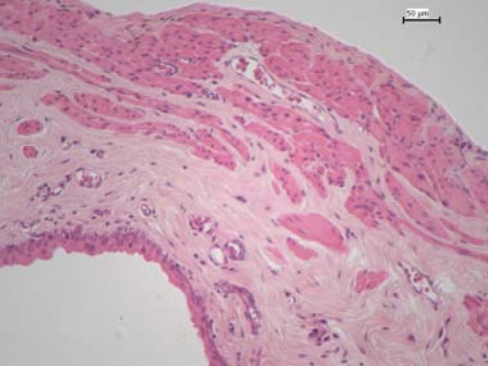
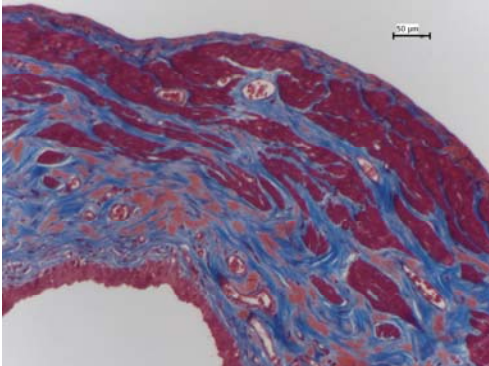
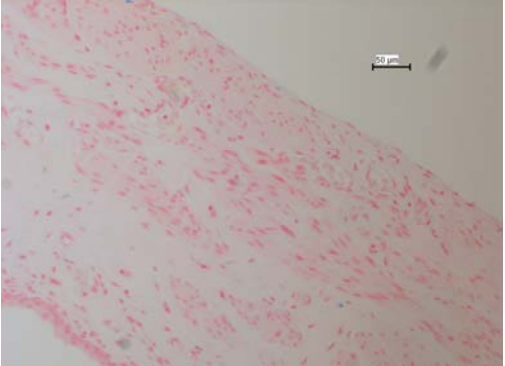
Nuclei are stained braun.  
Muscle is stained pink red.  
Collagen is stained blue

Prussian Blue

Iron (hemosiderine) is stained blue.  
Asbestos bodies are stained blue-black.  
Nuclei are stained red



Fibrin gel with TG-IGF1

<p>Hematoxylin &amp; Erythrosine staining Nuclei are stained blue-black. Muscle is stained deep pink red</p>	<p>Masson's Trichrome staining Nuclei are stained braun. Muscle is stained pink red. Collagen is stained blue</p>	<p>Prussian Blue Iron (hemosiderine) is stained blue. Asbestos bodies are stained blue-black. Nuclei are stained red</p>	
			
			

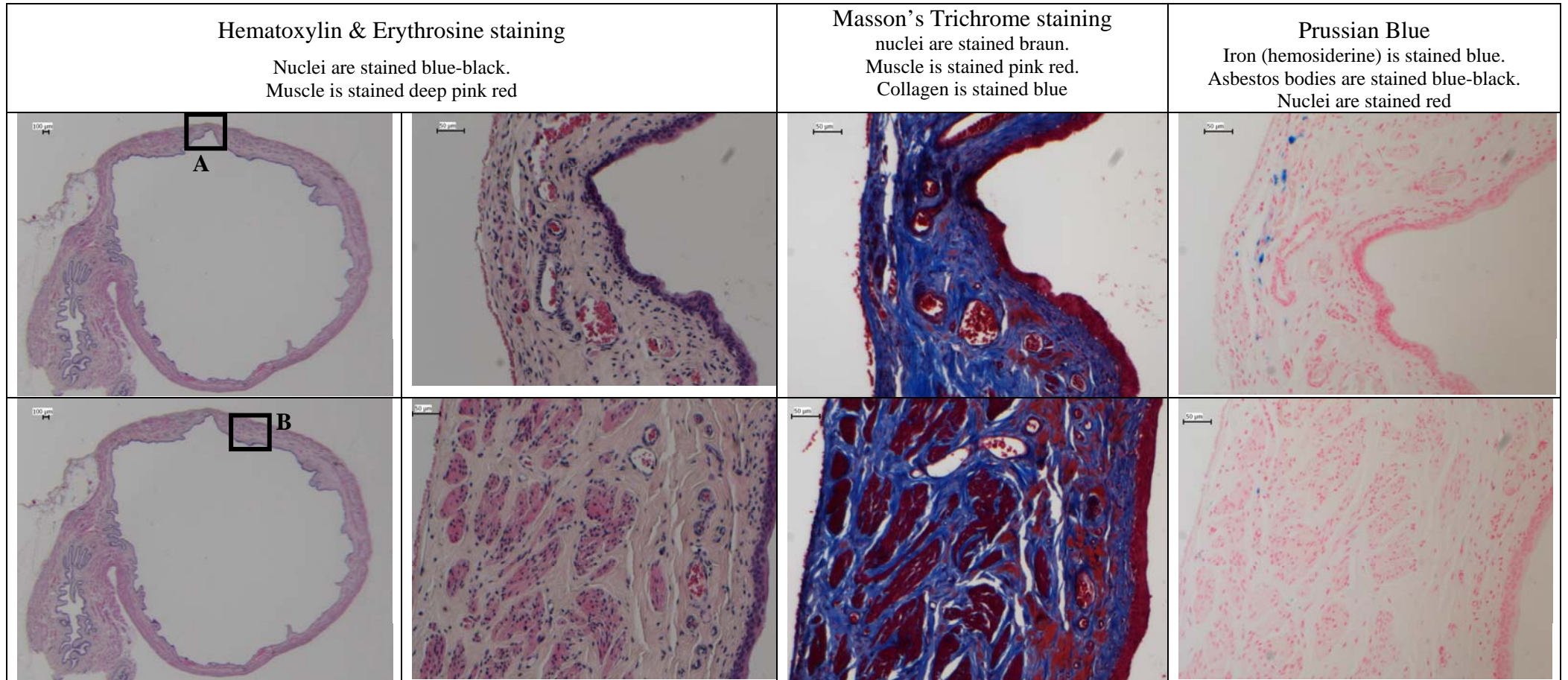
**Annex 2. Histology staining of rat bladder specimens at 4 weeks for second series experiment**



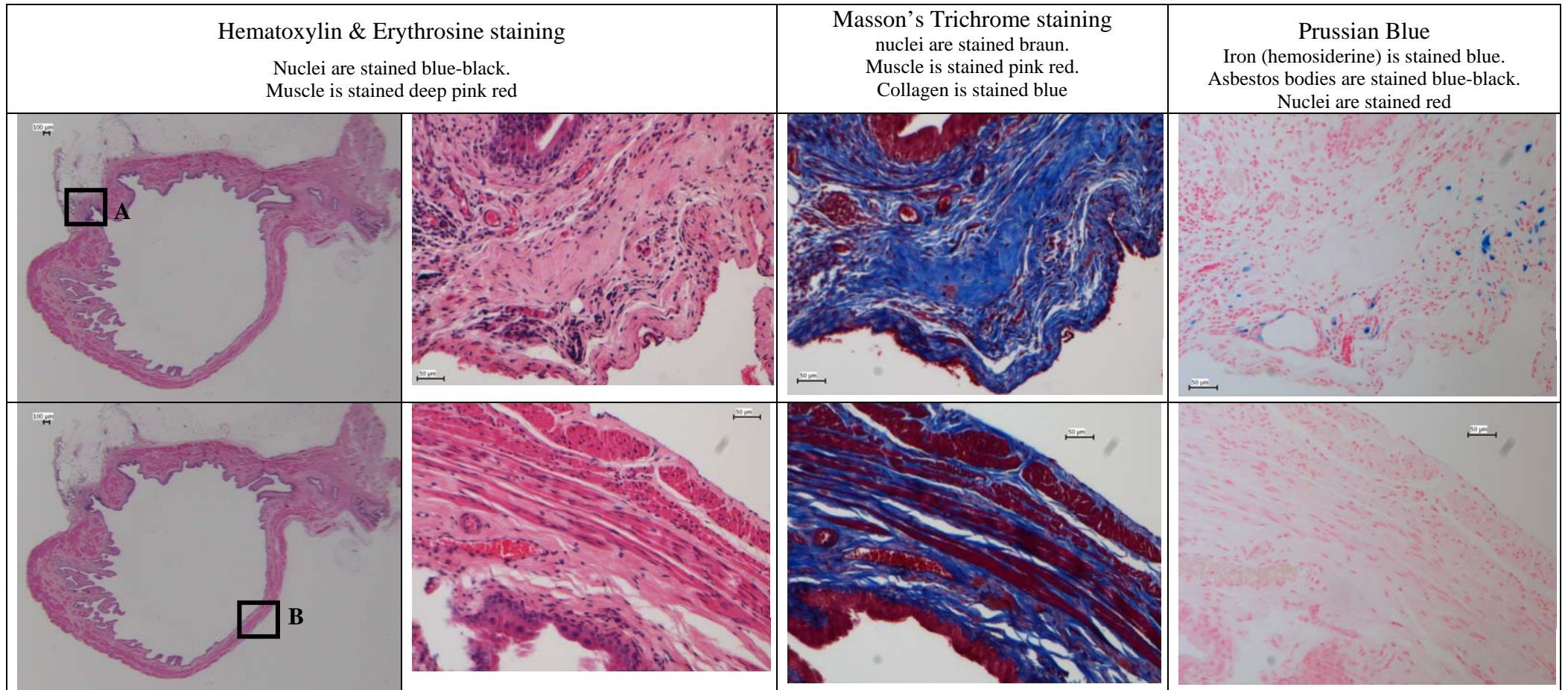


Resection only

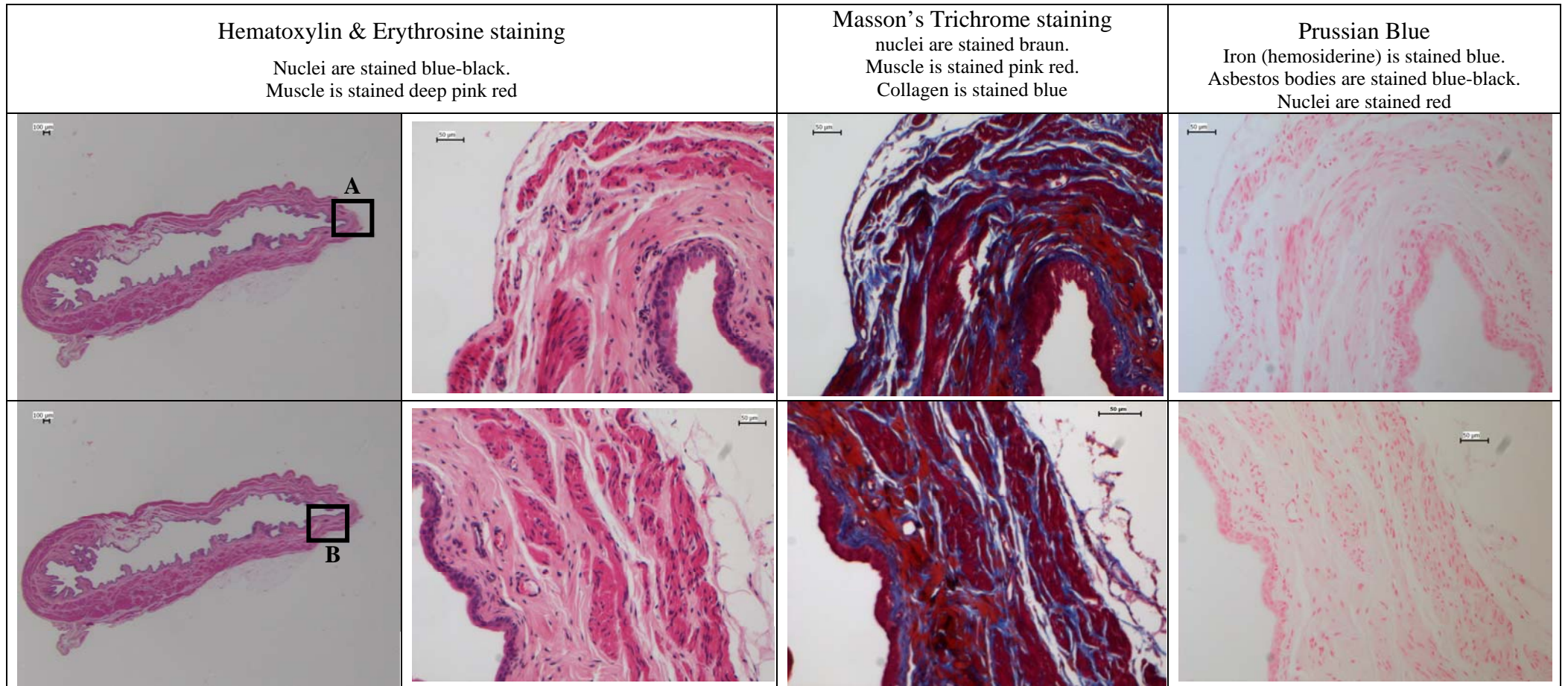
## Resection only



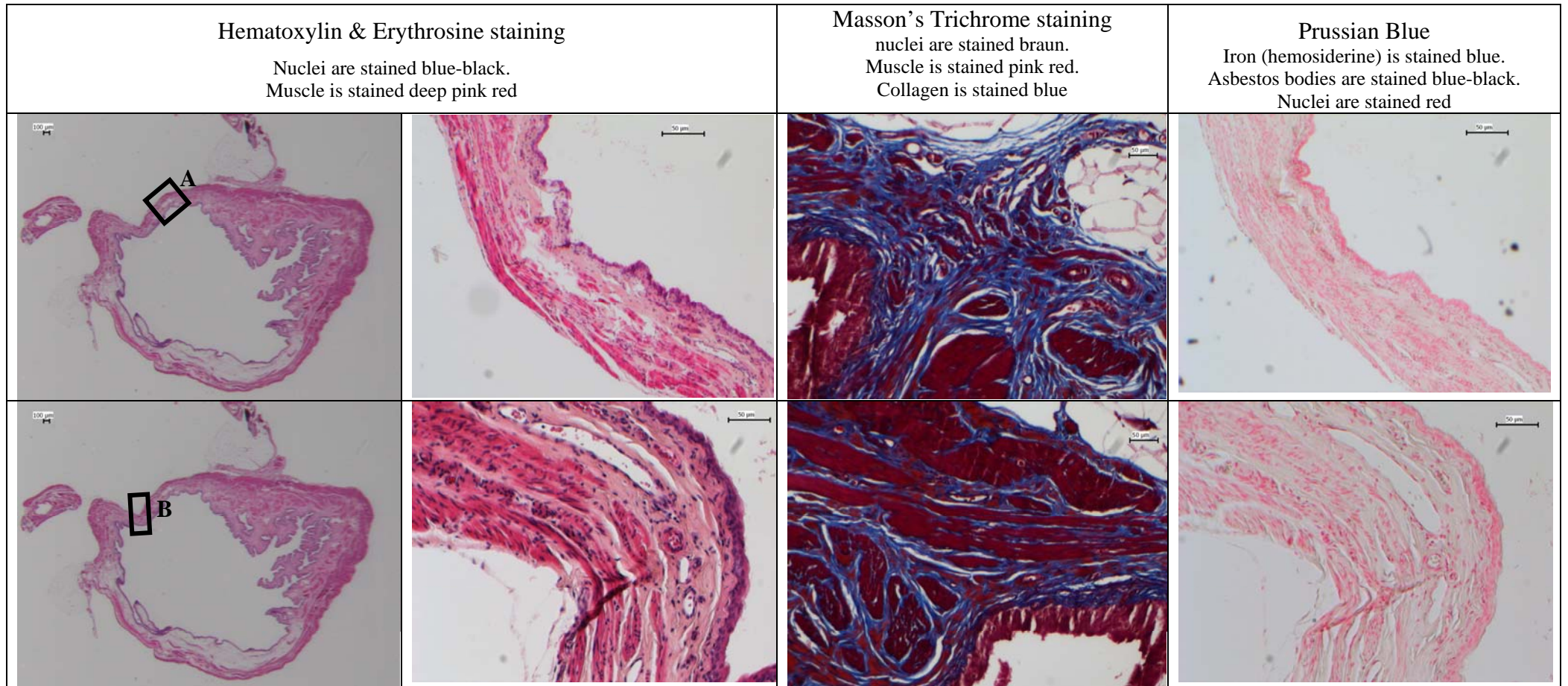
Resection only



Resection only



Resection only



Resection only

<p>Hematoxylin &amp; Erythrosine staining</p> <p>Nuclei are stained blue-black. Muscle is stained deep pink red</p>	<p>Masson's Trichrome staining</p> <p>nuclei are stained braun. Muscle is stained pink red. Collagen is stained blue</p>	<p>Prussian Blue</p> <p>Iron (hemosiderine) is stained blue. Asbestos bodies are stained blue-black. Nuclei are stained red</p>
		



Fibrin gel only

### Fibrin gel only

#### Hematoxylin & Erythrosine staining

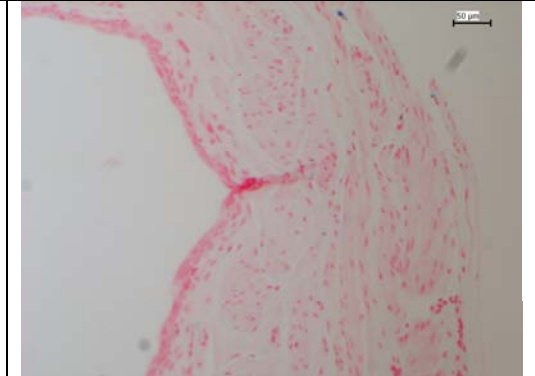
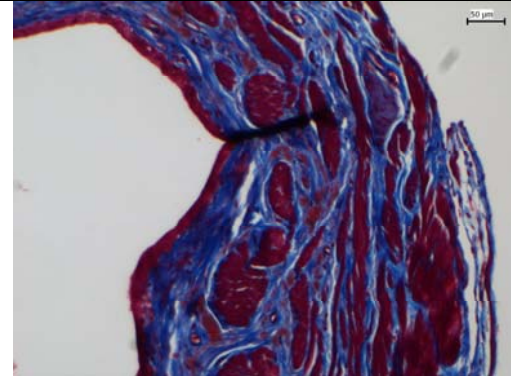
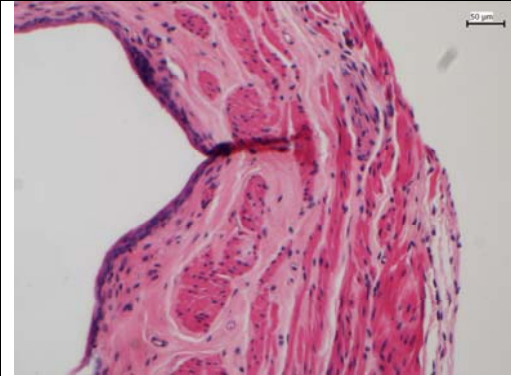
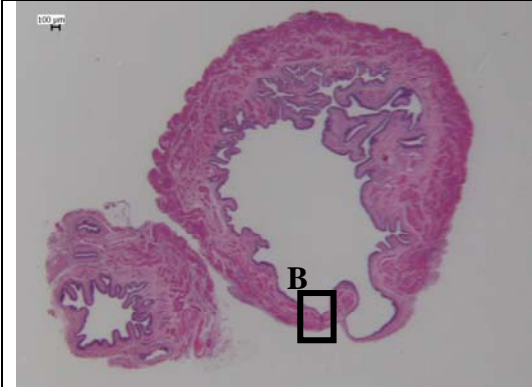
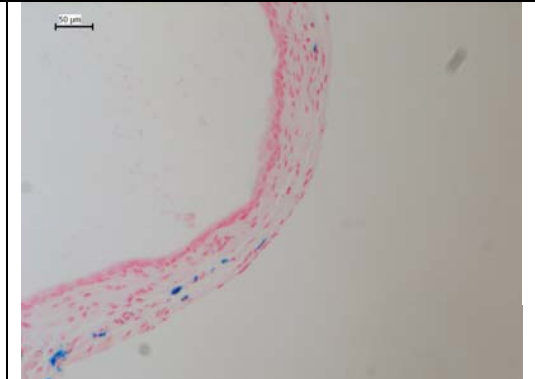
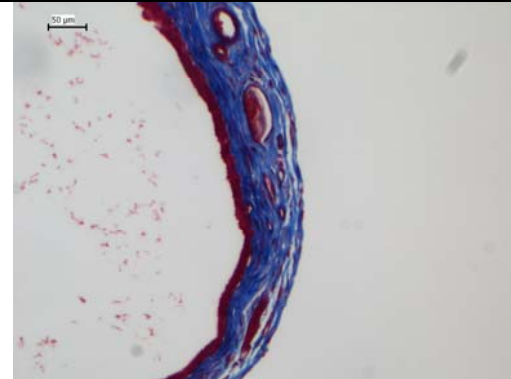
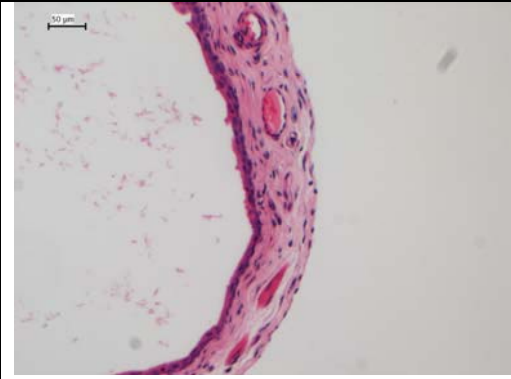
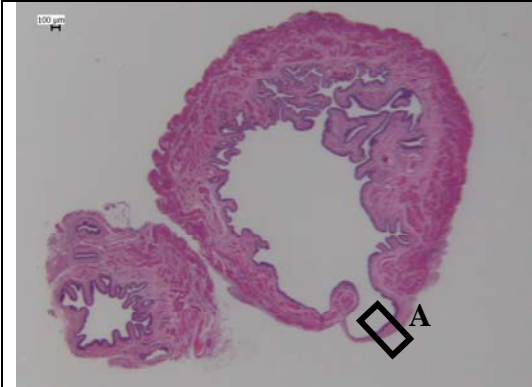
Nuclei are stained blue-black.  
Muscle is stained deep pink red

#### Masson's Trichrome staining

nuclei are stained braun.  
Muscle is stained pink red.  
Collagen is stained blue

#### Prussian Blue

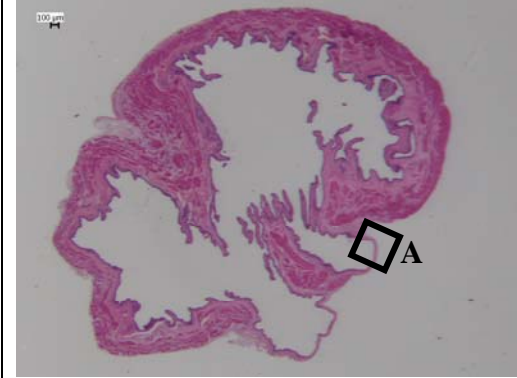
Iron (hemosiderine) is stained blue.  
Asbestos bodies are stained blue-black.  
Nuclei are stained red



Fibrin gel only

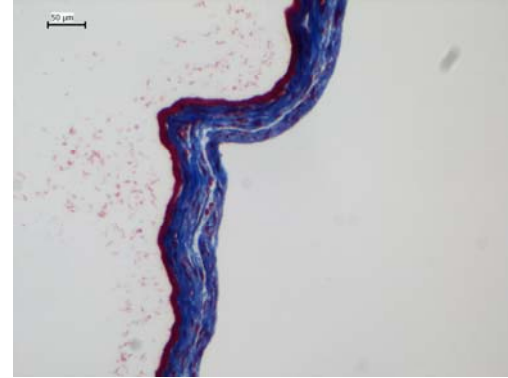
Hematoxylin & Erythrosine staining

Nuclei are stained blue-black.  
Muscle is stained deep pink red



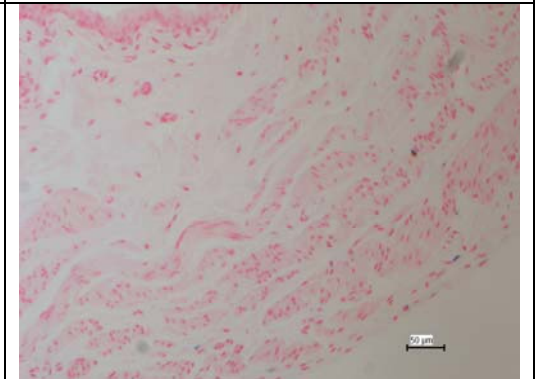
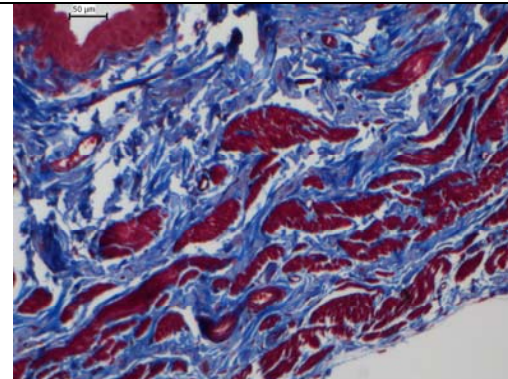
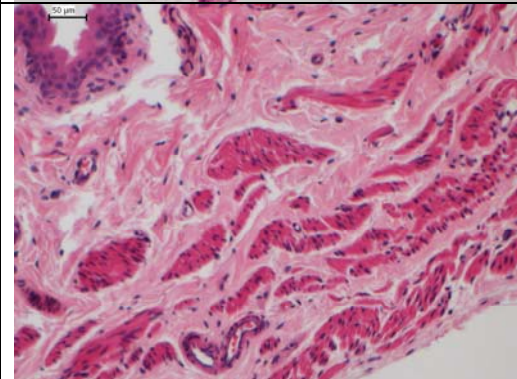
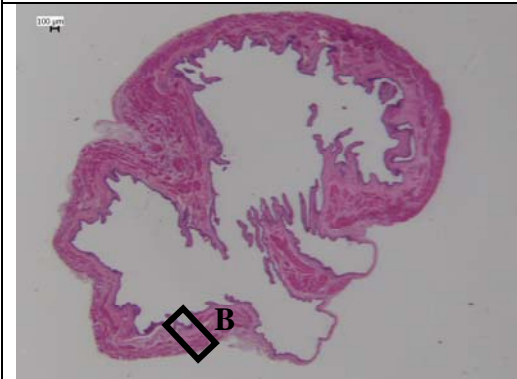
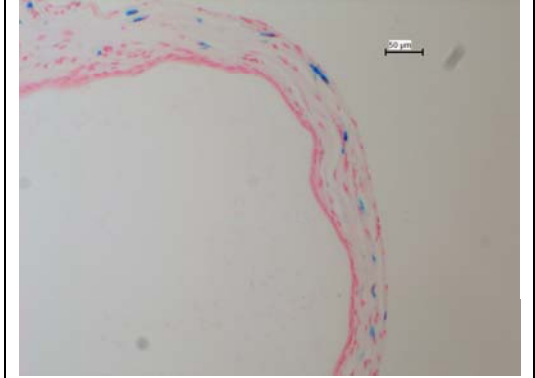
Masson's Trichrome staining

nuclei are stained braun.  
Muscle is stained pink red.  
Collagen is stained blue



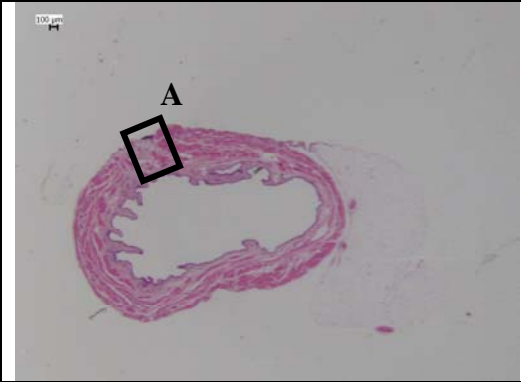
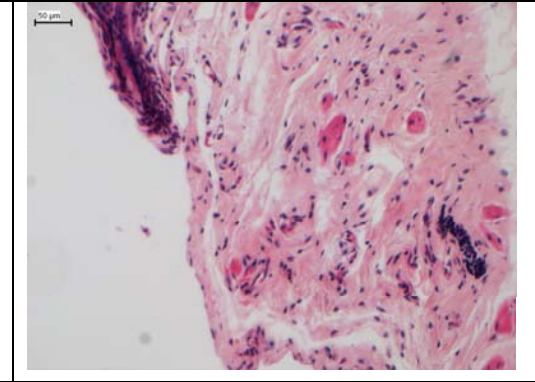
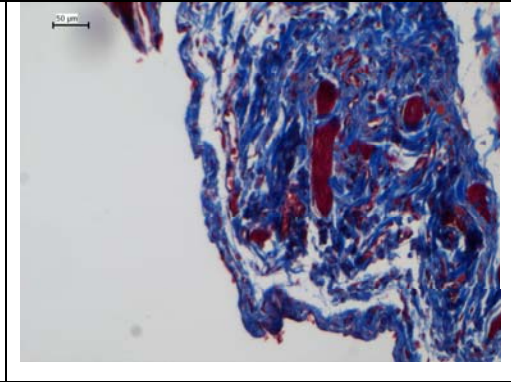
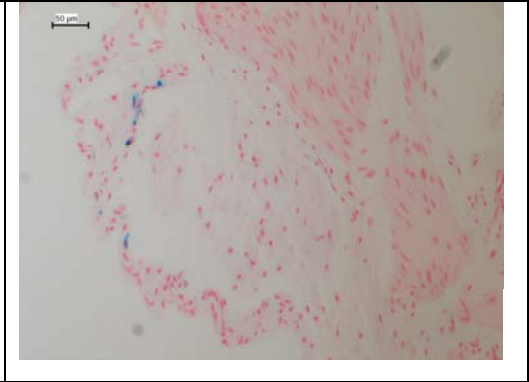
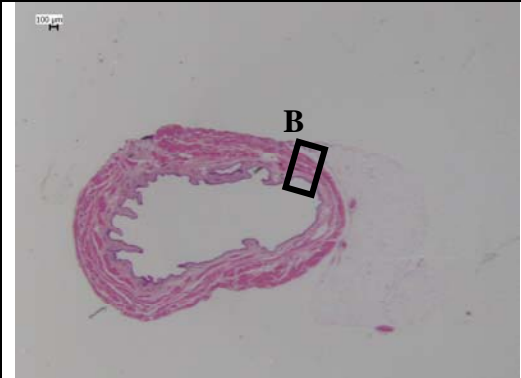
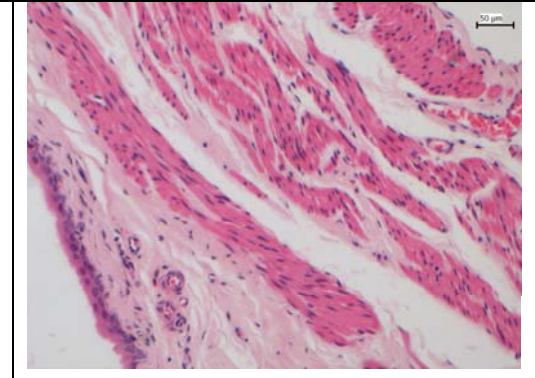
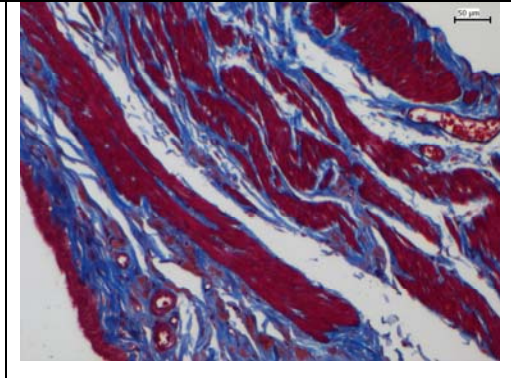
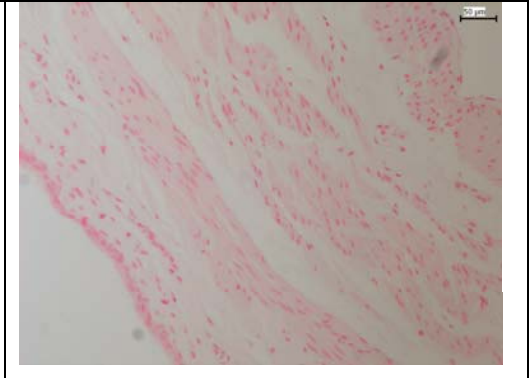
Prussian Blue

Iron (hemosiderine) is stained blue.  
Asbestos bodies are stained blue-black.  
Nuclei are stained red

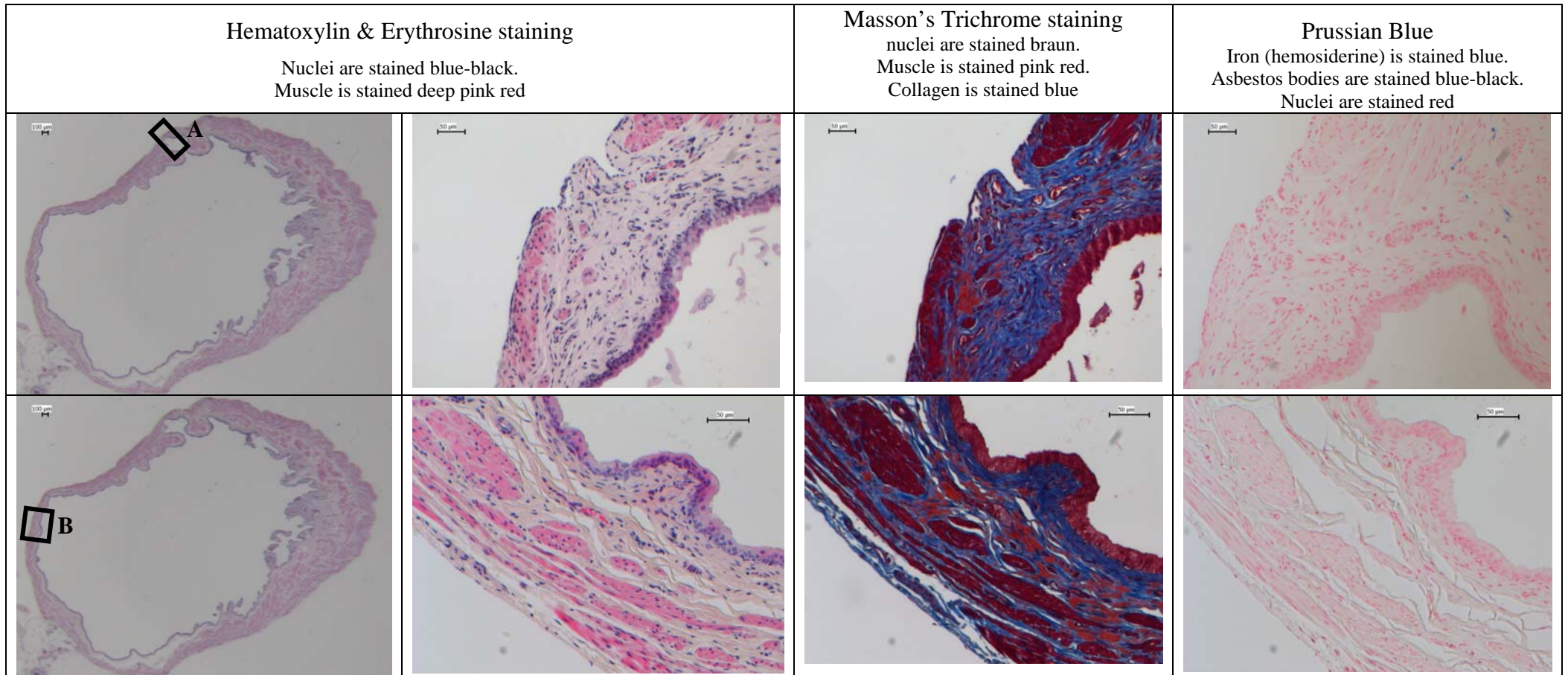




Fibrin gel only

<p>Hematoxylin &amp; Erythrosine staining Nuclei are stained blue-black. Muscle is stained deep pink red</p>	<p>Masson's Trichrome staining nuclei are stained braun. Muscle is stained pink red. Collagen is stained blue</p>	<p>Prussian Blue Iron (hemosiderine) is stained blue. Asbestos bodies are stained blue-black. Nuclei are stained red</p>	
			
			

Fibrin gel only



Fibrin gel only

Hematoxylin & Erythrosine staining

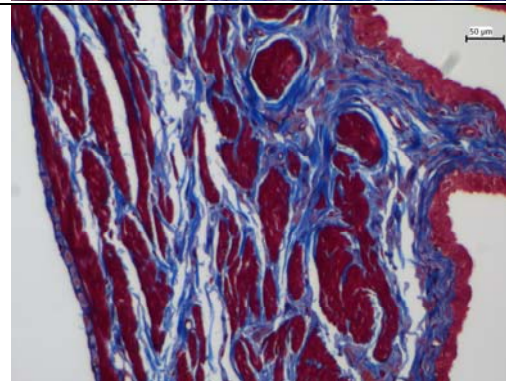
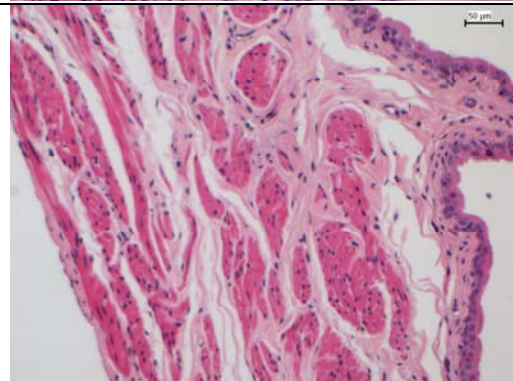
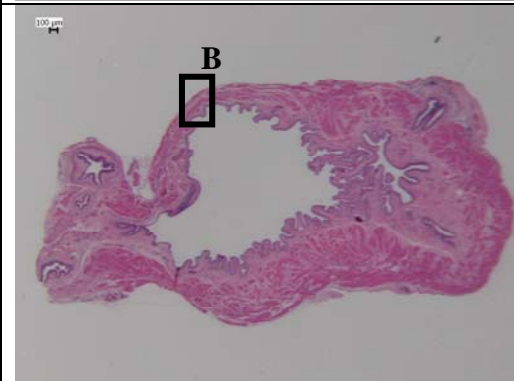
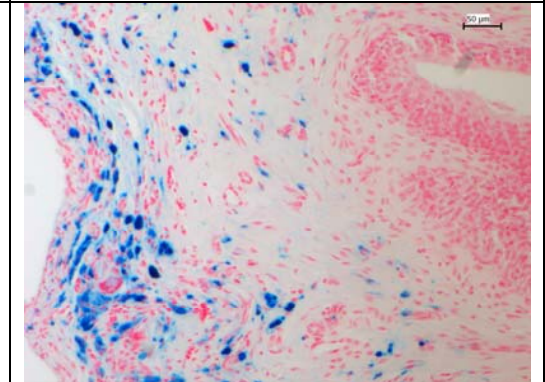
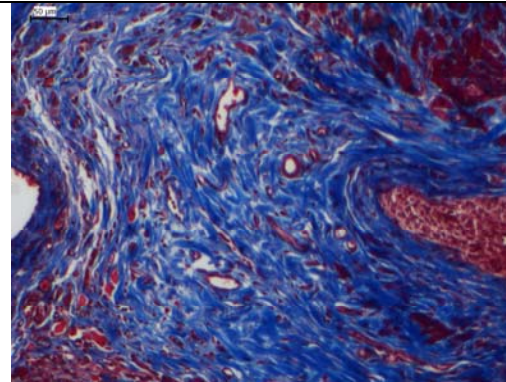
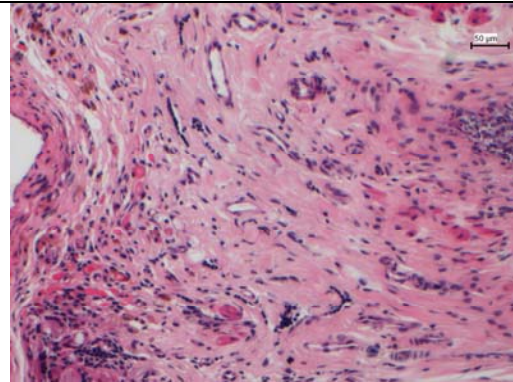
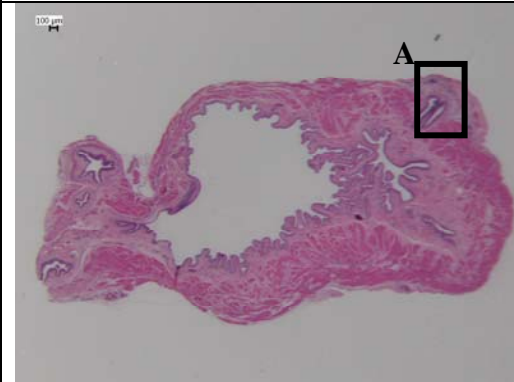
Nuclei are stained blue-black.  
Muscle is stained deep pink red

Masson's Trichrome staining

nuclei are stained braun.  
Muscle is stained pink red.  
Collagen is stained blue

Prussian Blue

Iron (hemosiderine) is stained blue.  
Asbestos bodies are stained blue-black.  
Nuclei are stained red

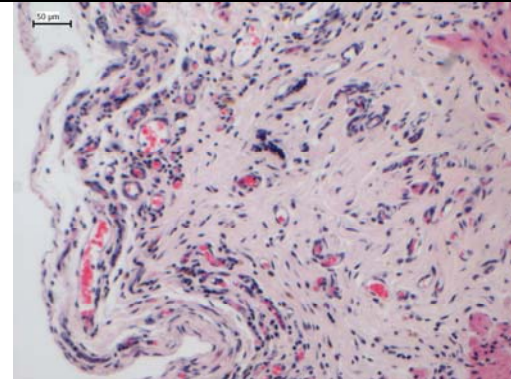
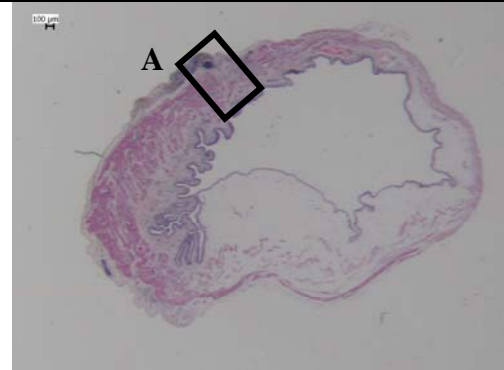




## Fibrin gel with recombinant native IGF1

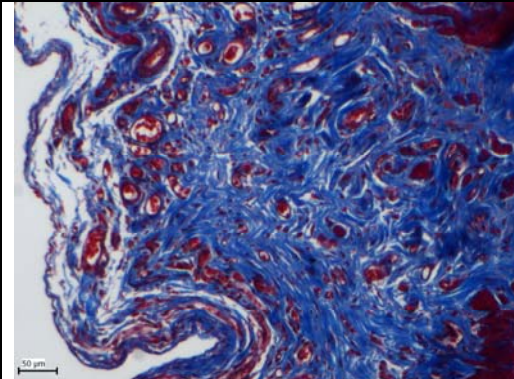
### Hematoxylin & Erythrosine staining

Nuclei are stained blue-black.  
Muscle is stained deep pink red



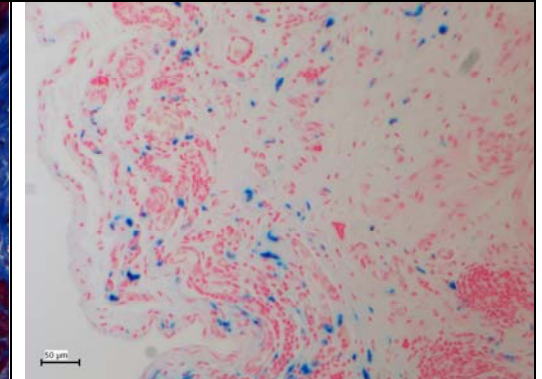
### Masson's Trichrome staining

Nuclei are stained brown.  
Muscle is stained pink red.  
Collagen is stained blue

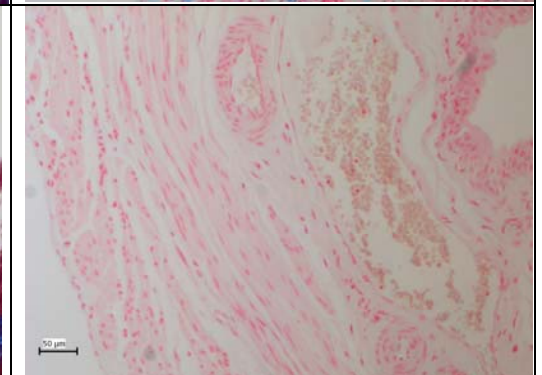
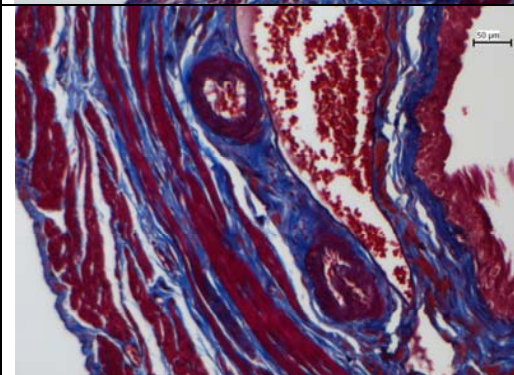
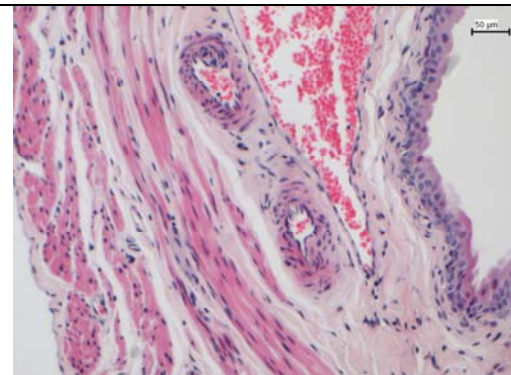
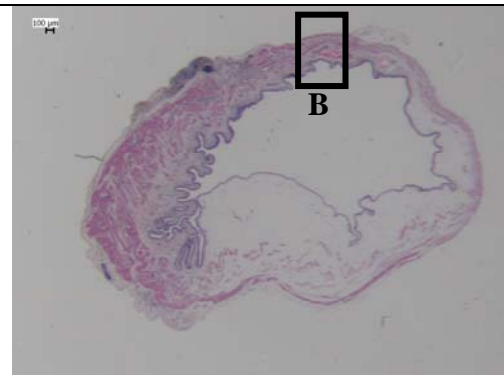


### Prussian Blue

Iron (hemosiderine) is stained blue.  
Asbestos bodies are stained blue-black.  
Nuclei are stained red



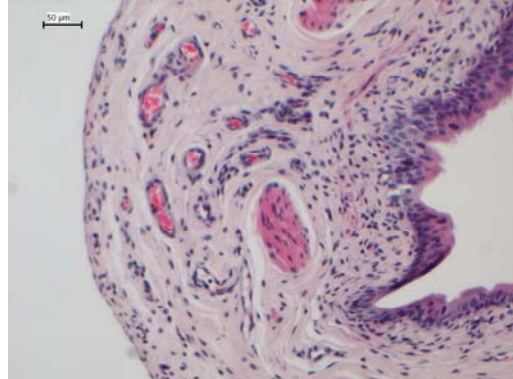
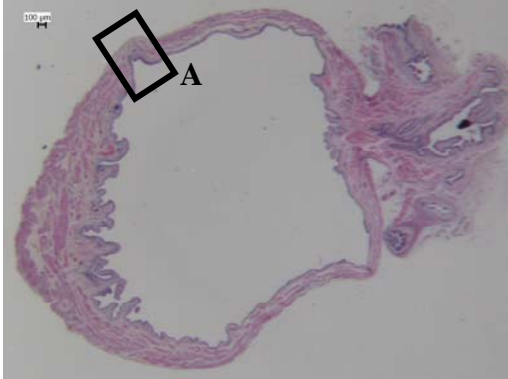
### B



Fibrin gel with recombinant native IGF1

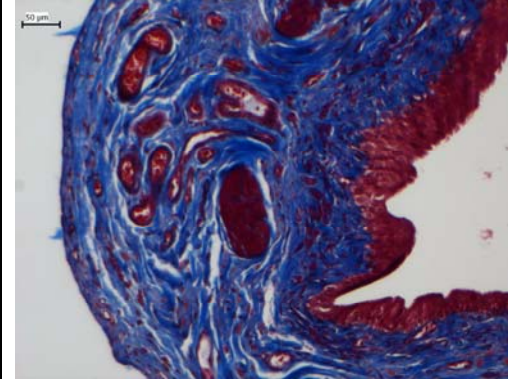
Hematoxylin & Erythrosine staining

Nuclei are stained blue-black.  
Muscle is stained deep pink red



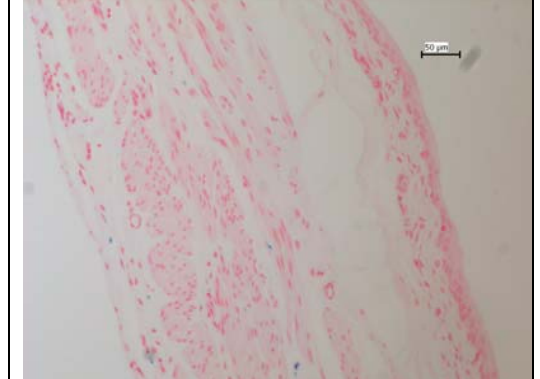
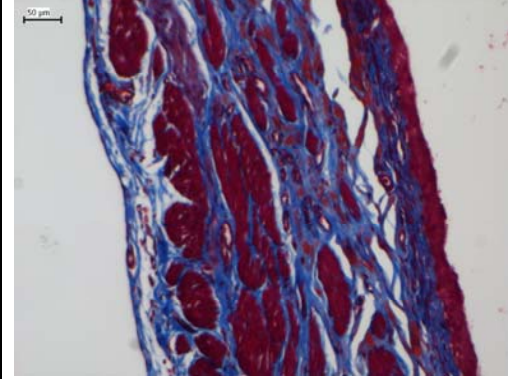
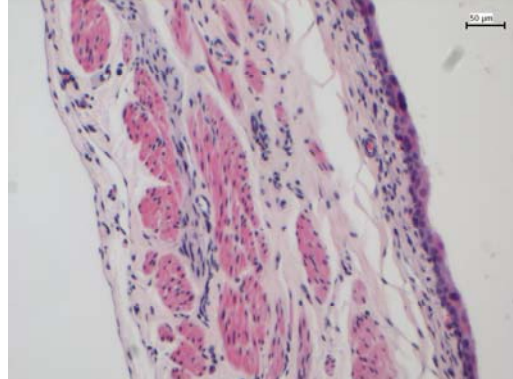
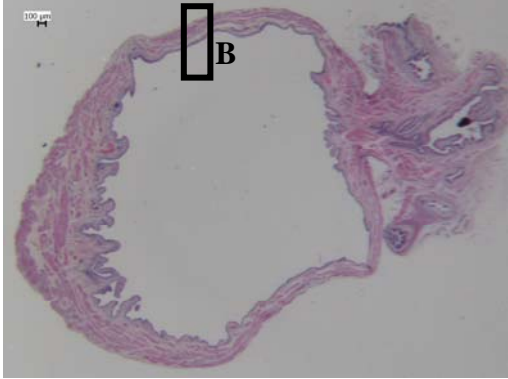
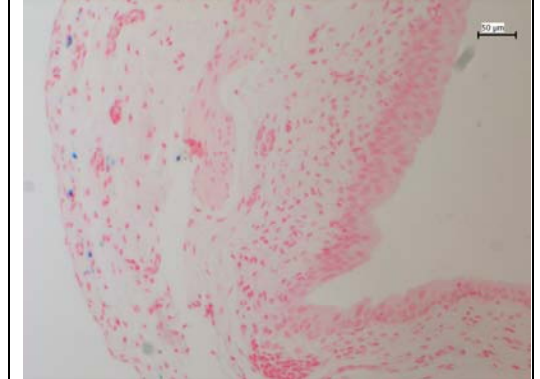
Masson's Trichrome staining

Nuclei are stained braun.  
Muscle is stained pink red.  
Collagen is stained blue



Prussian Blue

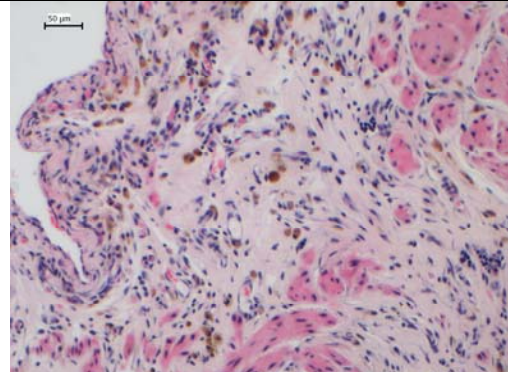
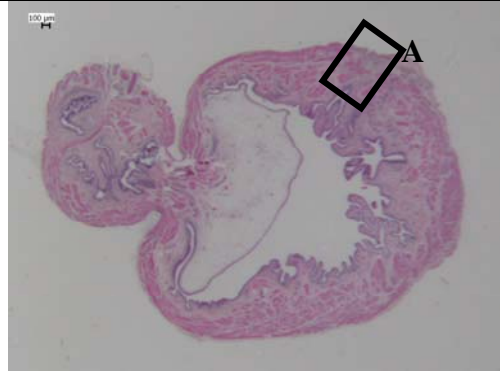
Iron (hemosiderine) is stained blue.  
Asbestos bodies are stained blue-black.  
Nuclei are stained red



Fibrin gel with recombinant native IGF1

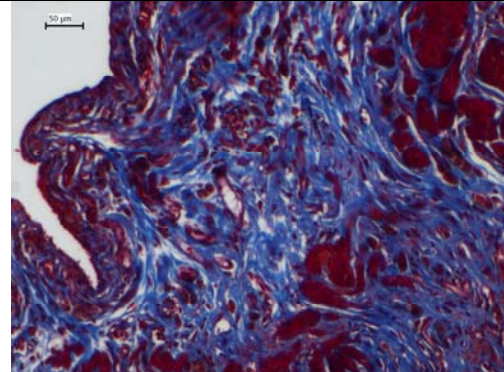
Hematoxylin & Erythrosine staining

Nuclei are stained blue-black.  
Muscle is stained deep pink red



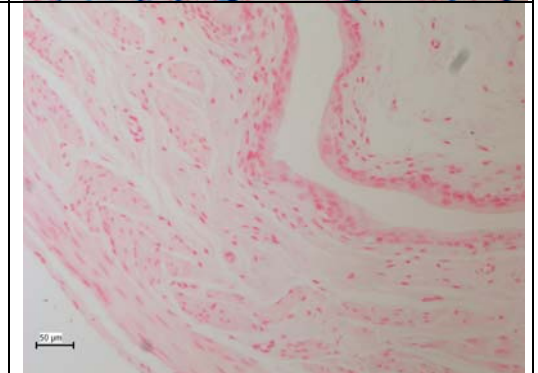
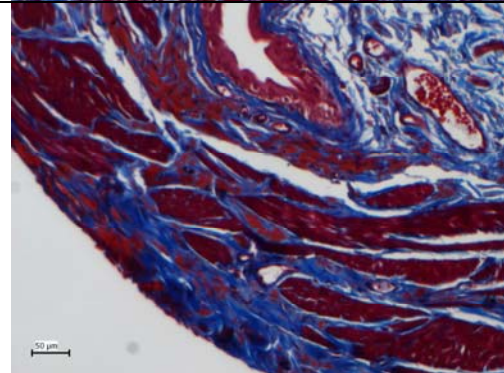
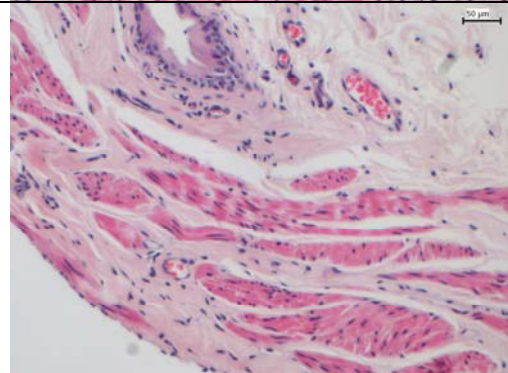
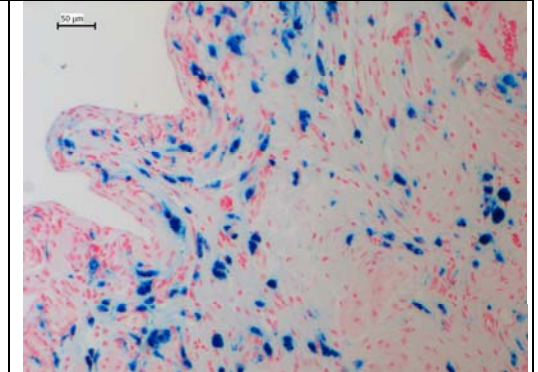
Masson's Trichrome staining

Nuclei are stained braun.  
Muscle is stained pink red.  
Collagen is stained blue

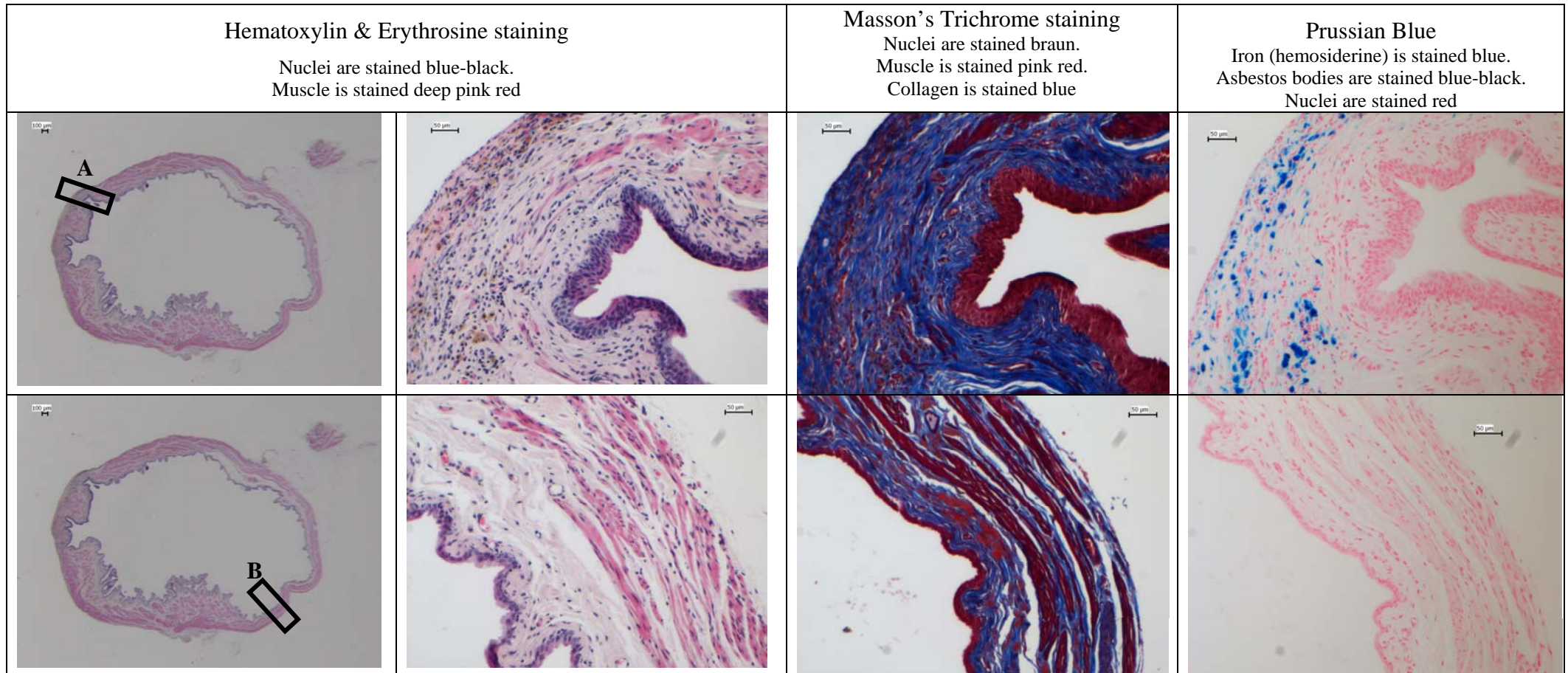


Prussian Blue

Iron (hemosiderine) is stained blue.  
Asbestos bodies are stained blue-black.  
Nuclei are stained red

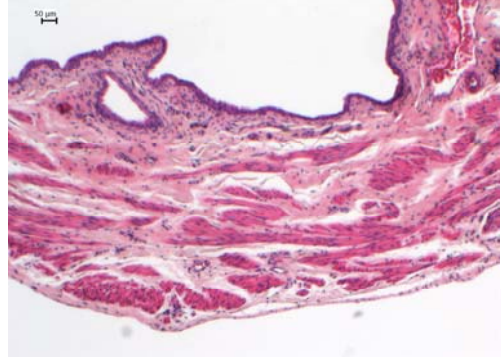


Fibrin gel with recombinant native IGF1



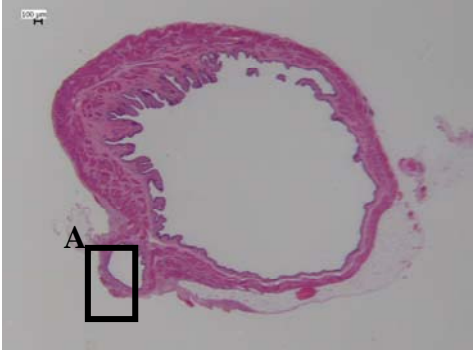
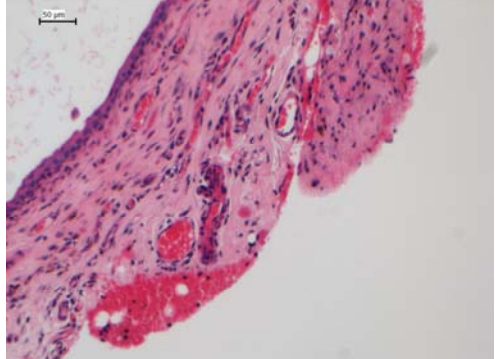
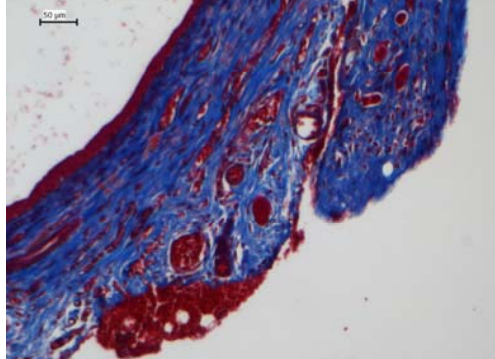
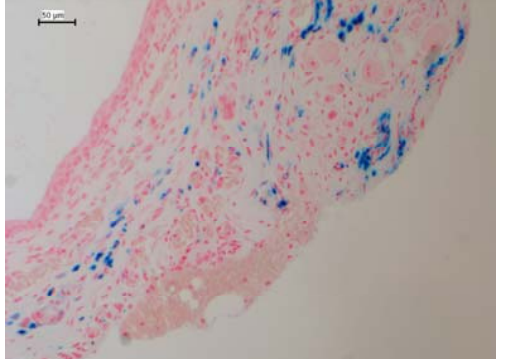
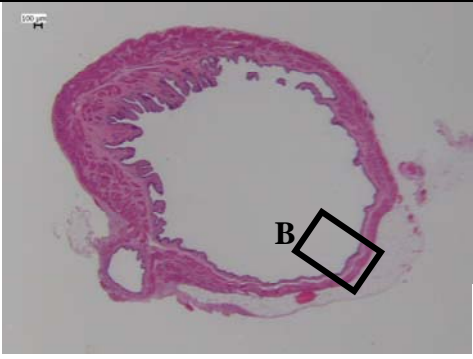
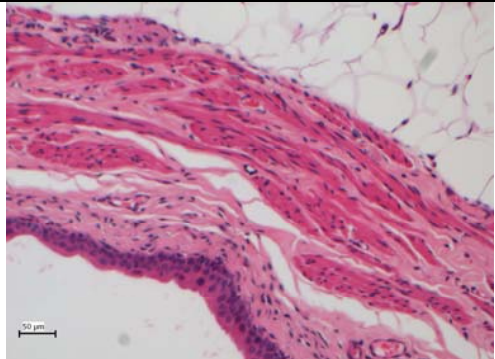
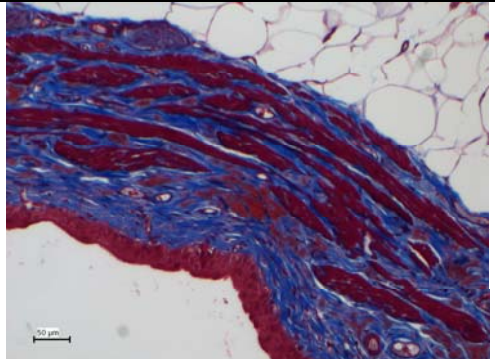



Fibrin gel with recombinant native IGF1

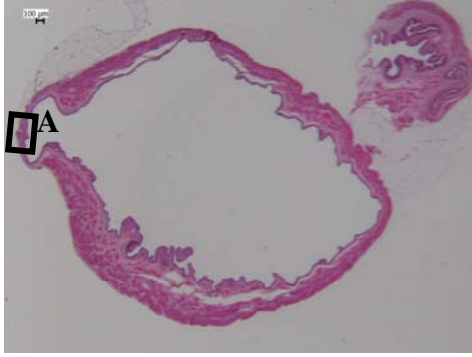
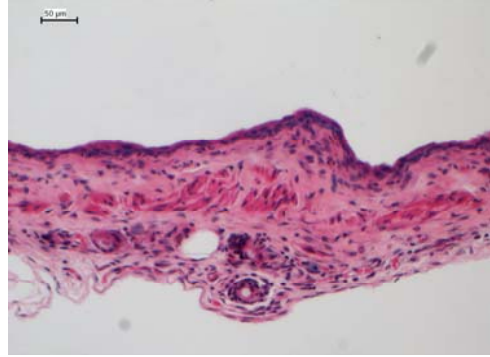
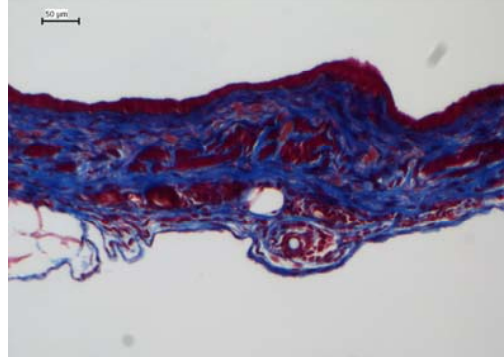
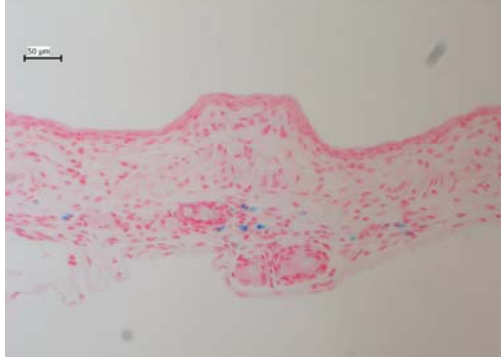
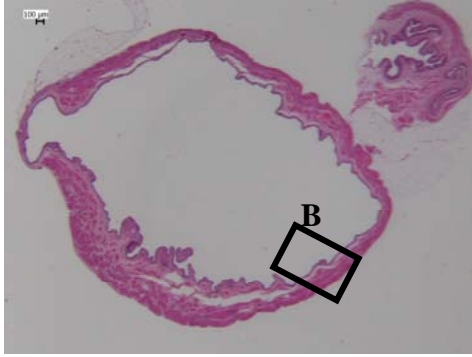
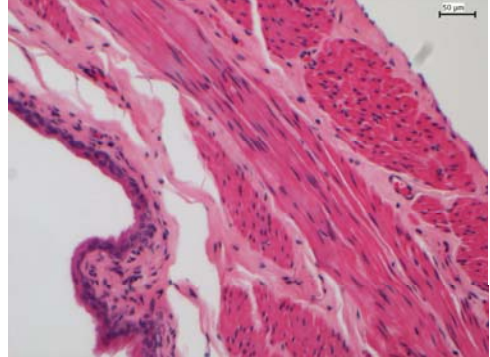
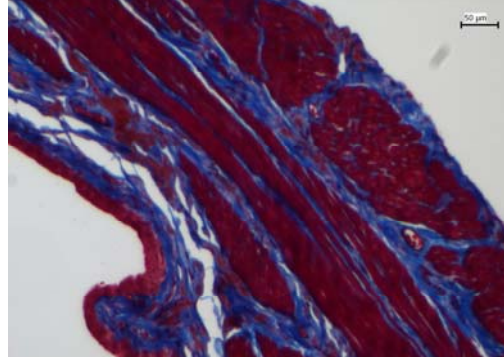
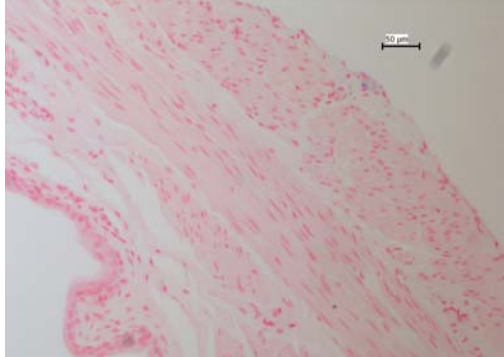
<p><b>Hematoxylin &amp; Erythrosine staining</b></p> <p>Nuclei are stained blue-black. Muscle is stained deep pink red</p>	<p><b>Masson's Trichrome staining</b></p> <p>Nuclei are stained braun. Muscle is stained pink red. Collagen is stained blue</p>	<p><b>Prussian Blue</b></p> <p>Iron (hemosiderine) is stained blue. Asbestos bodies are stained blue-black. Nuclei are stained red</p>	
			



### Fibrin gel with TG-IGF1

<p><b>Hematoxylin &amp; Erythrosine staining</b> Nuclei are stained blue-black. Muscle is stained deep pink red</p>	<p><b>Masson's Trichrome staining</b> Nuclei are stained braun. Muscle is stained pink red. Collagen is stained blue</p>	<p><b>Prussian Blue</b> Iron (hemosiderine) is stained blue blue. Asbestos bodies are stained blue-black. Nuclei are stained red</p>	
 <p>100 µm</p>	 <p>50 µm</p>	 <p>50 µm</p>	 <p>50 µm</p>
 <p>100 µm</p>	 <p>50 µm</p>	 <p>50 µm</p>	 <p>50 µm</p>

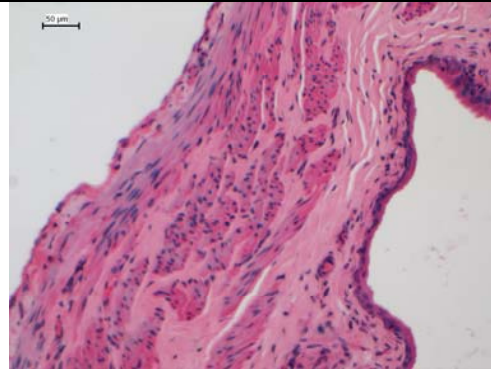
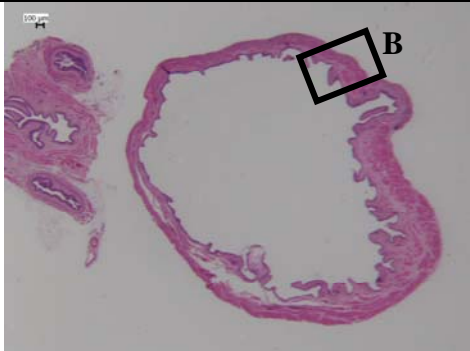
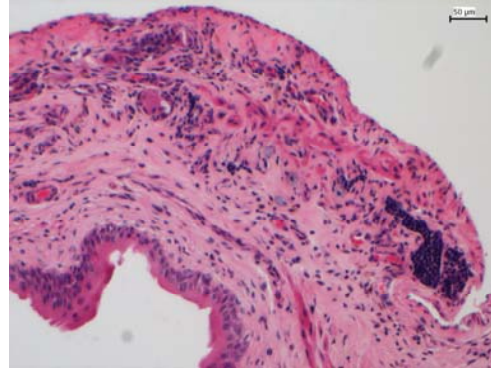
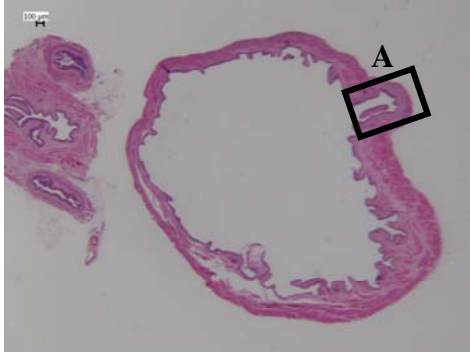
Fibrin gel with TG-IGF1

<p>Hematoxylin &amp; Erythrosine staining</p> <p>Nuclei are stained blue-black. Muscle is stained deep pink red</p>	<p>Masson's Trichrome staining</p> <p>Nuclei are stained braun. Muscle is stained pink red. Collagen is stained blue</p>	<p>Prussian Blue</p> <p>Iron (hemosiderine) is stained blue. Asbestos bodies are stained blue-black. Nuclei are stained red</p>	
			
			

Fibrin gel with TG-IGF1

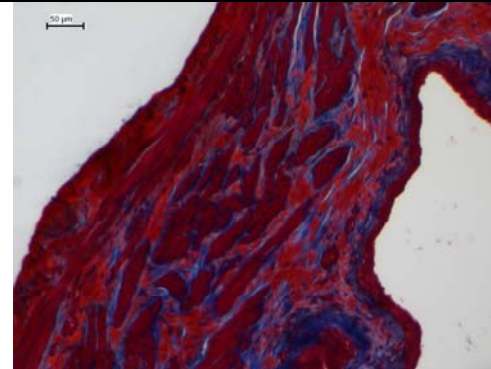
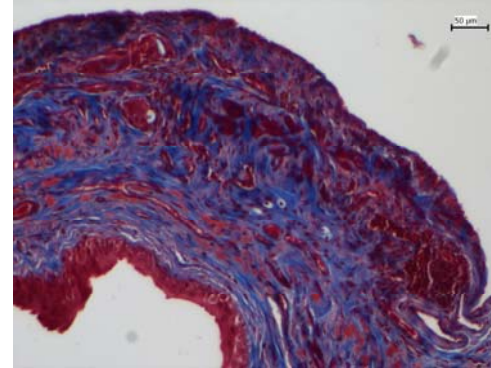
Hematoxylin & Erythrosine staining

Nuclei are stained blue-black.  
Muscle is stained deep pink red



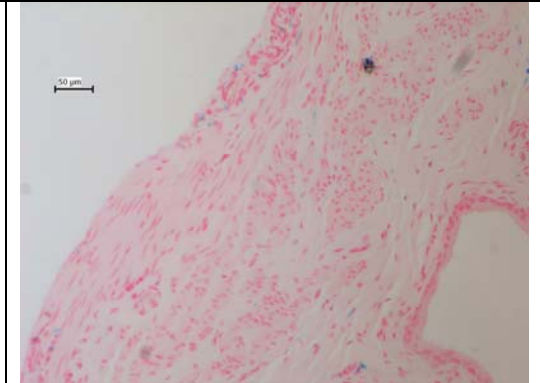
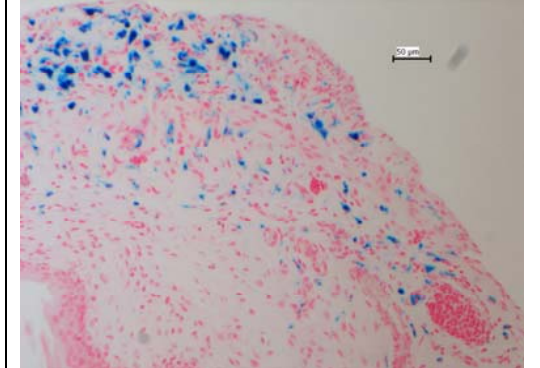
Masson's Trichrome staining

Nuclei are stained braun.  
Muscle is stained pink red.  
Collagen is stained blue

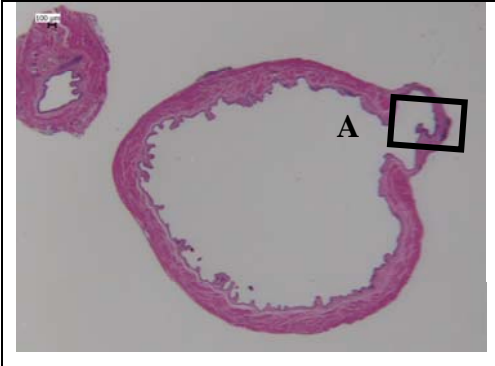
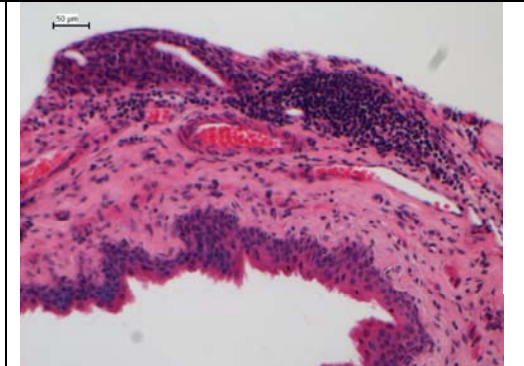
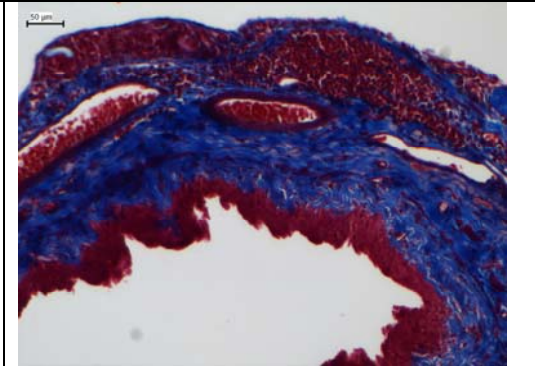
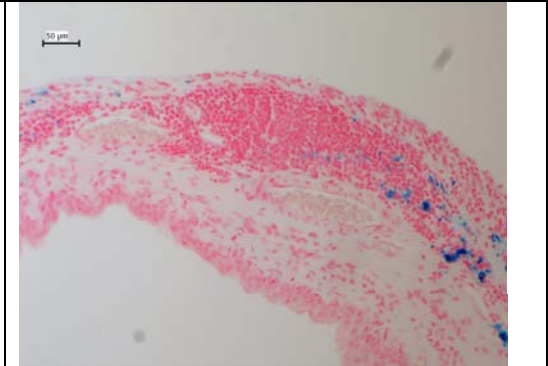
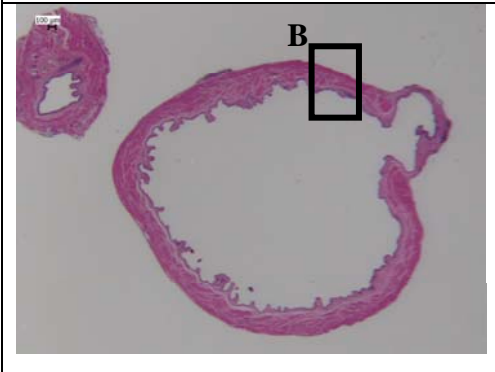
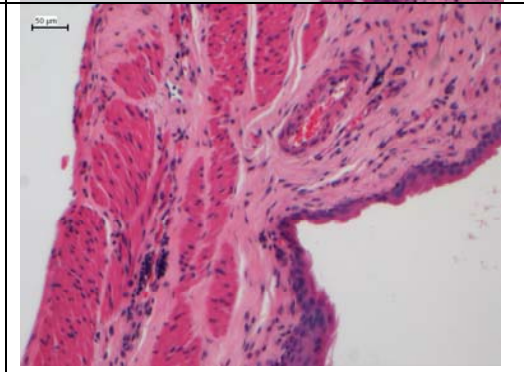
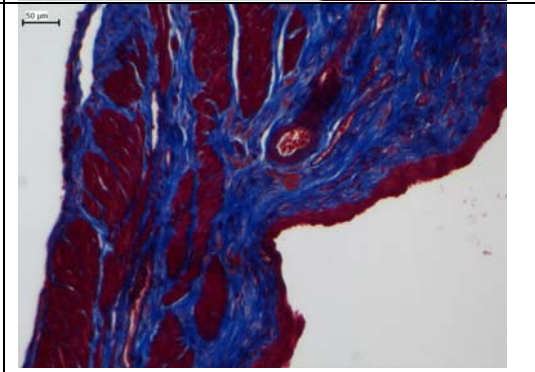
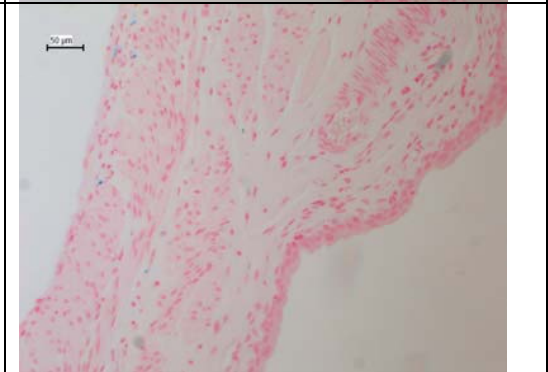


Prussian Blue

Iron (hemosiderine) is stained blue.  
Asbestos bodies are stained blue-black.  
Nuclei are stained red



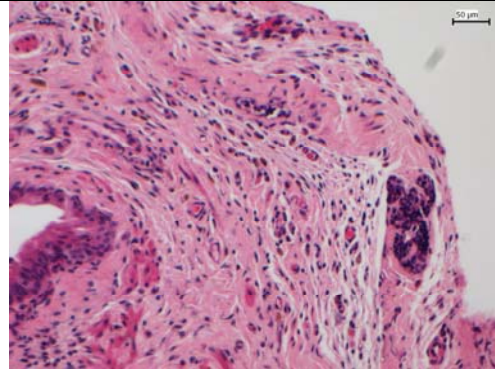
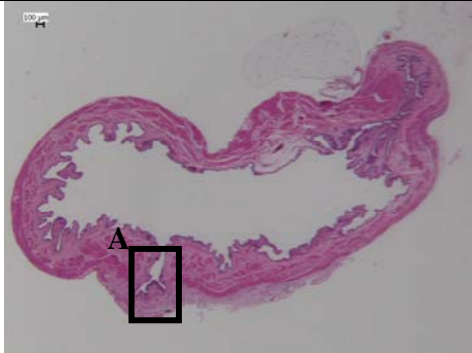
Fibrin gel with TG-IGF1

<p>Hematoxylin &amp; Erythrosine staining Nuclei are stained blue-black. Muscle is stained deep pink red</p>	<p>Masson's Trichrome staining Nuclei are stained braun. Muscle is stained pink red. Collagen is stained blue</p>	<p>Prussian Blue Iron (hemosiderine) is stained blue. Asbestos bodies are stained blue-black. Nuclei are stained red</p>	
			
			

Fibrin gel with TG-IGF1

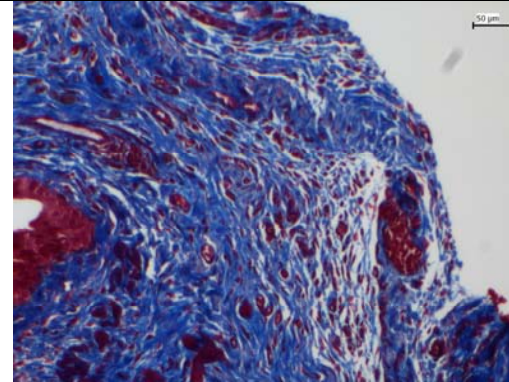
Hematoxylin & Erythrosine staining

Nuclei are stained blue-black.  
Muscle is stained deep pink red



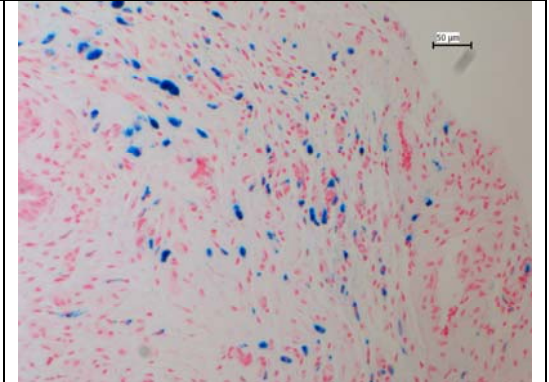
Masson's Trichrome staining

Nuclei are stained brown.  
Muscle is stained pink red.  
Collagen is stained blue



Prussian Blue

Iron (hemosiderine) is stained blue.  
Asbestos bodies are stained blue-black.  
Nuclei are stained red



B

